SOFIA II MODEL
TELESCOPE WIND TUNNEL TEST

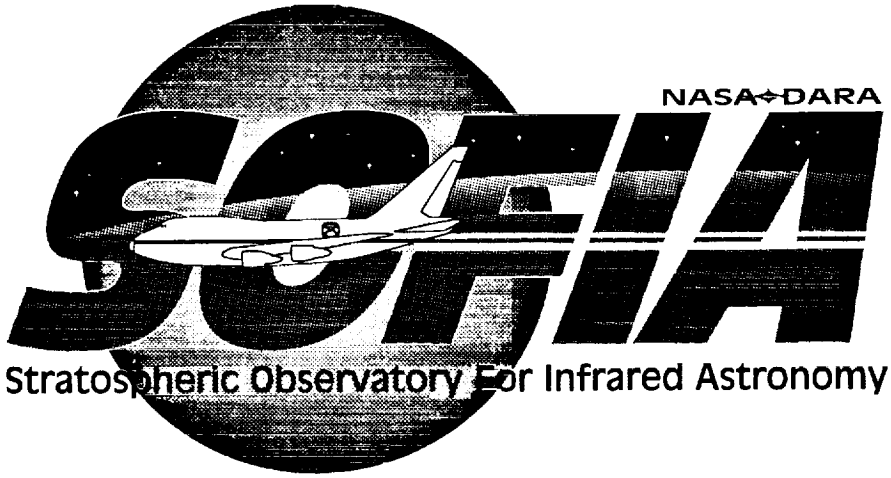

January 12, 1995

Paul Keas

CONTENTS

PURPOSE OF DOCUMENT 3
INTRODUCTION 3
TEST STRATEGY
Analog of the Physical System 4
Method of Calculation 5
MATRIX$_X$™ Calculations 6
EQUIPMENT USED 7
TEST SETUP 8
ESTIMATED ACCURACY OF TEST RESULTS 9
TELESCOPE CAVITY ENVIRONMENT
Bulkhead Vibration 12
Baseline Configuration 13
COMPARISON OF TORQUE MEASUREMENT TECHNIQUES
Measurement Methods 15
Measurement Results 15
SOFIA WIND TUNNEL MODEL TELESCOPE TEST RESULTS
Conditions Tested 17
Naming and Sign Conventions for Forces and Moments 17
Model Scale Vs Full Scale Physical Units 18
747 Configurations 65 Through 67 (favorite cavity treatment for 200) 19
747 Configurations 86 Through 88 (favorite cavity treatment for SP) 19
Dependency on Angle of Attack (alpha) 20
Dependency on Side Slip (beta) 22
Dependency on Elevation Angle (gamma) 24
Dependency on Airspeed (Mach) 26
Static LOS Normal Force "N" Vs Static Cross Elevation Moment "PM" 28
Overview of Static Forces and Moments 29
CONCLUSION 34
SUMMARY OF FULL-SCALE EQUIVALENT FORCES AND MOMENTS 36

APPENDIX A
Data Spreadsheet for configurations 65 through 67 (200) A1
Data Spreadsheet for configurations 86 through 88 (SP) A2

APPENDIX B
How to Use Appendix B B0
Model Scale Dynamic Cross Elevation Moment PSD plots
for configurations 65 through 67 (200) ..... B1 - B72
Model Scale Dynamic Cross Elevation Moment PSD plots
for configurations 86 through 88 (SP) ..... B72 - B144
APPENDIX C
Dynamic Signal Scaling Factors C1
PSD Scaling C1
Dynamic Disturbance Calculations C2

PURPOSE OF DOCUMENT

This document outlines the tests performed to make aerodynamic force and torque measurements on the SOFIA wind tunnel model telescope. These tests were performed during the SOFIA II wind tunnel test in the 14 ft wind tunnel during the months of June through August, 1994. A brief description is given of the test methodology, and the instrumentation used. A summary of the test results follows.

INTRODUCTION

The test described in this report was designed to measure the dynamic cross elevation moment acting on the SOFIA model telescope due to aerodynamic loading. The measurements were taken with the telescope mounted in an open cavity in the tail section of the SOFIA model 747. The purpose of the test was to obtain an estimate of the full scale aerodynamic disturbance spectrum, by scaling up the wind tunnel results (taking into account differences in sail area, air density, cavity dimensions, etc.). An estimate of the full scale cross elevation moment spectrum was needed to help determine the impact this disturbance would have on the telescope positioning system requirements.

A model of the telescope structure, made of a light weight composite material, was mounted in the open cavity of the SOFIA wind tunnel model. This model was mounted via a force balance, to the cavity bulkhead. Despite efforts to use a "stiff" balance, and a lightweight model, the balance/telescope system had a very low resonant frequency (37 Hz) compared to the desired measurement bandwidth (1000 Hz). Due to this mechanical resonance of the balance/telescope system, the balance alone could not provide an accurate measure of applied aerodynamic force at the high frequencies desired. A method of measurement was developed that incorporated accelerometers in addition to the balance signal, to calculate the aerodynamic force.

TEST STRATEGY

The following is an overview of the test strategy used to calculate the cross elevation moment spectrum. For a more detailed description of the development of this strategy, please refer the SOFIA documents: "SOFIA WIND TUNNEL MODEL TELESCOPE TEST PLAN" (May 31, 1994), and "SOFIA WIND TUNNEL MODEL TELESCOPE BENCH TEST RESULTS" (July 11, 1994).

Analog of the Physical System

Figure #1 shows a simplified, single degree of freedom system that will be used to illustrate the method that was used to solve for the cross elevation moment spectrum.

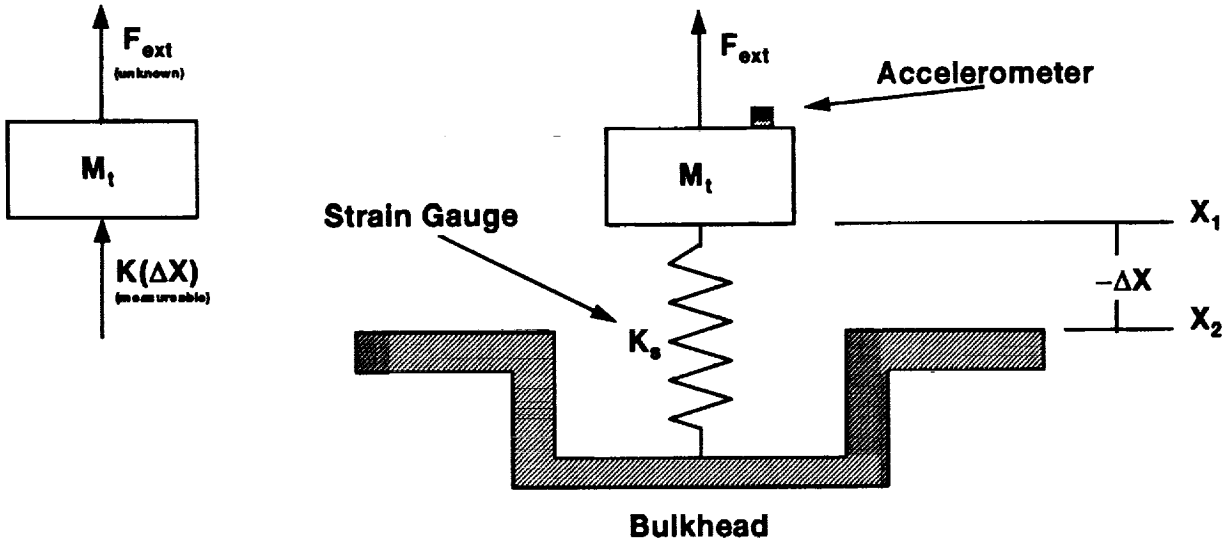

Figure #1: Analog of telescope/balance dynamic system.

The mass (*telescope*) is supported by a strain gauge (*balance*) with spring constant K_S, and an external disturbance F_{ext} is applied to the block as shown above. The system can be excited by the external force (F_{ext}), or by motion of the bulkhead (a change in X_2).

In ANY case, (regardless of the source of the excitation) The following equation will hold true:

$$\text{(i)}\quad \Sigma F = M_t(a) = K(\Delta X) + F_{ext}$$

The physical system pictured above can also be represented in a block diagram form which will better illustrate the states which are measured in an attempt to solve for F_{ext}, and how the physical states are related.

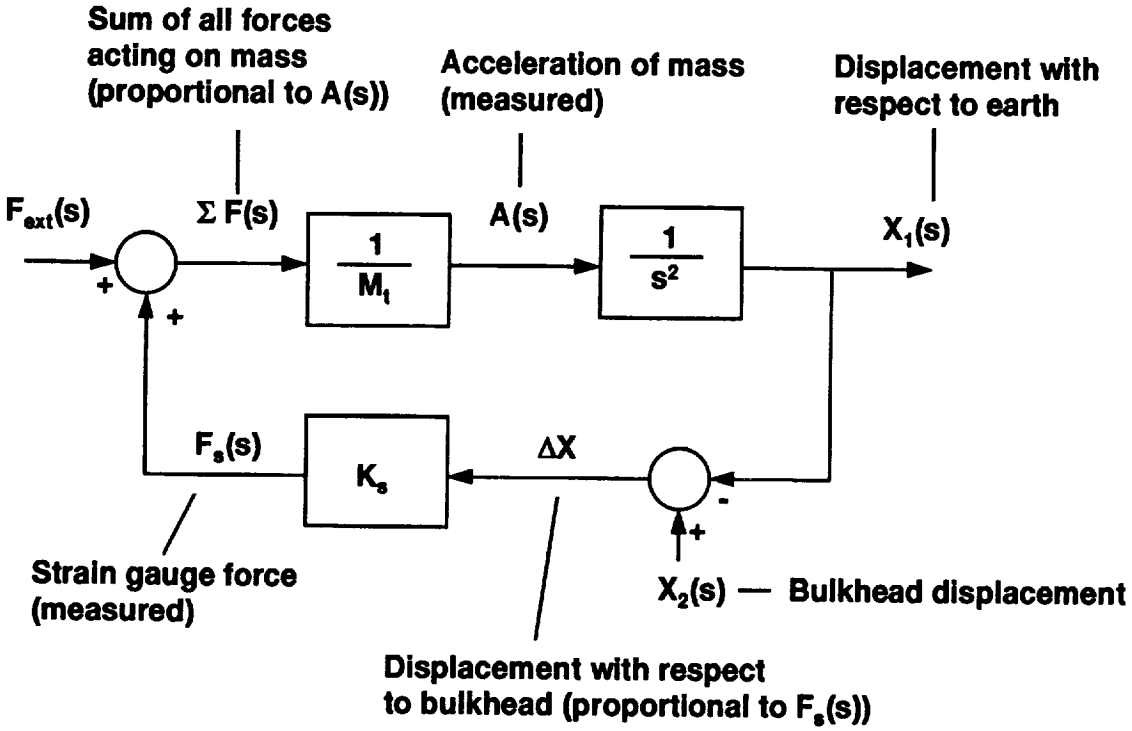

Figure #2: Block diagram of physical system in figure #1.

This diagram shows the system as having two inputs. One input is the external disturbance we wish to solve for, and the other "undesired" input is due to a bulkhead vibration.

Method of Calculation

An examination of the block diagram above will reveal that the external disturbance can be calculated directly from ($K_S(\Delta X)$), and ($A(s)*M_t$). $\Delta X(t)$ is given by the strain gauge signal, and the acceleration A(t) is measured by the accelerometer mounted on the moving mass. The known spring constant K_S and mass M_t can be used to scale these two signals, and solve for the external disturbance at any time (t). This calculation makes no assumptions about what portion of a physical state is due to bulkhead movement, and which is due to the external force.

The block diagram illustrates the fact that the strain gauge displacement and mass acceleration are due to both bulkhead movement and external forces. It also shows that both acceleration and ΔX are necessary to calculate F_{ext}. The nature of the measurements determine their relative importance as a function of frequency. Because the strain gauge signal is a measure of deflection, it will become negligible at high frequencies, where the

deflection of the strain gauge becomes very small. At low frequencies, the balance forces will dominate, since deflection will become very large for a given acceleration. (The extreme case being for a static applied force which would result in a static strain gauge deflection, and no acceleration.)

The overall transfer function between $F_{ext}(s)$ and A(s) is an issue, but only by virtue of the fact that the calculation of F_{ext} becomes difficult when the system resonates, since the F_{ext} is small compared to the measured outputs. (At the resonant frequency, a large amount of energy is stored in the strain gauge, and large strain gauge forces result). This simply means that the relatively narrow band of frequencies around the resonant peak may be inaccurate. This effect did not turn out to be a significant problem in determining the RMS value of F_{ext}.

$MATRIX_X$ Calculations

Once the balance and accelerometer data was collected, it was scaled to physical units, and used to calculate a time function of F_{ext}. $MATRIX_X$ was used to do this operation in the time domain. The equations of motion were simple algebraic equations. The operation performed was equivalent to rearranging equation (i) from the simplified example outlined above:

$$\text{(i)}\quad \Sigma F = M_t(a) = K(\Delta X) + F_{ext}$$

$$F_{ext} = M_t(a) - K(\Delta X)$$

Where a(t) would be obtained from the accelerometer signal, and $\Delta X(t)$ would be obtained from the strain gauge signal.

Care was taken to collect the data in a way that would preserve the phase relationships between the measured accelerations and displacements, so that meaningful time domain calculations could be performed.

The method of calculation was basically an application of Newton's 2nd law to the telescope model. The actual calculation was the same type as outlined above, except it was applied to a system having additional degrees of freedom. For a detailed summary of the actual scale factors and calculations used to compute the dynamic cross elevation moment applied to the model telescope, please refer to appendix C.

EQUIPMENT USED

1.) TO.75 MK XX force balance.
2.) BLAMS balance load alarm and monitoring system.
3.) Four ENDEVCO 2250A-10 crystal accelerometers.
4.) Two ENDEVCO Type 102 signal conditioners.
5.) One ENDEVCO type 109 power supply.
6.) Two KISTLER crystal accelerometers.
7.) One KISTLER signal amplifier.
8.) One H.P. Dynamic Signal Analyzer.
9.) 16 Channel Metrum recorder.
10.) 4mm DAT. Tape Drive.
11.) $MATRIX_X$ System Build and DSP modules.

All the signals were input to the Metrum recorder wide-band. The Metrum recorder was configured to filter the incoming signals in a way that preserved the phase relationships between the signals that would be used in time domain calculations. The cutoff frequency (0.5 DB down) for the ENDEVCO accelerometers and the TO.75 MK XX force balance was 1.25 KHz (4 pole Chebechev low-pass) with a sampling rate of 5 KHz. The two KISTLER accelerometers were cutoff at 10 KHz with a sampling rate of 40 KHz.

TEST SETUP

The instrumentation was set up to measure the forces and moments that act in the telescope's plane of symmetry (the X' Z' plane). Figure 3 illustrates the orientation of the telescope model and the instrumentation in relation to the aircraft's coordinate system.

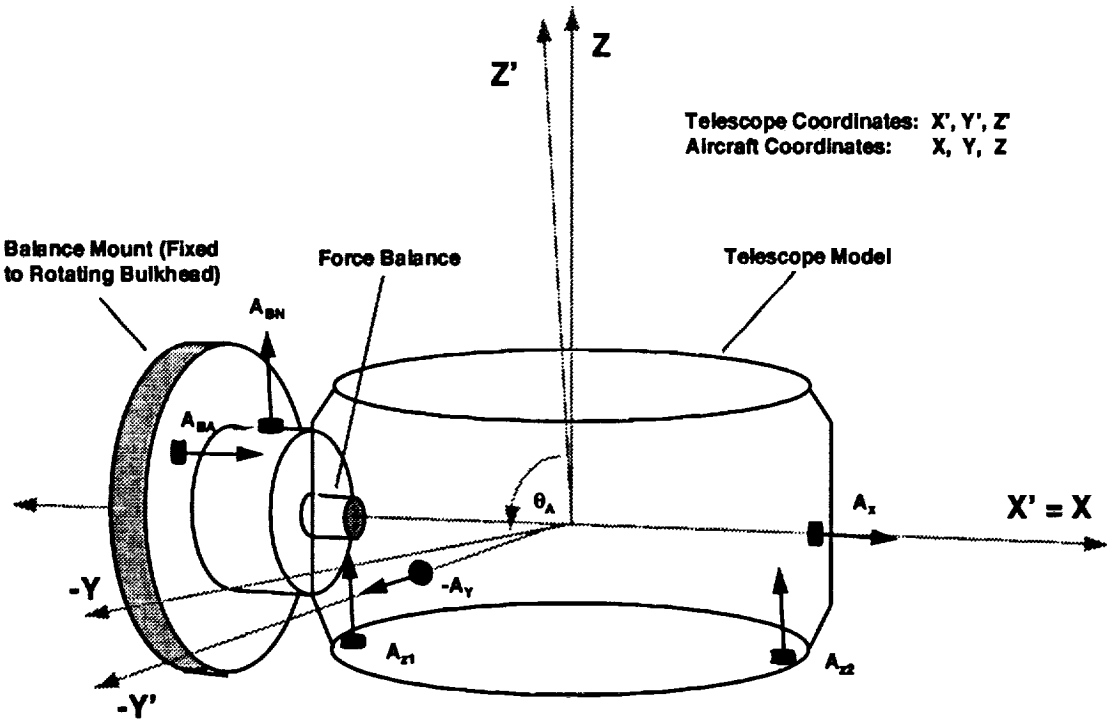

FIGURE # 3: Test set up in SOFIA wind tunnel model

The telescope coordinate system rotated about the X axis as the aperture angle changed. Z' was in the direction the telescope was "looking", and was always normal to the aperture opening. The aperture angle was formed between Z' and -Y. An aperture angle of 90 degrees resulted in the alignment of the two coordinate systems.

For all aperture positions: A_{BN}, A_{Z1}, and A_{Z2} were parallel to the Z' axis. A_X, and A_{BA} were parallel to the X' axis. A_Y was parallel to the Y' axis. The normal, lateral, and axial forces sensed by the balance remained parallel to the Z', Y' and X' axis respectively.

The accelerometers mounted on the bulkhead were used to monitor the bulkhead vibration. This data was not incorporated in the actual cross elevation moment calculation, however these signals were recorded so that questionable cross elevation moment results could be checked against any resonances that may have existed in the bulkhead.

A_Y and A_X were also not incorporated in the cross elevation moment measurements, however it was desired to record this information in case unexpectedly high lateral or axial

forces were encountered during the wind tunnel tests. Only the normal forces (in Z' direction) from the balance were incorporated in the dynamic cross elevation moment calculations, however all six degrees of freedom were recorded for future reference.

ESTIMATED ACCURACY OF TEST RESULTS
(as determined from the **BENCH TEST**)

The SOFIA wind tunnel model telescope bench test indicated that meaningful data could be obtained using the proposed strategy. The external disturbance could be calculated within a factor of 2 for frequencies under 1000 Hz and outside the band of frequencies from 500 to 700 Hz. Figure # 4 shows the "error" function expressed as the calculated cross elevation moment divided by the known input. This plot was generated from the results of a bench test that was performed prior to the wind tunnel test.

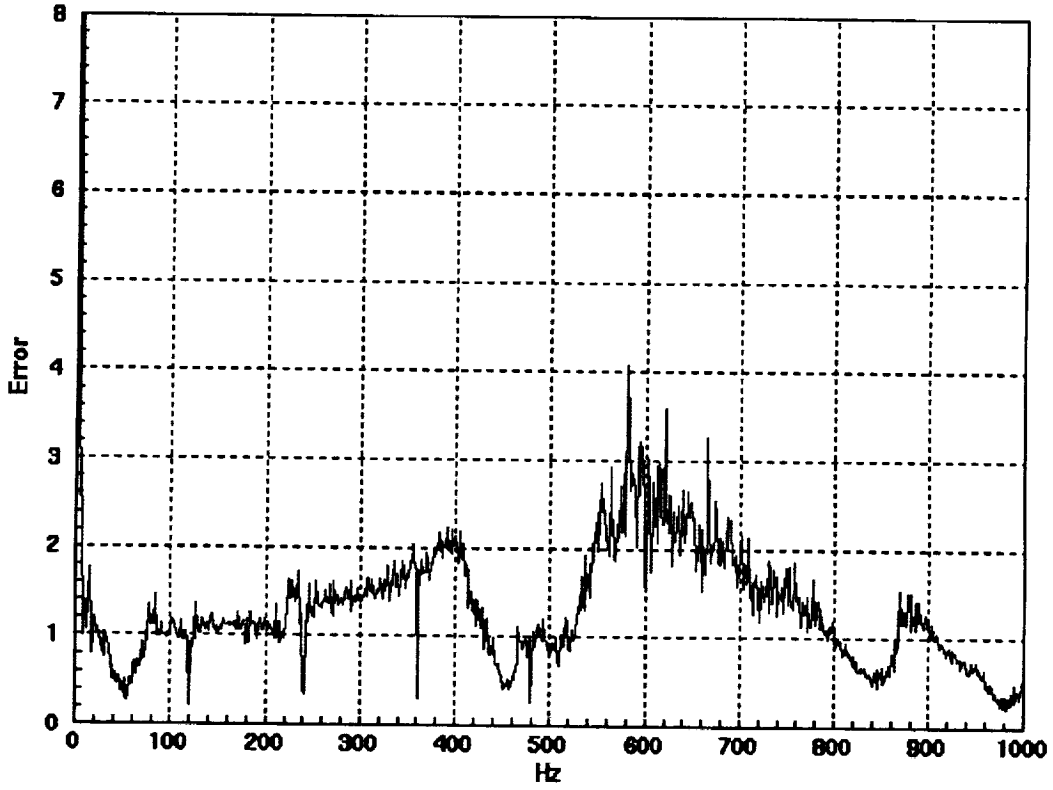

FIGURE 4: (Calculated)/(Known) for random disturbance during bench test.
(complete equation of motion results)

Three calculations were performed on the **bench test data**. The calculations performed were the complete equations of motion (EOM), a high frequency approximation that neglected the balance reaction forces, and a low frequency approximation that neglected the telescope acceleration. The complete EOM (results shown above) proved to be the most useful calculation for approximating the external disturbance spectrum.

The complete EOM performed well over the frequency range stated above, except from 1Hz down to DC, where the accelerometer responses rolled off and the accelerometer signals exhibited large amplitude variations in response to random temperature fluctuations. A low frequency approximation was necessary to calculate the bottom 1 Hz of the disturbance spectrum. The disturbance calculation was tested in the presence of a 6 Hz 0.1 g bulkhead vibration. this vibration input did not corrupt the calculated external disturbance obtained from the complete EOM calculation. Figure 5 shows a comparison of the complete EOM, the high frequency approximation, and low frequency approximation for calculating the external disturbance. The spectrum of the known input is included at the bottom of the figure.

Note that the low frequency approximation yielded correct information down to DC, however, the inertial load due to the shaking bulkhead was added at 6 Hz. The high frequency approximation was not valid for any of the frequencies shown in the figure. The complete EOM calculation was very well correlated with the known input spectrum, even at 6 Hz in the presence of the 0.1 G bulkhead vibration. The complete EOM broke down under 1 Hz, where an error was introduced by the crystal accelerometers.

Figure 5 illustrates the fact that the complete EOM were needed to calculate the external disturbance separate from the inertial loading that results from bulkhead vibration.

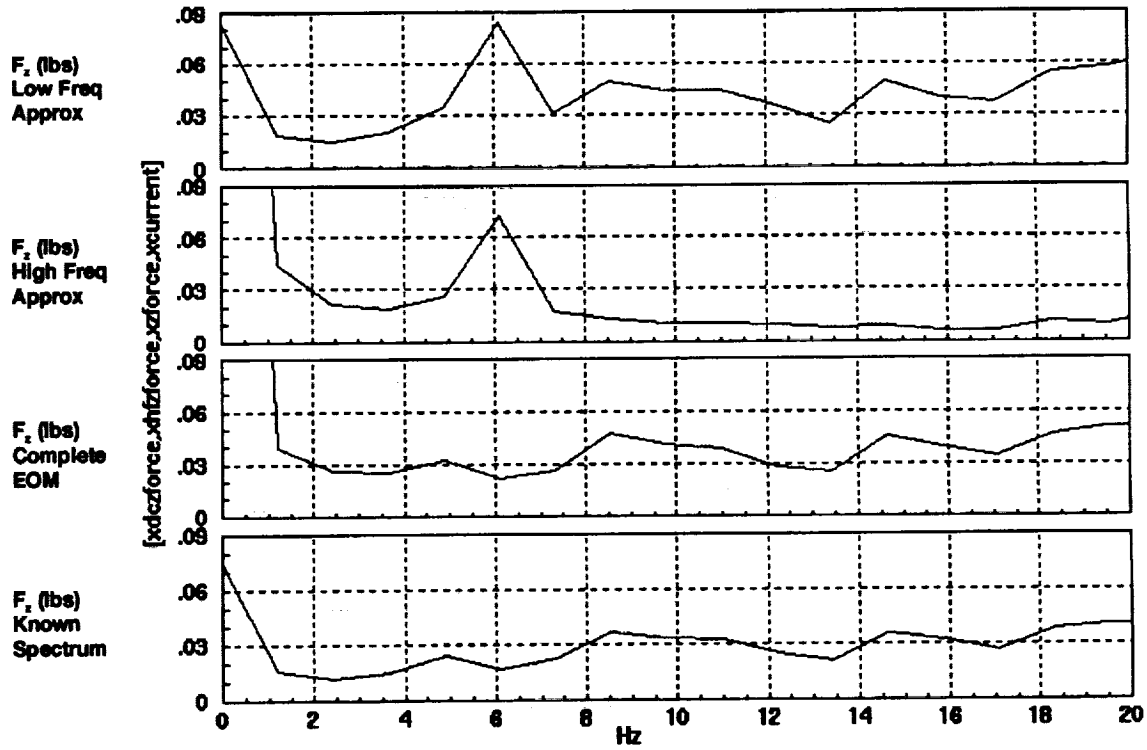

FIGURE 5: Frequency domain results of bench test external force calculations in an environment with a 6 Hz, 0.1g vibration.

The low frequency approximation performed extremely well from 60 Hz, down to DC. The low frequency approximation was however, vulnerable to bulkhead acceleration. This is because it assumed that the disturbance was equal and opposite to the balance force. Bulkhead vibration was added to the low frequency disturbance approximation as 1 lb/g.

The **bench test results** indicated that the proposed test strategy could provide meaningful information for a limited band of frequencies. The two factors that were identified as limiting frequency range of the test were the dynamics of the force balance, and the structural resonances in the telescope model. The dynamics internal to the force balance limited the range of frequencies over which the balance could provide accurate dynamic force information. The structural resonance of telescope model limited the range of frequencies over which the model would behave like a rigid body (a condition that was assumed in the calculations) to frequencies under 1000 Hz.

TELESCOPE CAVITY ENVIRONMENT

Bulkhead Vibration

The rotating bulkhead bearing was somewhat loose, and became excited during the open cavity wind tunnel tests. The resulting bulkhead motion contained much higher frequency components than were expected from the massive 747 model. Figure 6 shows the spectrum of the bulkhead vibration in the Z' direction and the X' direction.

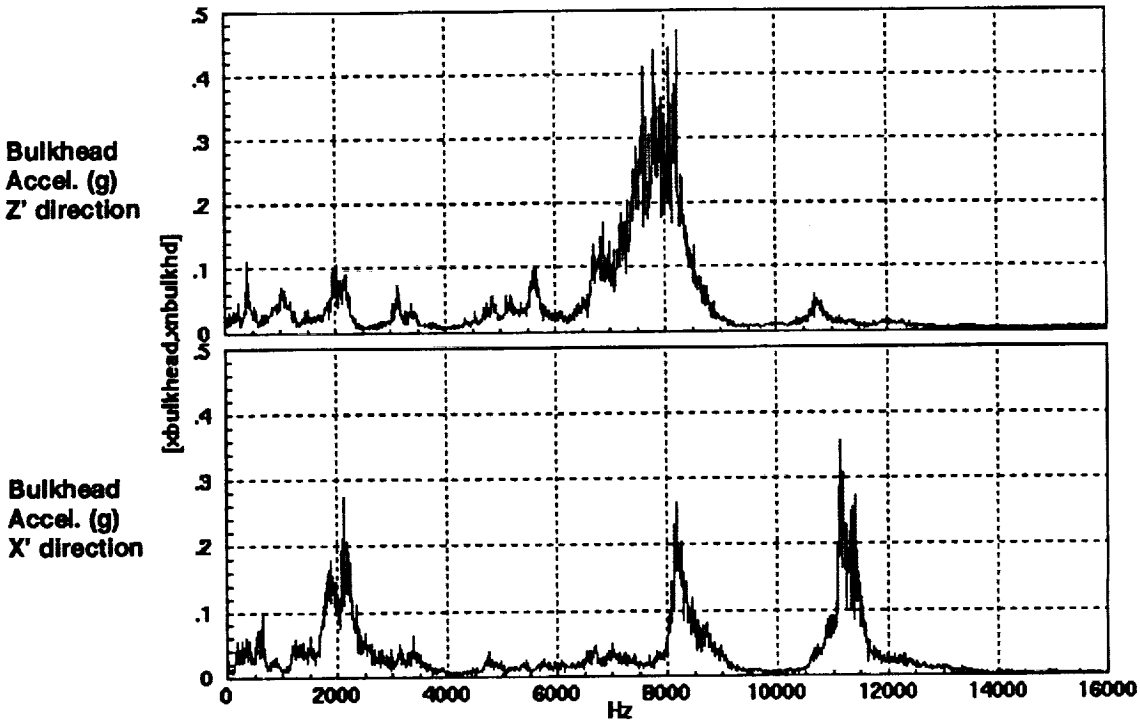

FIGURE 6: Spectrum of bulkhead vibration during a Mach 0.85 wind tunnel run.

The high frequency components seemed to be resonances in the bulkhead plate. In the time domain, the Z' acceleration showed evidence that the 8000 Hz component was a ringing that was excited 400 times a second (from the 400 Hz aerodynamic disturbance). See figure 7.

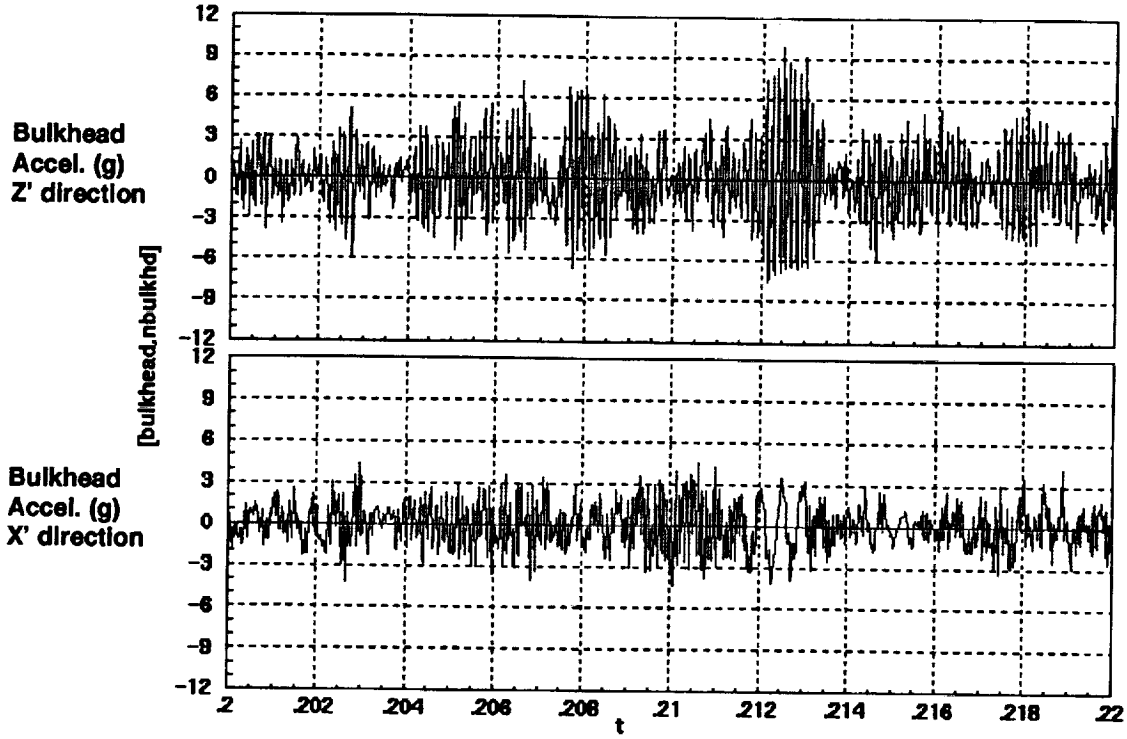

FIGURE 7: Time record of bulkhead vibration during a Mach 0.85 wind tunnel run.

The bulkhead vibration in the Z' and X' directions had acceleration levels of **2.4 g** RMS and **1.7 g** RMS respectively. However, most of this energy was at frequencies above 1000 Hz. The acceleration signals were digitally filtered to eliminate their content above 1000 Hz. The filtered acceleration levels for the Z' and X' directions became **0.26 g** RMS and **0.25 g** RMS respectively. The inertial loads due to these vibrations would be approximately 0.25 lb RMS within the frequency range of interest (0-1000 Hz).

Baseline Configuration

A dynamic cross elevation moment calculation was performed on the data taken from a closed cavity. Since it was known (by observing the SPL measurements during the closed cavity condition) that the cross elevation moments were very small during the closed cavity condition, this information could be used to estimate the levels of cross elevation moment that would be calculated in error, due to the bulkhead vibration.

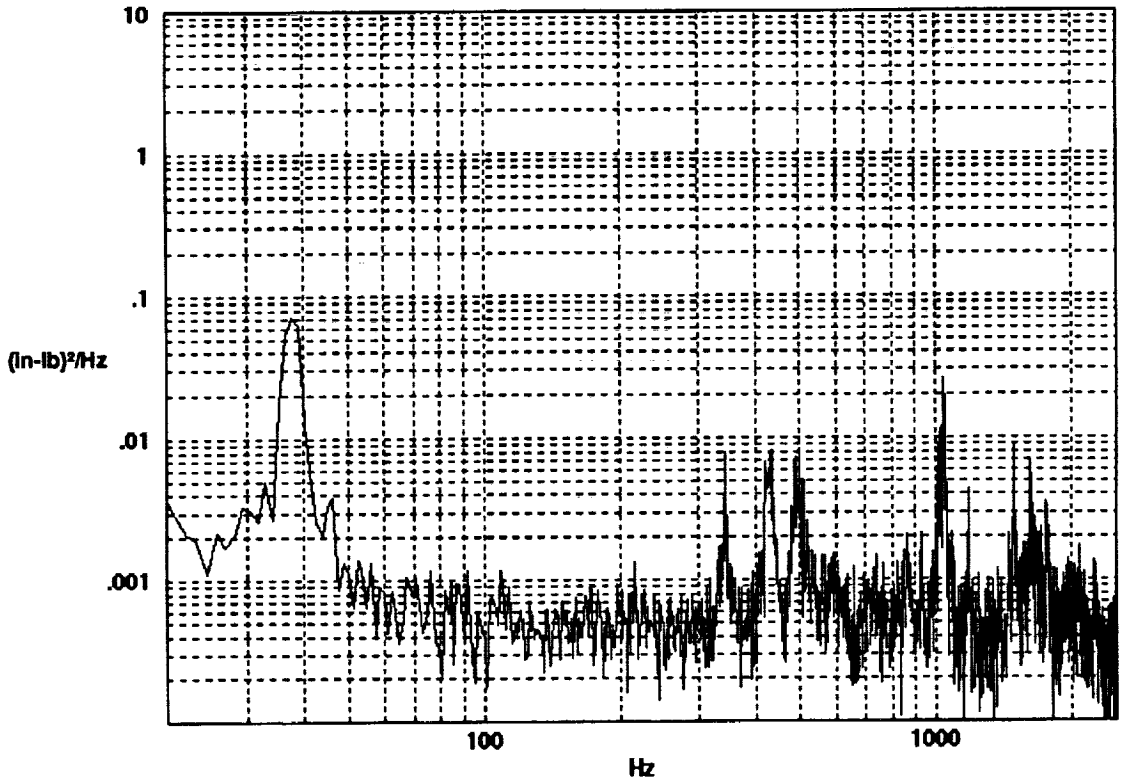

(Cavity Closed)

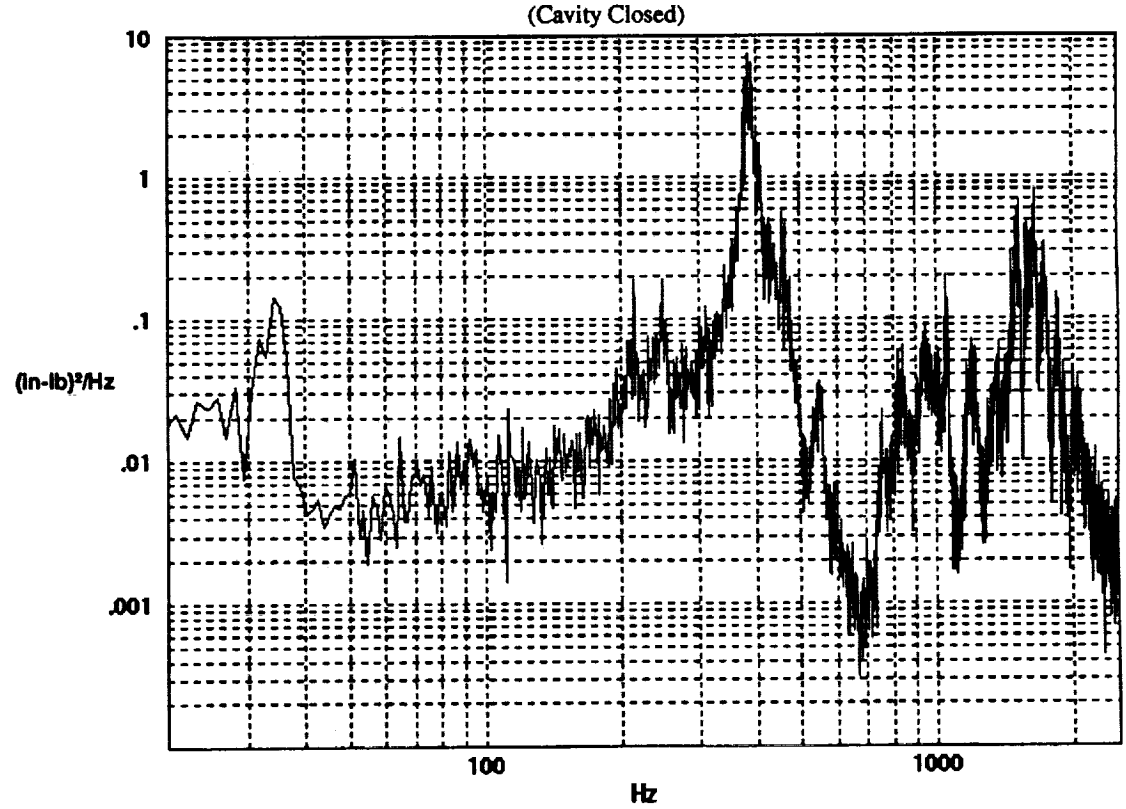

(Cavity Open)

FIGURES 8 and 9: "CROSS ELEVATION MOMENT" PSD for SP configuration, closed cavity and open cavity at cruise condition (Configurations 89 and 86 respectively).

Note that the PSD levels are several orders of magnitude lower for the closed cavity configuration than for the open cavity condition. The "Noise" introduced by the vibrating bulkhead did not seem to result in a significant output. The only significant error occurred at the natural frequency of the Balance/Telescope natural frequency of 37 Hz, as expected. The error at this resonance was two orders of magnitude lower than the major contributor to the RMS value of the cross elevation moment which was observed at 400 Hz during the open cavity condition.

COMPARISON OF TORQUE MEASUREMENT TECHNIQUES

Measurement Methods

The force balance/accelerometer method used the phase locked balance and accelerometer signals to solve for the dynamic cross elevation moment as outlined in this report.

The dynamic pressure method used eight kulites to measure the dynamic differential pressure from one side of the primary mirror to the other. The dynamic pressure information could then be used to calculate torque when multiplied by the appropriate sail area and moment arm. A report generated be Dan Machak, who performed the dynamic pressure analysis, will give a much more complete description of that method.

Measurement Results

The dynamic pressure and balance/accelerometer method produced results that were well correlated. The percent difference in RMS torque results between the two methods for any given test condition was between 10 and 30 percent. The balance/accelerometer method yielded consistently higher values. figures 10 and 11 show a comparison between the results obtained from the two methods for configuration 8, cruise condition (Mach = .85, alpha = 2.5).

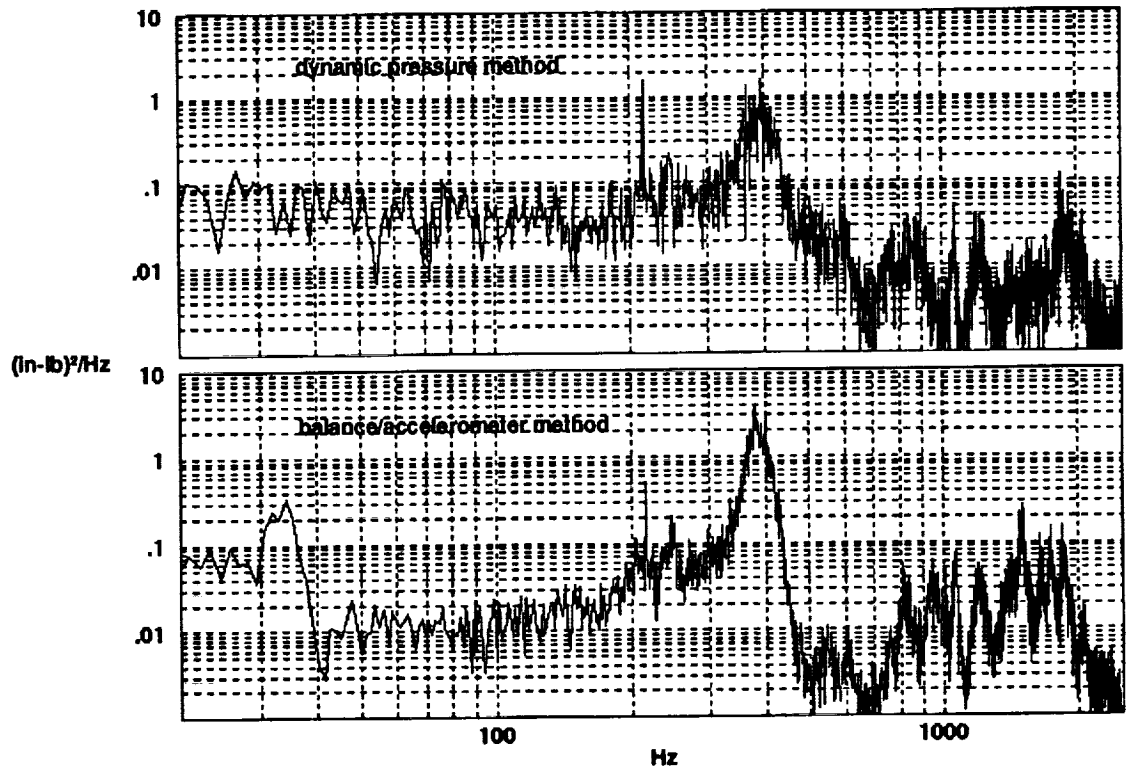

Cross elevation Moment PSD

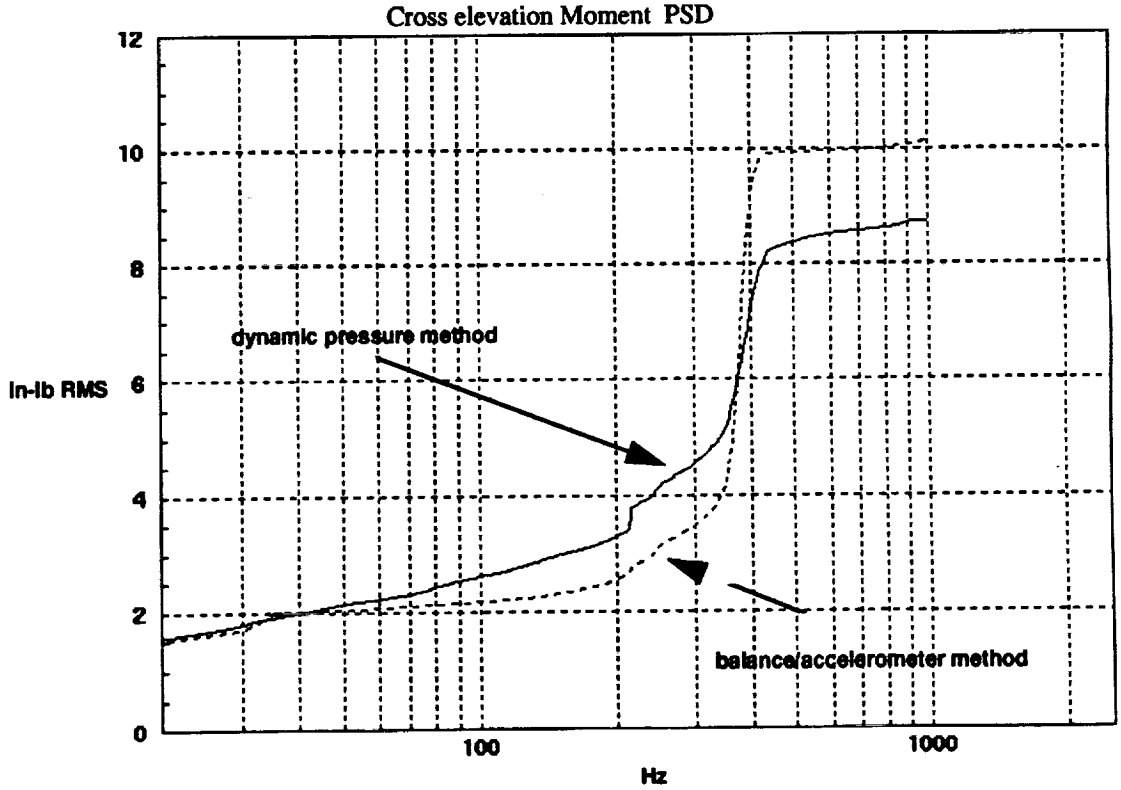

Cross elevation Moment Cumulative RMS

FIGURES 10 and 11: Cross elevation Moment calculations for both measurement methods for cruise condition (SP configuration 86, run 219, sequence 5.)

SOFIA II WIND TUNNEL MODEL TELESCOPE TEST RESULTS

Conditions Tested

Due to the delicate nature of the force balance and lightly damped dynamic response of the balance/telescope system, It was necessary to lock-out the balance during many of the test configurations to prevent damage to the force balance. For this reason, the method outlined in this report was only implemented during the testing of the "favorite" cavity treatments, where cross elevation moments were minimized. Fortunately, a second method was also in place to measure the cross elevation moment by sensing the dynamic pressure on the top and bottom of the primary mirror. This method (F=qA) was observed to produce results that closely matched those obtained using the method outlined here (F=Ma). The dynamic pressure method was in place for even the most violent test conditions.

Since the balance/accelerometer method was used for only certain test conditions, the scope of this report is limited to the optimum configurations for the 200 and SP 747 cavity. The balance information also contains static load information which could not be obtained from the kulites. The static loading, as well as its apparent dependency on any test condition variables (like Mach, angle of attack, elevation angle etc...) is presented in detail. A report written by Dan Machak, with the dynamic pressure results will provide a better overall picture by which to compare the cross elevation moment levels for all the configurations that were tested.

Naming and Sign Conventions for Forces and Moments

Complete accelerometer data was limited to motion in the X'Z' plane. Therefore, **dynamic** torques were only calculated about an axis parallel to the Y' axis, passing through the location where the (model scale) air bearing would be located (see figure 12 on following page). **Static** data was gathered for all six degrees of freedom since all this information was available from the force balance signal. The following page summarizes the naming and sign conventions for these forces and moments.

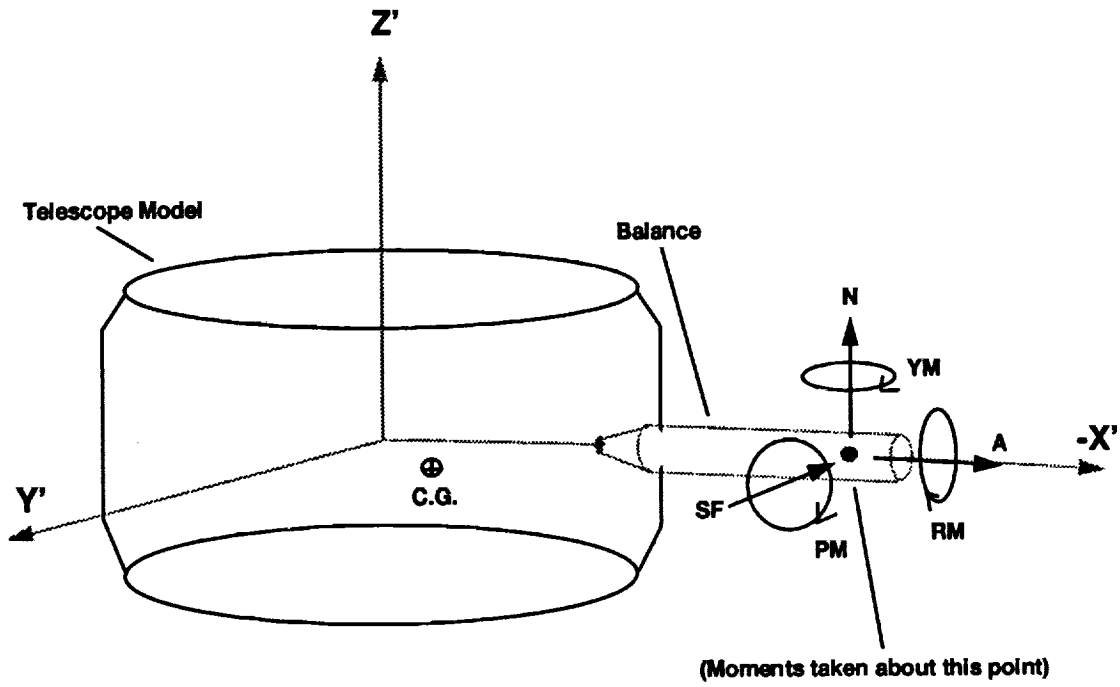

Figure 12: Sign Conventions for forces A, SF, N, and moments RM, PM, YM. (The orientation of the forces and moments rotates with the telescope coordinant system as the telescope elevation angle is changed).

A = Nasmyth Axial Force	RM = Elevation Moment
SF = Side Force	PM = Cross Elevation Moment
N = LOS Normal Force	YM = LOS Moment

Model Scale Vs Full Scale Physical Units

Note that the RMS torque levels presented in this report are in inch-pounds MODEL SCALE. To convert from **inch-pounds model scale** to the approximate **full scale torque in foot-pounds**, MULTIPLY the model scale torque by a factor of **70** (for scaling purposes, some of the static moments are plotted in ft-lb, making their conversion factor approximately 5.8). To convert the **model scale frequency** units to approximate **full scale equivalent**; DIVIDE the model scale frequency by a factor of **17**.

It is important to note that the RMS values for **dynamic** torques presented in this report **do not include the mean value.** The RMS values were calculated by summing the elements of the PSD in $(\text{in-lb})^2$ units, and then taking the square root of the sum. RMS values were calculated for two bandwidths: 1 - 1000 Hz, and 300 - 500 Hz. This was done to provide a separate measure of the main aerodynamic resonance centered at 400 Hz. From these two separate calculations, it is made graphically evident that most of the energy is contained within the 300 - 500 Hz range.

747 Configurations 65 Through 67 (favorite cavity treatment for 200)

The dynamic cross elevation moment observed at cruise condition in configuration 65 averaged 9.88 in-lb RMS (approximately 692 ft-lb full scale). Most of this energy was concentrated at an aerodynamic resonant peak centered at 400 Hz (approximately 23.5 Hz full scale). The energy contained in the spectrum between 300 and 500 Hz was 9.08 in-lb RMS. The static cross elevation moment observed at cruise condition was approximately -5.4 in-lb.

747 Configurations 86 Through 88 (favorite cavity treatment for SP)

The dynamic cross elevation moment levels observed at cruise condition in configuration 86 averaged 11.0 in-lb RMS (approximately 721 ft-lb full scale). Most of this energy was concentrated at an aerodynamic resonant peak centered at 400 Hz (approximately 23.5 Hz full scale). The energy contained in the spectrum between 300 and 500 Hz was 10.1 in-lb RMS. The static cross elevation moment observed at cruise condition was approximately -3.8 in-lb.

The following pages are a summary of how the Cross elevation moment levels varied with changes in Mach, angle of attack, side slip, and telescope elevation angle for the above configurations.

Dependency on Angle of Attack (alpha)

The angle of attack was varied at a Mach 0.85 and an elevation angle of 40 degrees (centered). The dynamic cross elevation moments of configuration 65 did not exhibit a large dependency on alpha, increasing only slightly for values of alpha over 2 degrees. The static cross elevation moment increased with increasing angle of attack. The static moment was negative for the range of alpha tested (see figures 13 and 14).

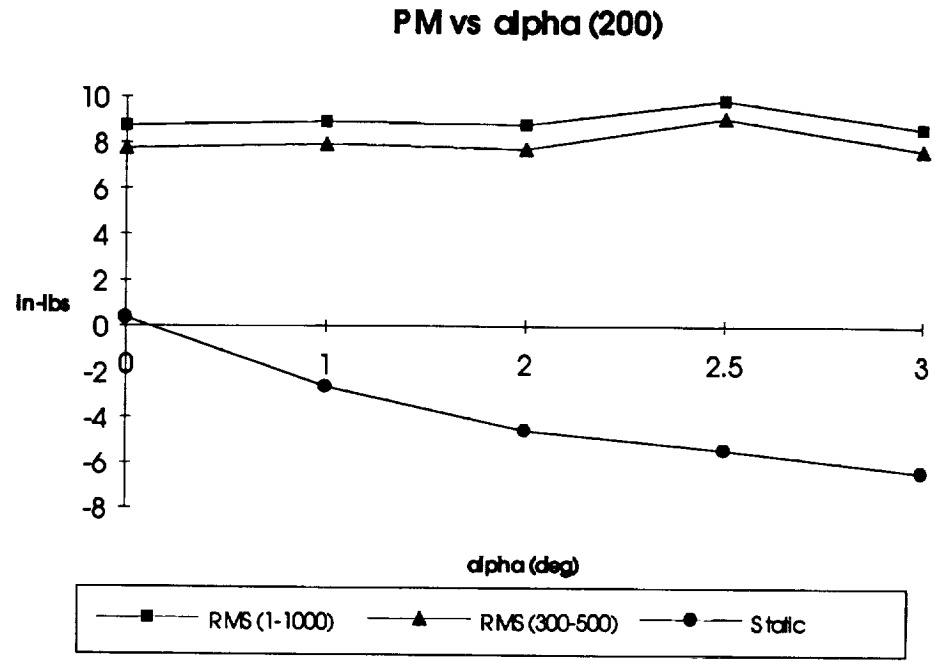

Figure 13: Cross elevation Moment Vs Alpha for Configuration 65, beta = 0, gamma = 40, Mach = 0.85.

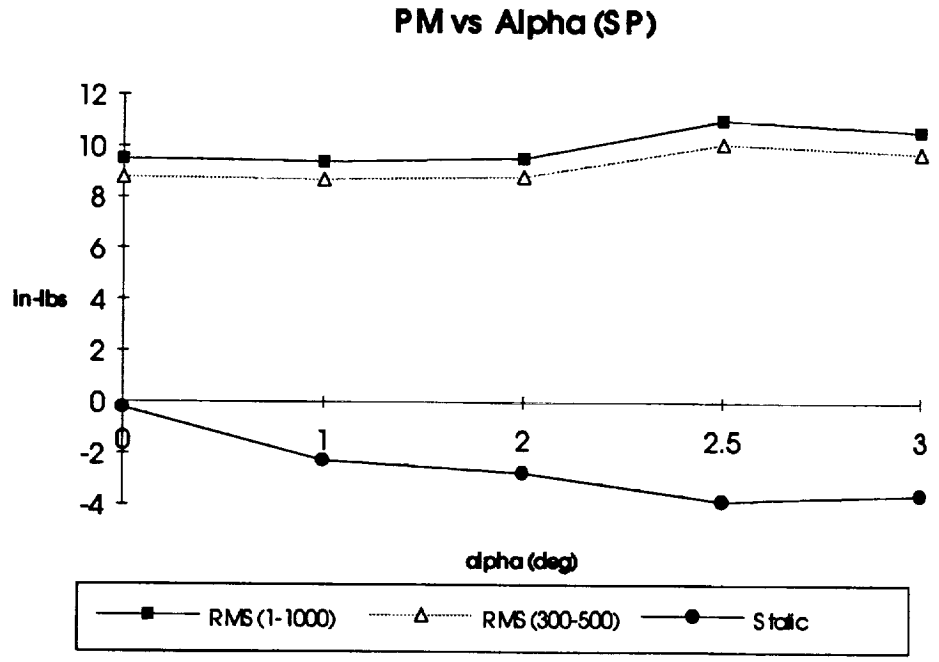

Figure 14: Cross elevation Moment Vs Alpha for Configuration 86, beta = 0, gamma = 40, Mach = 0.85.

Dependency on Side Slip (beta)

The figures 15 through 16 show how the cross elevation moments varied at cruise condition for different values of beta. The dynamic moment was largest for positive side slip ("wind in the right ear"), while the static moment was maximum for negative side slip. for a beta of positive one, the static load actually changed direction and became positive.

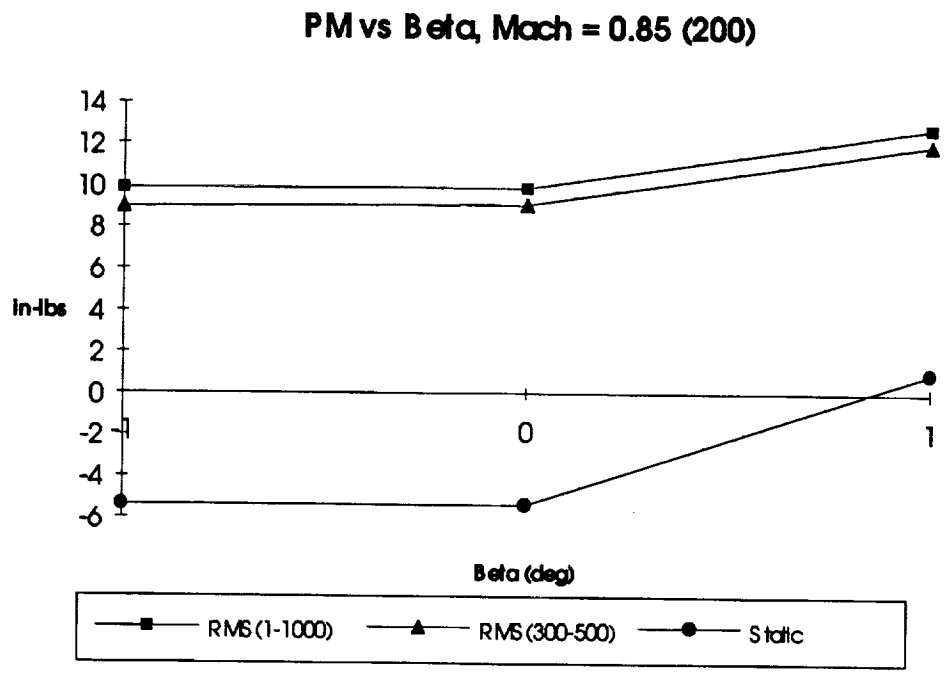

Figure 15: Cross elevation Moment Vs beta for Configuration 65, 66, 67, alpha = 2.5, gamma = 40, Mach=0.85.

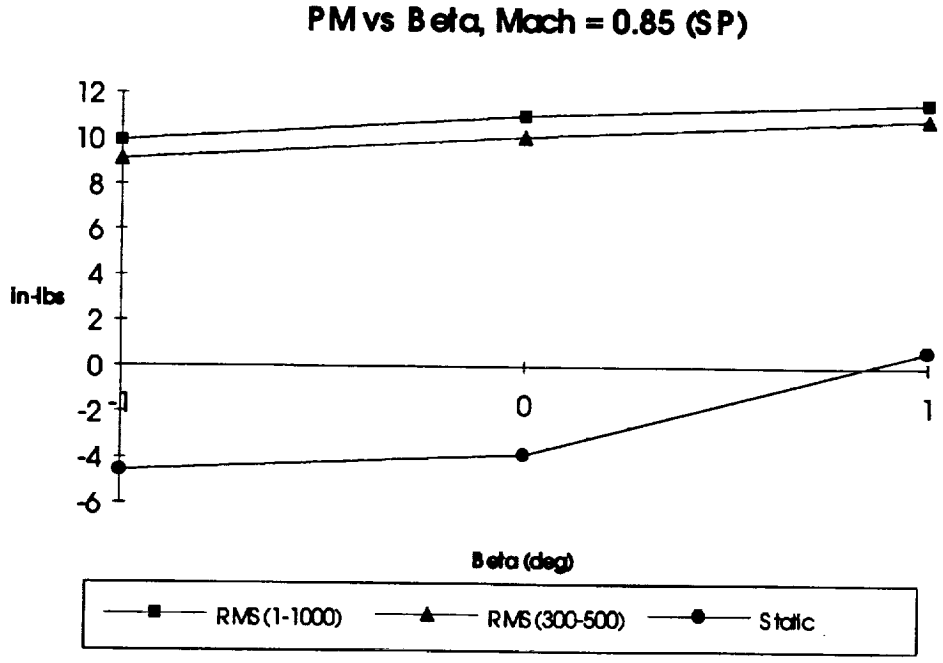

Figure 16: Cross elevation Moment Vs beta for Configuration 86, 87, 88, alpha = 2.5, gamma = 40, Mach=0.85.

Dependency on Elevation Angle (gamma)

The elevation angle was varied at a Mach of 0.85 and an angle of attack of 0.25 degrees (cruise condition). The dynamic cross elevation moment did not seem to have much dependency on elevation angle. The dynamic torque levels increased only slightly in the center of the range of travel. The static cross elevation moment had a large apparent dependency on elevation angle. As shown in figures 17 and 18, the static moment increased as the elevation angle increased to 40 degrees.

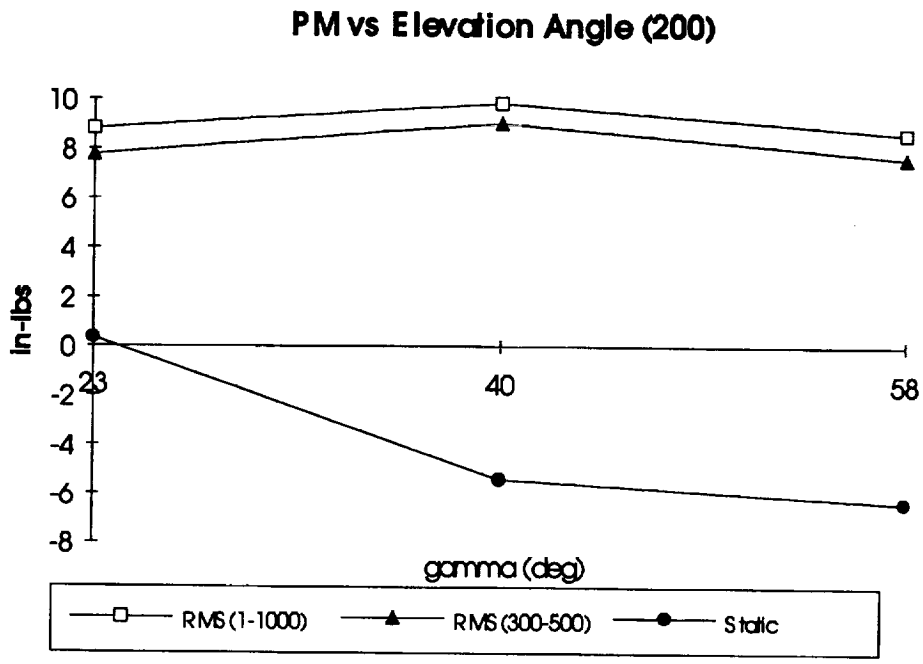

Figure 17: Cross elevation Moment Vs gamma for Configuration 65, alpha = 2.5, beta = 0, Mach = 0.85.

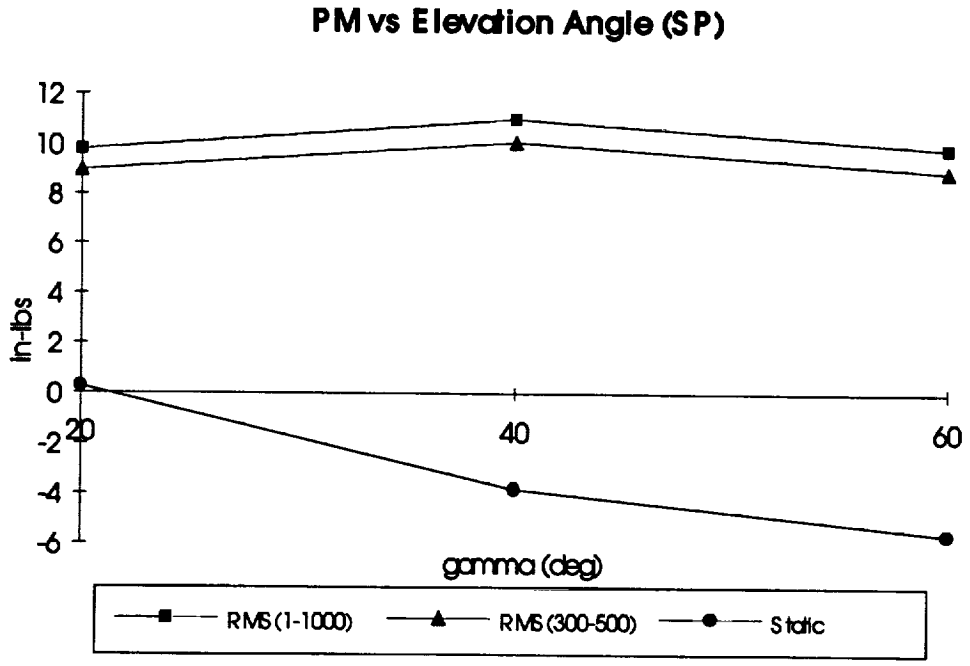

Figure 18: Cross elevation Moment Vs gamma for Configuration 86, alpha = 2.5, beta = 0, Mach = 0.85.

Dependency on Airspeed (Mach)

Mach was varied from 0.63 to 0.88 at an angle of attack of 2.5 degrees. The dynamic cross elevation moment was observed to reach a maximum near Mach 0.75, and then drop slowly as the Mach number continued to increase. The static moment was observed to reach a maximum at a higher Mach.

An interesting result at low mach numbers was a spike in the PSD at 900 Hz (model scale). This spike was consistently present at mach 0.63, and would vanish at higher mach numbers. Note that figures 19 and 20 show a greater portion of the energy outside the 300-500 Hz band for Mach 0.63. Refer to appendix B for the PSD plots of the dynamic cross elevation moment. The 900 Hz spike is plainly visible on the first page of appendix B (run 177, sequence 1).

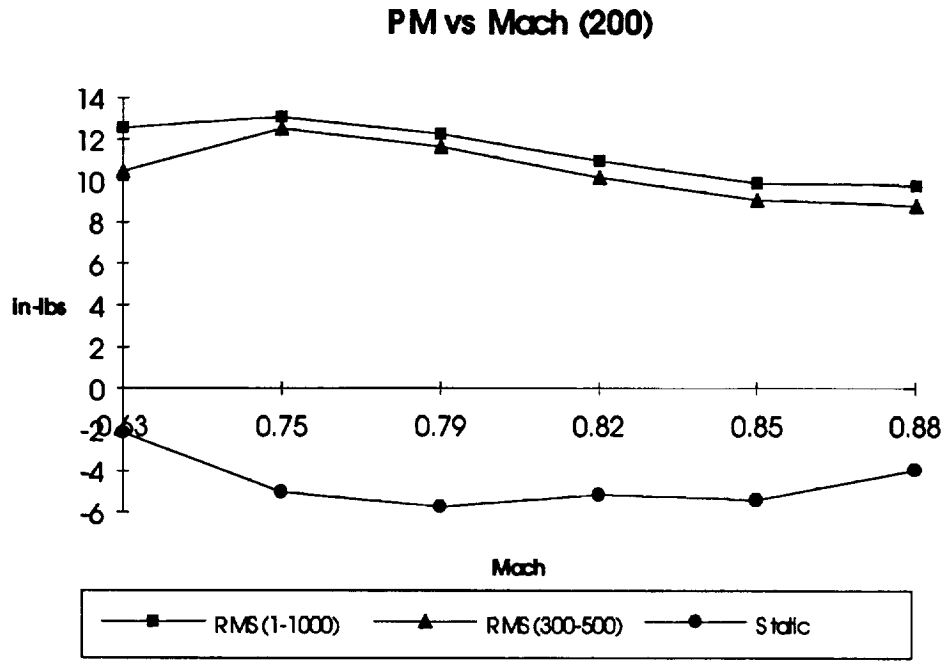

Figure 19: Cross elevation Moment Vs Mach for Configuration 65, alpha = 2.5, beta = 0, gamma = 40..

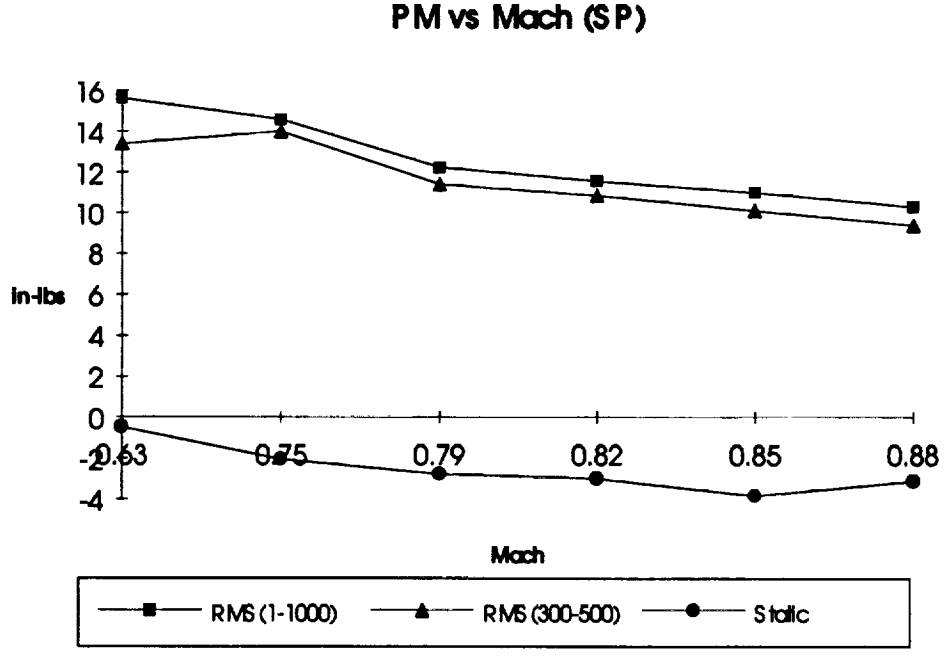

Figure 20: Cross elevation Moment Vs Mach for Configuration 86, alpha = 2.5, beta = 0, gamma = 40.

Static LOS normal Force "N" Vs Static Cross elevation Moment "PM".

While the dynamic cross elevation moment seemed to be primarily due to a dynamic LOS normal force applied near the center of the primary mirror, this did not seem to be the case for the static cross elevation moment. In fact, there are some cases where the resultant LOS normal force is directed into the cavity, while the cross elevation moment "PM" is in the opposite direction that one would expect if the LOS normal force "N" were applied in the vicinity of the primary mirror center. This suggests that the sides, as well as the spider structure supporting the secondary mirror were subject to "DC" aerodynamic forces. There is not enough data to determine exactly where on the structure, these aerodynamic forces were applied. Figures 21 and 22 show a comparison of the static LOS normal force load to the static cross elevation moment load for changes in alpha, beta, gamma, and Mach.

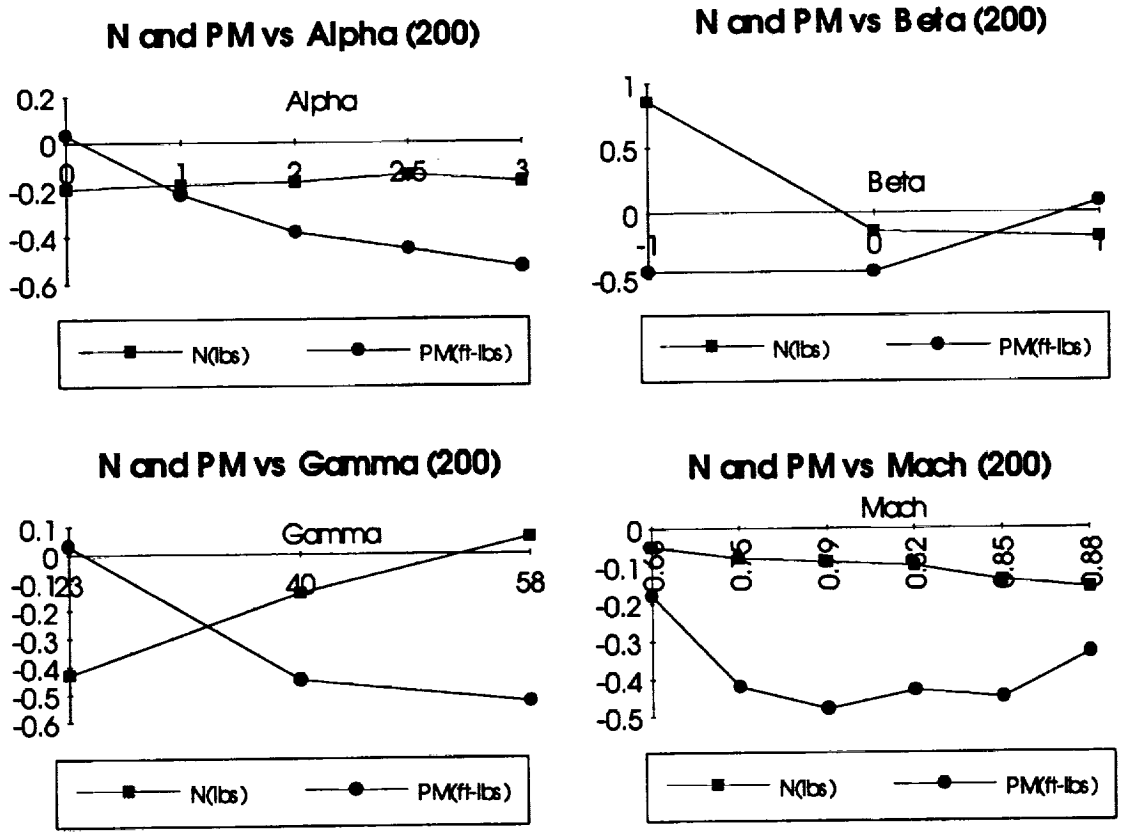

Figure 21: N Vs PM for tested values of alpha, beta, gamma, and Mach. (200 configuration)

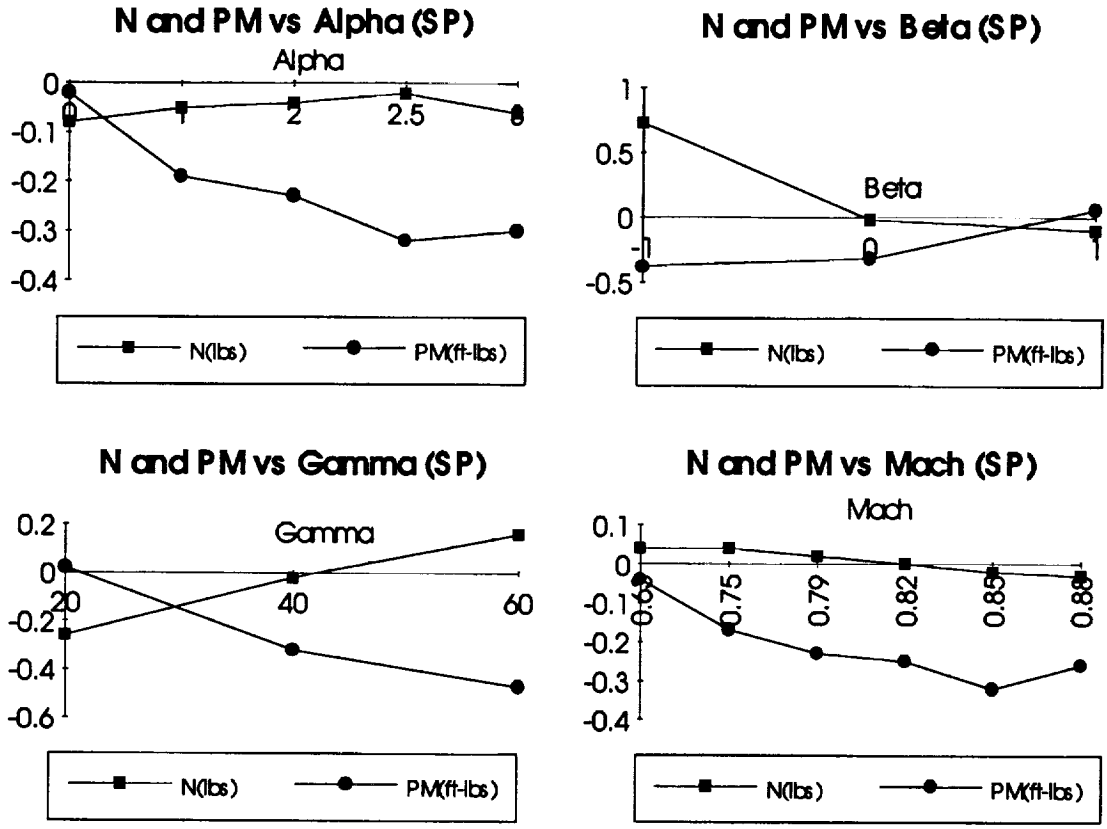

Figure 22: N Vs PM for tested values of alpha, beta, gamma, and Mach. (SP configuration)

Overview of Static Forces and Moments

An overview of all the static forces and moments on the telescope shows that high nasmyth axial forces were measured, and that the nasmyth axial force seems to have contributed to the cross elevation moment (PM). Note the apparent relationship between A and PM in figures 23 through 30. This, in addition to the possibility of pure couples being applied (which do not contribute to the resultant forces), may account for the unexpected lack of a proportional relationship between N and PM.

An examination of these figures will also reveal that the LOS moment (YM) is mainly related to the side force. For variations in alpha an mach, there seems to be a relationship between side force (SF) and elevation moment (RM).

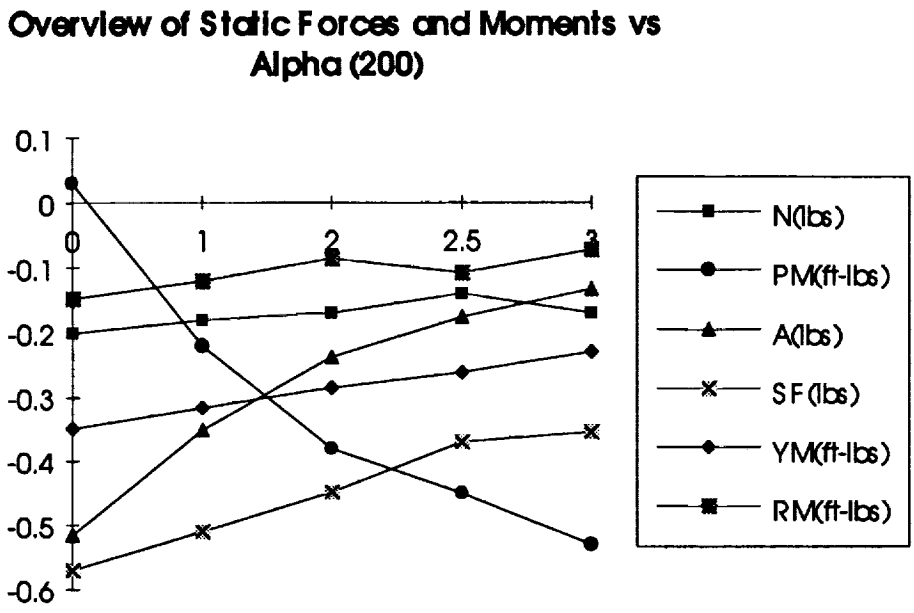

Figure 23

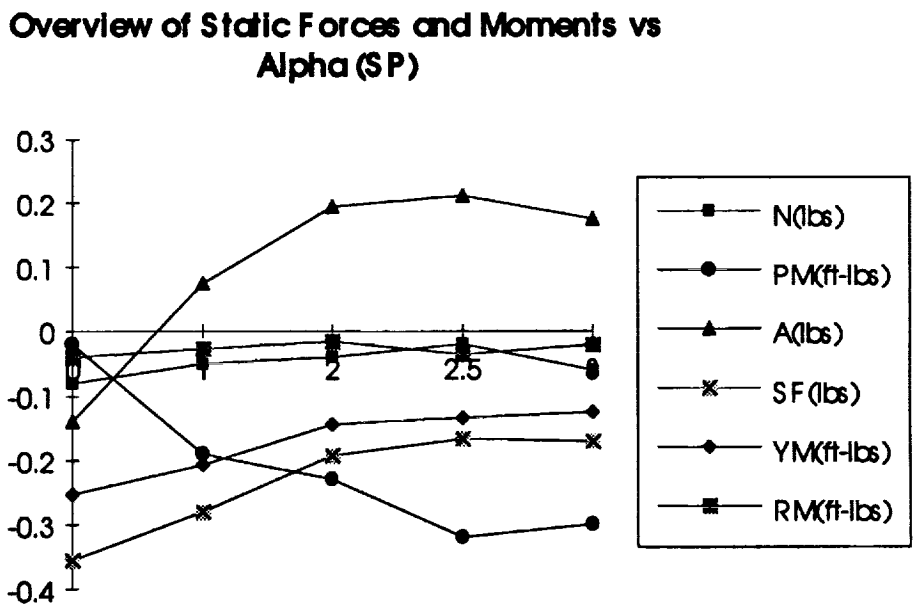

Figure 24

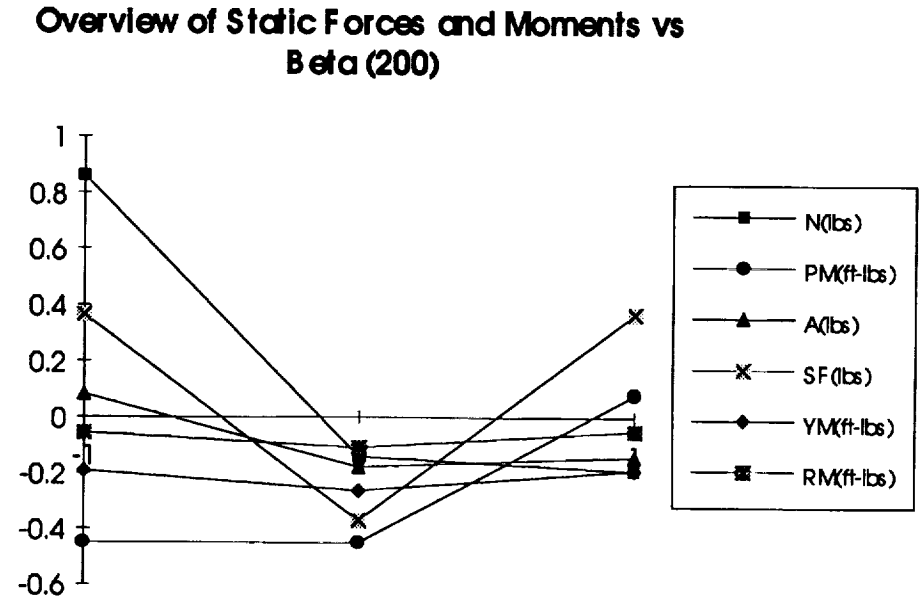

Figure 25

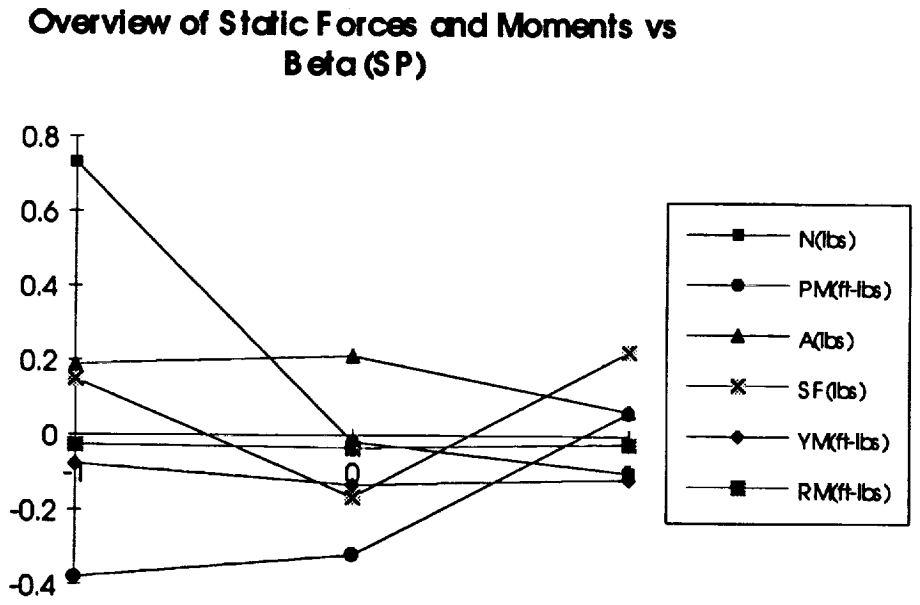

Figure 26

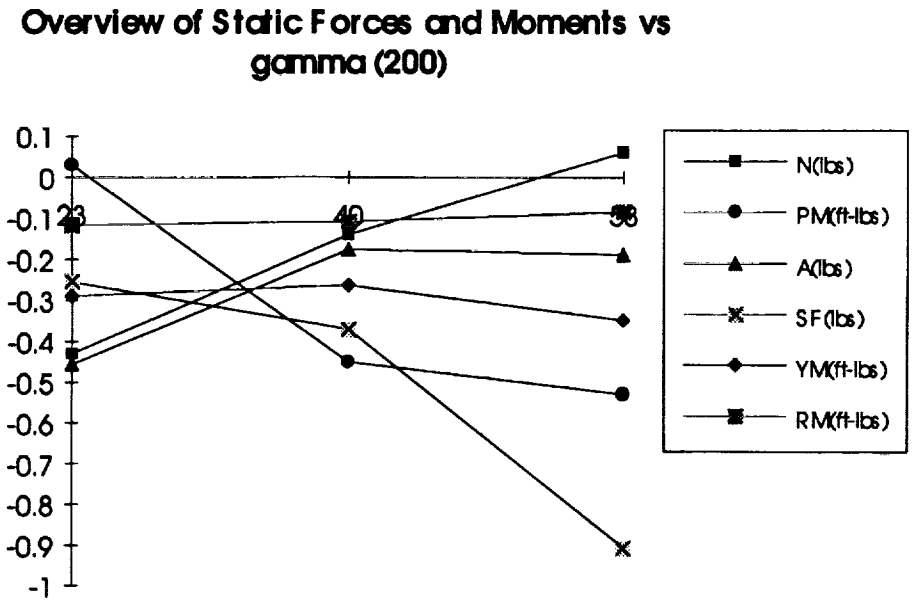

Figure 27

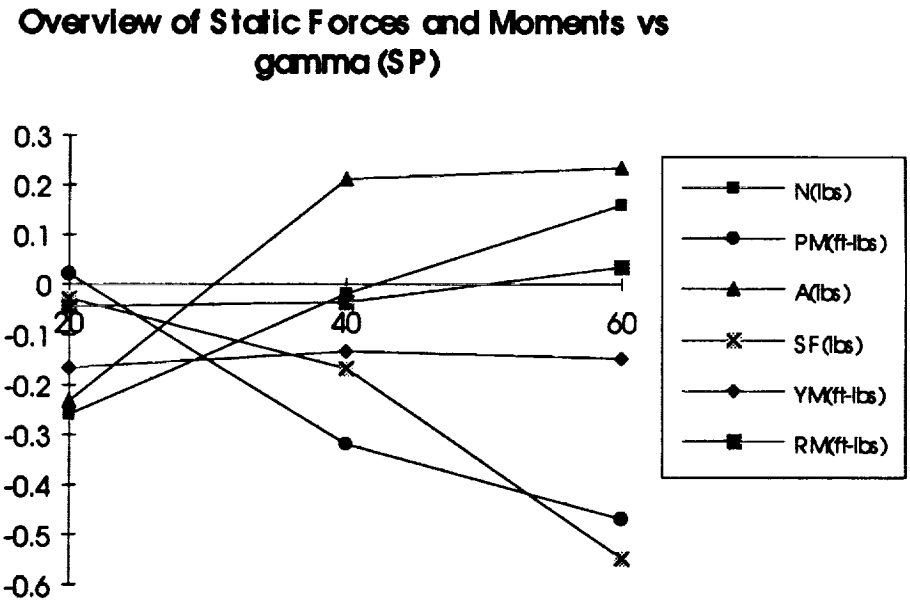

Figure 28

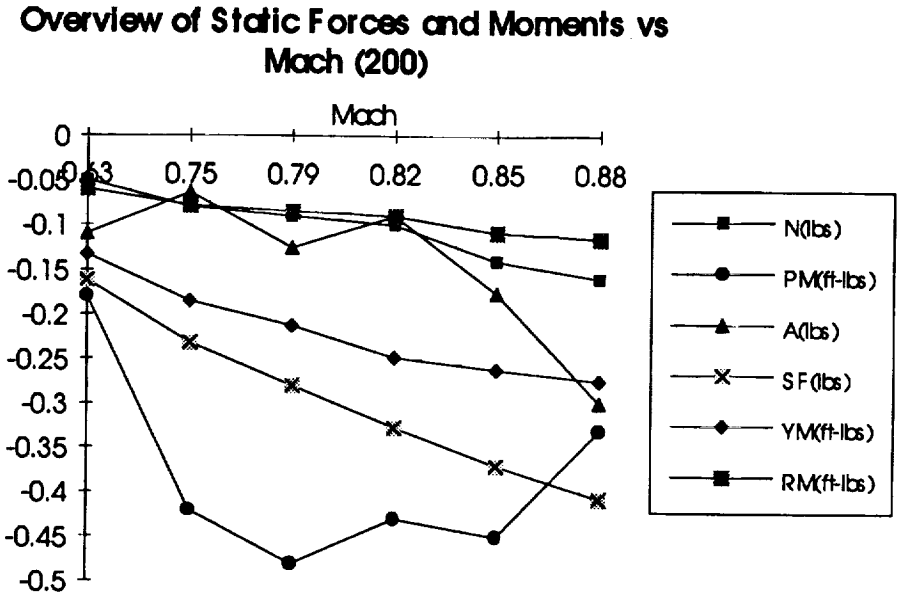

Figure 29

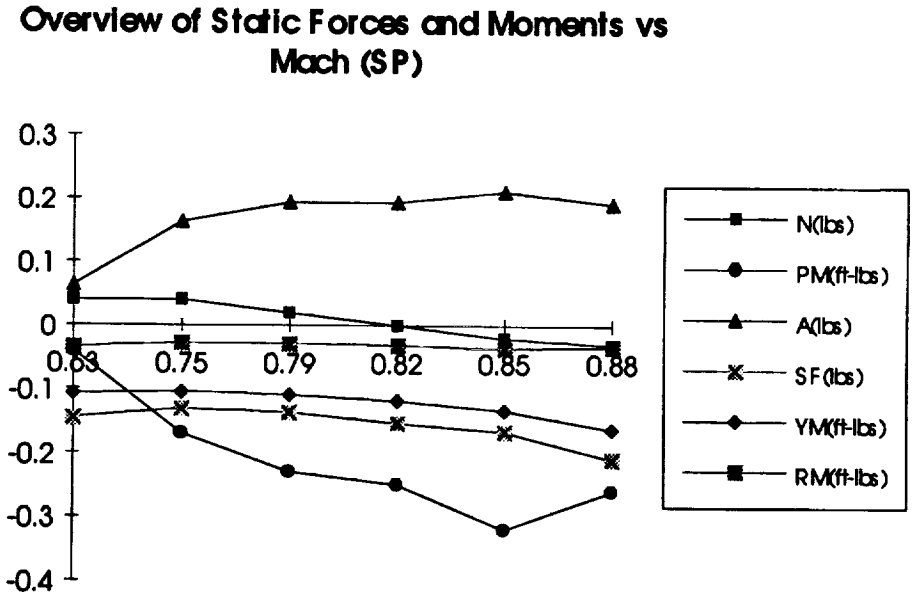

Figure 30

CONCLUSION

During the SOFIA II wind tunnel test, measurements were taken to determine the aerodynamic forces that acted on the telescope in the cavity of the 747 model. The **dynamic cross elevation moment** on the telescope was calculated using two independent methods. One method using a dynamic pressure measurement (F=qA). A second method (outlined in this report) used a combination of force balance and accelerometer data (F=ma). These independent methods yielded RMS cross elevation moment values that differed by only 10 to 30 percent. The second method predicted cross elevation moments constantly higher than the first. **Static forces and moments** were measured in all **six degrees of freedom** with the force balance by which the telescope model was mounted to the cavity wall.

The scope of this report was limited to the "favorite" cavity treatments for the 200 and SP version of the 747. The results presented here were obtained using the second (F=ma) method mentioned above.

747 Configurations 65 Through 67 (favorite cavity treatment for 200)

The **full scale dynamic cross elevation moment levels** predicted for cruise condition in configuration 65 averaged approximately **692 ft-lb RMS** at frequencies below 60 Hz. Most of this energy was concentrated at an aerodynamic resonant peak centered at approximately 23.5 Hz (full scale). The energy predicted in the spectrum between 17.6 and 29.4 Hz was 636 ft-lb RMS. The **static cross elevation moment** predicted at cruise condition was approximately **-378 ft-lb.**

747 Configurations 86 Through 88 (favorite cavity treatment for SP)

The **full scale dynamic cross elevation moment levels** predicted for cruise condition in configuration 86 averaged approximately **772 ft-lb RMS** at frequencies below 60 Hz. Most of this energy was concentrated at an aerodynamic resonant peak centered at approximately 23.5 Hz (full scale). The energy predicted in the spectrum between 17.6 and 29.4 Hz was 708 ft-lb RMS. The **static cross elevation moment** predicted at cruise condition was approximately **-269 ft-lb.**

The test data was analyzed to determine if the forces and moments showed any apparent dependencies on test condition variables such as mach, angle of attack, side slip angle, and elevation angle. The results show relatively small variations in the dynamic cross elevation moment about the cruise condition level for the conditions tested. The static cross elevation moment however, did vary considerably with changes in mach, angle of attack, side slip and elevation angle.

The way in which the static cross elevation moment acted on the telescope was much different from the dynamic cross elevation moment. The dynamic cross elevation moment seemed to be primarily due to a LOS normal force acting on the primary mirror. The

static cross elevation moment was observed to be fairly uncorrelated with the LOS normal force resultant on the telescope as the test conditions were varied. Apparent reasons for this include a large static nasmyth axial force resultant which seemed to contribute to the cross elevation moment, and possibly some static pure couples applied about the cross elevation axis, which did not contribute to the LOS normal force resultant. An overview of all the static forces and moments was presented for a graphic comparison for the various test conditions.

SUMMARY OF FULL SCALE EQUIVALENT AERODYNAMIC FORCES AND MOMENTS FOR SOFIA II TELESCOPE

CRUISE CONDITIONS: Mach = 0.85, α=2.5 deg, β = 0, elevation angle = 40 deg.

200

Dynamic Cross Elevation Moment (ft-lb RMS)

(300-500Hz)	(1-1000Hz)
636	**692**

Static Forces (lb)		**Static Moments (ft-lb)**	
Nasmyth Axial	**-12.6**	Elevation	**-92.4**
Side	**-25.9**	Cross Elevation	**-378**
LOS Normal	**-9.8**	LOS	**-218**

SP

Dynamic Cross Elevation Moment (ft-lb RMS)

(300-500Hz)	(1-1000Hz)
708	**772**

Static Forces (lb)		**Static Moments (ft-lb)**	
Nasmyth Axial	**14.77**	Elevation	**-33.6**
Side	**-11.69**	Cross Elevation	**-269**
LOS Normal	**-1.4**	LOS	**-109.2**

Config	Run	Seq	alpha	beta	gamma	Mach	RMS(1-1000)	RMS(300-500)	N	PM	A	SF	YM	RM
65	177	1	2.5	0	40	0.63	12.542	10.452	-0.05	-0.18	-0.11	-0.162	-0.13	-0.06
65	177	2	2.5	0	40	0.75	13.062	12.499	-0.08	-0.42	-0.06	-0.232	-0.19	-0.06
65	177	3	2.5	0	40	0.79	12.273	11.639	-0.09	-0.48	-0.13	-0.279	-0.21	-0.09
65	177	4	2.5	0	40	0.82	10.951	10.159	-0.1	-0.43	-0.09	-0.327	-0.25	-0.09
65	177	5	2.5	0	40	0.85	9.8797	9.0796	-0.14	-0.45	-0.18	-0.37	-0.26	-0.11
65	177	6	2.5	0	40	0.88	9.7242	8.7637	-0.16	-0.33	-0.3	-0.407	-0.27	-0.12
65	178	1	0	0	40	0.85	8.7334	7.7342	-0.2	0.03	-0.52	-0.57	-0.35	-0.15
65	178	2	1	0	40	0.85	8.9088	7.9415	-0.18	-0.22	-0.35	-0.509	-0.32	-0.12
65	178	3	2	0	40	0.85	8.8194	7.7378	-0.17	-0.38	-0.24	-0.448	-0.29	-0.09
65	178	4	3	0	40	0.85	8.6365	7.6892	-0.17	-0.53	-0.13	-0.355	-0.23	-0.07
65	179	1	2.5	0	58	0.85	8.6479	7.6544	0.06	-0.53	-0.19	-0.907	-0.35	-0.09
65	179	2	2.5	0	23	0.85	8.8142	7.7595	-0.43	0.03	-0.46	-0.255	-0.29	-0.12
66	181	1	2.5	-1	40	0.63	10.302	9.6391	0.58	-0.3	0.026	0.196	-0.1	-0.04
66	181	3	2.5	-1	40	0.75	11.495	10.766	0.77	-0.4	0.07	0.279	-0.14	-0.05
66	181	4	2.5	-1	40	0.79	10.682	9.9494	0.79	-0.42	0.068	0.317	-0.16	-0.05
66	181	5	2.5	-1	40	0.82	9.9407	8.9292	0.86	-0.45	0.081	0.34	-0.18	-0.06
66	181	6	2.5	-1	40	0.85	9.8426	8.9538	0.86	-0.45	0.081	0.366	-0.19	-0.06
66	181	7	2.5	-1	40	0.88	9.2706	8.3152	0.86	-0.46	0.038	0.477	-0.26	-0.07
66	182	1	0	-1	40	0.85	9.8696	8.8755	0.24	-0.13	-0.23	0.535	-0.31	-0.09
66	182	2	1	-1	40	0.85	9.2738	8.2758	0.61	-0.33	-0.11	0.617	-0.34	-0.08
66	182	3	2	-1	40	0.85	8.7847	7.8555	0.74	-0.4	0.018	0.523	-0.28	-0.07
66	182	4	3	-1	40	0.85	8.7139	7.5702	0.98	-0.52	0.162	0.28	-0.15	-0.05
66	183	1	2.5	-1	58	0.85	8.3072	7.2733	1.2	-0.63	0.282	0.331	-0.17	-0.05
66	183	2	2.5	-1	23	0.85	9.0315	7.9301	0.2	-0.12	-0.16	0.48	-0.28	-0.08
67	184	1	2.5	1	40	0.63	12.306	11.699	-0.18	0.08	-0.04	0.22	-0.1	-0.02
67	184	2	2.5	1	40	0.75	15.122	14.674	0.04	-0.04	-0.12	0.288	-0.15	-0.05
67	184	3	2.5	1	40	0.79	14.461	13.899	-0.13	0.05	-0.11	0.34	-0.18	-0.05
67	184	4	2.5	1	40	0.82	13.475	12.882	-0.11	0.04	-0.1	0.343	-0.18	-0.05
67	184	5	2.5	1	40	0.85	12.758	11.958	-0.19	0.08	-0.14	0.368	-0.19	-0.05
67	184	6	2.5	1	40	0.88	12.408	11.596	-0.52	0.24	-0.08	0.306	-0.15	-0.03
67	185	1	0	1	40	0.85	11.734	10.776	-0.64	0.29	-0.1	0.296	-0.14	-0.01
67	185	2	1	1	40	0.85	12.067	11.341	-0.53	0.26	-0.11	0.308	-0.15	-0.02
67	185	3	2	1	40	0.85	11.944	11.115	-0.24	0.11	-0.1	0.397	-0.2	-0.05
67	185	4	3	1	40	0.85	11.303	10.55	-0.2	0.08	-0.09	0.337	-0.17	-0.05
67	186	1	2.5	1	58	0.85	11.368	10.437	0.31	-0.13	-0.11	0.502	-0.29	-0.07
67	186	2	2.5	1	23	0.85	10.476	9.6384	-0.25	0.1	-0.21	0.358	-0.21	-0.07

Config	Run	Seq	alpha	beta	gamma	Mach	RMS(1-1000)	RMS(300-500)	N	PM	A	SF	YM	RM
86	219	1	2.5	0	40	0.63	15.625	13.376	0.04	-0.04	0.063	-0.145	-0.11	-0.03
86	219	2	2.5	0	40	0.75	14.59	14.023	0.04	-0.17	0.163	-0.131	-0.11	-0.03
86	219	3	2.5	0	40	0.79	12.241	11.443	0.02	-0.23	0.194	-0.137	-0.11	-0.03
86	219	4	2.5	0	40	0.82	11.594	10.862	0	-0.25	0.194	-0.154	-0.12	-0.03
86	219	5	2.5	0	40	0.85	11.033	10.113	-0.02	-0.32	0.211	-0.167	-0.13	-0.04
86	219	6	2.5	0	40	0.88	10.321	9.4112	-0.03	-0.26	0.192	-0.21	-0.16	-0.03
86	220	1	3	0	40	0.85	10.612	9.7737	-0.06	-0.3	0.175	-0.171	-0.13	-0.02
86	220	2	2	0	40	0.85	9.5464	8.819	-0.04	-0.23	0.194	-0.193	-0.14	-0.02
86	220	3	1	0	40	0.85	9.4061	8.6872	-0.05	-0.19	0.074	-0.28	-0.21	-0.03
86	220	4	0	0	40	0.85	9.4857	8.7721	-0.06	-0.02	-0.14	-0.355	-0.25	-0.04
86	221	1	2.5	0	60	0.85	9.8495	8.9361	0.16	-0.47	0.234	-0.549	-0.15	0.034
86	221	2	2.5	0	20	0.85	9.7579	8.953	-0.26	0.02	-0.23	-0.029	-0.17	-0.05
87	222	1	2.5	-1	40	0.63	11.698	10.698	0.28	-0.14	0.14	0.149	-0.07	-0.01
87	222	2	2.5	-1	40	0.75	12.927	12.394	0.52	-0.27	0.171	0.14	-0.08	-0.02
87	222	3	2.5	-1	40	0.79	12.009	11.388	0.62	-0.31	0.163	0.158	-0.08	-0.03
87	222	5	2.5	-1	40	0.82	11.231	10.449	0.66	-0.34	0.162	0.107	-0.06	-0.02
87	222	6	2.5	-1	40	0.85	9.9143	9.1092	0.73	-0.38	0.188	0.149	-0.08	-0.03
87	222	7	2.5	-1	40	0.88	9.7792	8.8245	0.75	-0.39	0.206	0.168	-0.09	-0.03
87	223	1	3	-1	40	0.85	10.914	9.7877	0.78	-0.4	0.191	0.218	-0.11	-0.03
87	223	2	2	-1	40	0.85	9.2911	8.5805	0.75	-0.39	0.195	0.184	-0.1	-0.03
87	223	3	1	-1	40	0.85	9.0423	8.3406	0.58	-0.31	0.269	0.389	-0.2	-0.04
87	223	4	0	-1	40	0.85	9.4011	8.6831	0.5	-0.27	0.154	0.506	-0.27	-0.05
87	224	1	2.5	-1	60	0.85	9.9895	9.2508	1.03	-0.52	0.308	0.267	-0.15	0.01
87	224	2	2.5	-1	20	0.85	9.3629	8.4344	0.02	-0.01	0.032	0.324	-0.16	-0.06
88	225	1	2.5	1	40	0.63	14.125	13.202	-0.21	0.12	0.037	0.05	-0.03	-0.01
88	225	3	2.5	1	40	0.75	15.318	14.797	-0.22	0.12	0.065	0.165	-0.08	-0.02
88	225	4	2.5	1	40	0.79	13.682	13.06	-0.18	0.1	0.057	0.194	-0.1	-0.02
88	225	5	2.5	1	40	0.82	12.702	11.996	-0.1	0.07	0.063	0.213	-0.11	-0.02
88	225	6	2.5	1	40	0.85	11.613	10.921	-0.1	0.06	0.064	0.225	-0.12	-0.02
88	225	7	2.5	1	40	0.88	11.211	10.389	-0.24	0.13	0.063	0.242	-0.12	-0.02
88	226	1	3	1	40	0.85	10.723	9.9666	-0.13	0.08	0.077	0.205	-0.11	-0.02
88	226	2	2	1	40	0.85	10.93	10.156	-0.24	0.13	0.042	0.254	-0.13	-0.02
88	226	3	1	1	40	0.85	10.899	10.257	-0.33	0.17	0.026	0.296	-0.13	-0.02
88	226	4	0	1	40	0.85	10.842	10.169	-0.52	0.26	0.006	0.091	-0.05	-0.01
88	227	1	2.5	1	60	0.85	10.582	9.7755	0.7	-0.32	0.378	0.153	-0.1	0.016
88	227	2	2.5	1	20	0.85	10.829	10.143	-0.26	0.14	-0.1	0.196	-0.1	-0.06

How to Use Appendix B

Appendix B contains PSD plots of the dynamic pitching moments applied to the model telescope. Each plot has a name printed in the top left corner. The last 5 digits of this name correspond to a run and sequence number. For example: "R3017701" corresponds to run 177, sequence 01 of the SOFIA II wind tunnel test. This information can be used to look up the test conditions for that run and sequence in appendix A.

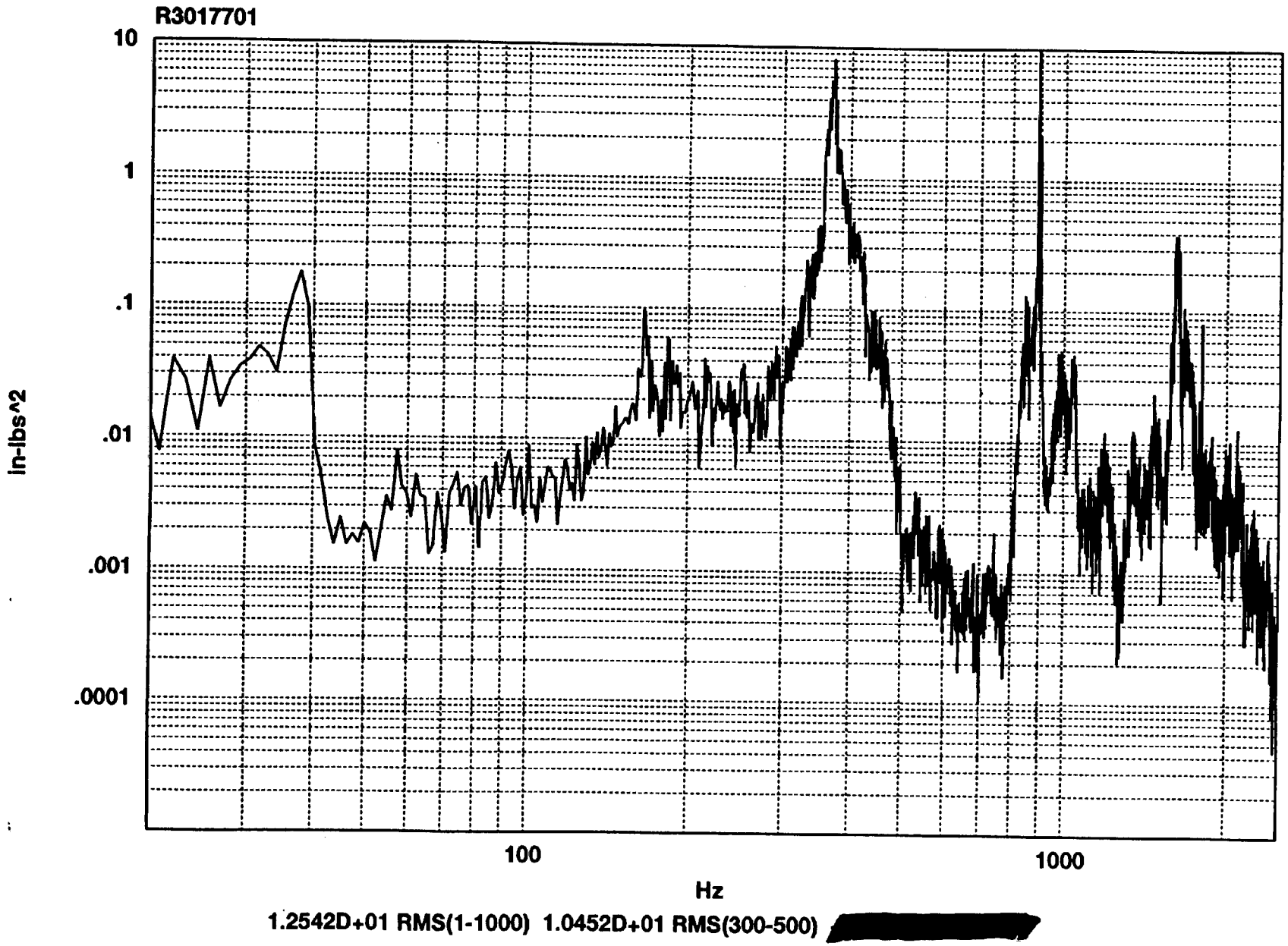
R3017701
10
1
.1
.01
.001
.0001
in-lbs^2
100
1000
Hz
1.2542D+01 RMS(1-1000) 1.0452D+01 RMS(300-500)
[redacted]

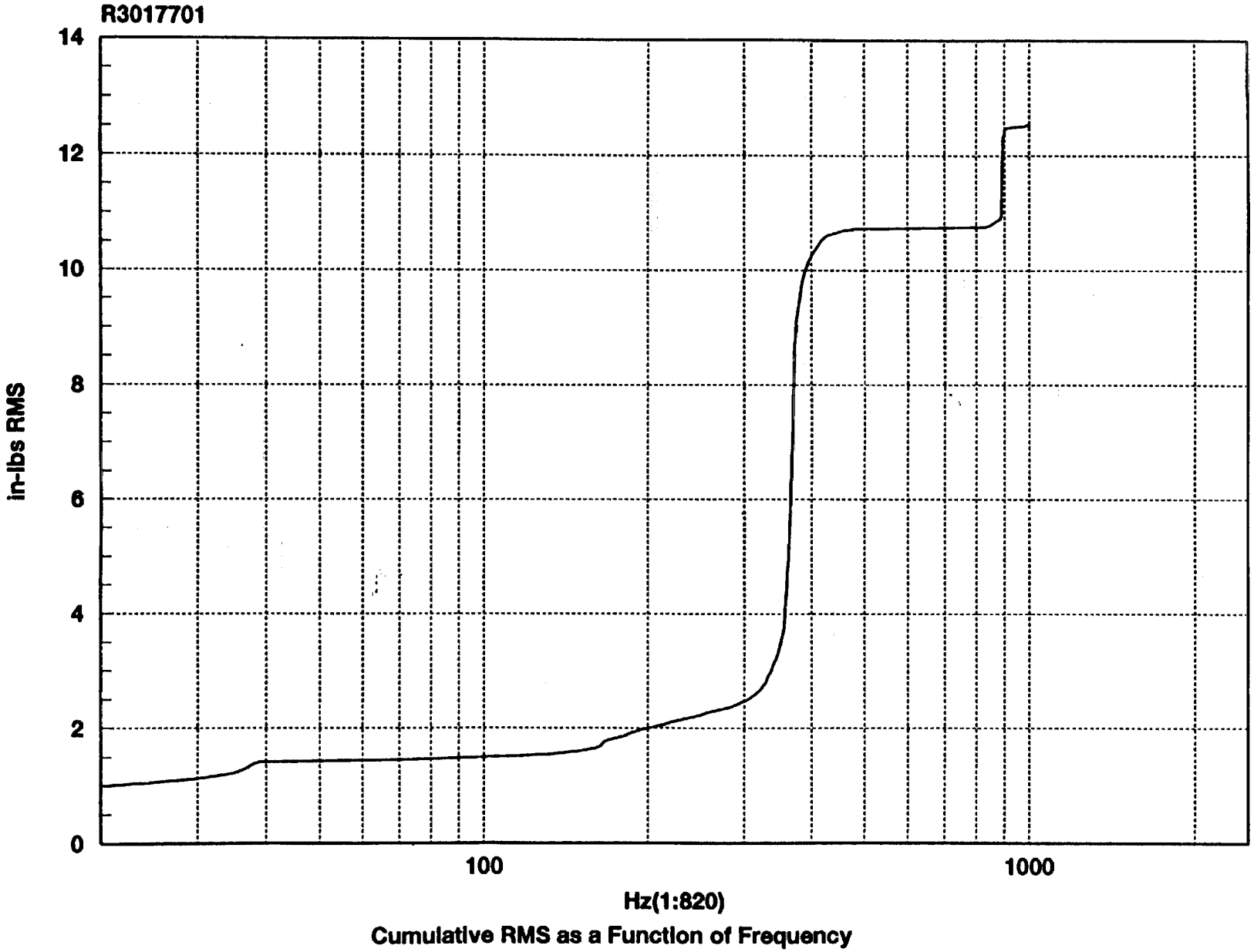

Cumulative RMS as a Function of Frequency

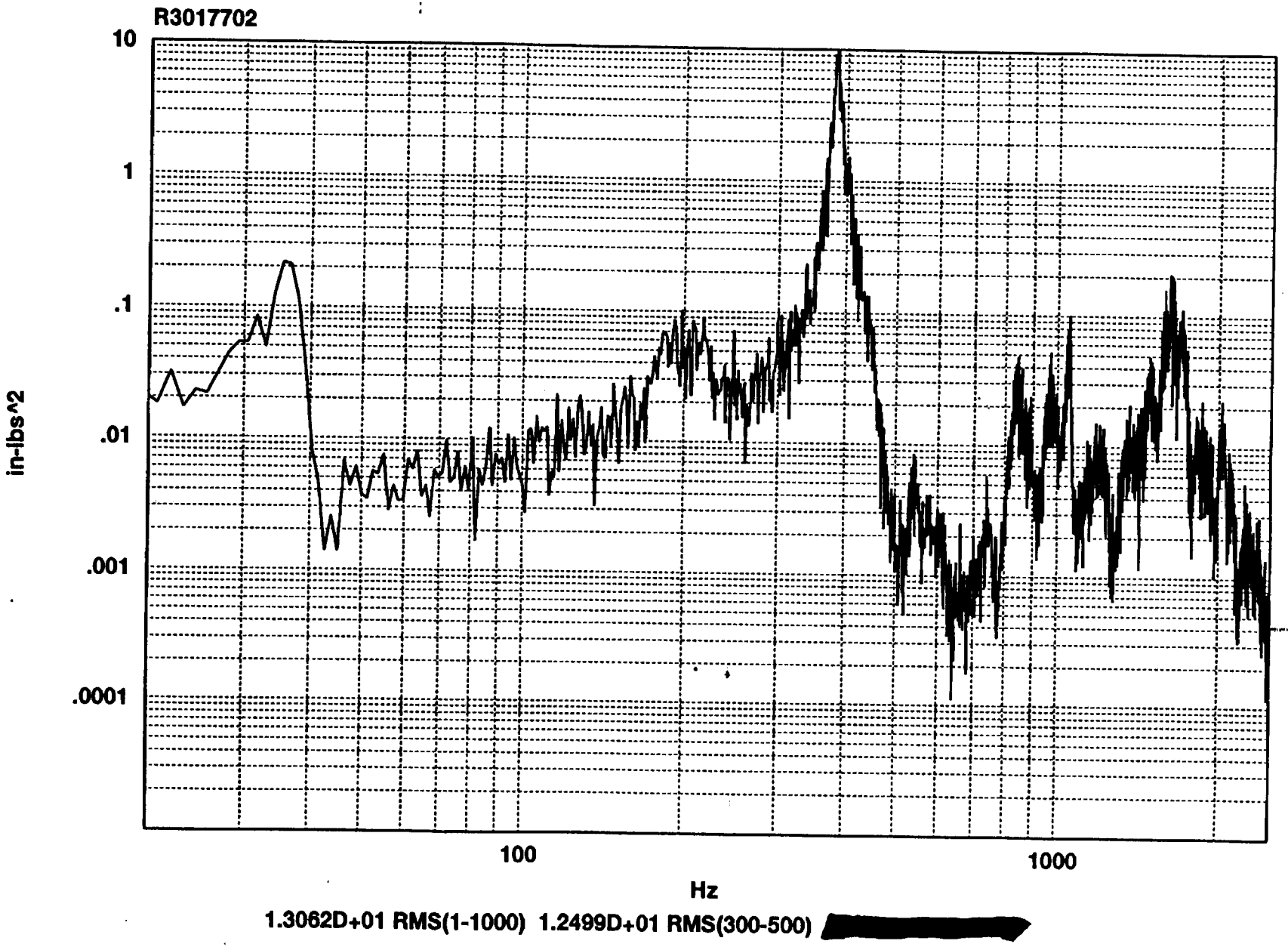
R3017702
10
1
.1
.01
.001
.0001
in-lbs^2
100
1000
Hz
1.3062D+01 RMS(1-1000) 1.2499D+01 RMS(300-500)

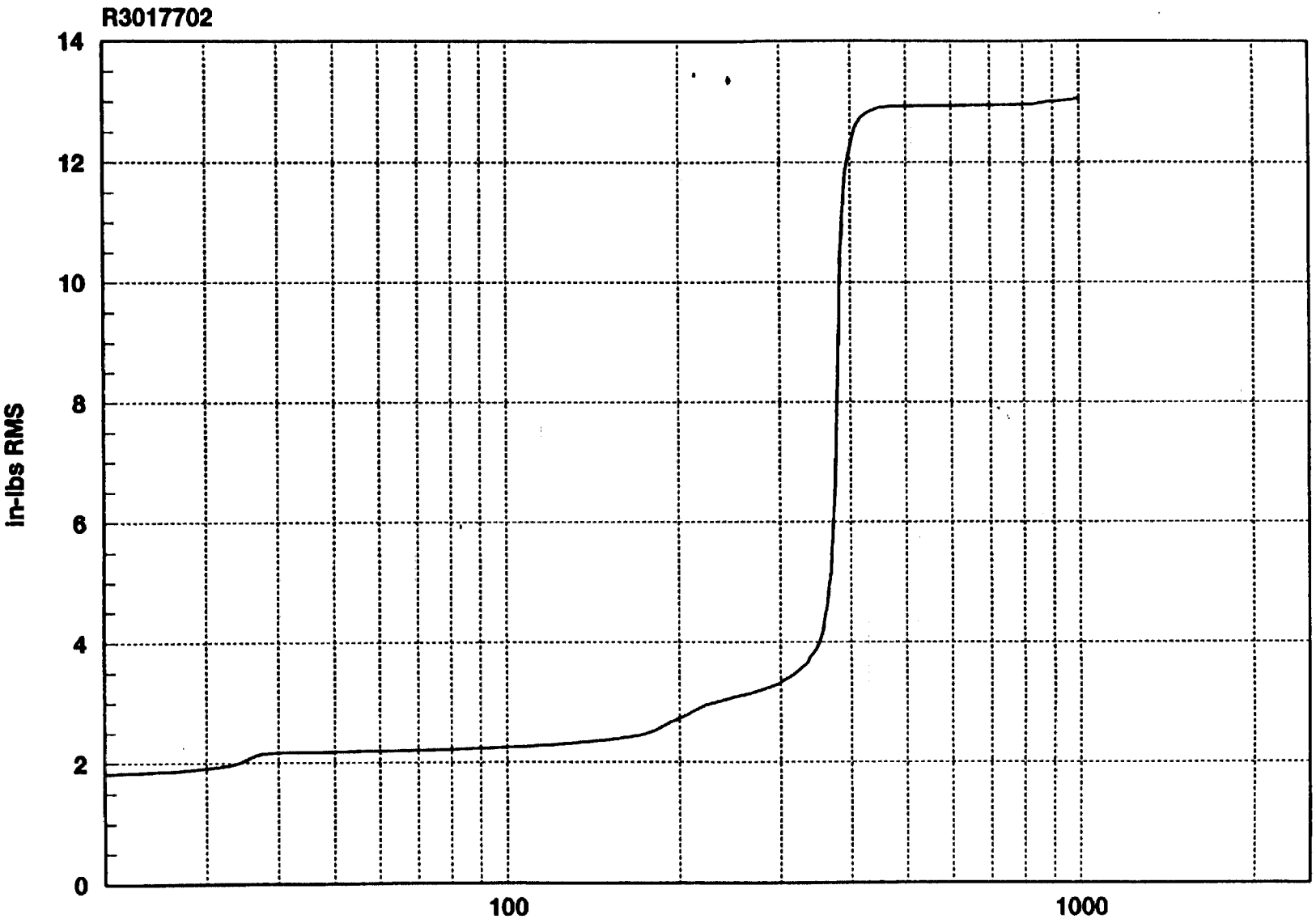

Cumulative RMS as a Function of Frequency

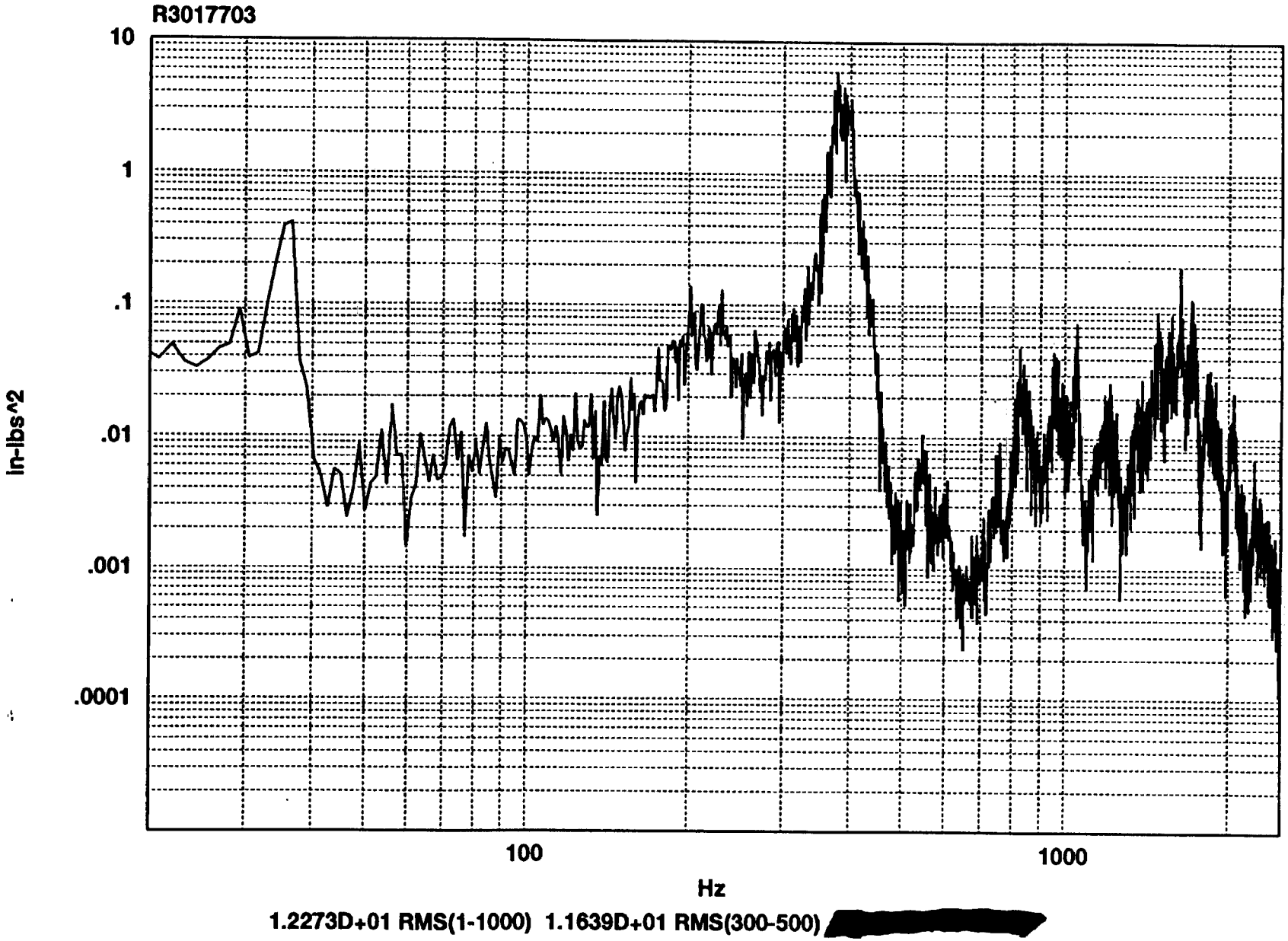
R3017703
10
1
.1
.01
.001
.0001
In-lbs^2
100
1000
Hz
1.2273D+01 RMS(1-1000) 1.1639D+01 RMS(300-500)

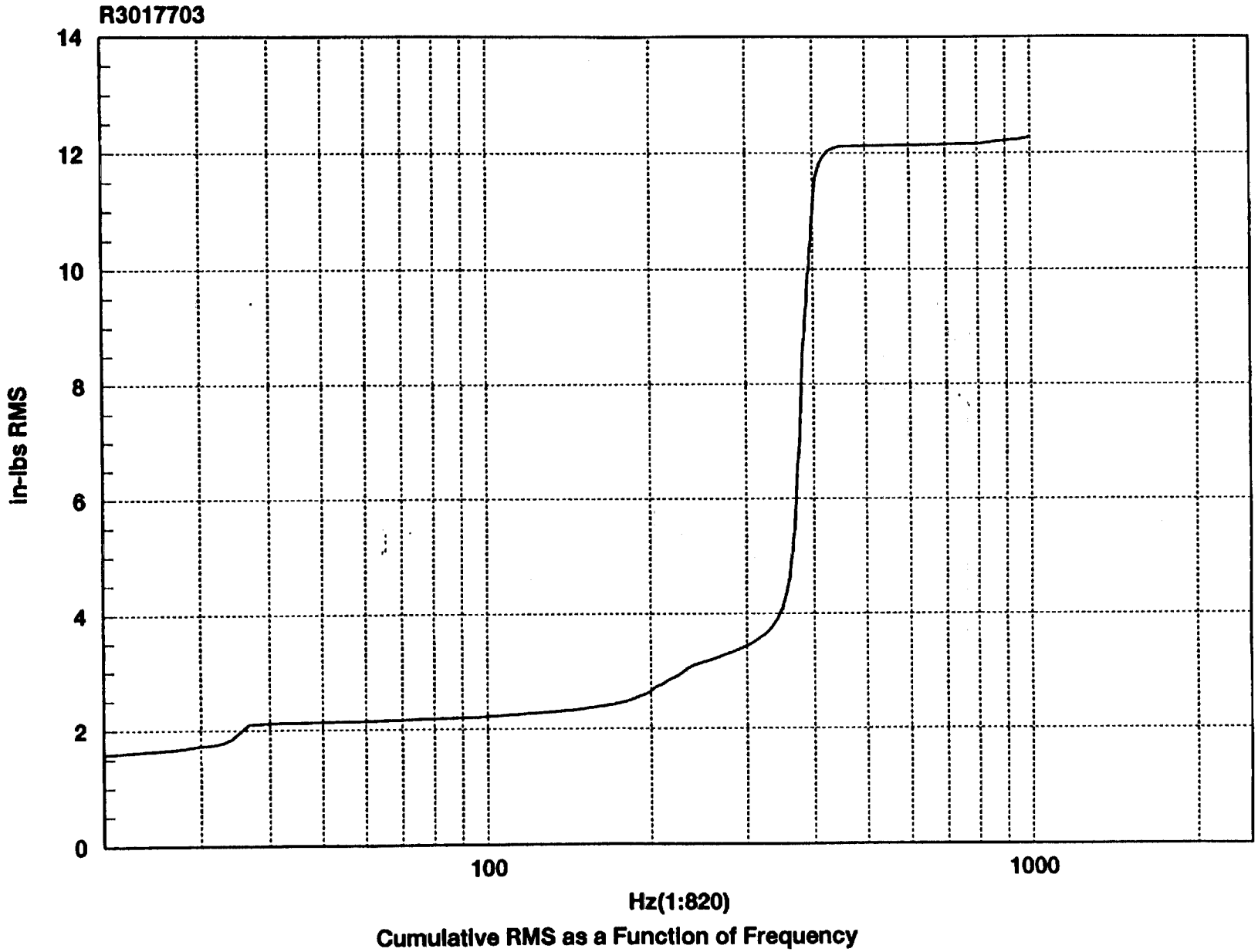

Cumulative RMS as a Function of Frequency

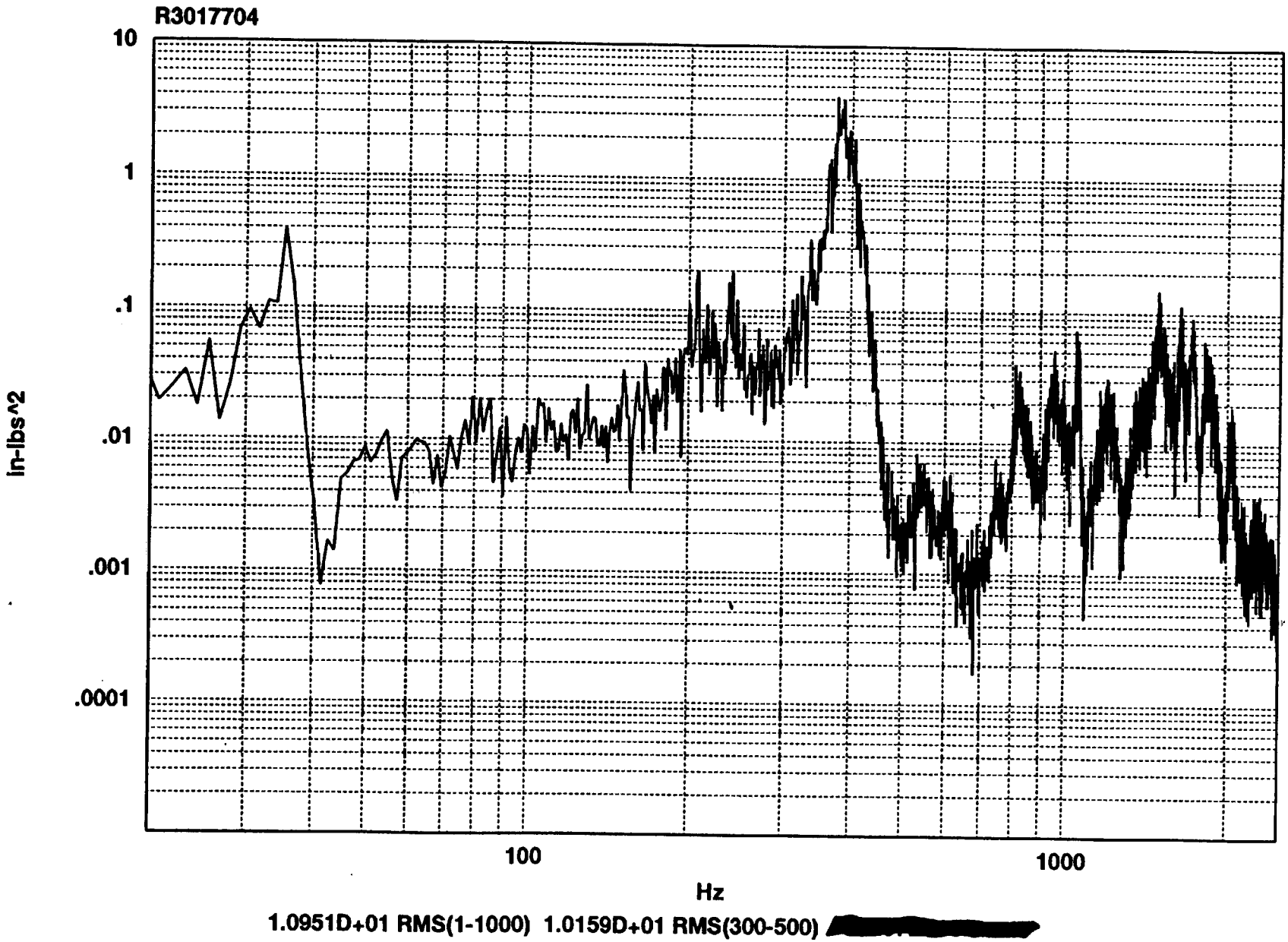
R3017704
10
1
.1
.01
.001
.0001
in-lbs^2
100
1000
Hz
1.0951D+01 RMS(1-1000) 1.0159D+01 RMS(300-500)

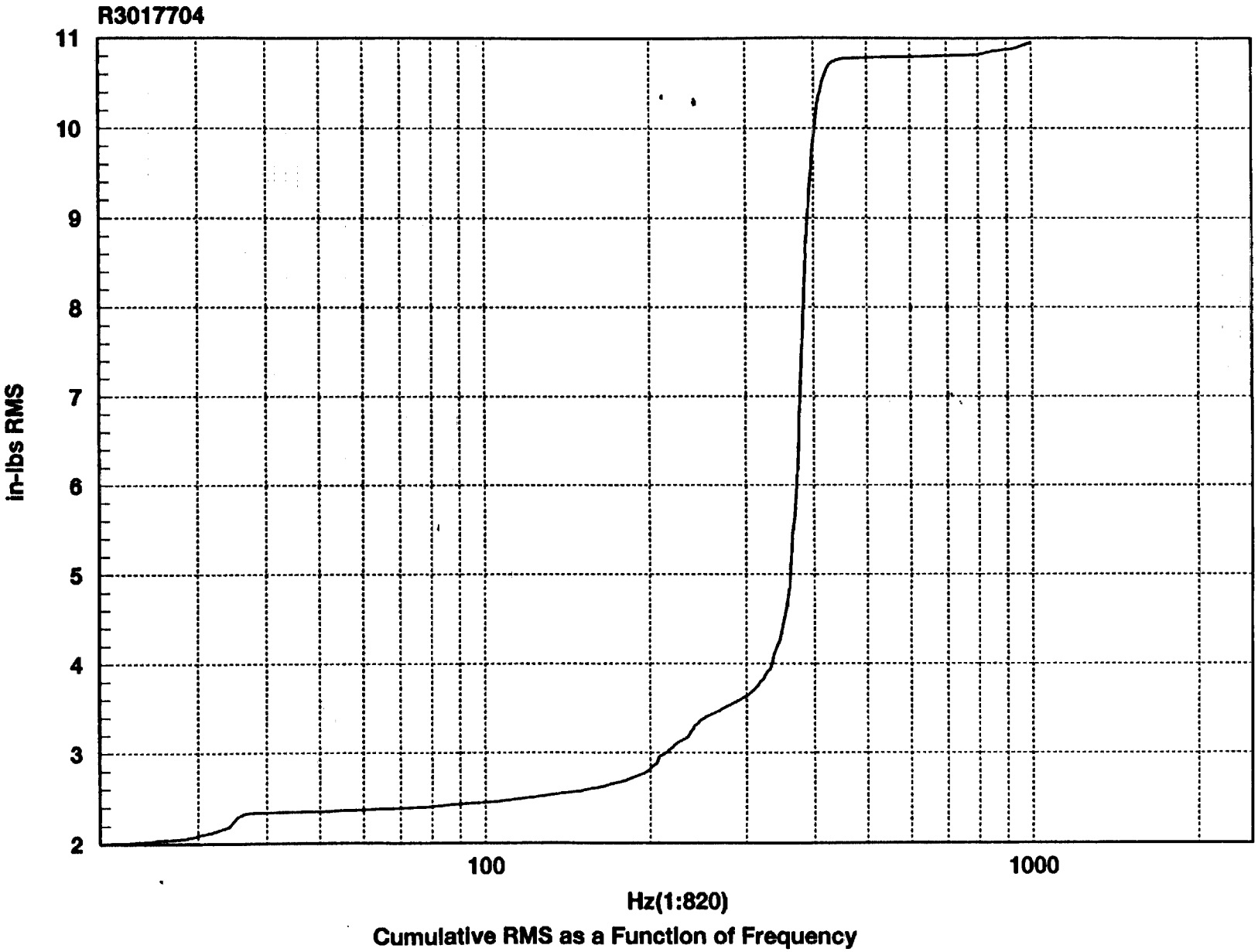

Cumulative RMS as a Function of Frequency

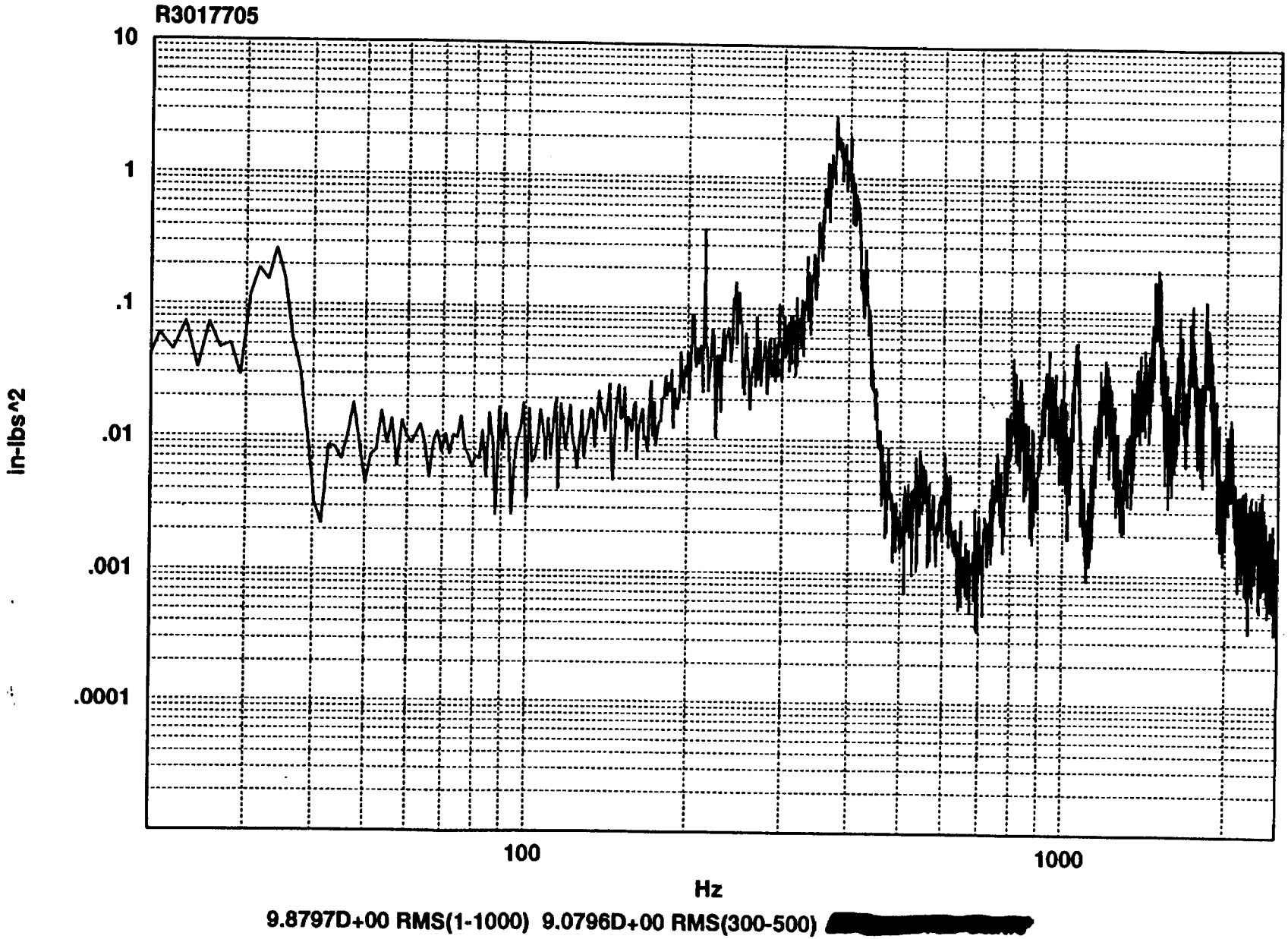
R3017705
10
1
.1
.01
.001
.0001
in-lbs^2
100
1000
Hz
9.8797D+00 RMS(1-1000) 9.0796D+00 RMS(300-500)

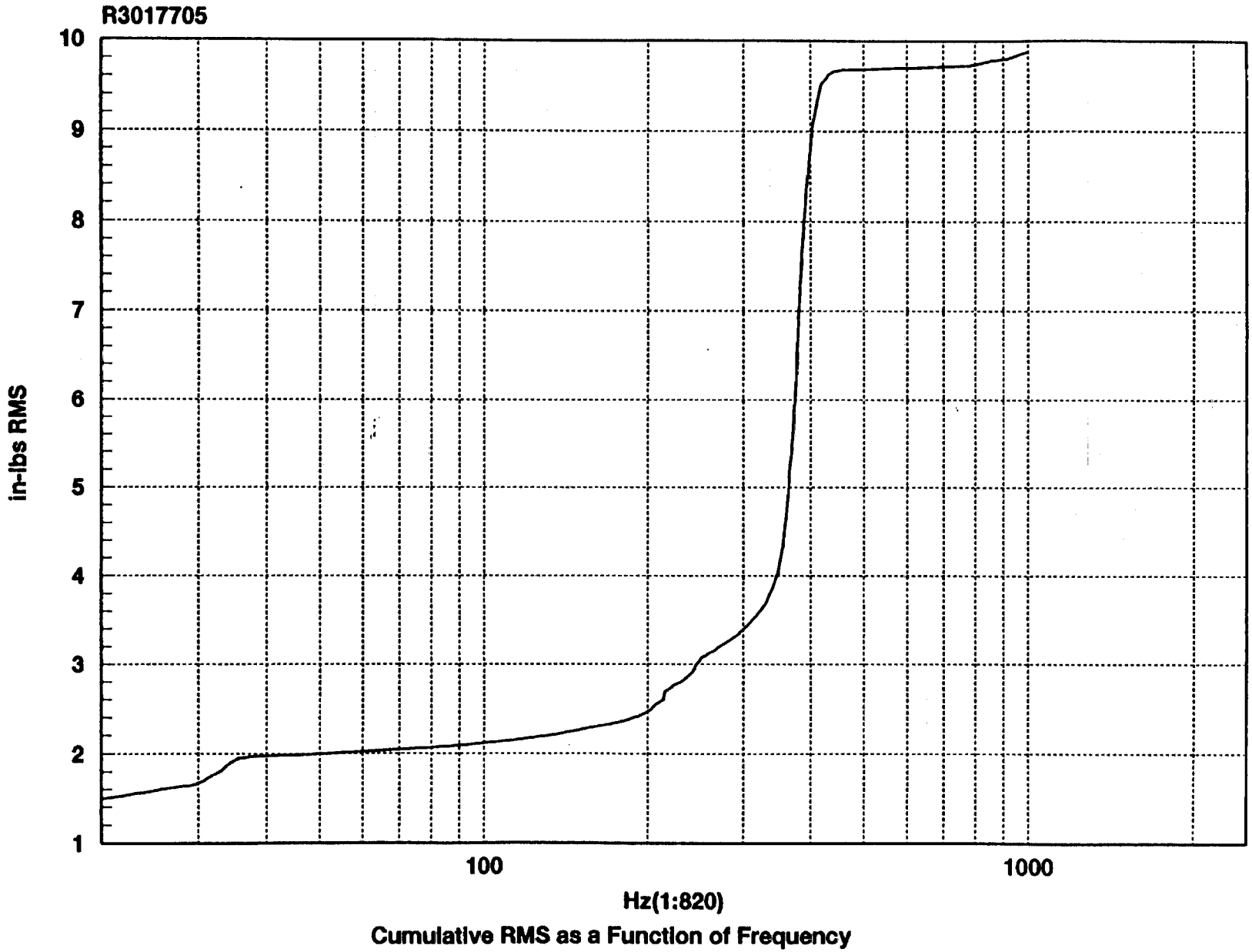

Cumulative RMS as a Function of Frequency

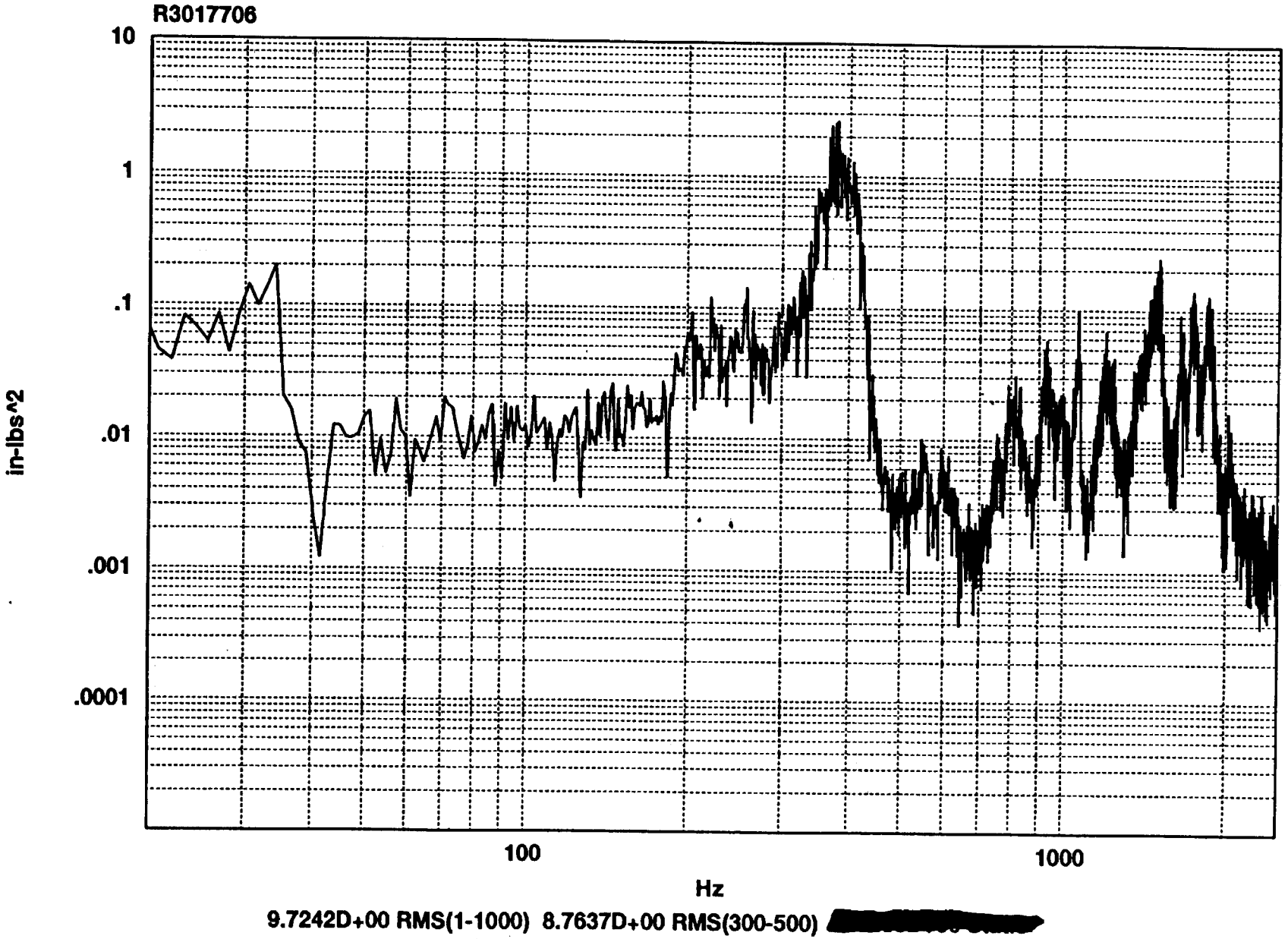
R3017706
10
1
.1
.01
.001
.0001
in-lbs^2
100
1000
Hz
9.7242D+00 RMS(1-1000) 8.7637D+00 RMS(300-500)

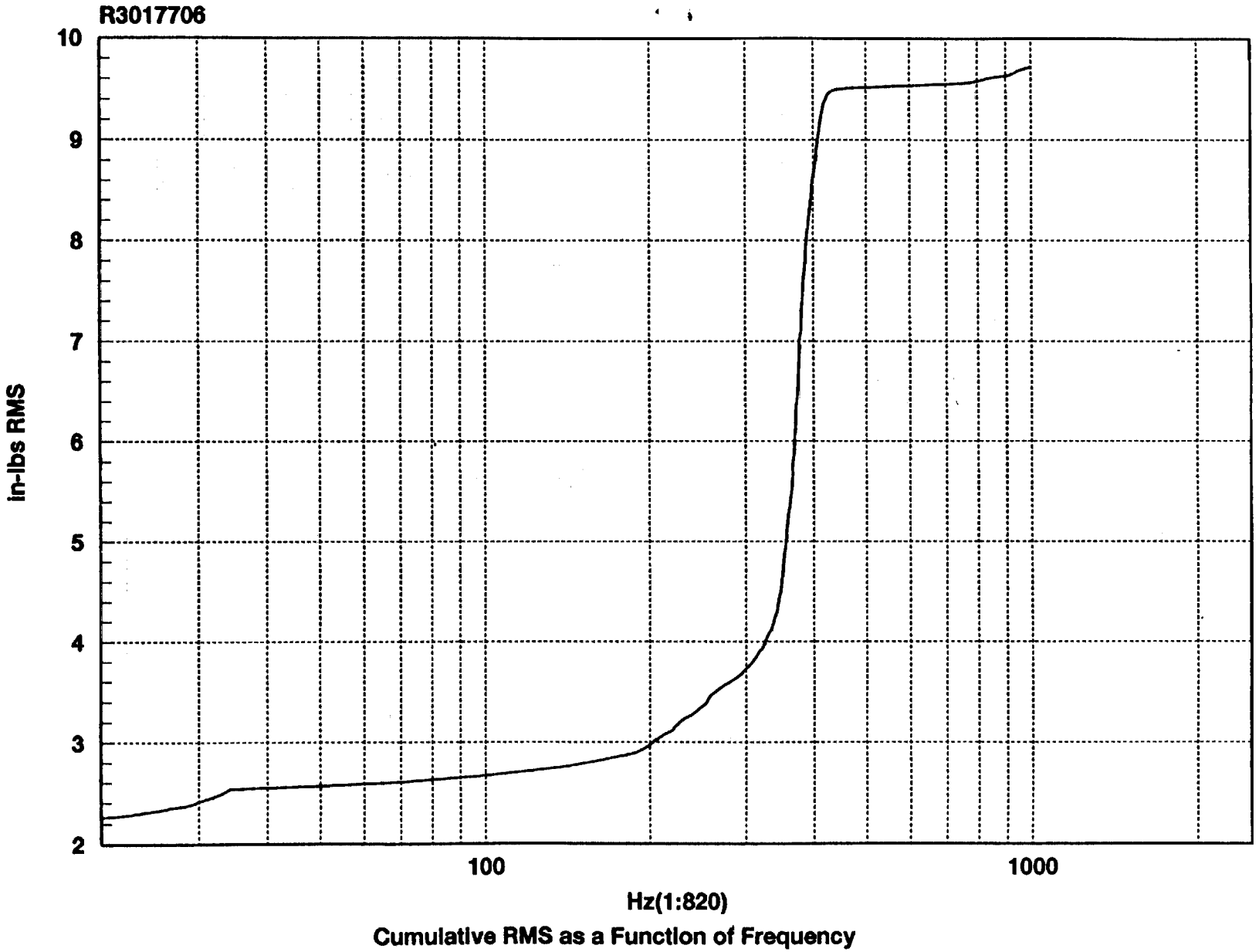

Cumulative RMS as a Function of Frequency

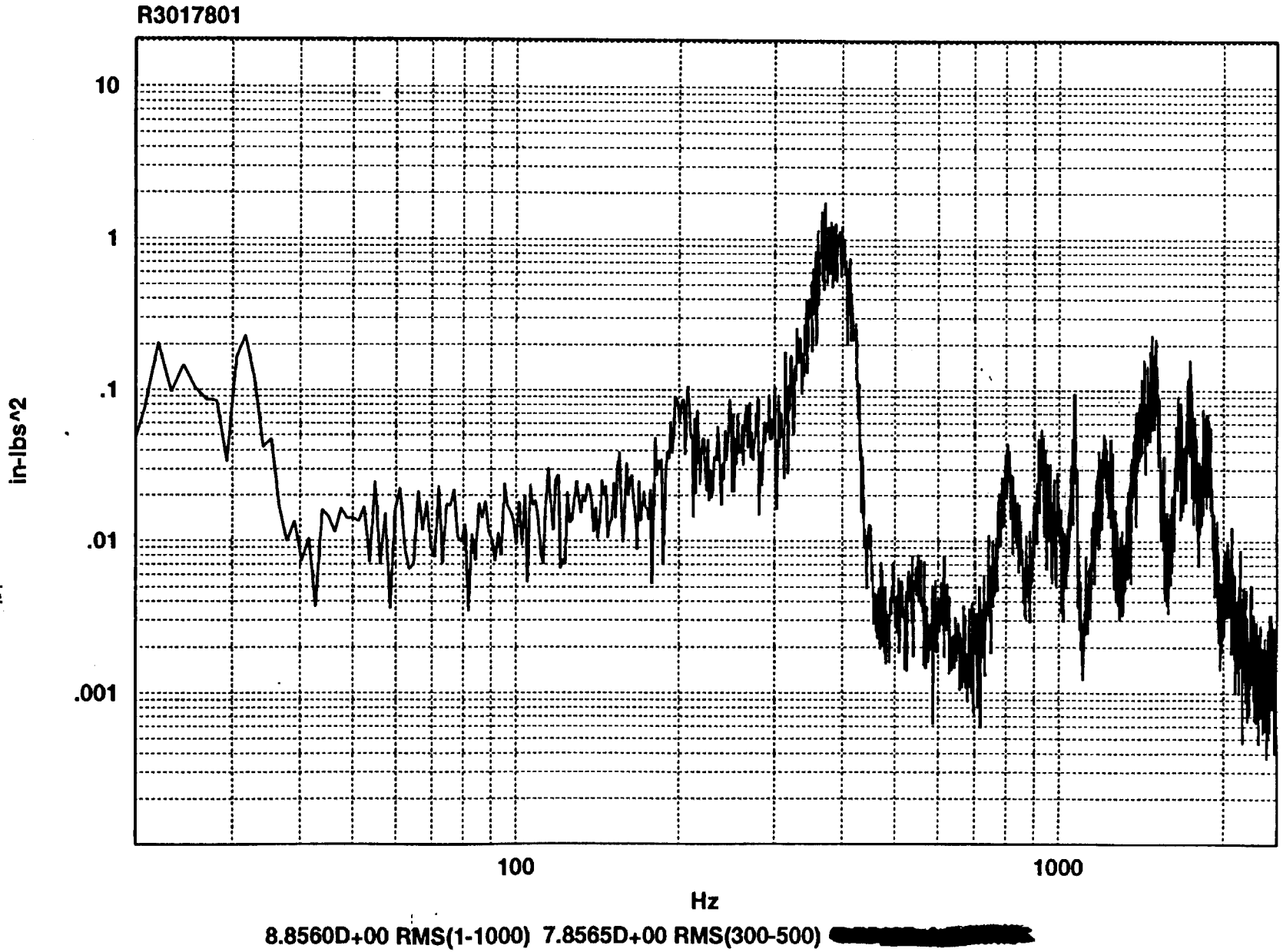
R3017801
10
1
.1
.01
.001
in-lbs^2
100
1000
Hz
8.8560D+00 RMS(1-1000) 7.8565D+00 RMS(300-500)

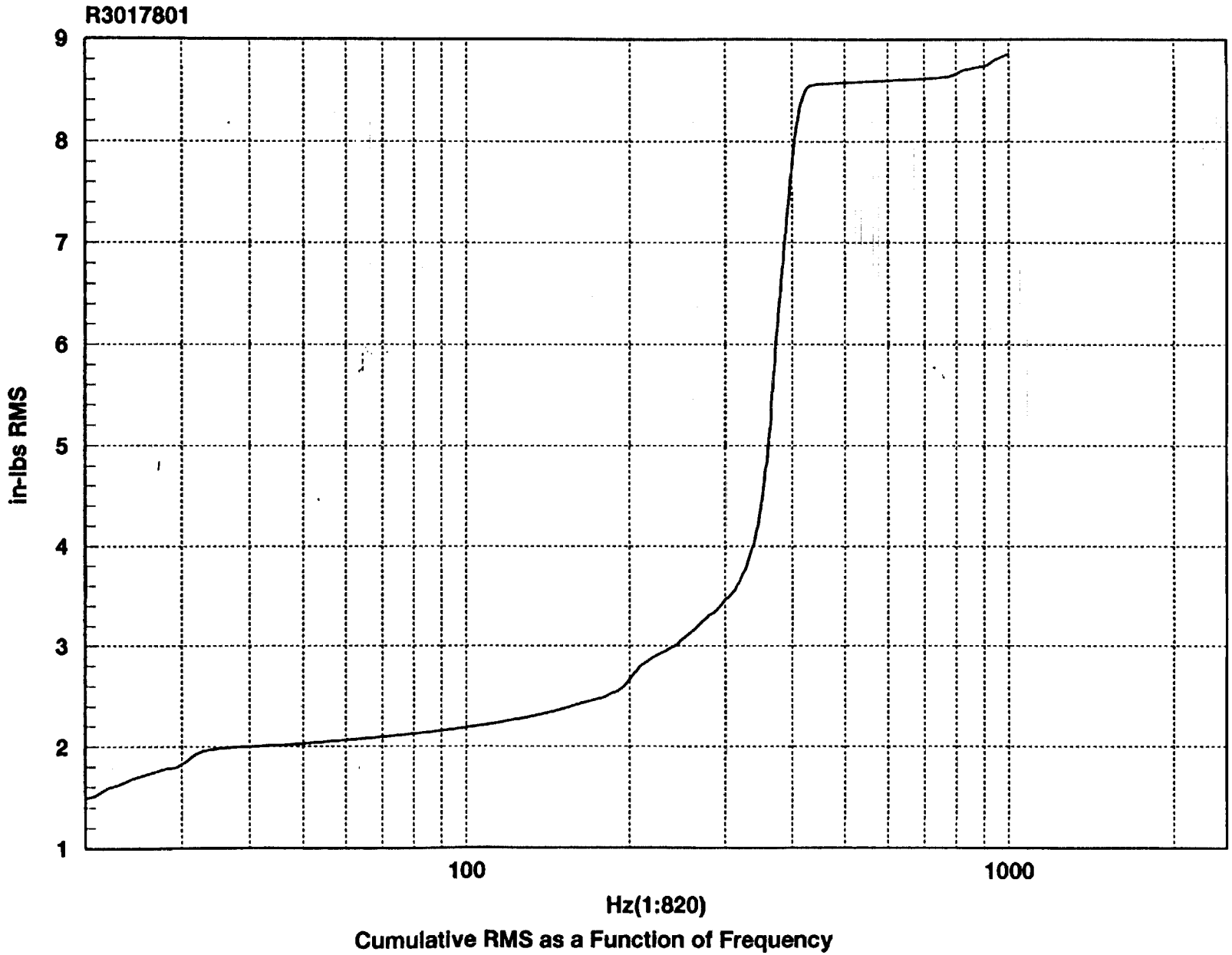

Cumulative RMS as a Function of Frequency

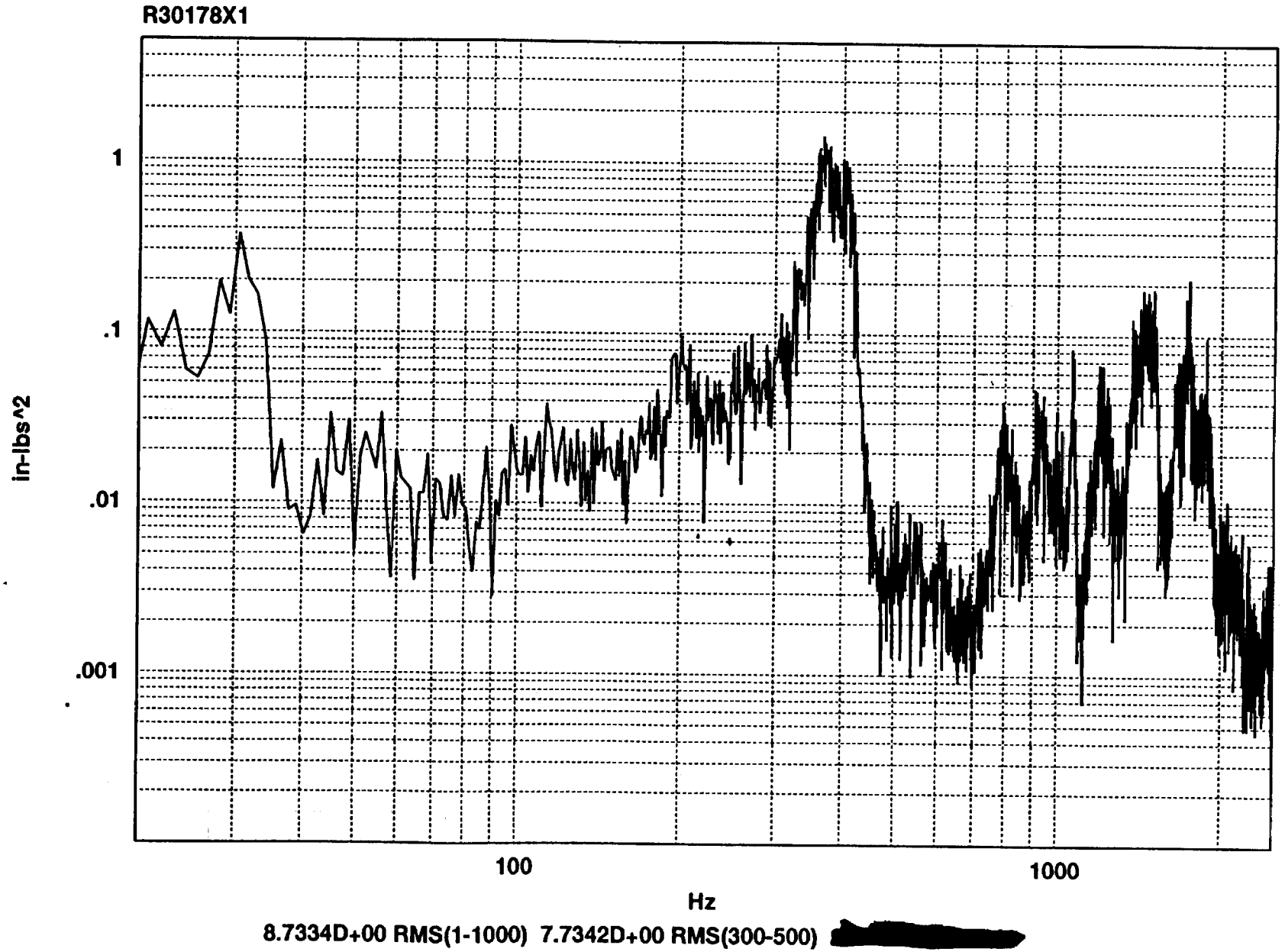
R30178X1
1
.1
.01
.001
in-lbs^2
100
1000
Hz
8.7334D+00 RMS(1-1000) 7.7342D+00 RMS(300-500)

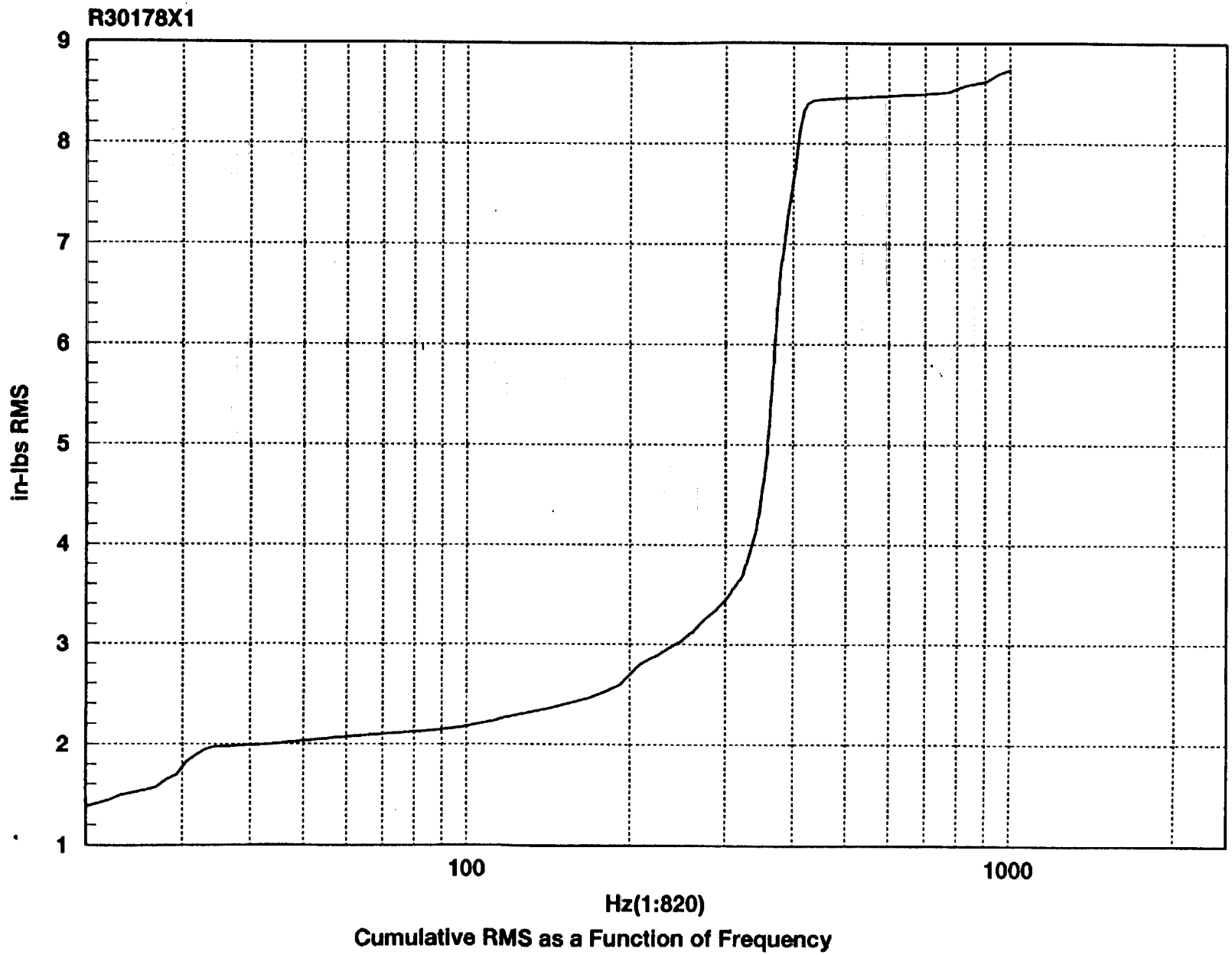

Cumulative RMS as a Function of Frequency

R3017802

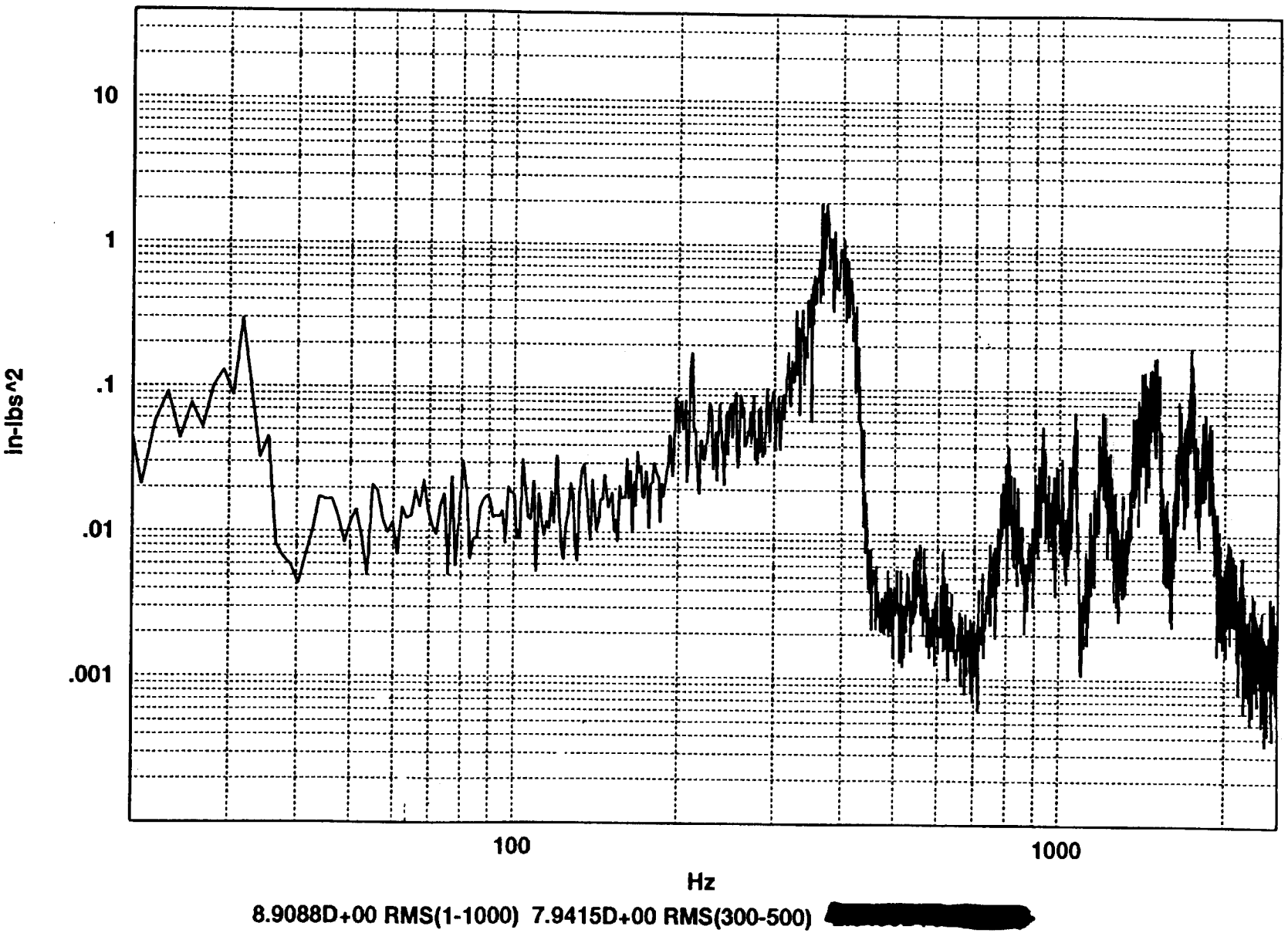

8.9088D+00 RMS(1-1000) 7.9415D+00 RMS(300-500) [redacted]

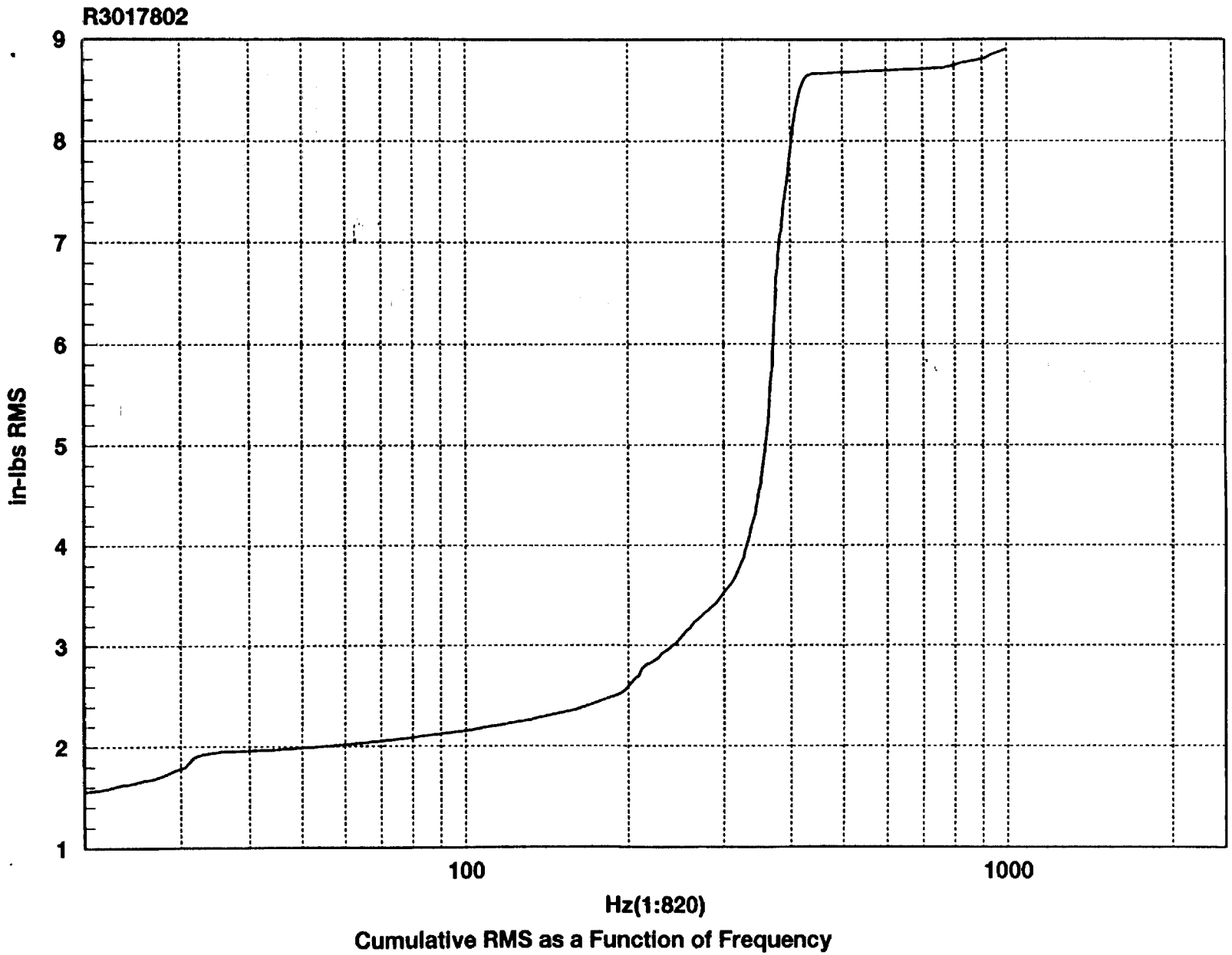

Cumulative RMS as a Function of Frequency

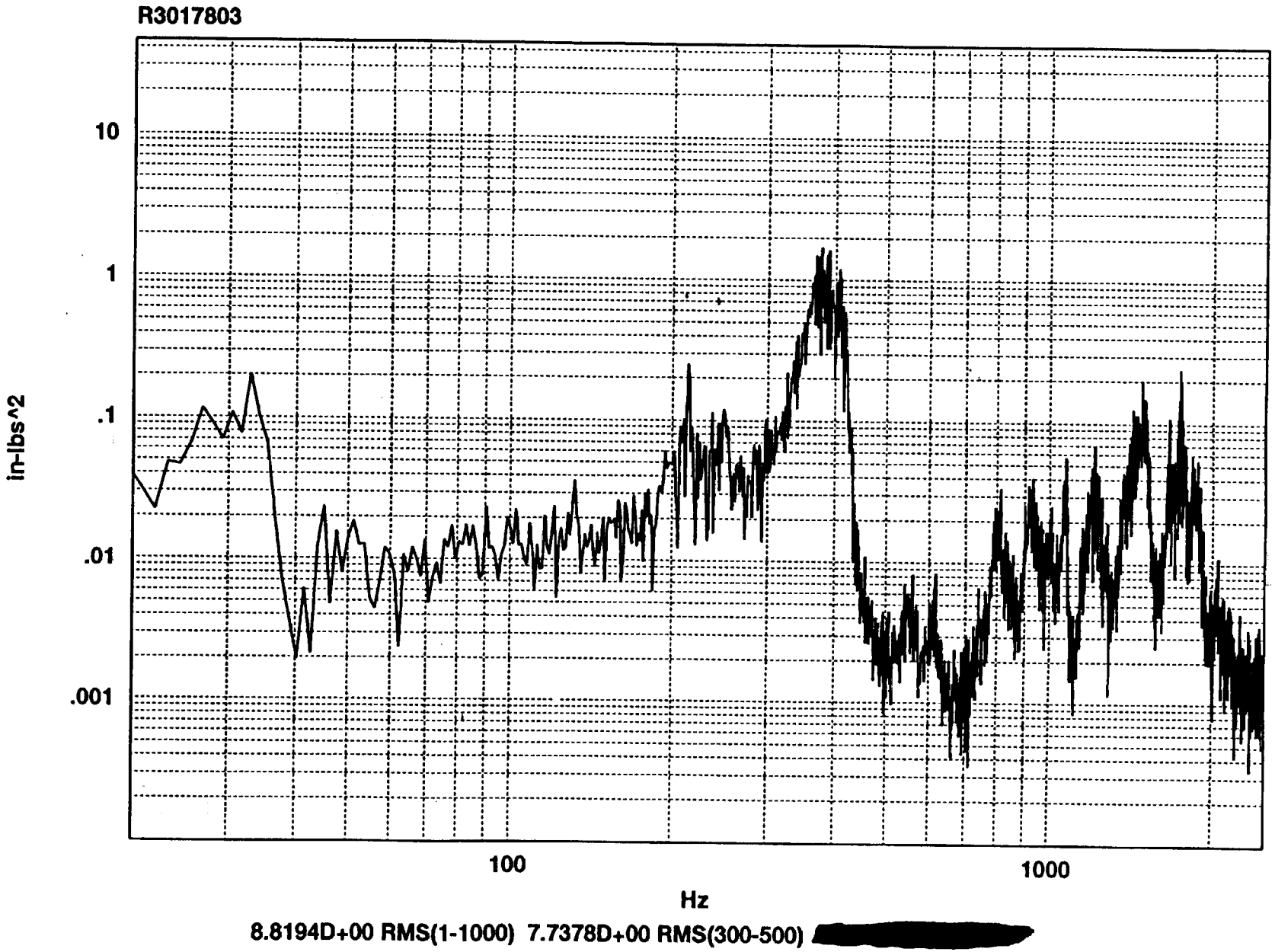
R3017803
10
1
.1
.01
.001
in-lbs^2
100
1000
Hz
8.8194D+00 RMS(1-1000) 7.7378D+00 RMS(300-500)

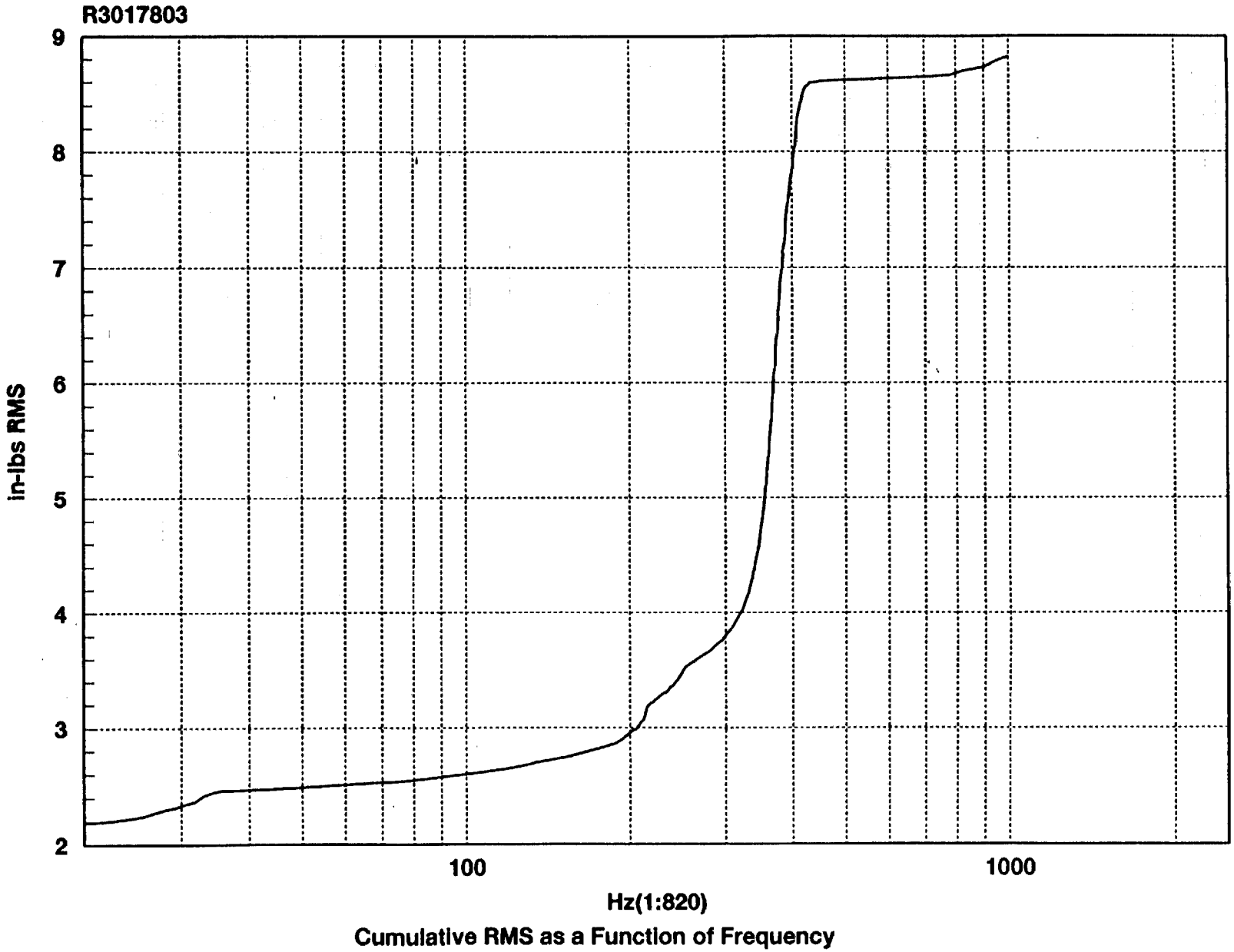
R3017803
9
8
7
6
5
4
3
2
in-lbs RMS
100
1000
Hz(1:820)
Cumulative RMS as a Function of Frequency

R3017804

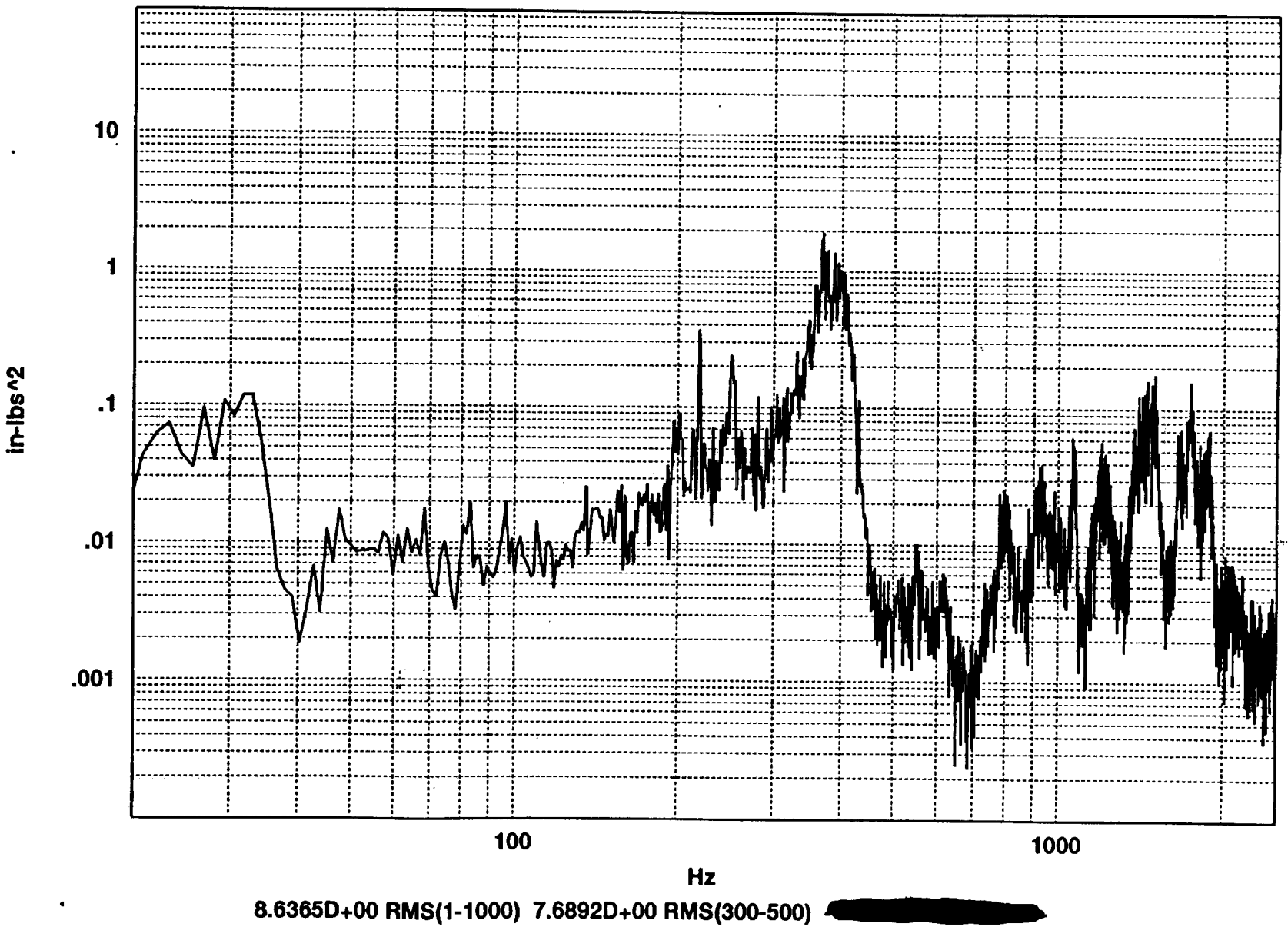

8.6365D+00 RMS(1-1000) 7.6892D+00 RMS(300-500) [redacted]

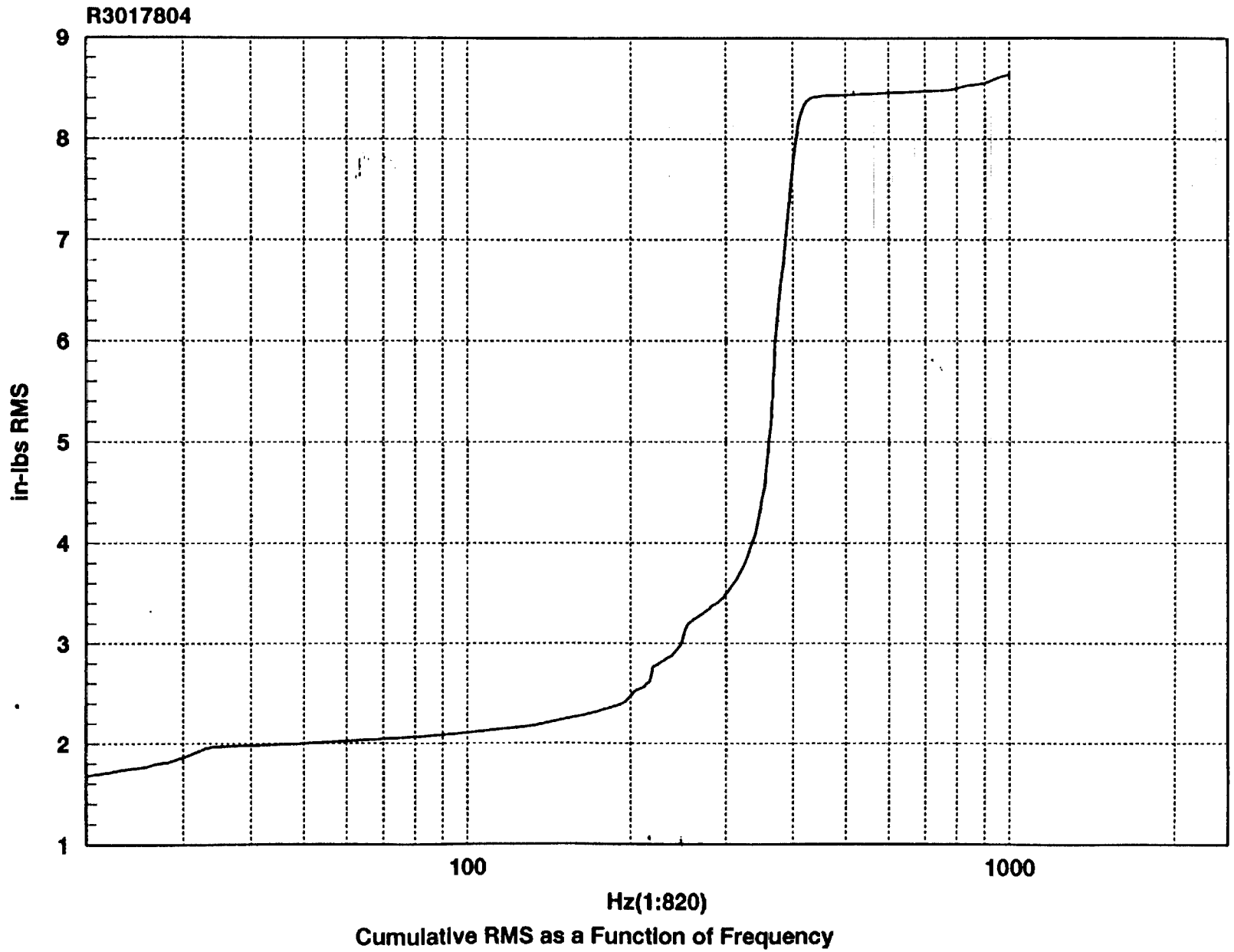

Cumulative RMS as a Function of Frequency

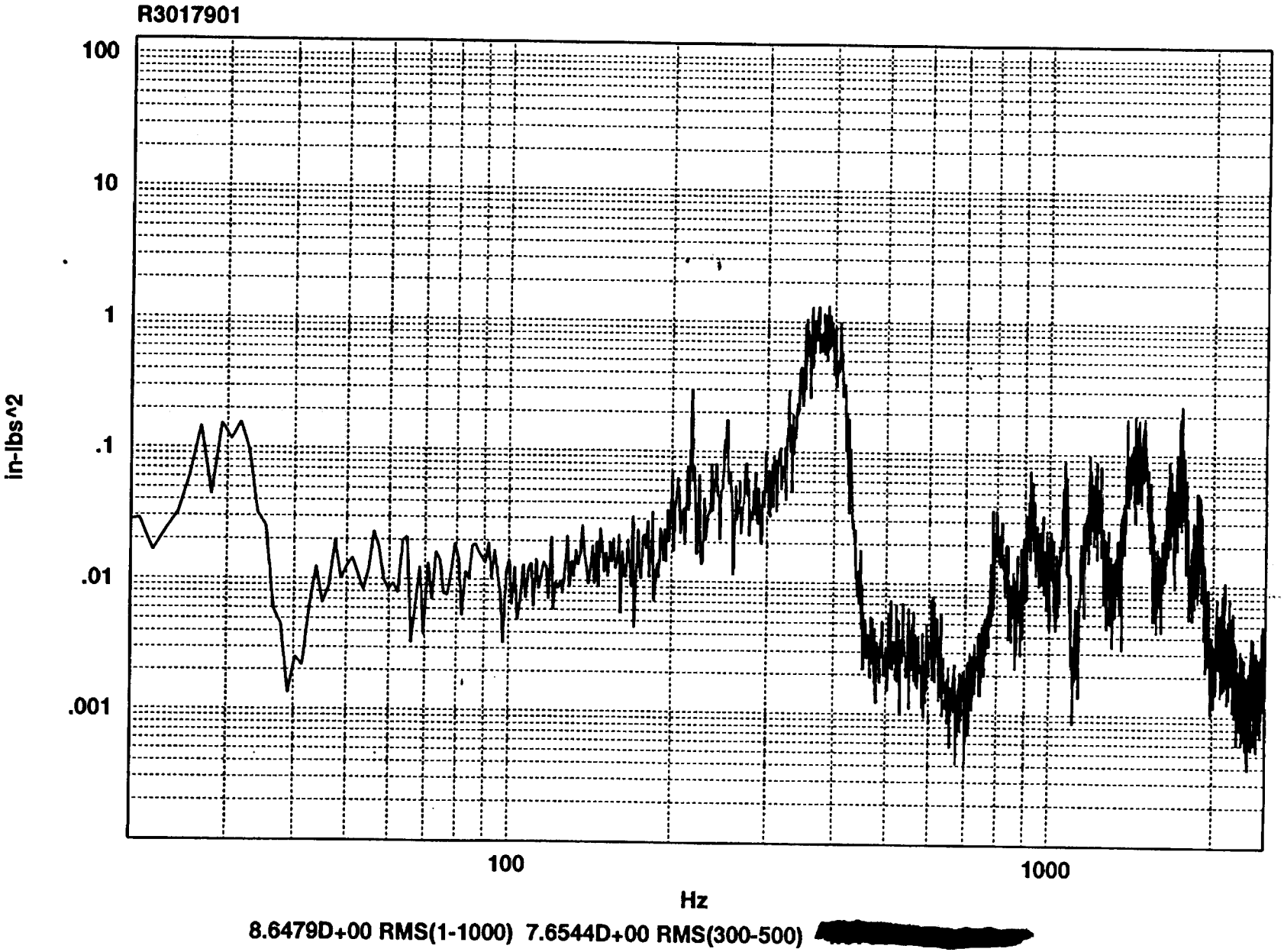
R3017901
100
10
1
.1
.01
.001
in-lbs^2
100
1000
Hz
8.6479D+00 RMS(1-1000) 7.6544D+00 RMS(300-500)

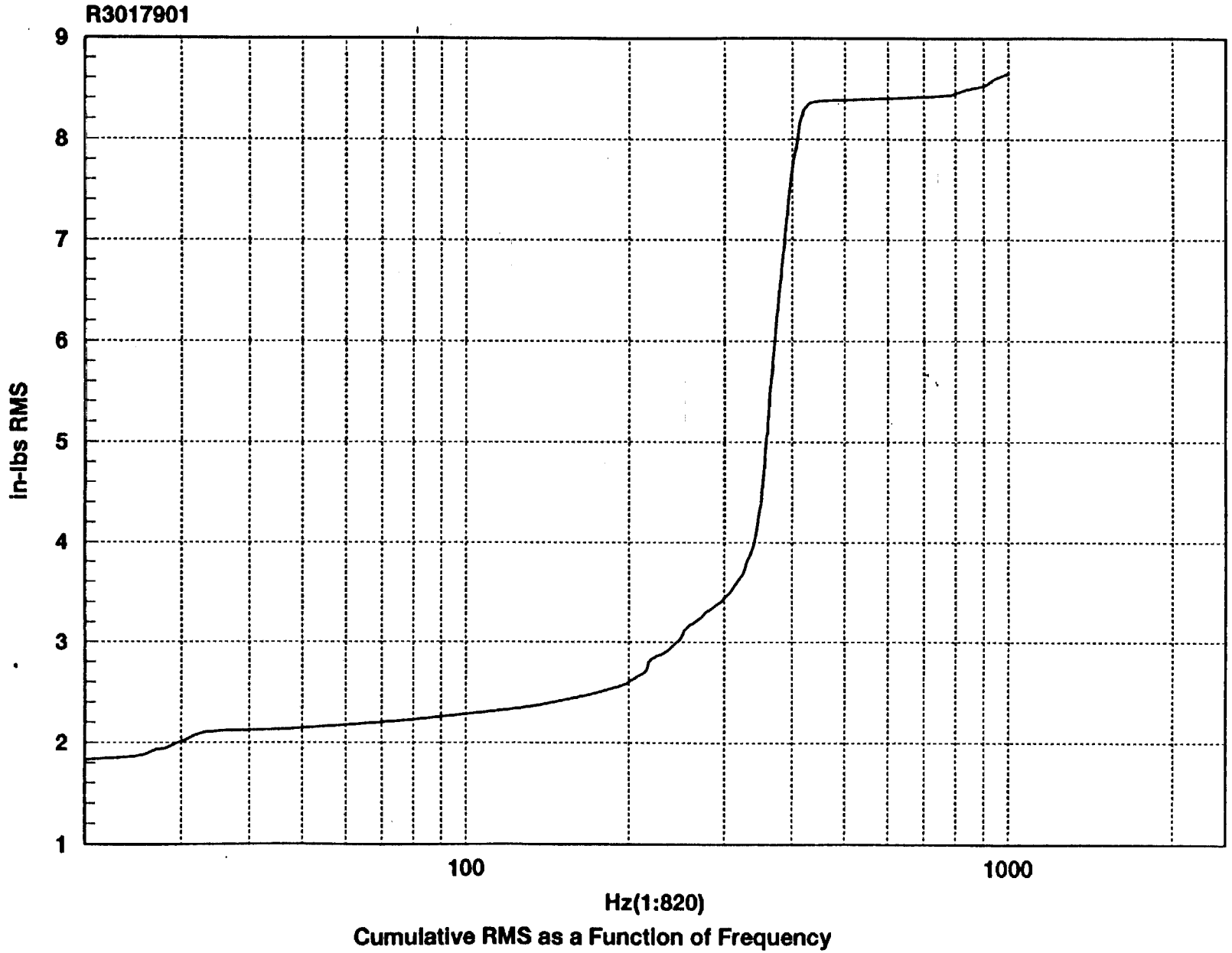

Cumulative RMS as a Function of Frequency

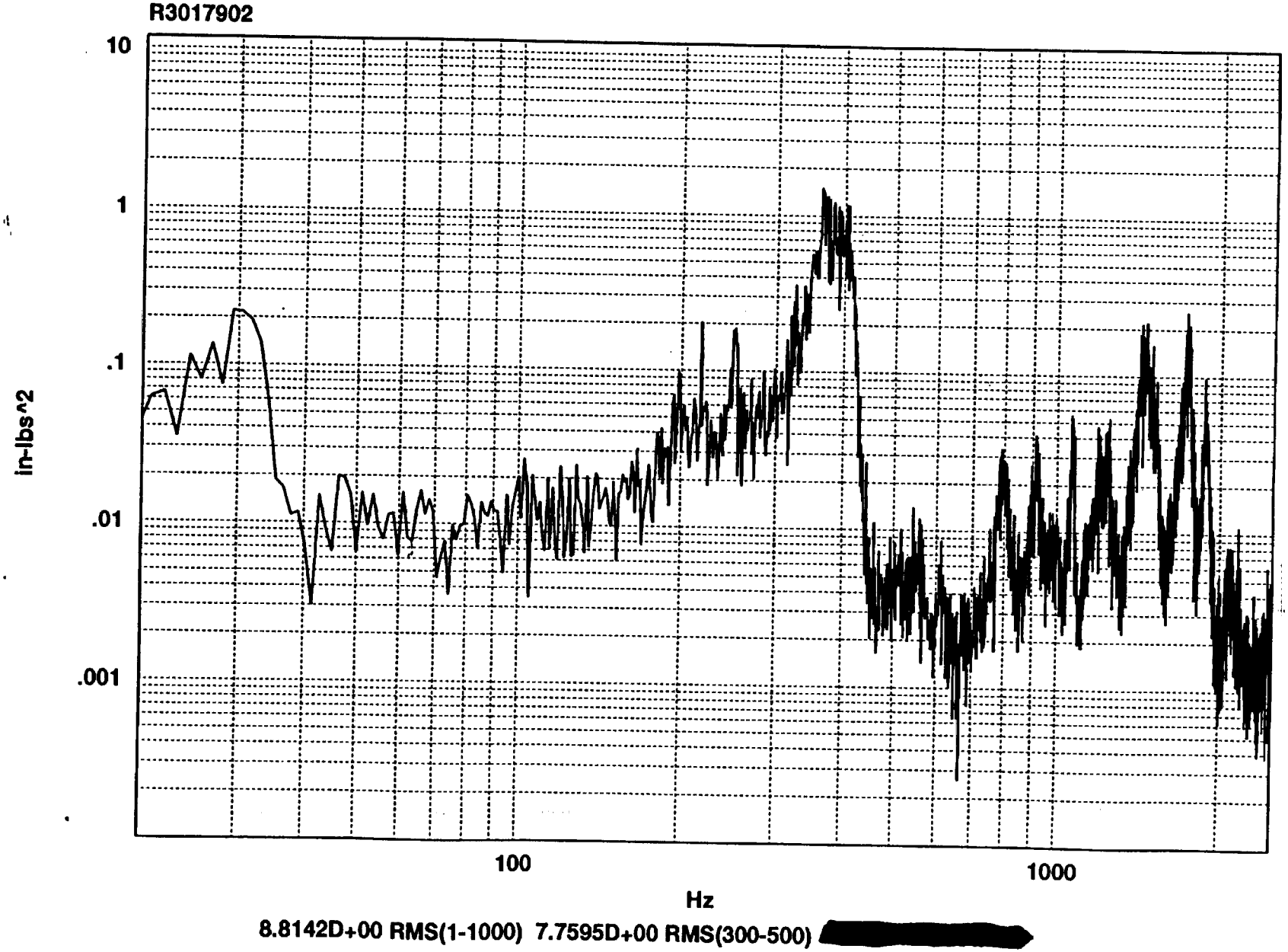
R3017902
10
1
.1
.01
.001
in-lbs^2
100
1000
Hz
8.8142D+00 RMS(1-1000) 7.7595D+00 RMS(300-500)

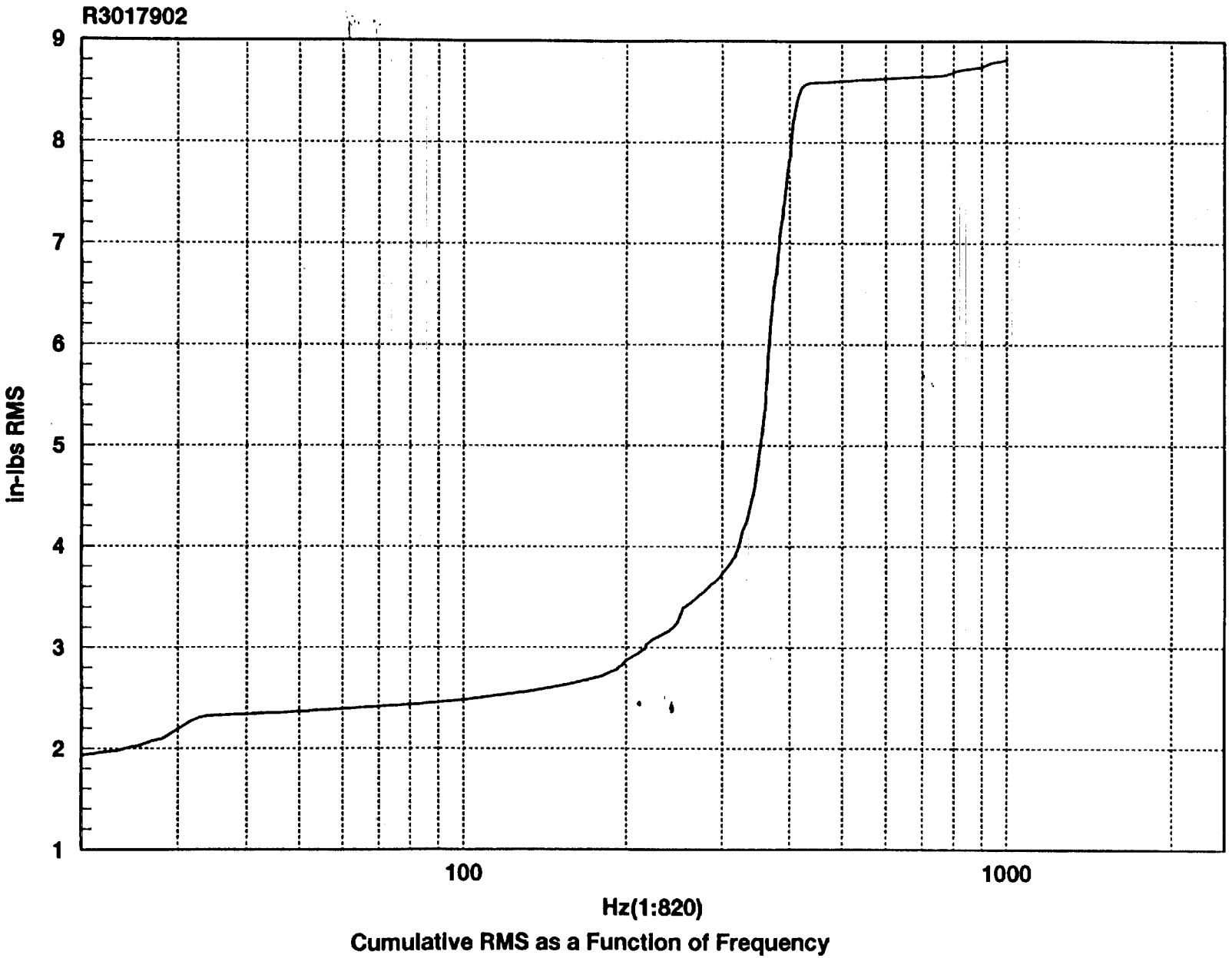

Cumulative RMS as a Function of Frequency

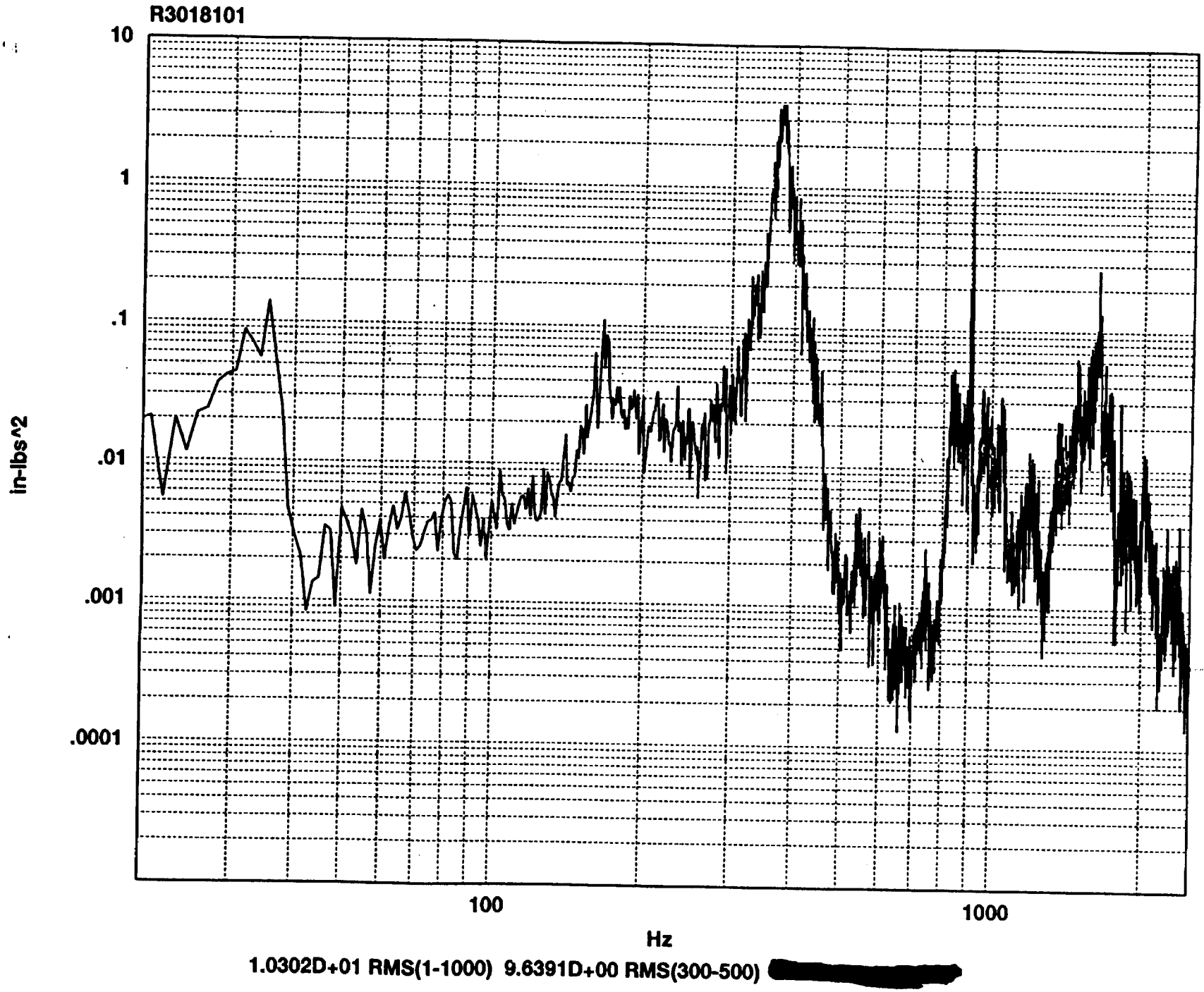
R3018101
10
1
.1
.01
.001
.0001
in-lbs^2
100
1000
Hz
1.0302D+01 RMS(1-1000) 9.6391D+00 RMS(300-500)
[redacted]

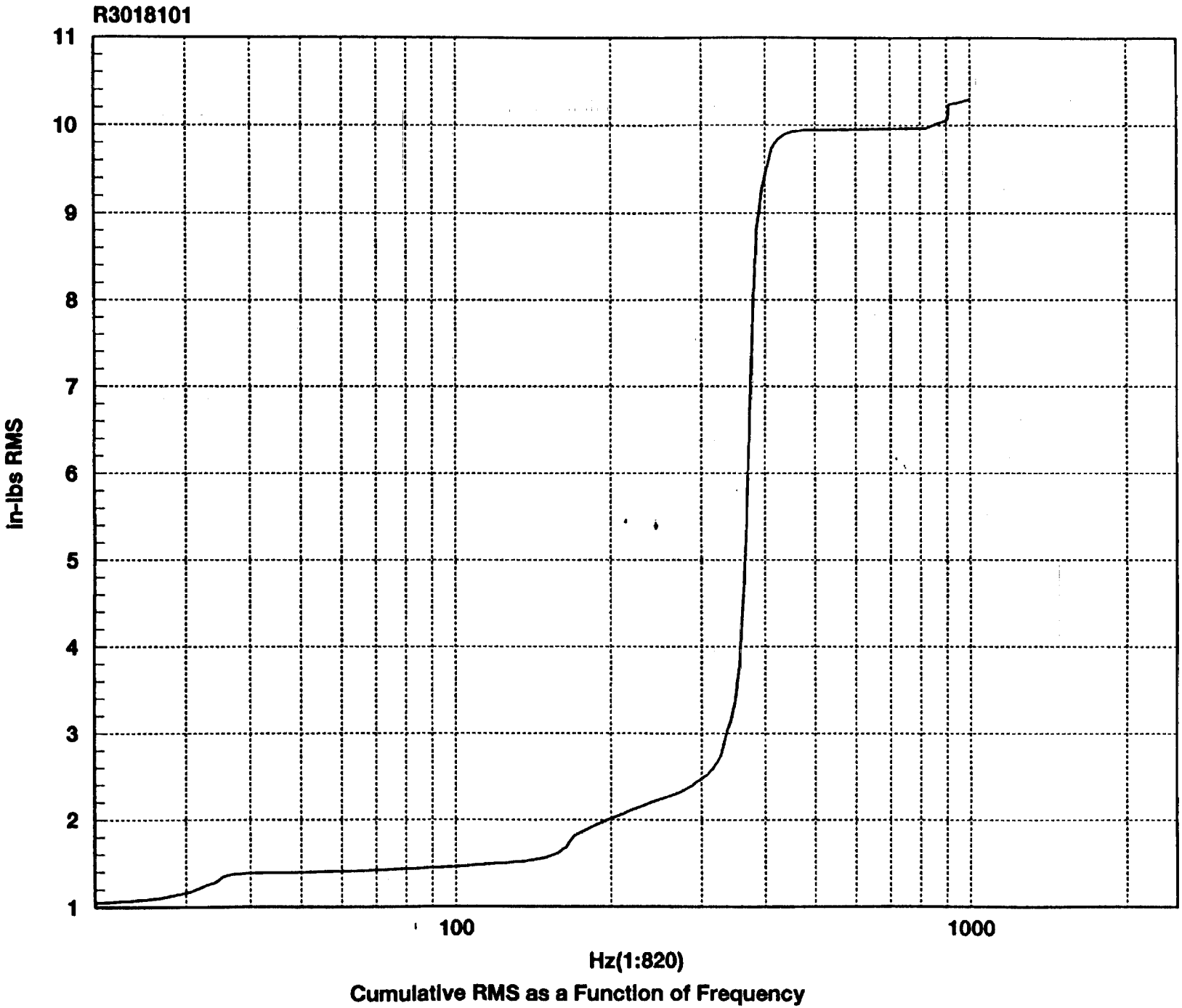

Cumulative RMS as a Function of Frequency

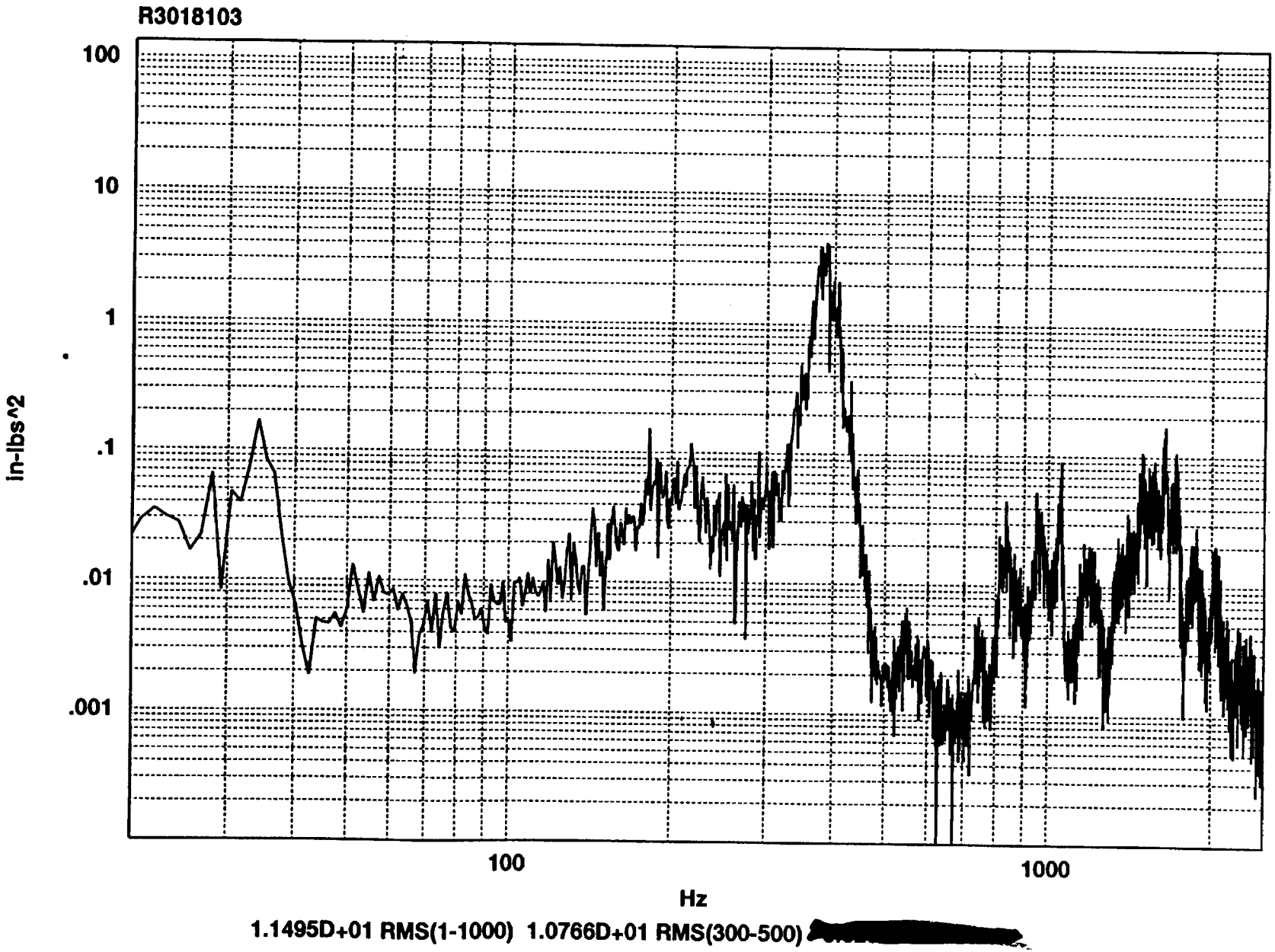
R3018103
100
10
1
.1
.01
.001
In-lbs^2
100
1000
Hz
1.1495D+01 RMS(1-1000) 1.0766D+01 RMS(300-500)

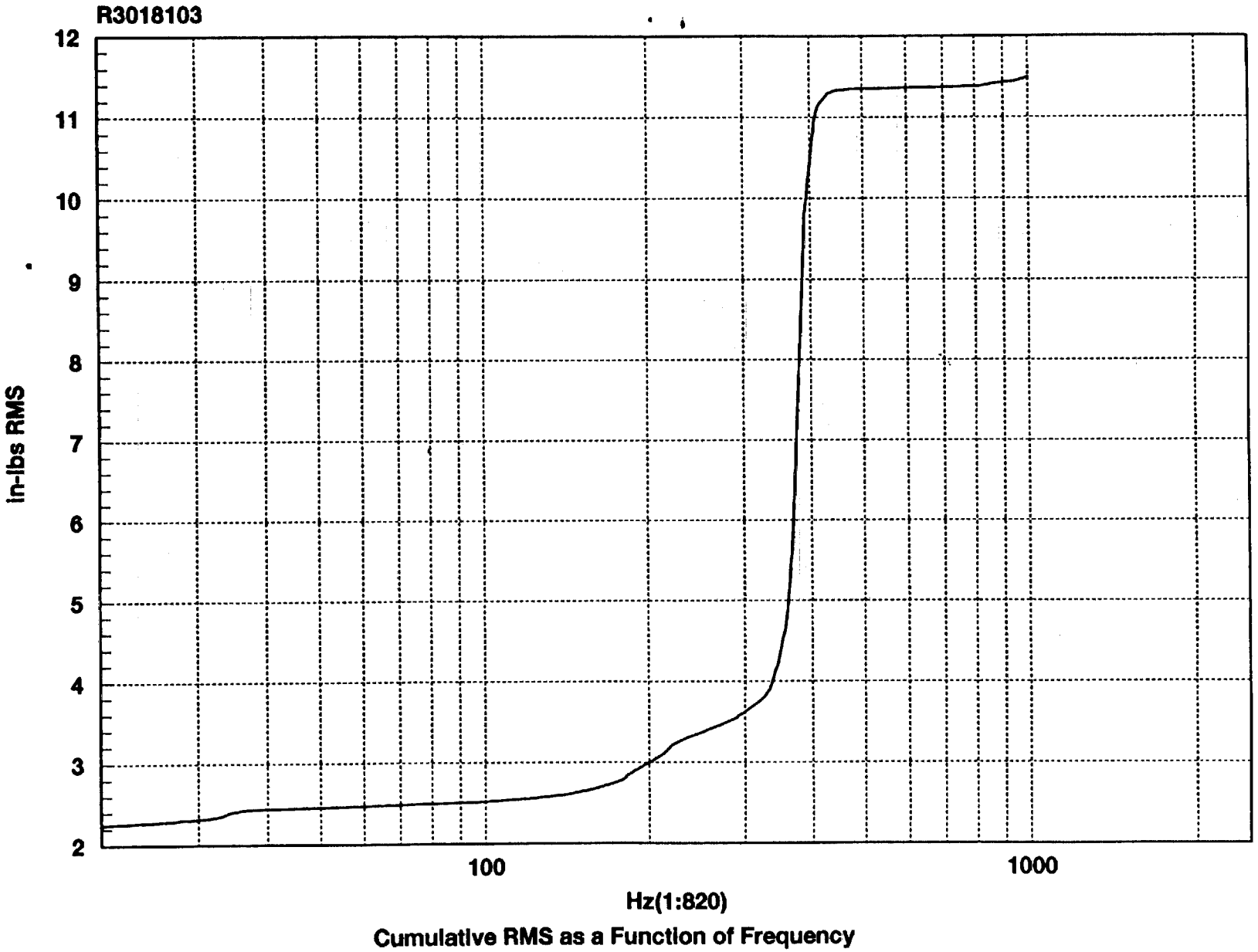

Cumulative RMS as a Function of Frequency

R3018104

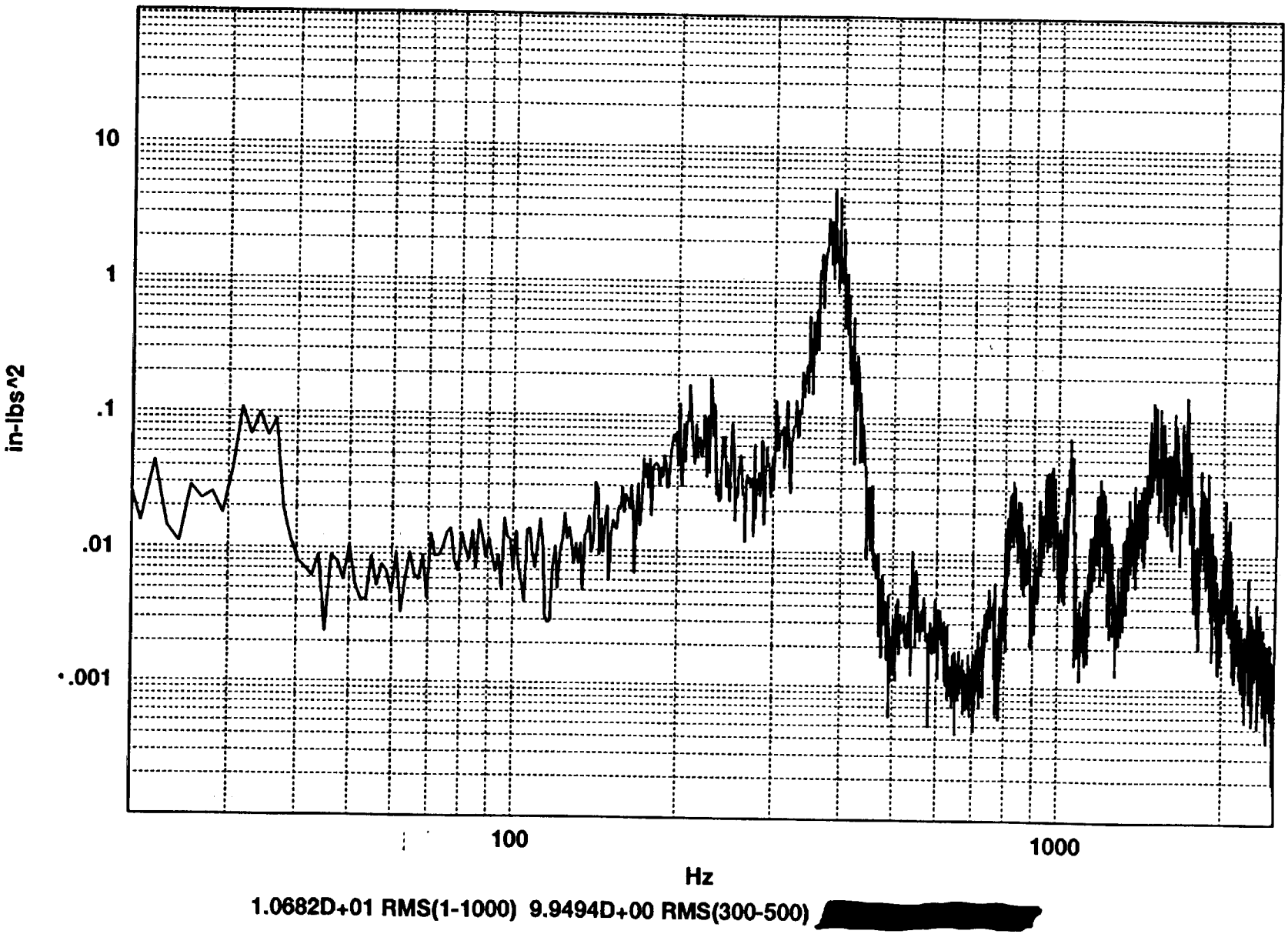

1.0682D+01 RMS(1-1000) 9.9494D+00 RMS(300-500) [redacted]

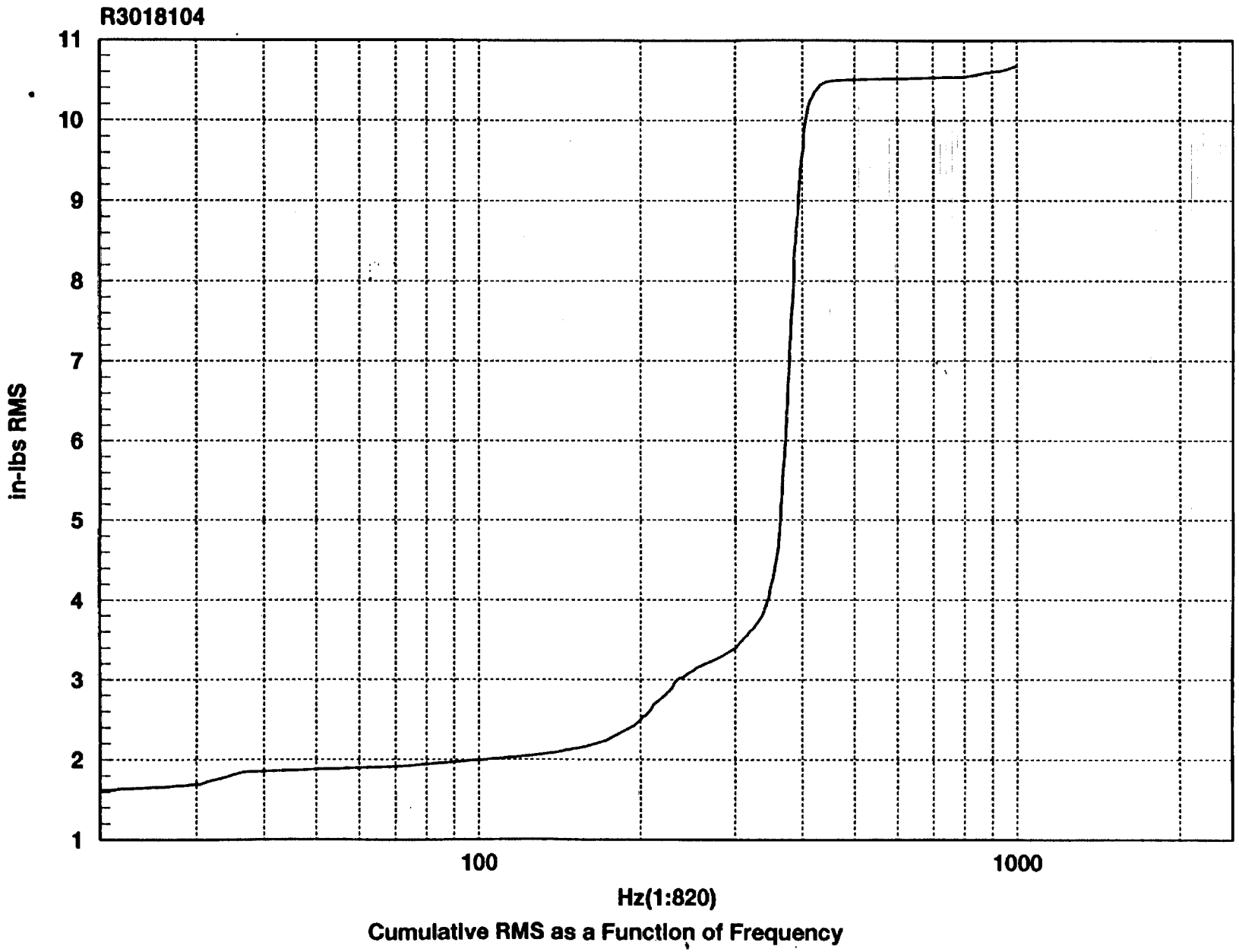

Cumulative RMS as a Function of Frequency

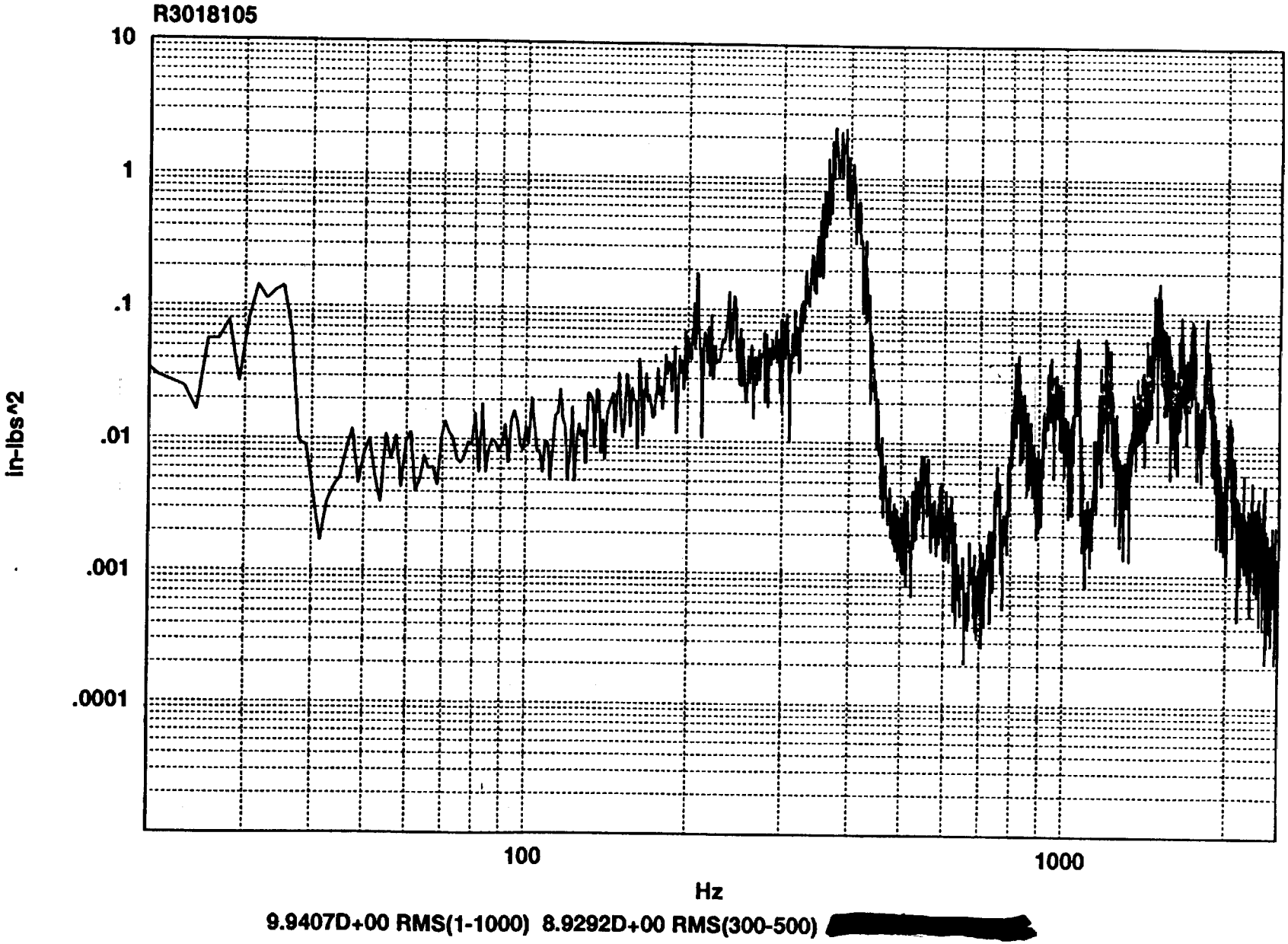
R3018105
10
1
.1
.01
.001
.0001
in-lbs^2
100
1000
Hz
9.9407D+00 RMS(1-1000) 8.9292D+00 RMS(300-500)

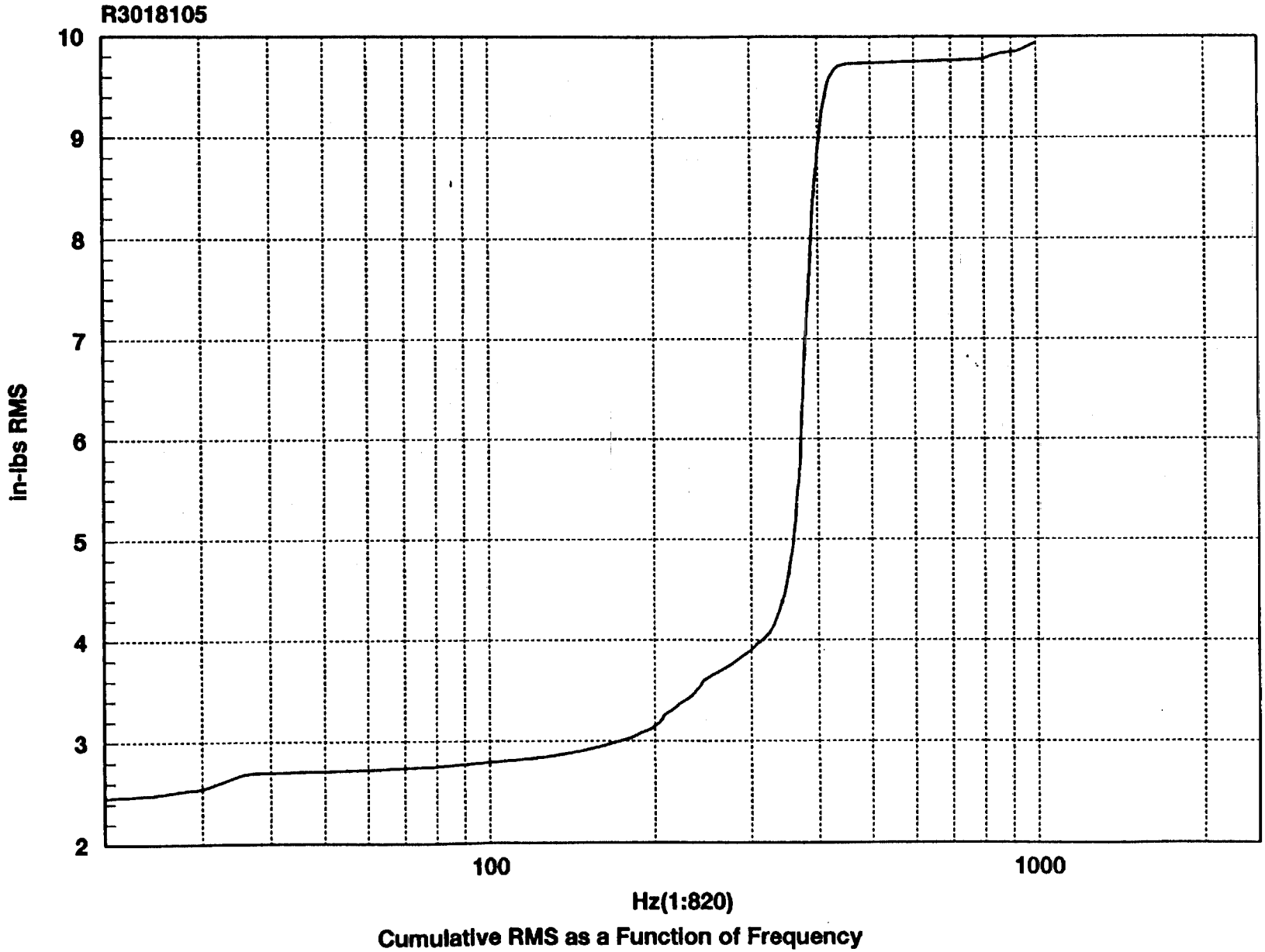

Cumulative RMS as a Function of Frequency

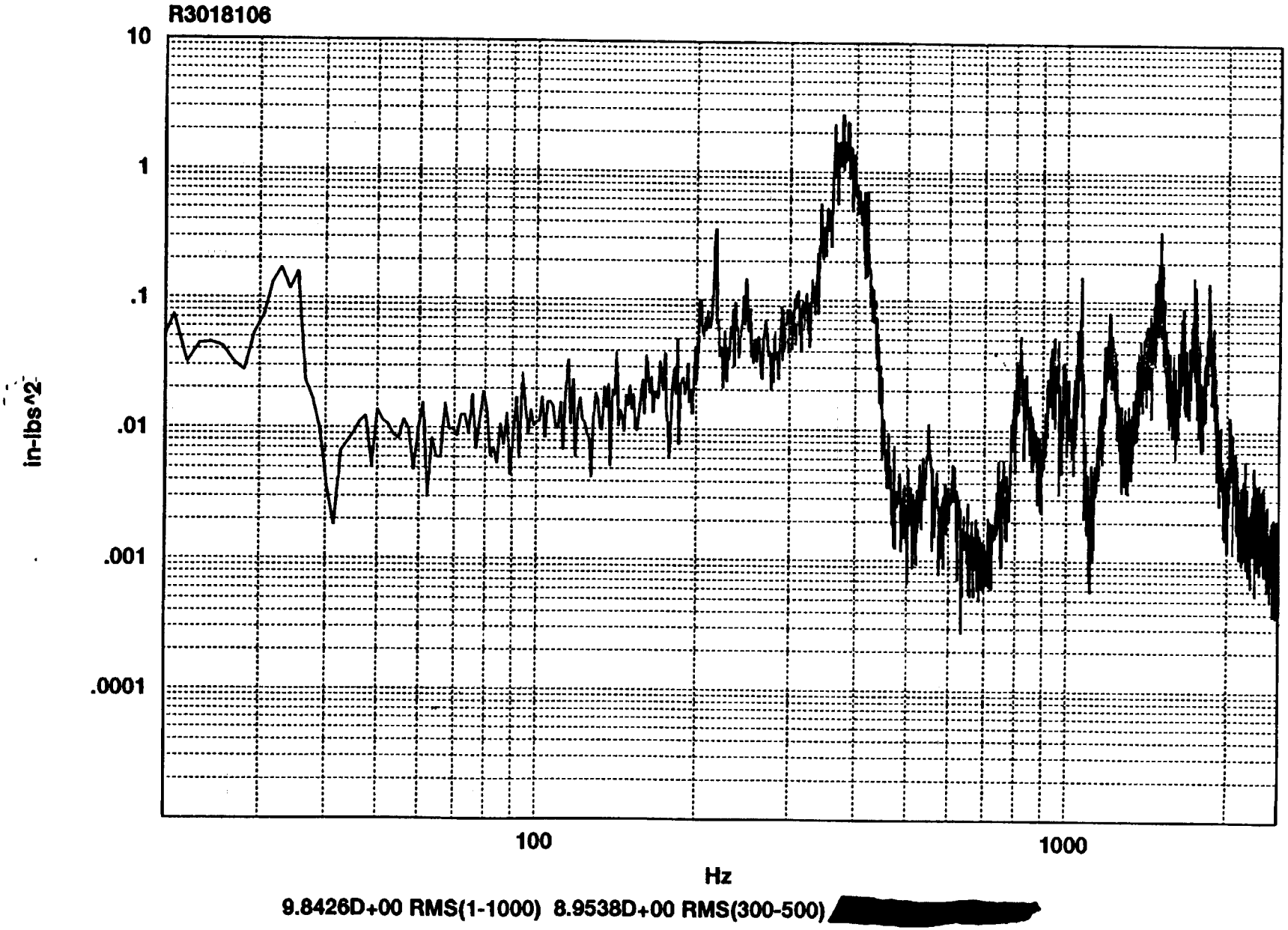
R3018106
10
1
.1
.01
.001
.0001
in-lbs^2
100
1000
Hz
9.8426D+00 RMS(1-1000) 8.9538D+00 RMS(300-500)

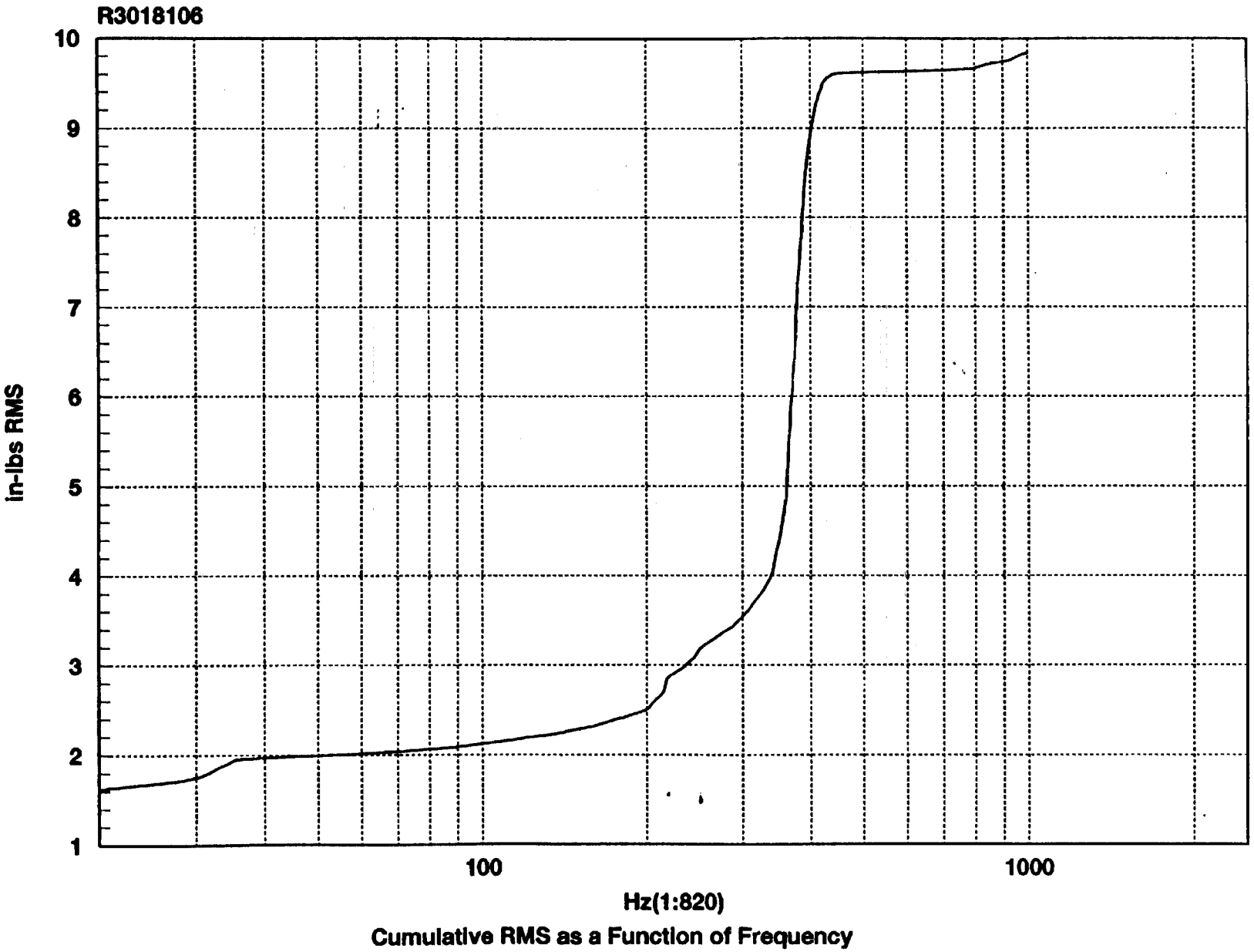

Cumulative RMS as a Function of Frequency

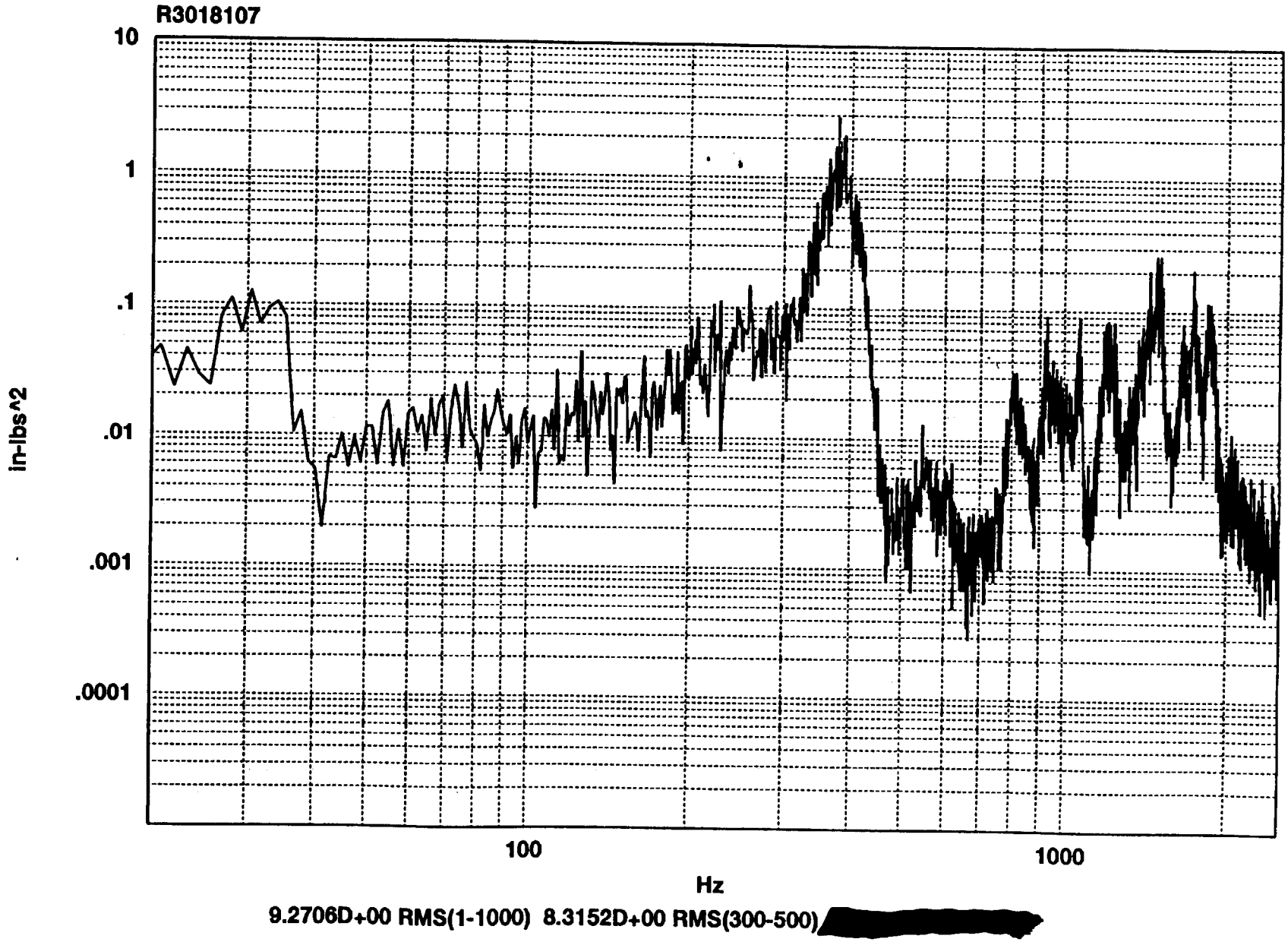
R3018107
10
1
.1
.01
.001
.0001
in-lbs^2
100
1000
Hz
9.2706D+00 RMS(1-1000) 8.3152D+00 RMS(300-500)

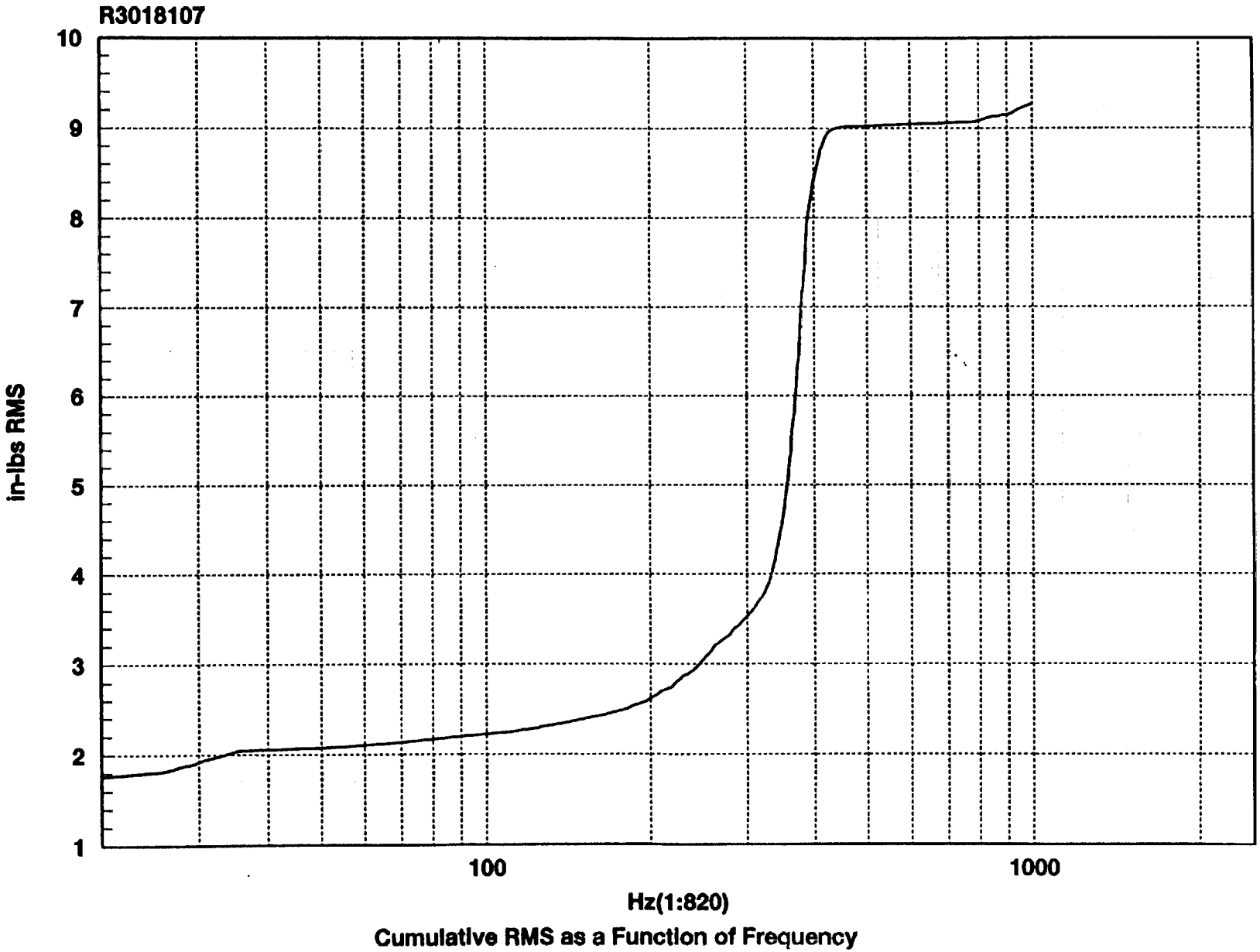
R3018107
10
9
8
7
6
5
4
3
2
1
in-lbs RMS
100
1000
Hz(1:820)
Cumulative RMS as a Function of Frequency

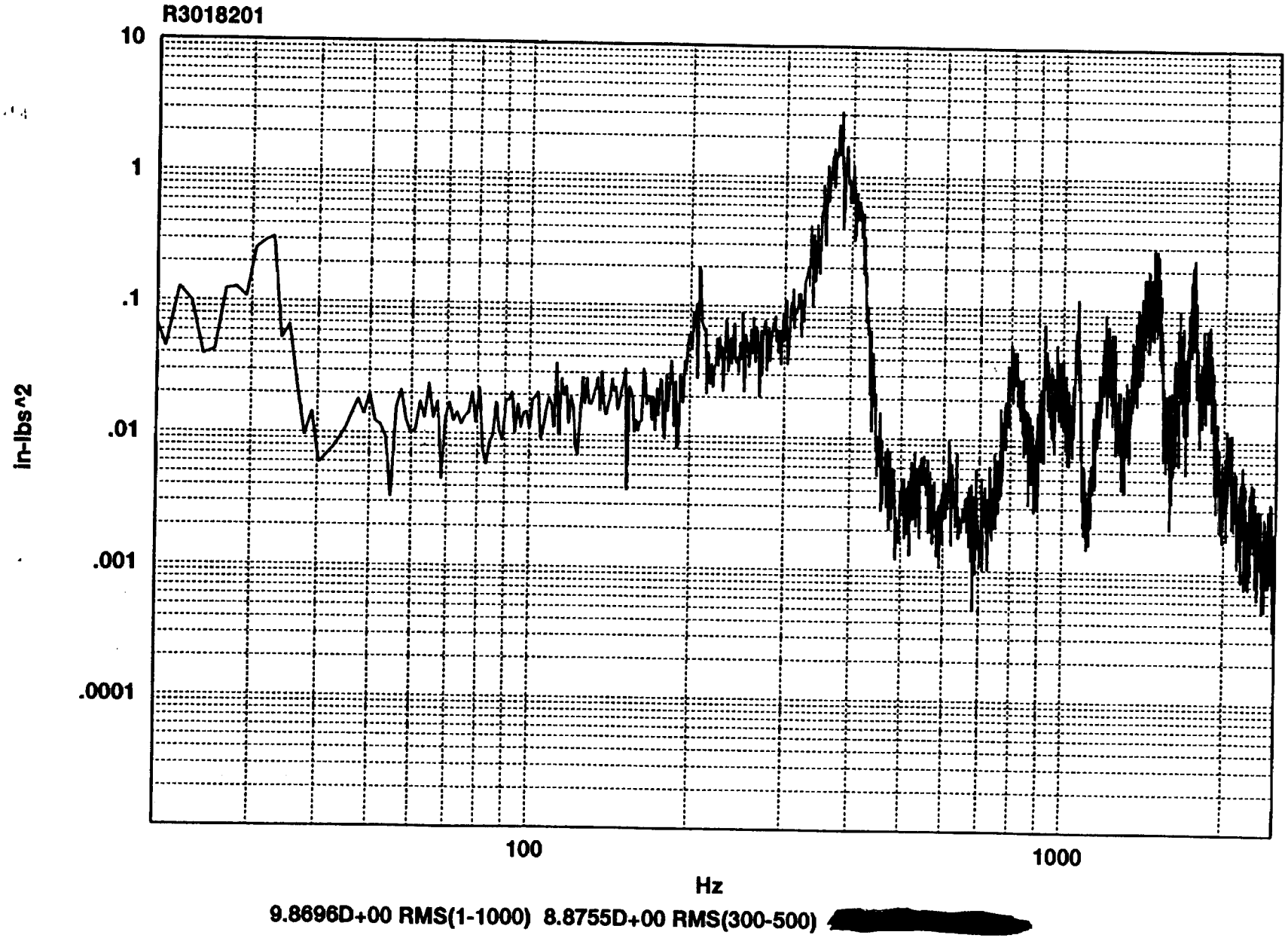
R3018201
10
1
.1
.01
.001
.0001
in-lbs^2
100
1000
Hz
9.8696D+00 RMS(1-1000) 8.8755D+00 RMS(300-500)

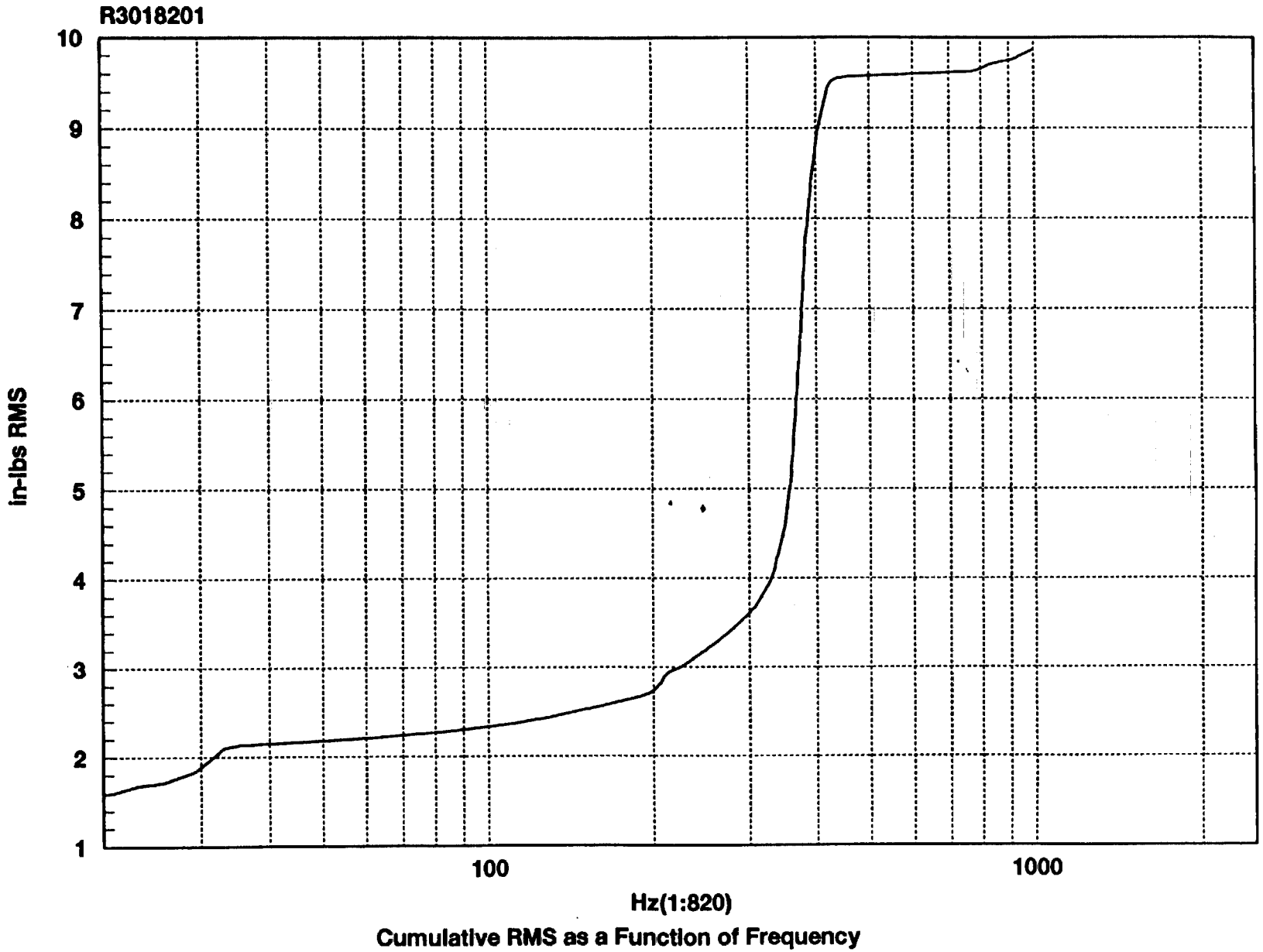
R3018201
10
9
8
7
6
5
4
3
2
1
in-lbs RMS
100
1000
Hz(1:820)
Cumulative RMS as a Function of Frequency

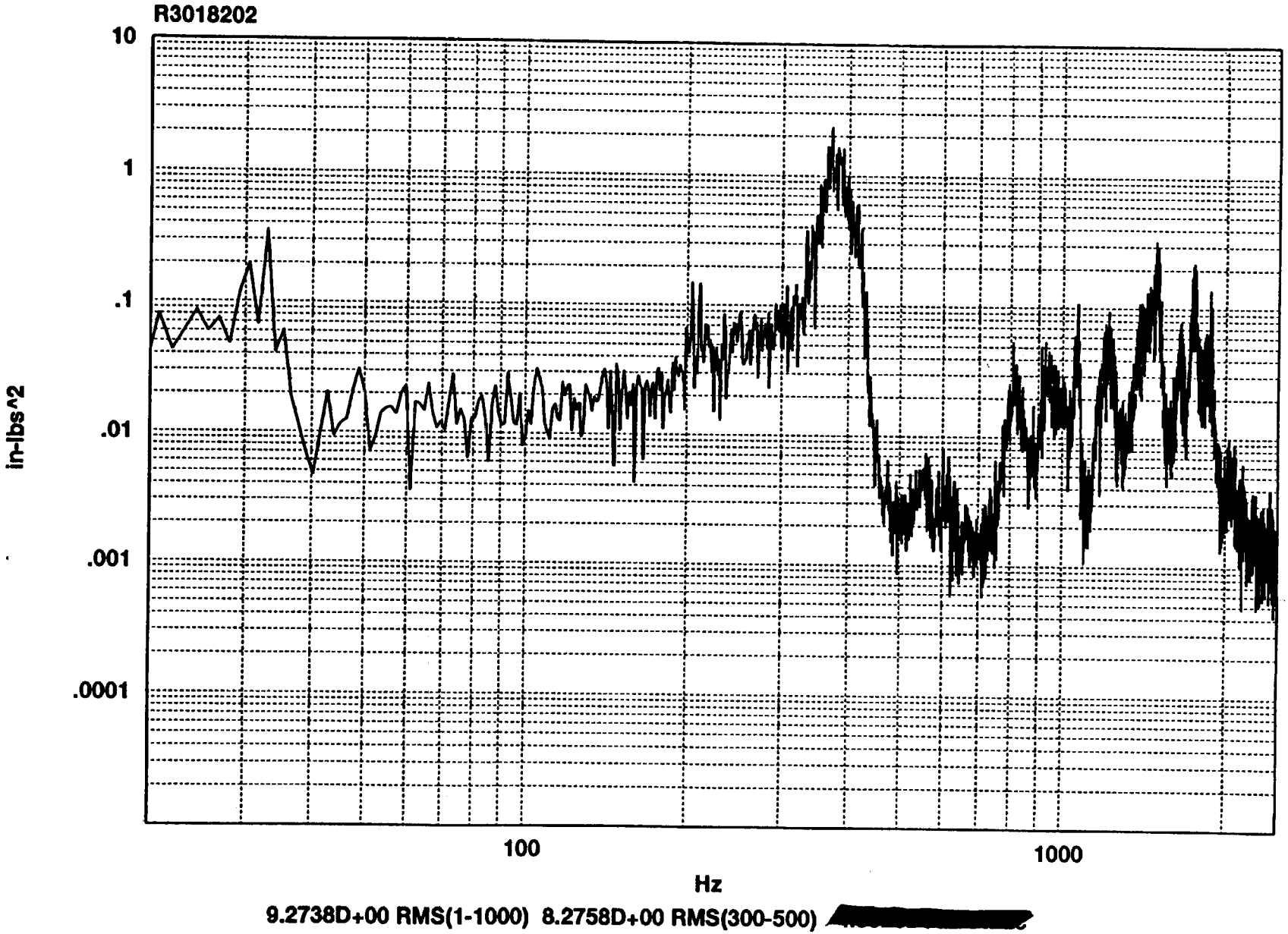
R3018202
10
1
.1
.01
.001
.0001
in-lbs^2
100
1000
Hz
9.2738D+00 RMS(1-1000) 8.2758D+00 RMS(300-500)

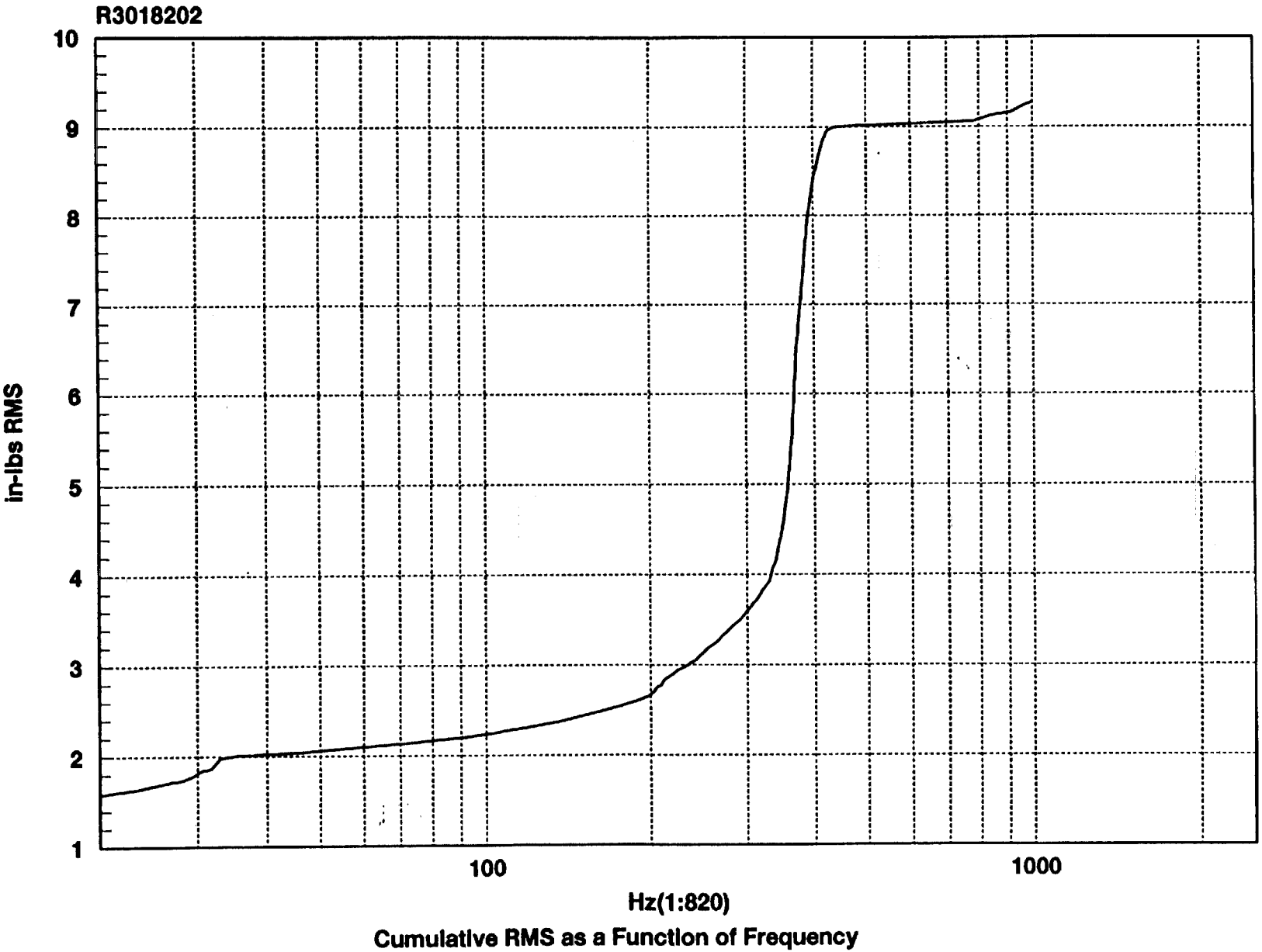

Cumulative RMS as a Function of Frequency

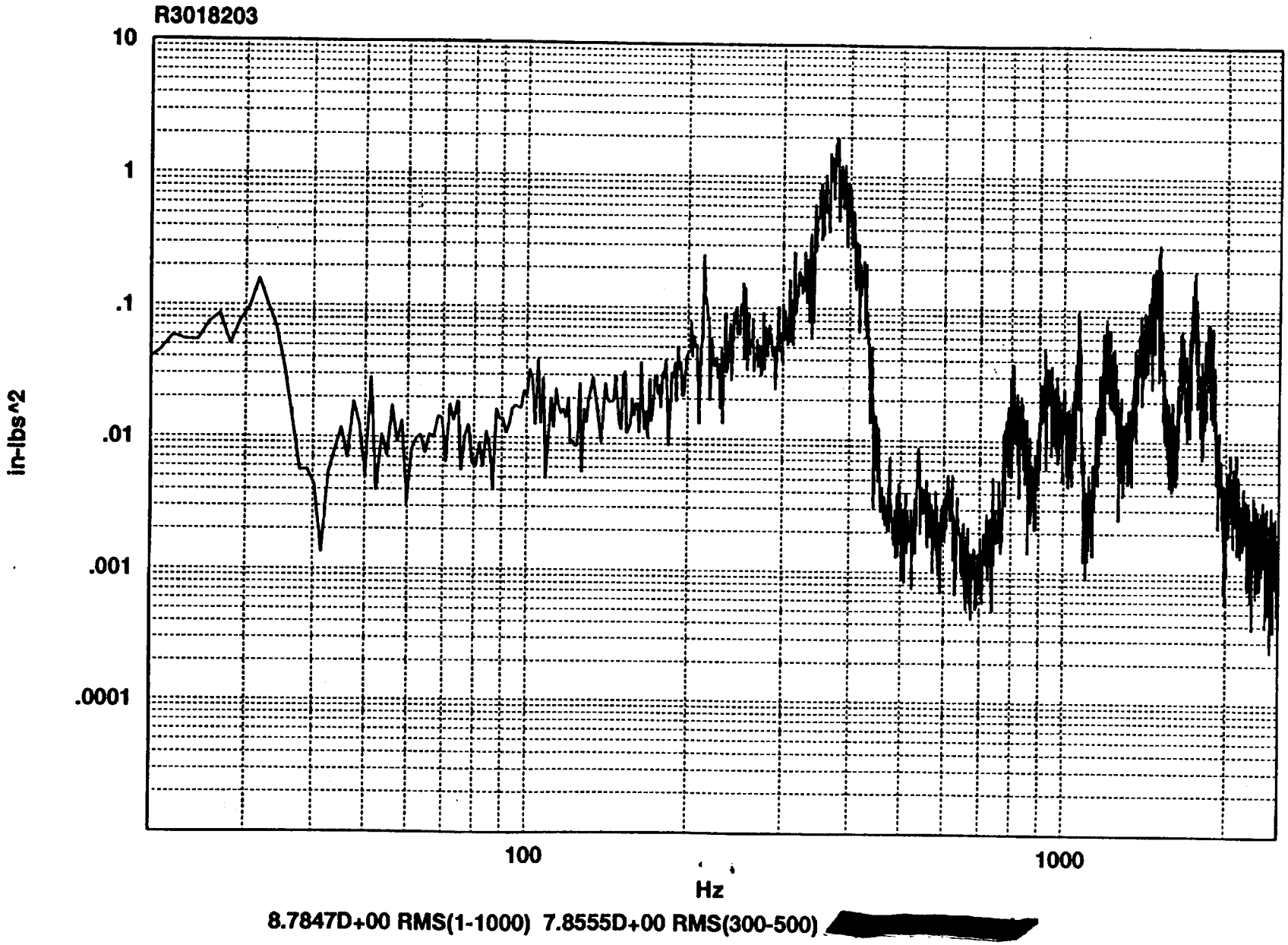
R3018203
10
1
.1
.01
.001
.0001
in-lbs^2
100
1000
Hz
8.7847D+00 RMS(1-1000) 7.8555D+00 RMS(300-500)

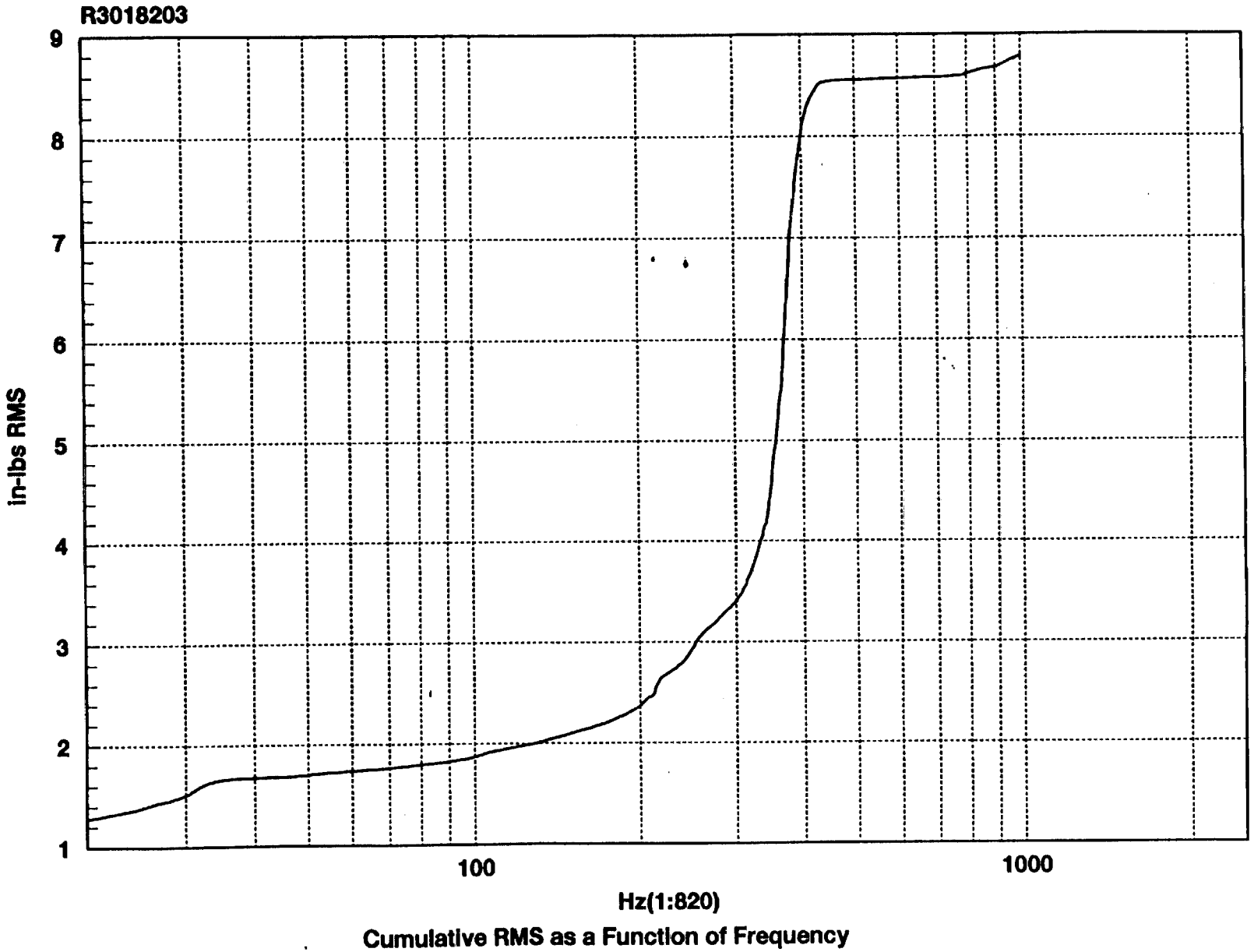

Cumulative RMS as a Function of Frequency

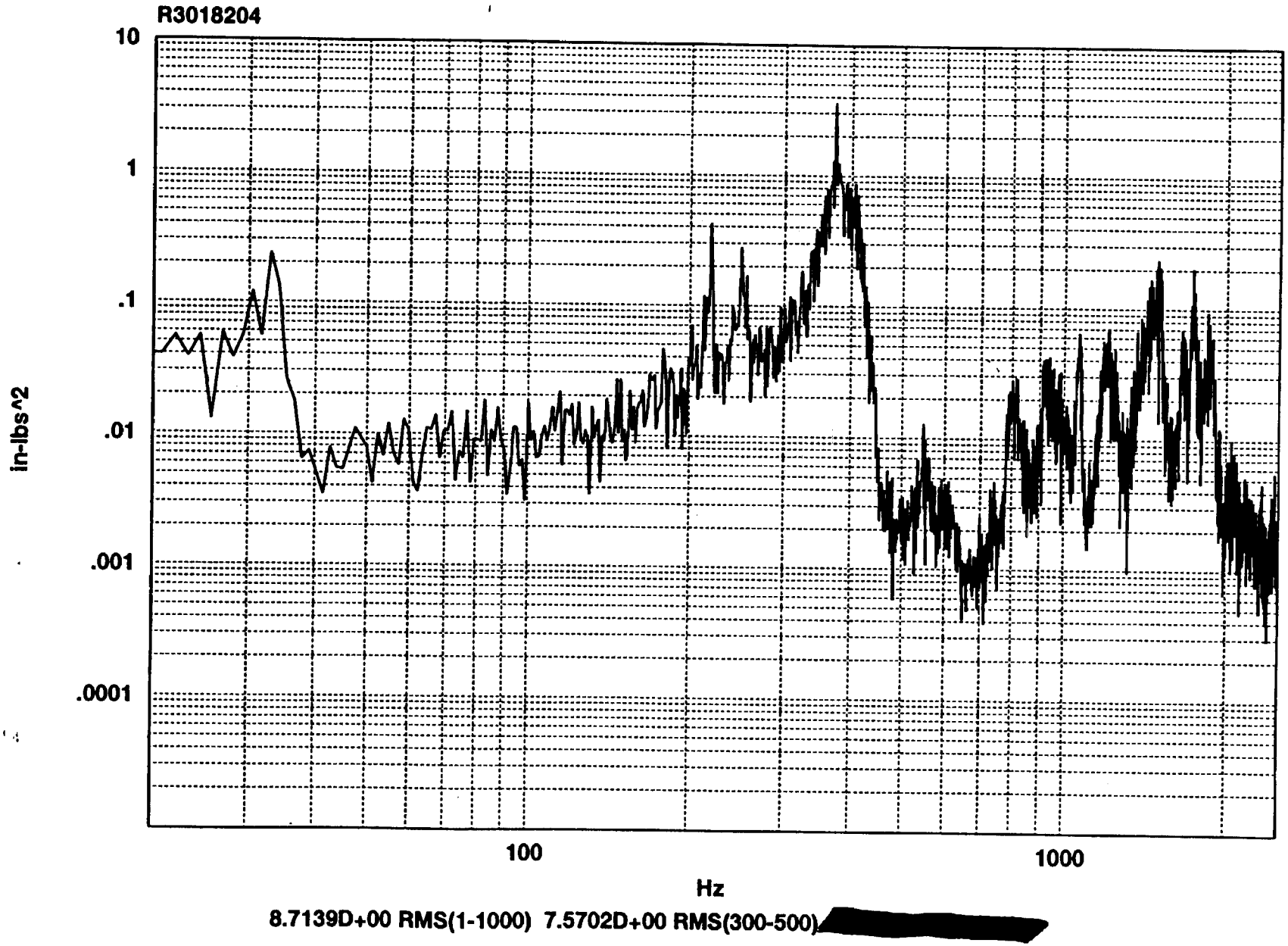
R3018204
10
1
.1
.01
.001
.0001
in-lbs^2
100
1000
Hz
8.7139D+00 RMS(1-1000) 7.5702D+00 RMS(300-500)

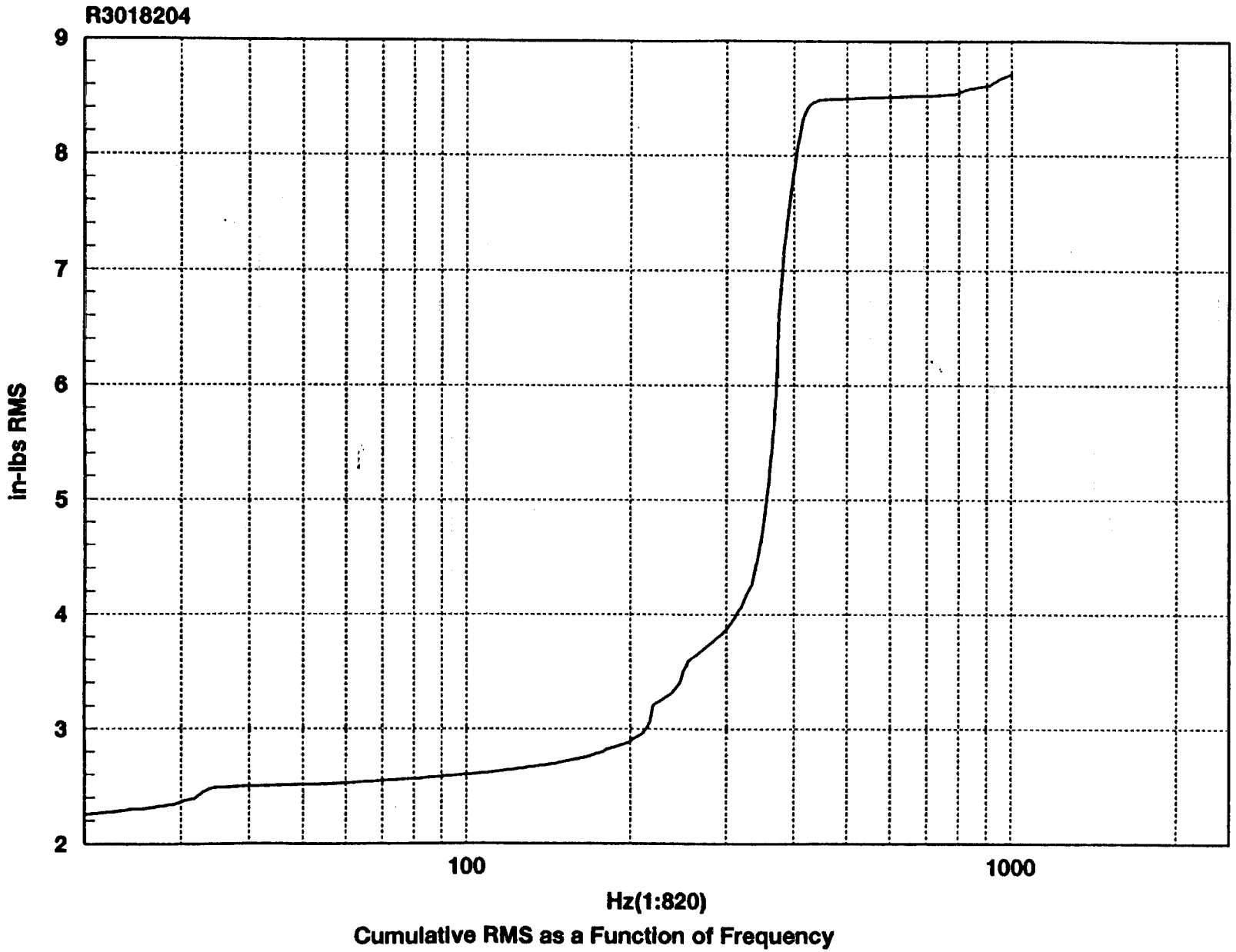

Cumulative RMS as a Function of Frequency

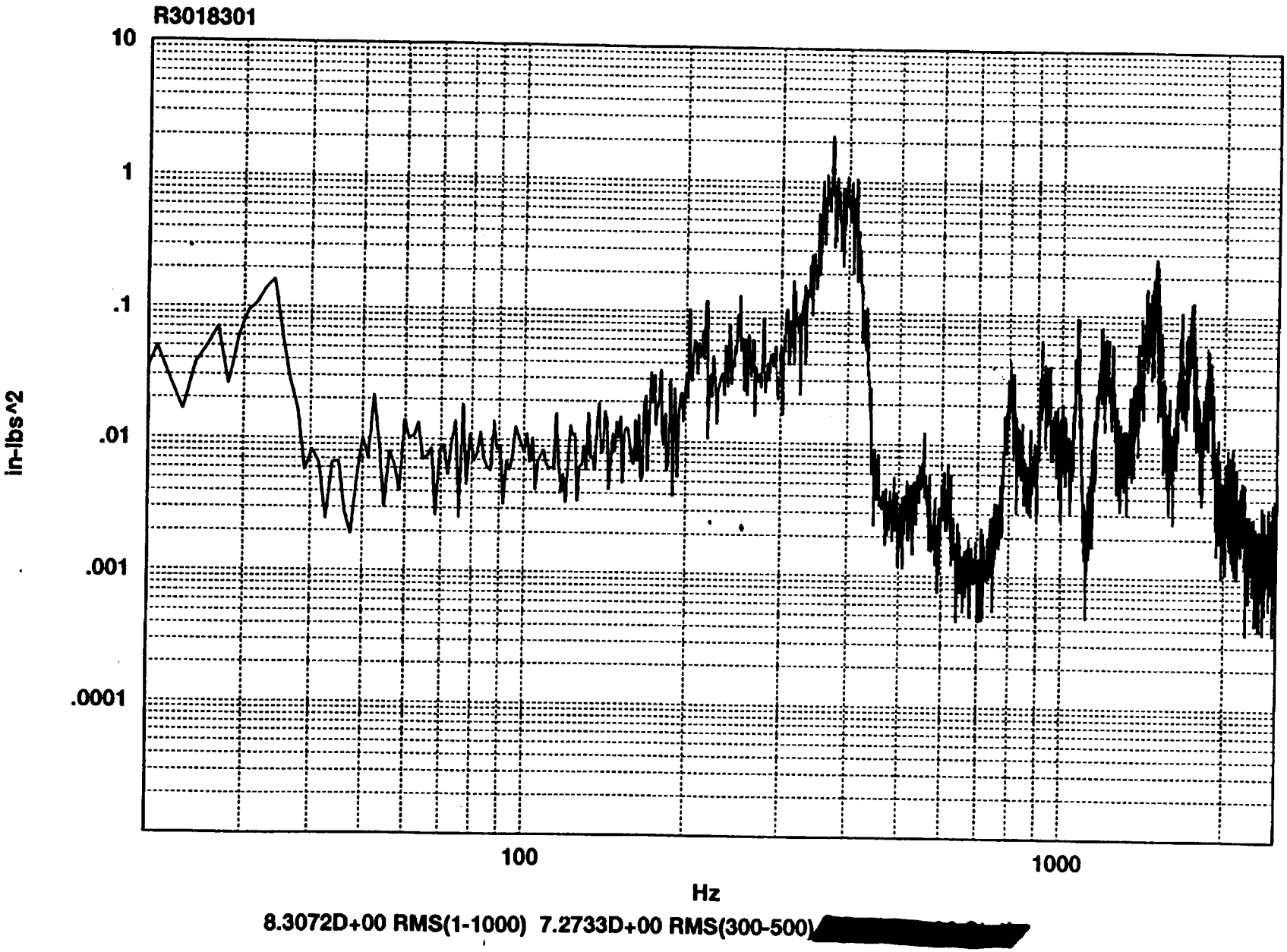
R3018301
10
1
.1
.01
.001
.0001
in-lbs^2
100
1000
Hz
8.3072D+00 RMS(1-1000) 7.2733D+00 RMS(300-500)

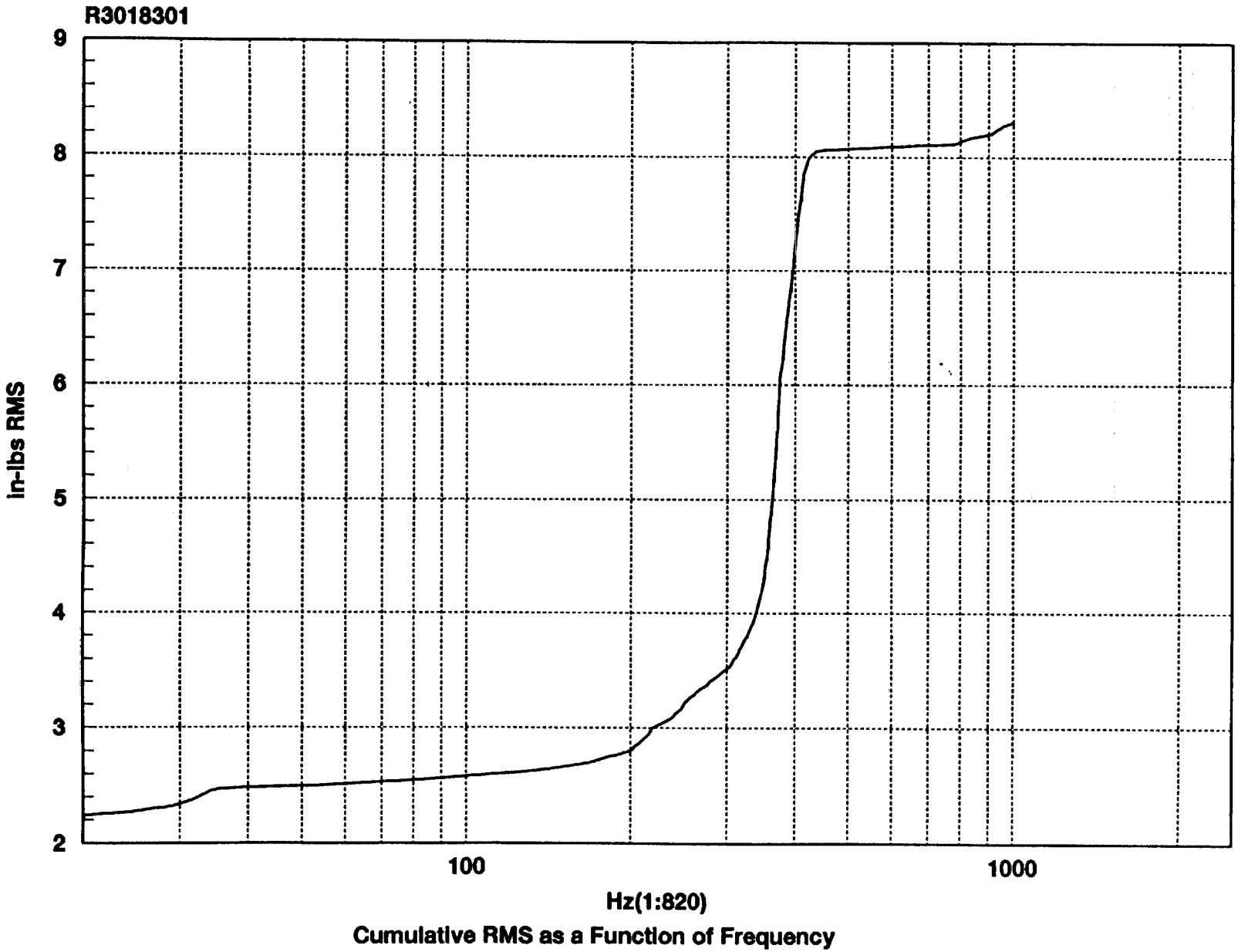

Cumulative RMS as a Function of Frequency

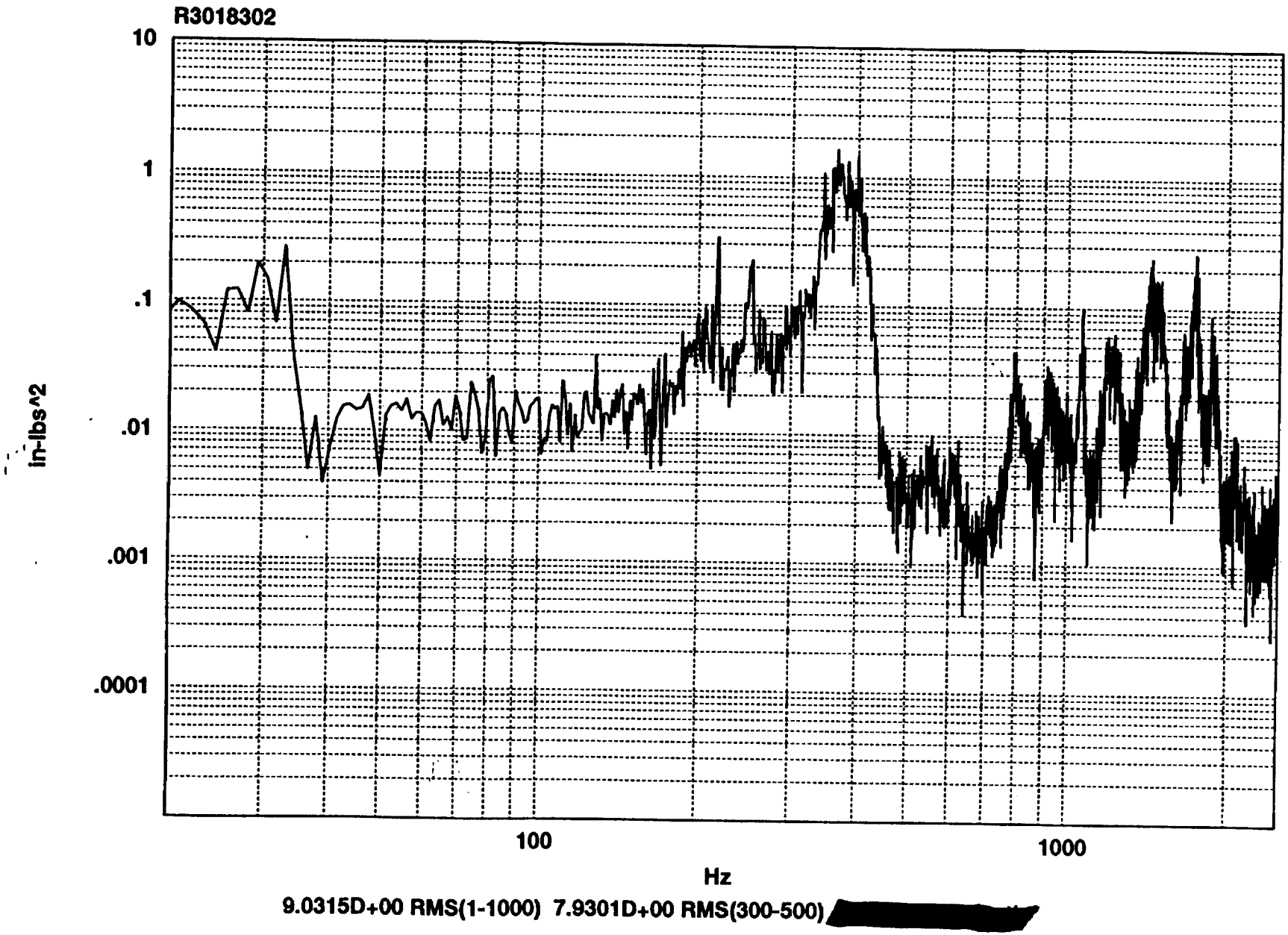
R3018302
10
1
.1
.01
.001
.0001
in-lbs^2
100
1000
Hz
9.0315D+00 RMS(1-1000) 7.9301D+00 RMS(300-500)

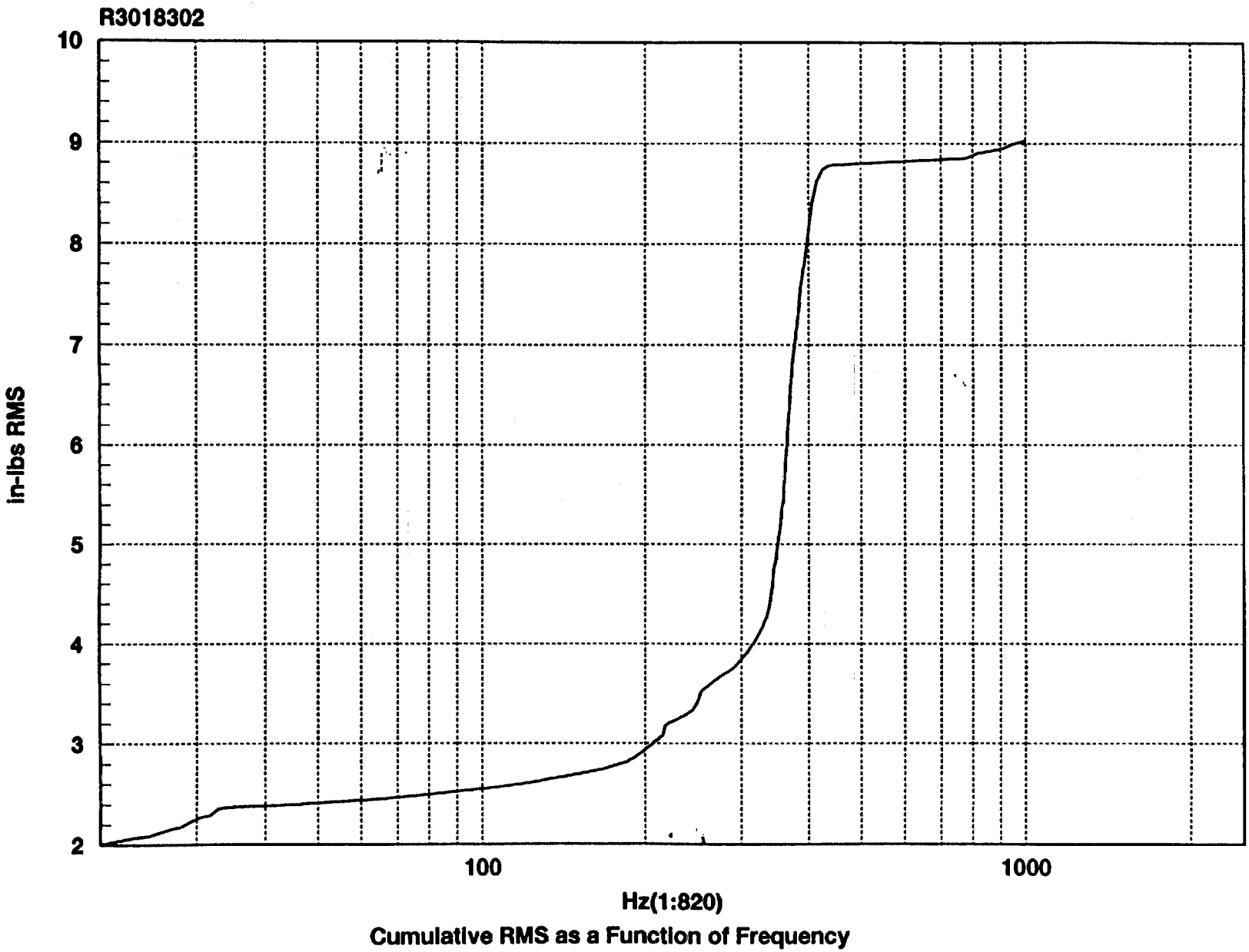
R3018302
10
9
8
7
6
5
4
3
2
in-lbs RMS
100
1000
Hz(1:820)
Cumulative RMS as a Function of Frequency

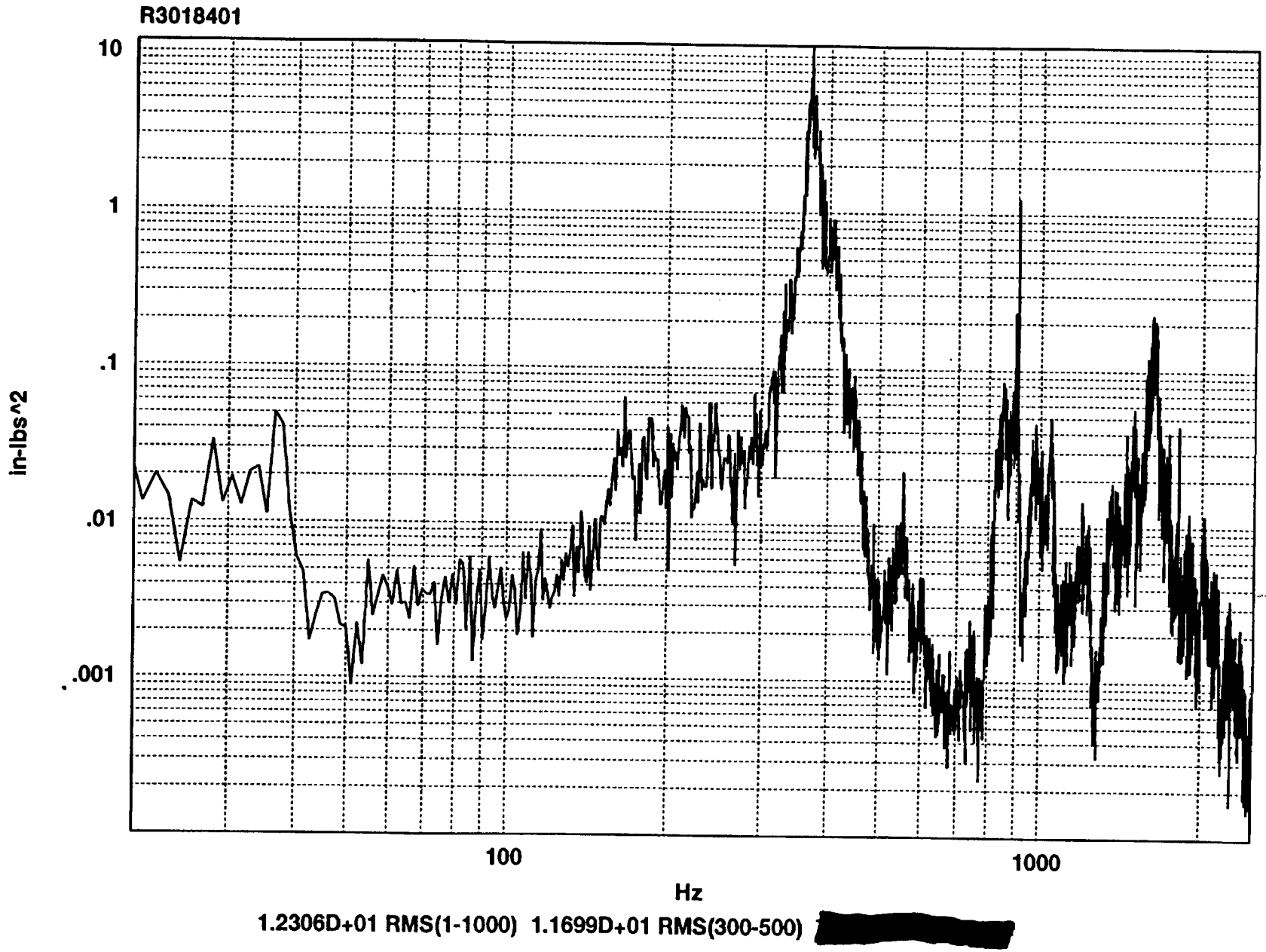
R3018401
10
1
.1
.01
.001
in-lbs^2
100
1000
Hz
1.2306D+01 RMS(1-1000) 1.1699D+01 RMS(300-500)

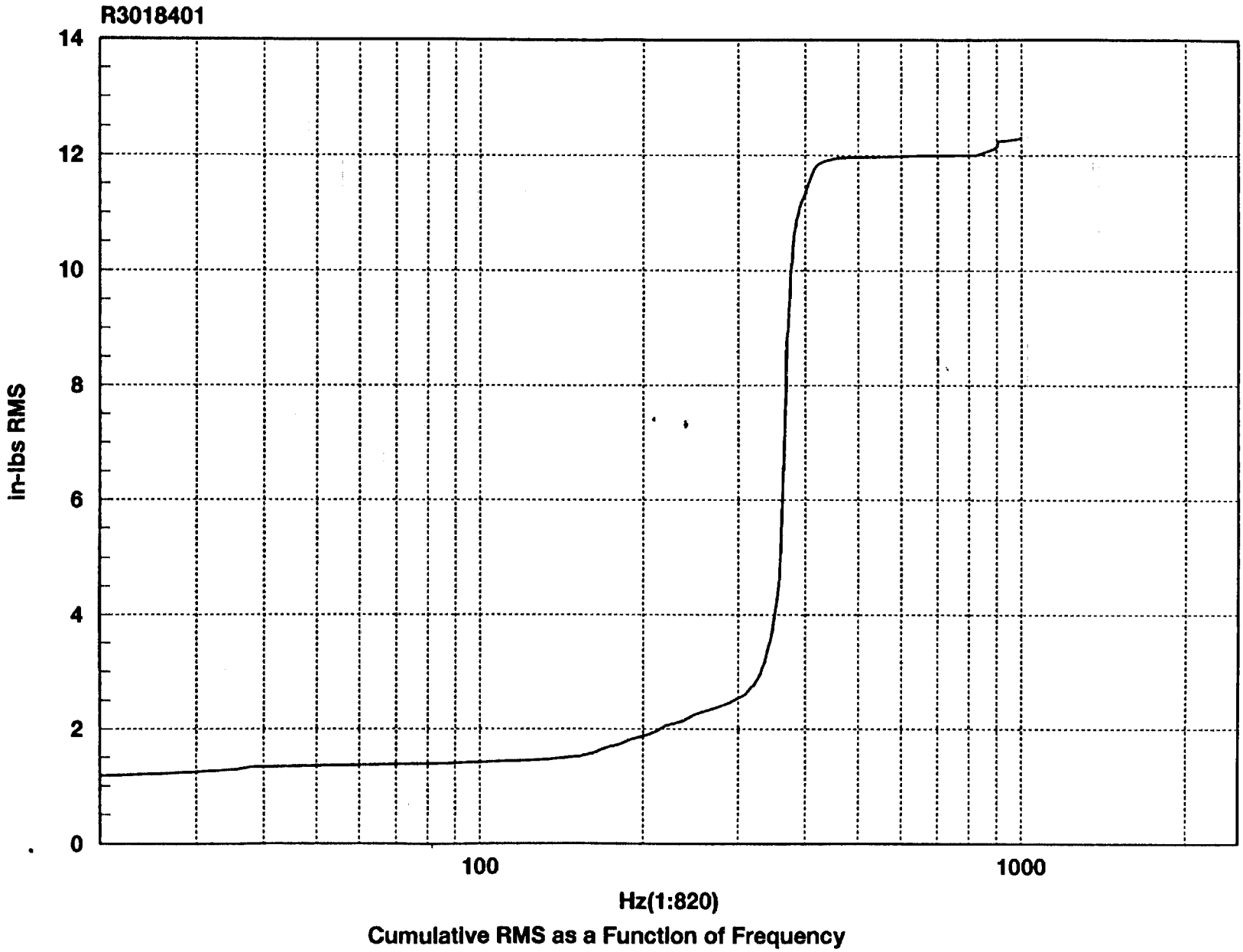
R3018401
14
12
10
8
6
4
2
0
in-lbs RMS
100
1000
Hz(1:820)
Cumulative RMS as a Function of Frequency

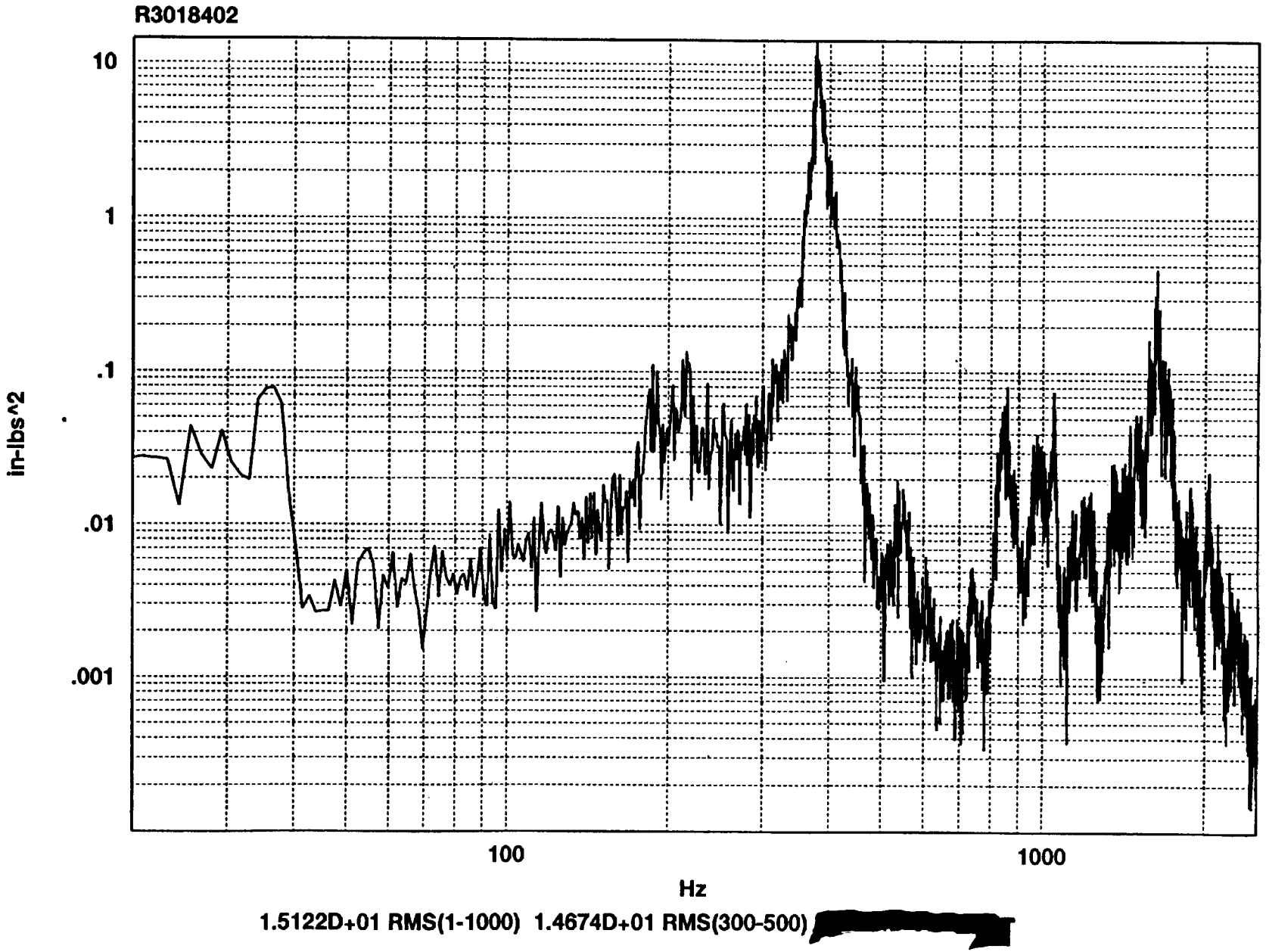
R3018402
10
1
.1
.01
.001
in-lbs^2
100
1000
Hz
1.5122D+01 RMS(1-1000) 1.4674D+01 RMS(300-500)

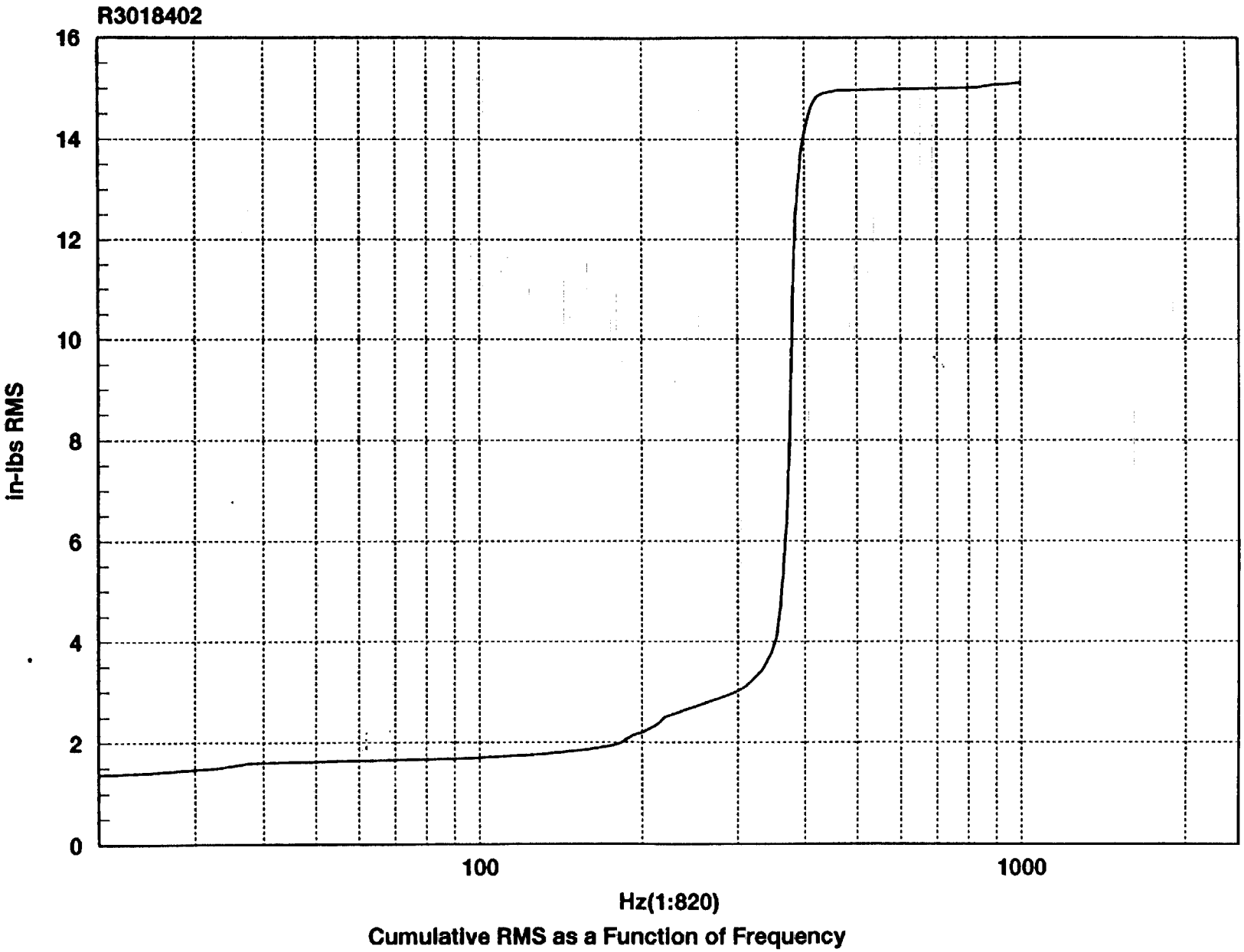
R3018402
16
14
12
10
8
6
4
2
0
in-lbs RMS
100
1000
Hz(1:820)
Cumulative RMS as a Function of Frequency

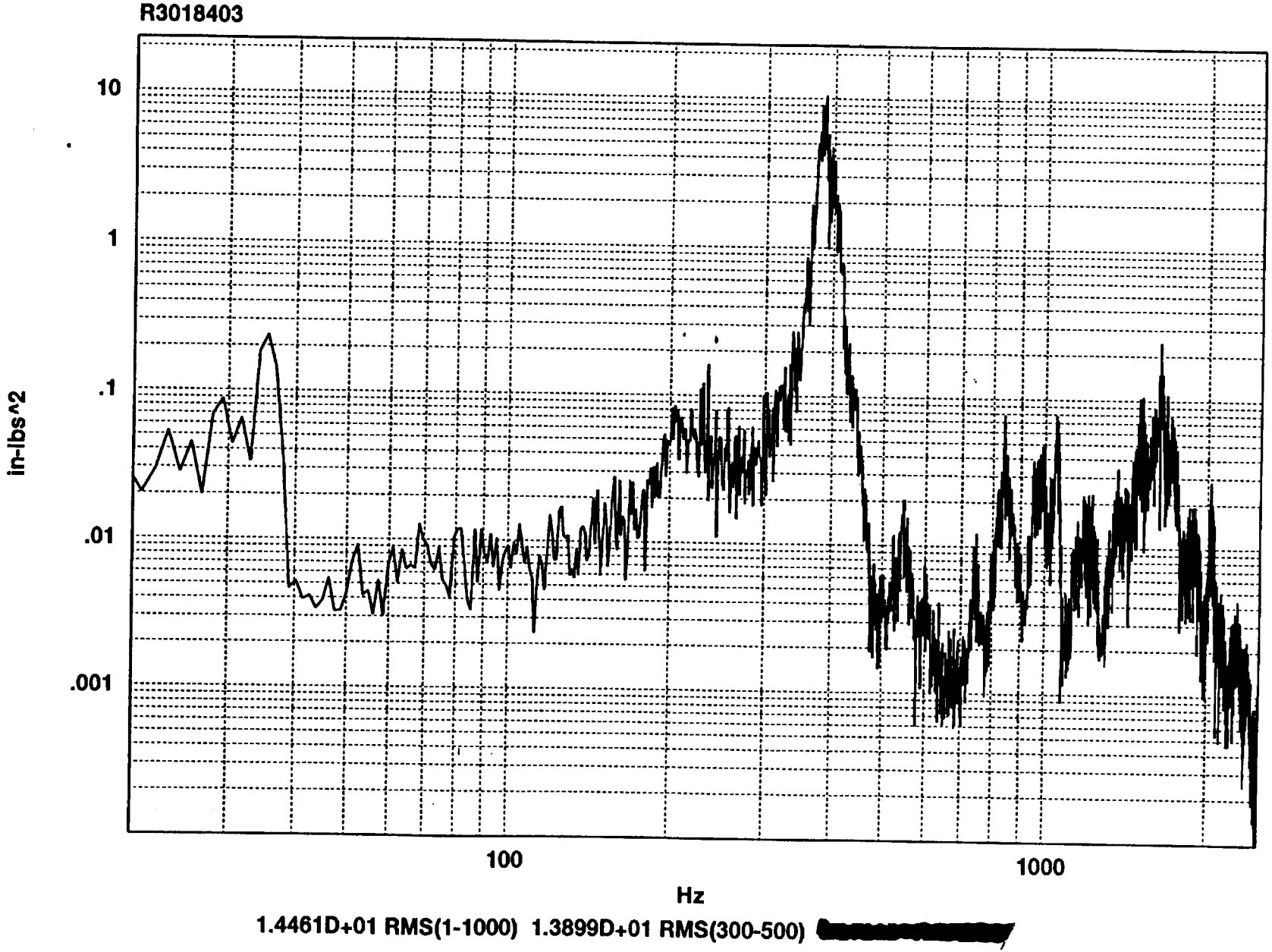
R3018403
10
1
.1
.01
.001
in-lbs^2
100
1000
Hz
1.4461D+01 RMS(1-1000) 1.3899D+01 RMS(300-500)

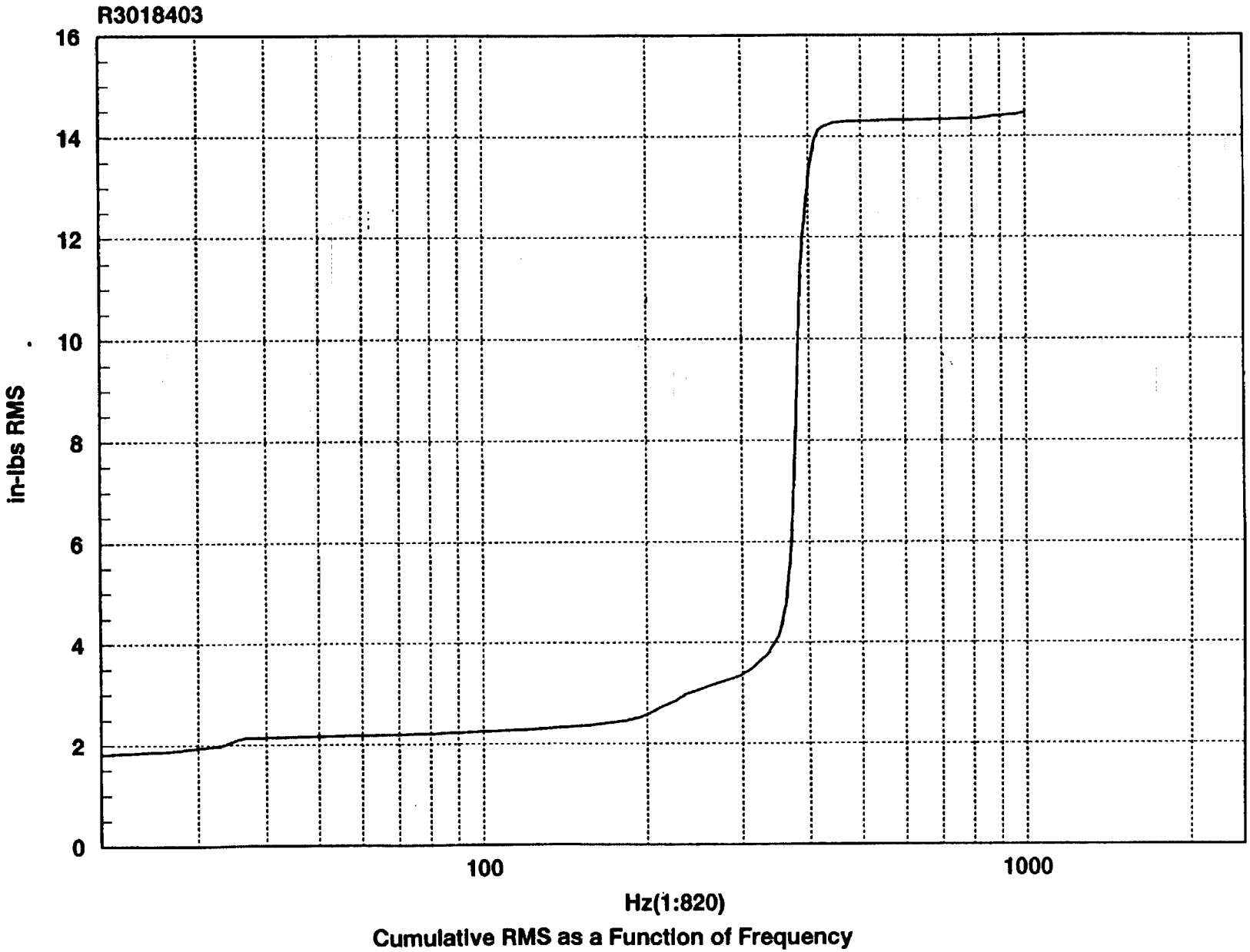

Cumulative RMS as a Function of Frequency

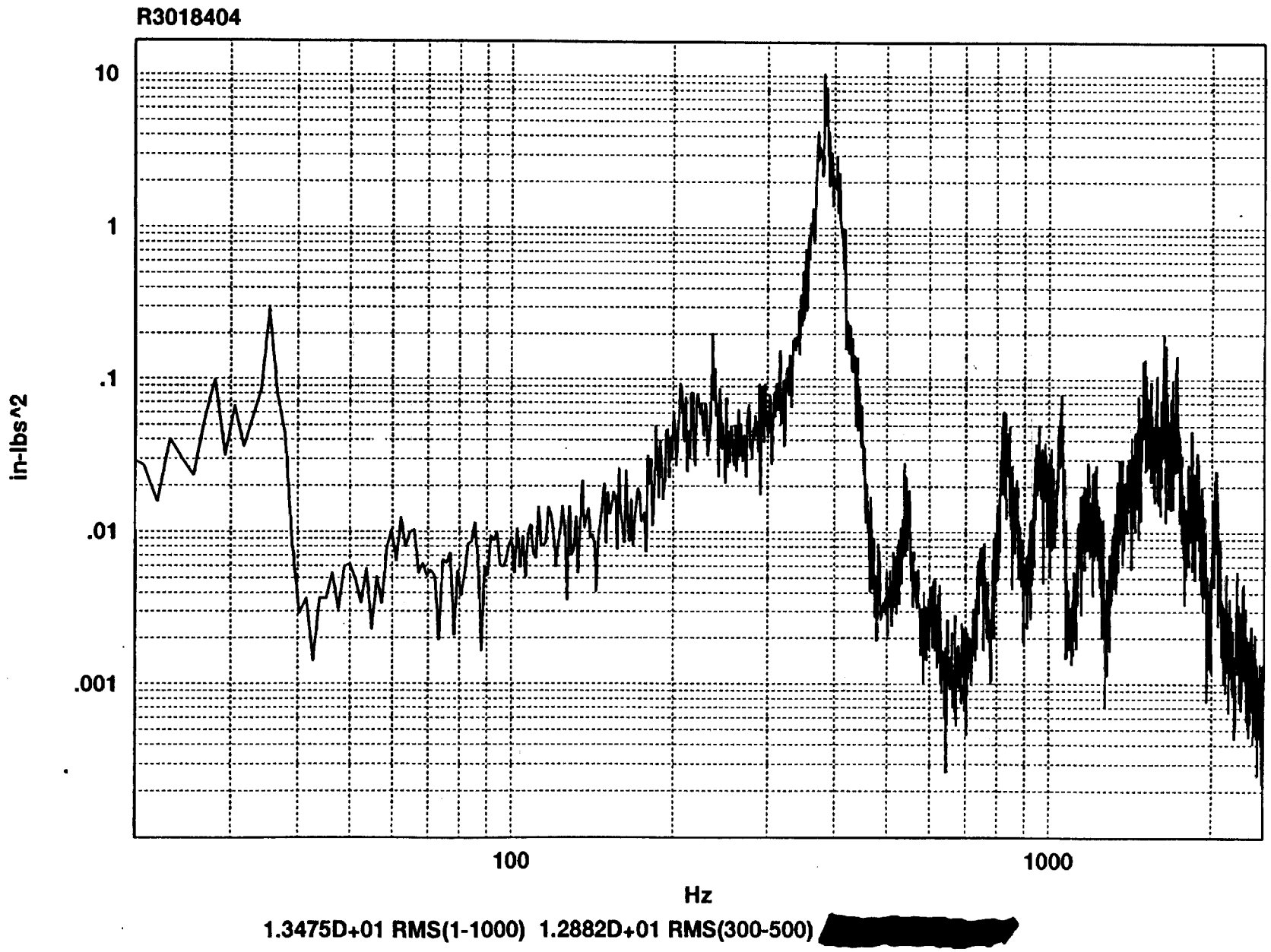
R3018404
10
1
.1
.01
.001
in-lbs^2
100
1000
Hz
1.3475D+01 RMS(1-1000) 1.2882D+01 RMS(300-500)

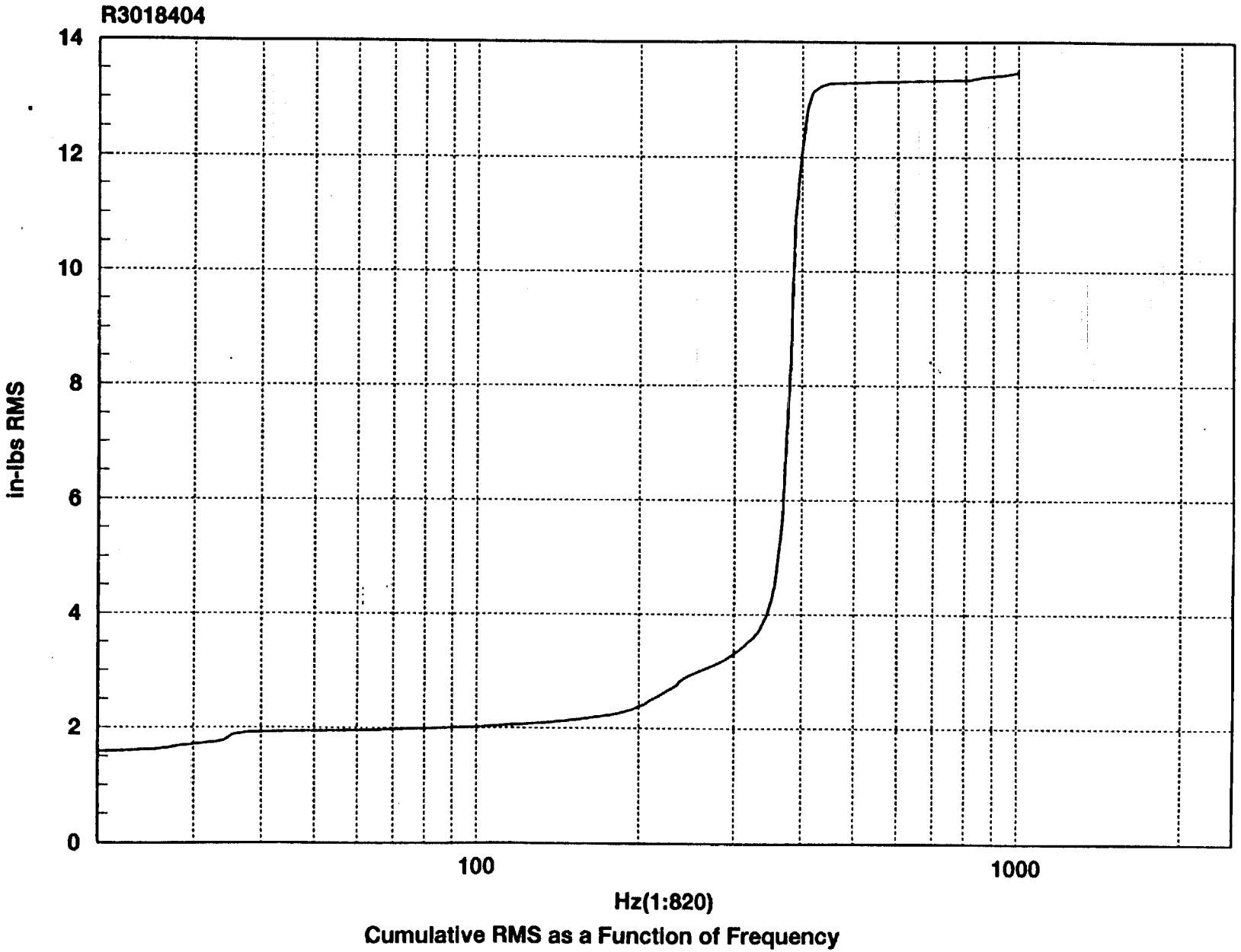

Cumulative RMS as a Function of Frequency

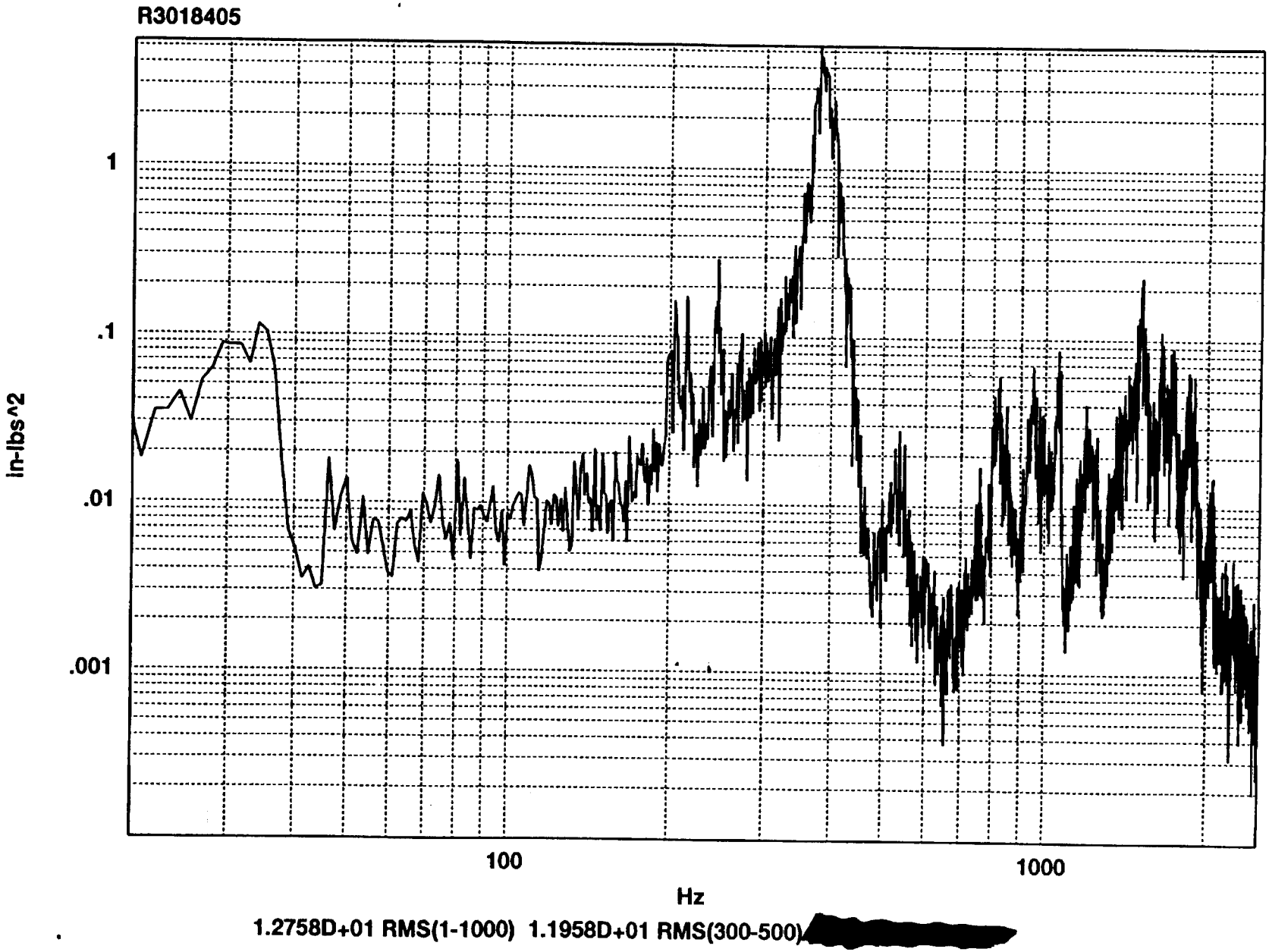
R3018405
1
.1
.01
.001
In-lbs^2
100
1000
Hz
1.2758D+01 RMS(1-1000) 1.1958D+01 RMS(300-500)

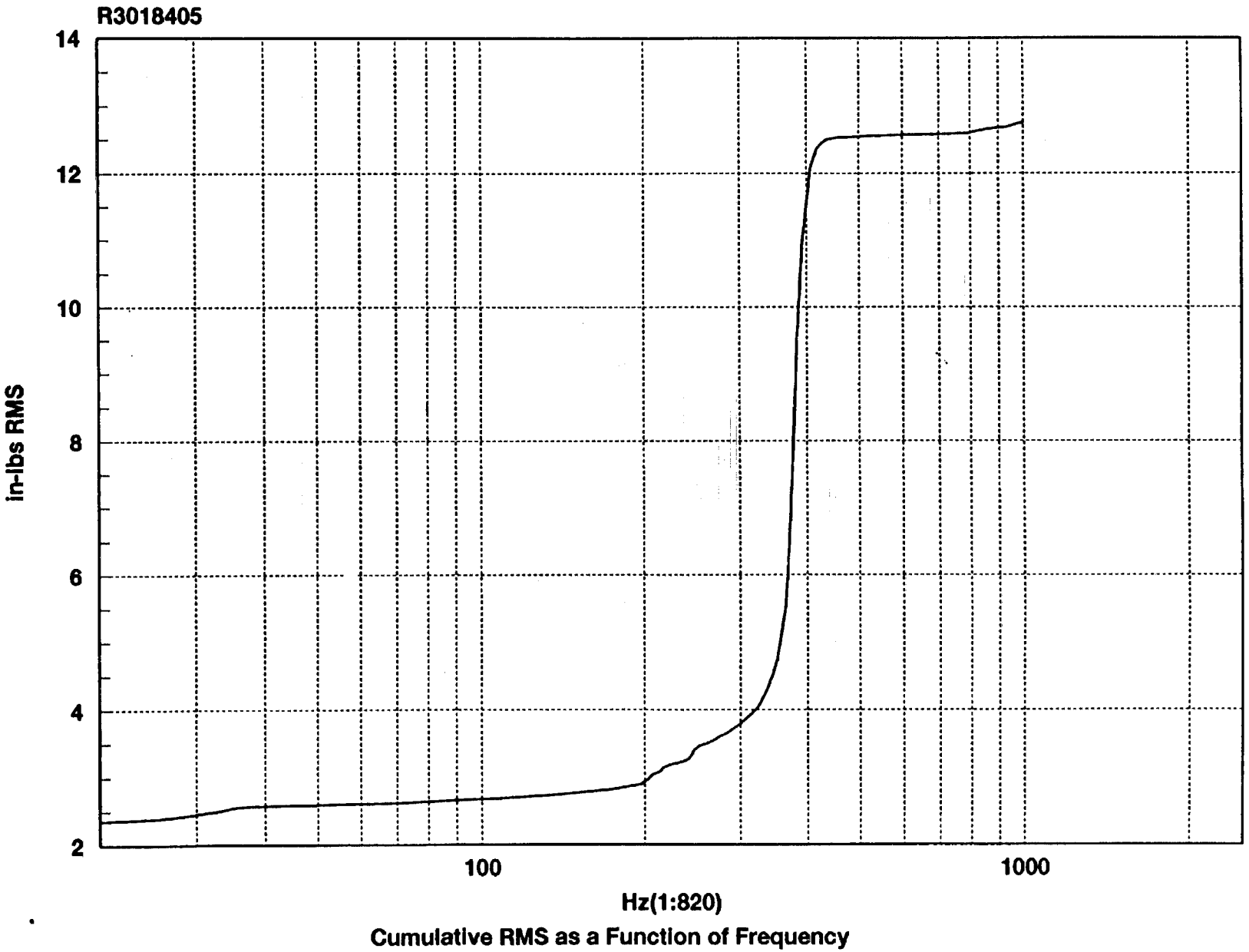
R3018405
14
12
10
8
6
4
2
in-lbs RMS
100
1000
Hz(1:820)
Cumulative RMS as a Function of Frequency

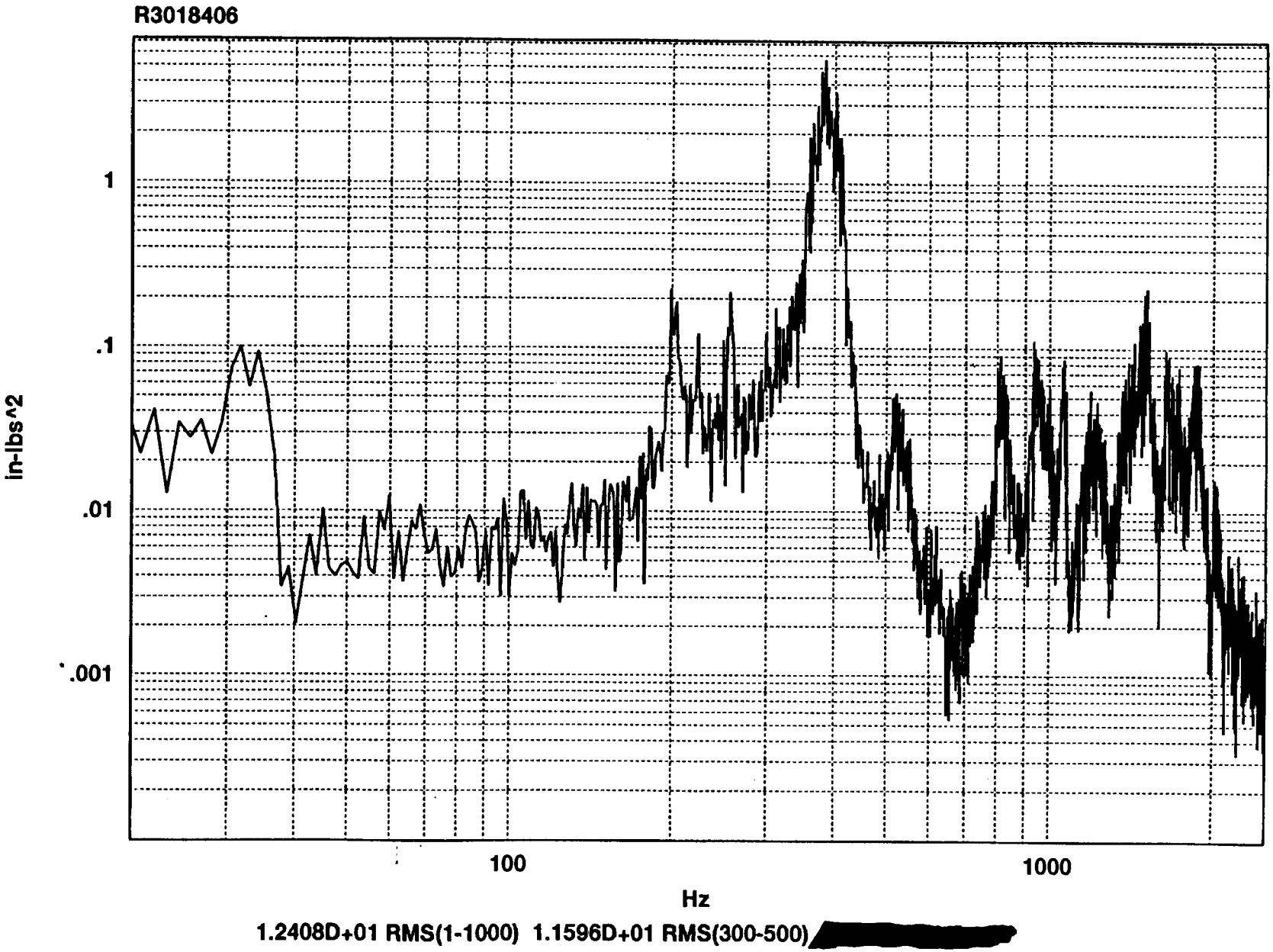
R3018406
1
.1
.01
.001
in-lbs^2
100
1000
Hz
1.2408D+01 RMS(1-1000) 1.1596D+01 RMS(300-500)

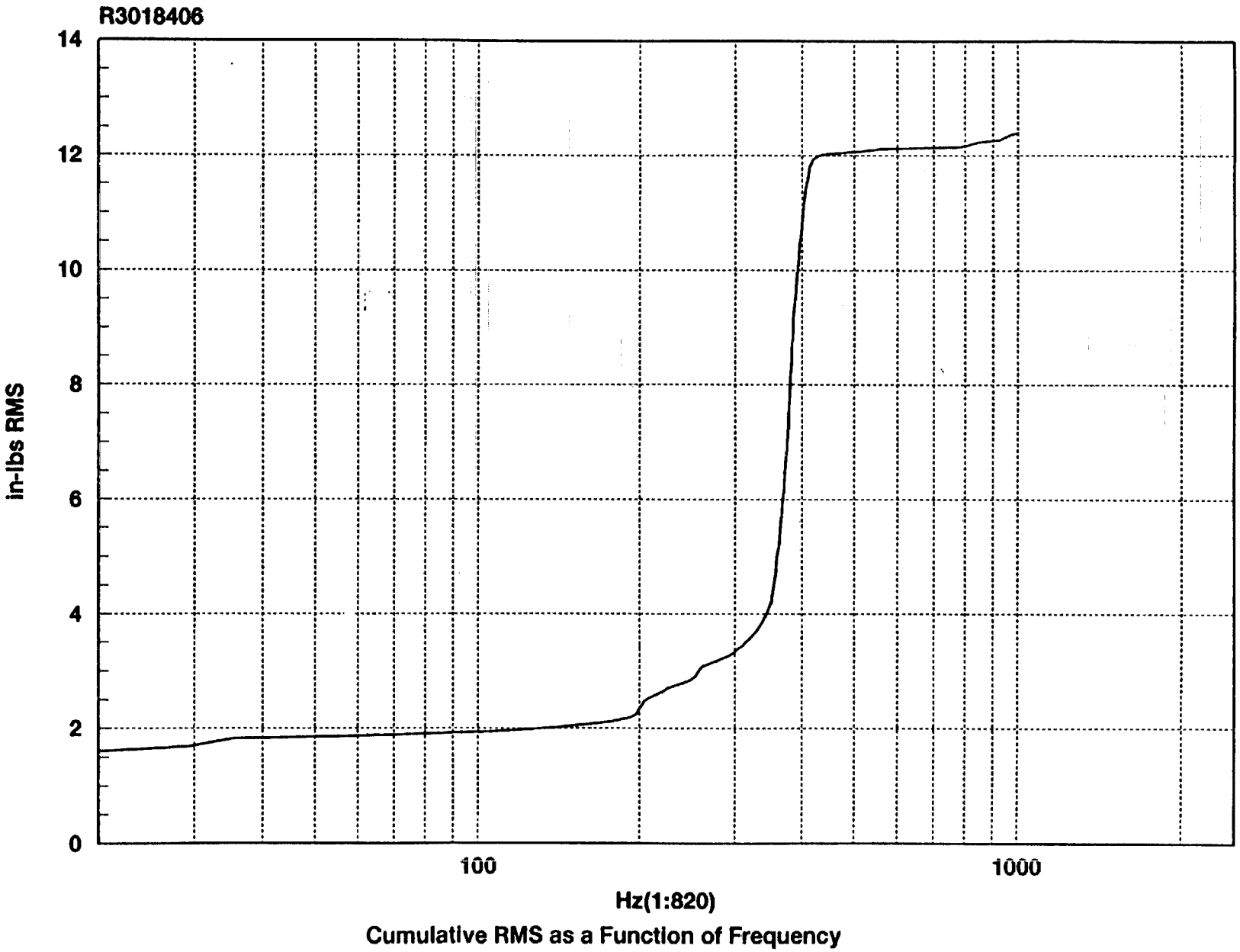
R3018406
14
12
10
8
6
4
2
0
in-lbs RMS
100
1000
Hz(1:820)
Cumulative RMS as a Function of Frequency

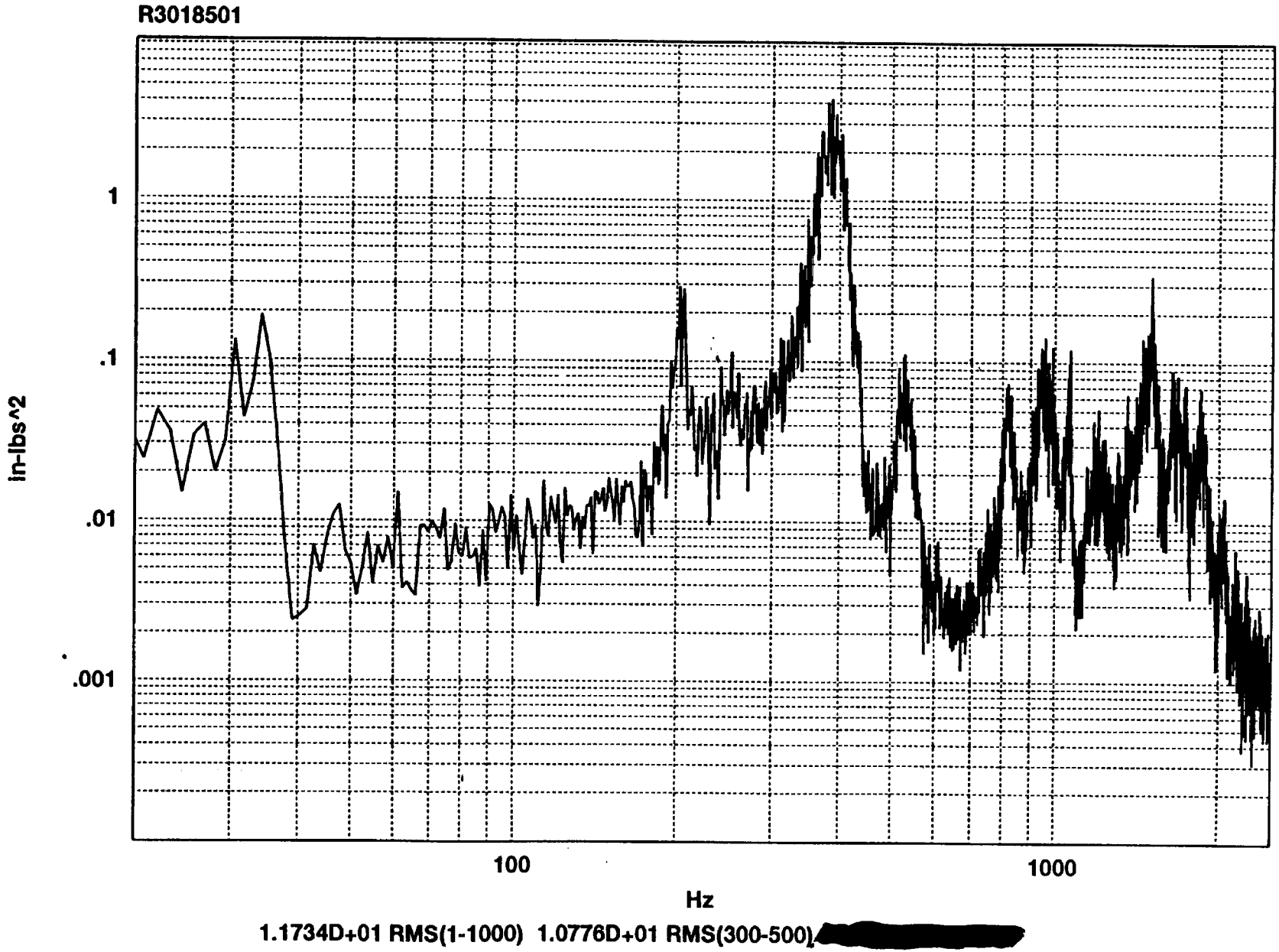
R3018501
1
.1
.01
.001
in-lbs^2
100
1000
Hz
1.1734D+01 RMS(1-1000) 1.0776D+01 RMS(300-500)

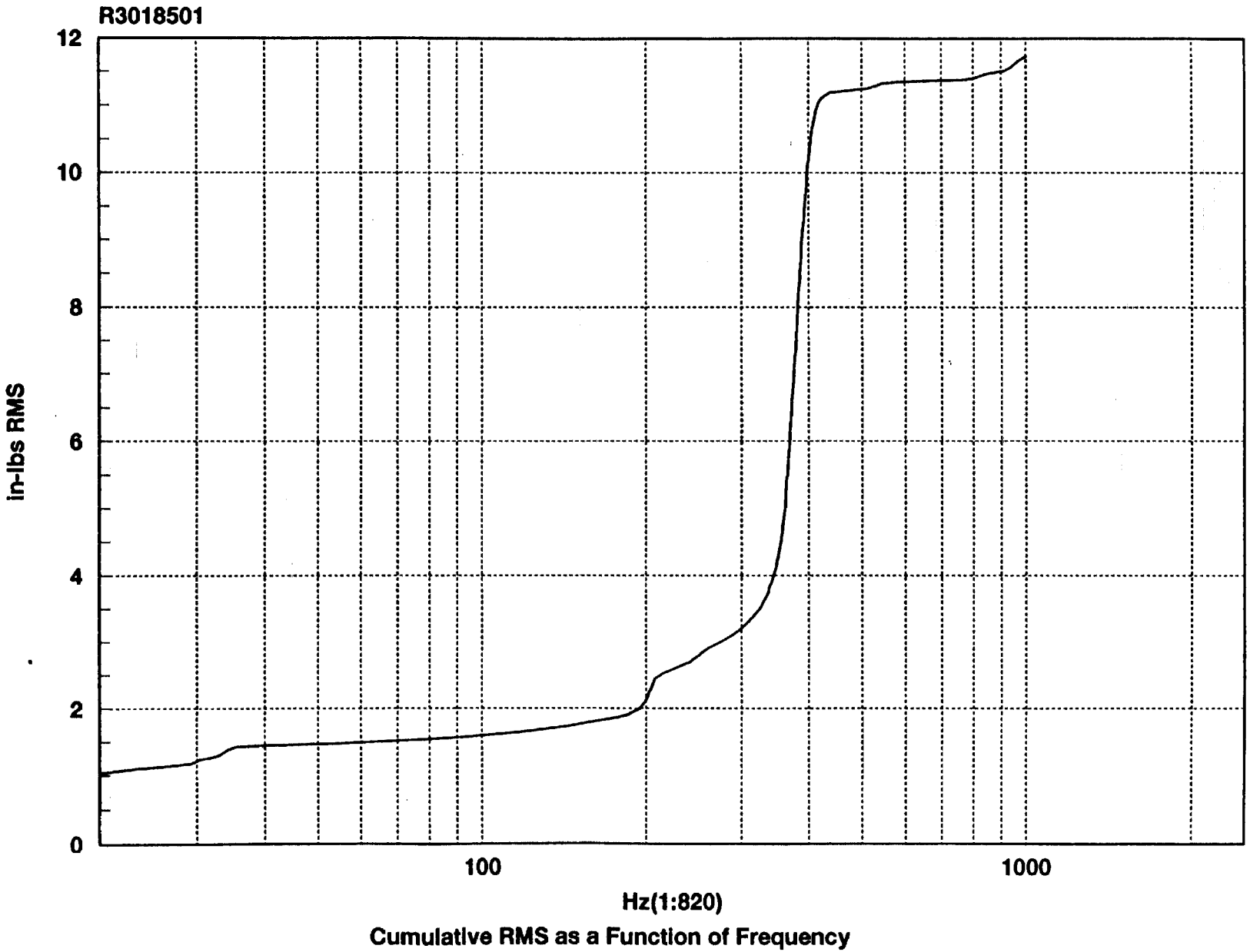

Cumulative RMS as a Function of Frequency

R3018502

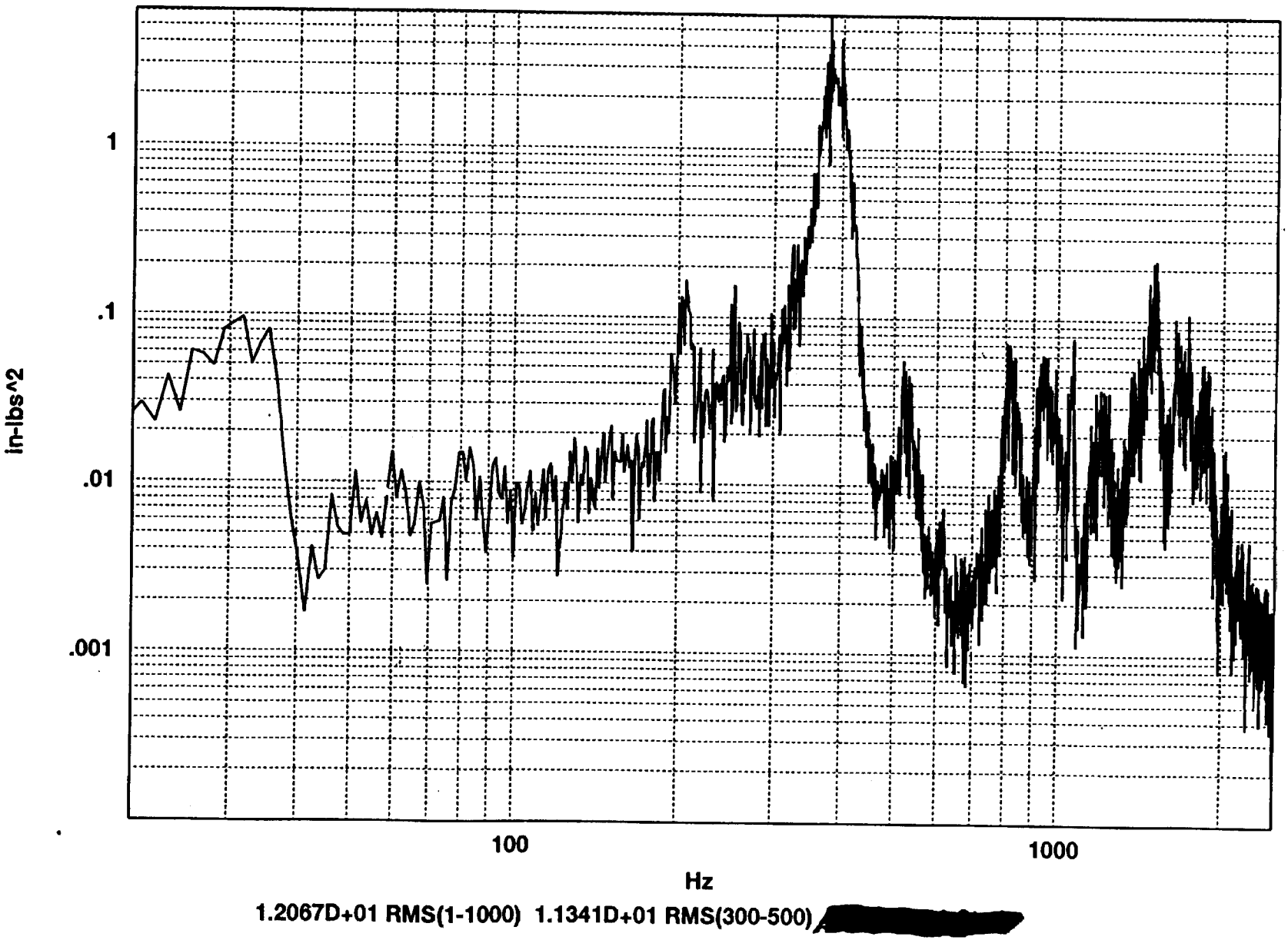

1.2067D+01 RMS(1-1000) 1.1341D+01 RMS(300-500) [redacted]

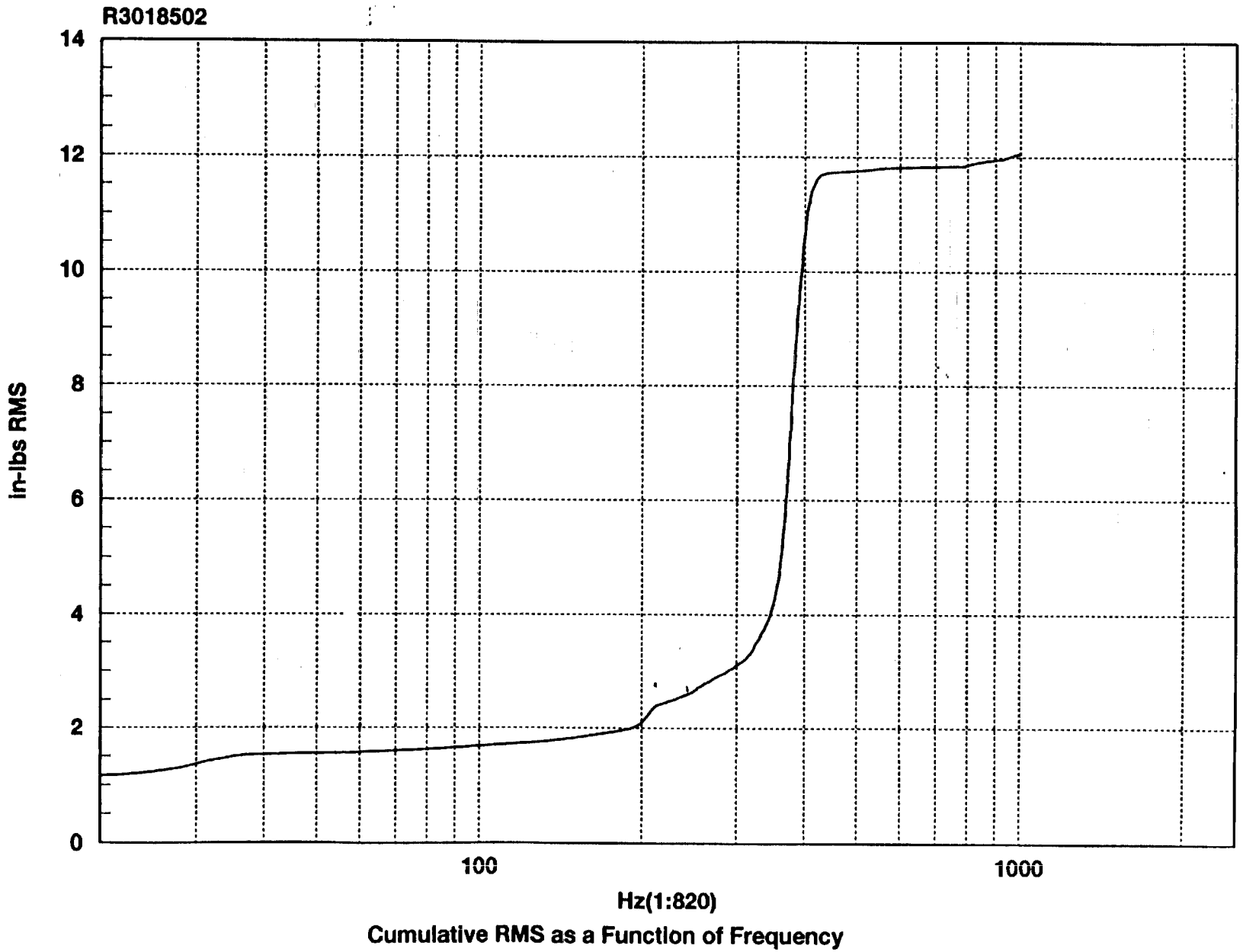
R3018502
14
12
10
8
6
4
2
0
in-lbs RMS
100
1000
Hz(1:820)
Cumulative RMS as a Function of Frequency

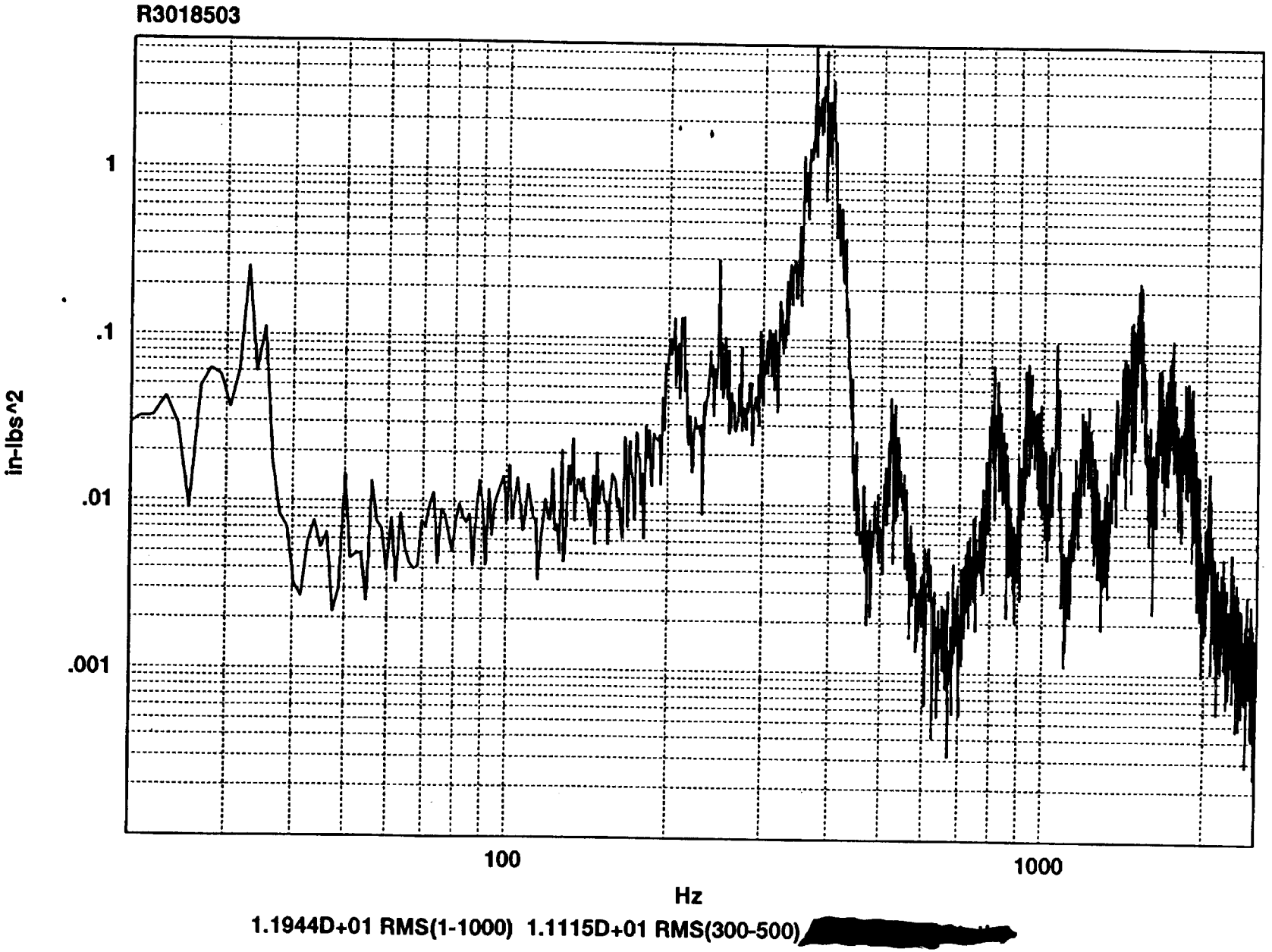
R3018503
1
.1
.01
.001
in-lbs^2
100
1000
Hz
1.1944D+01 RMS(1-1000) 1.1115D+01 RMS(300-500)

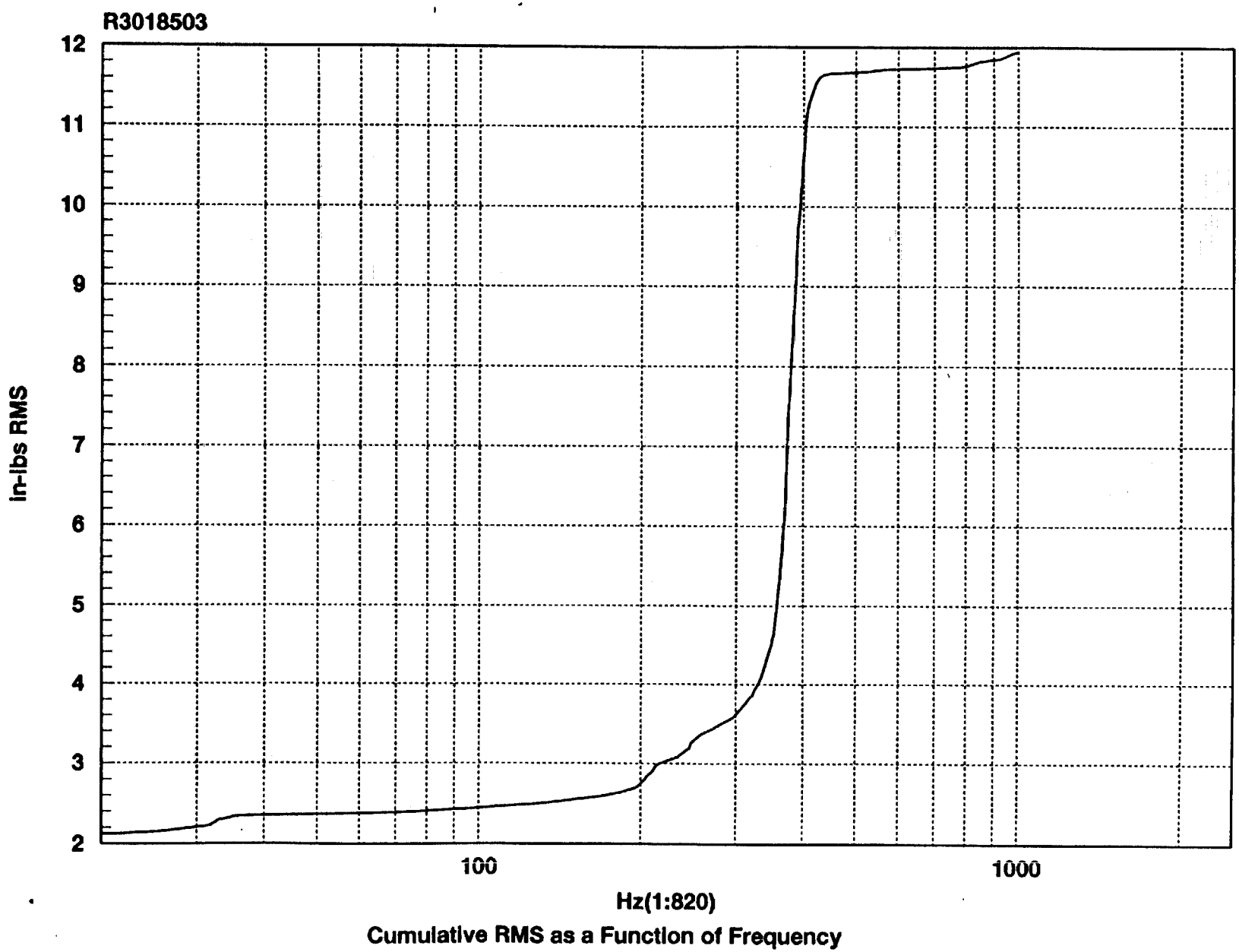

Cumulative RMS as a Function of Frequency

R3018504

1.1303D+01 RMS(1-1000) 1.0550D+01 RMS(300-500) [redacted]

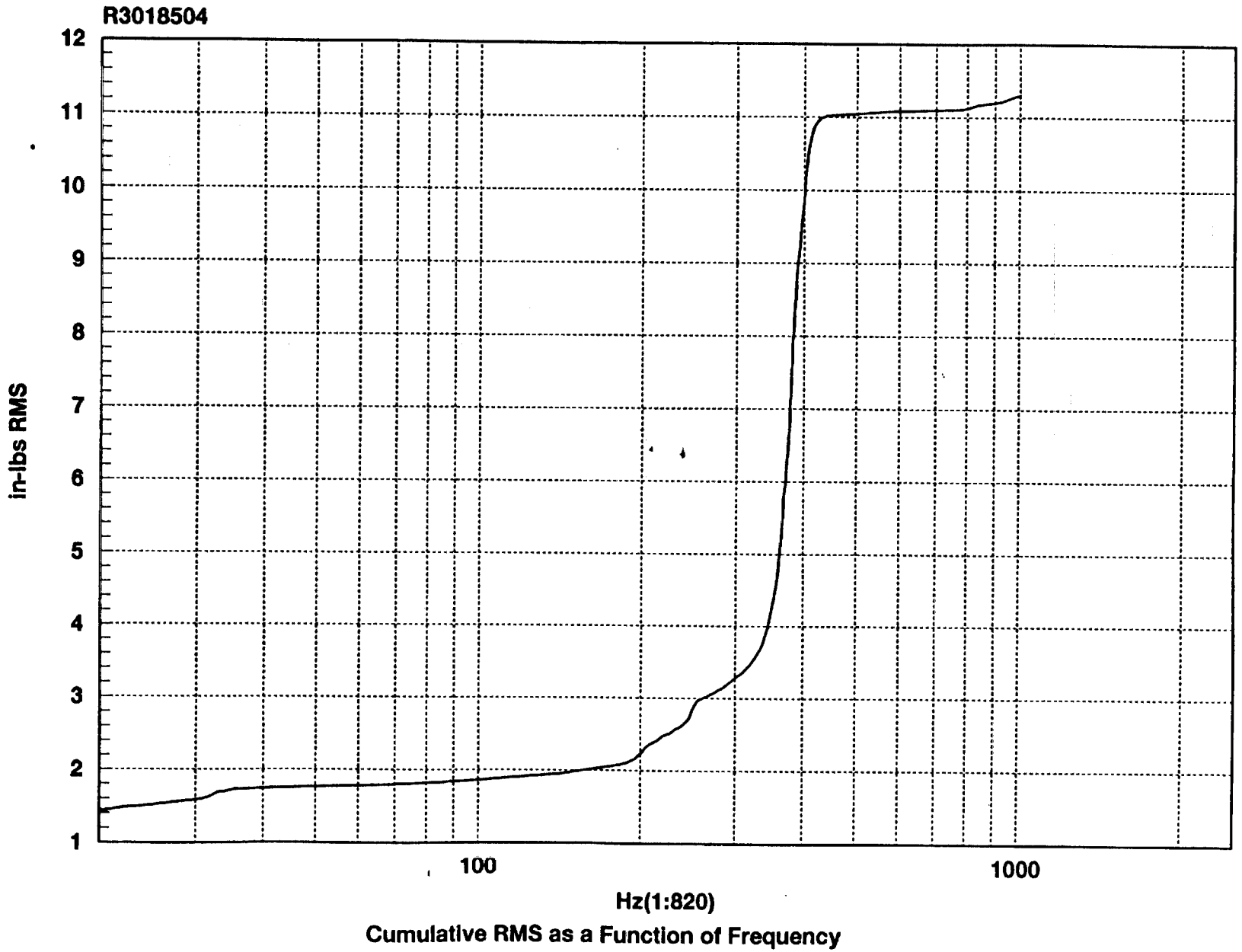

Cumulative RMS as a Function of Frequency

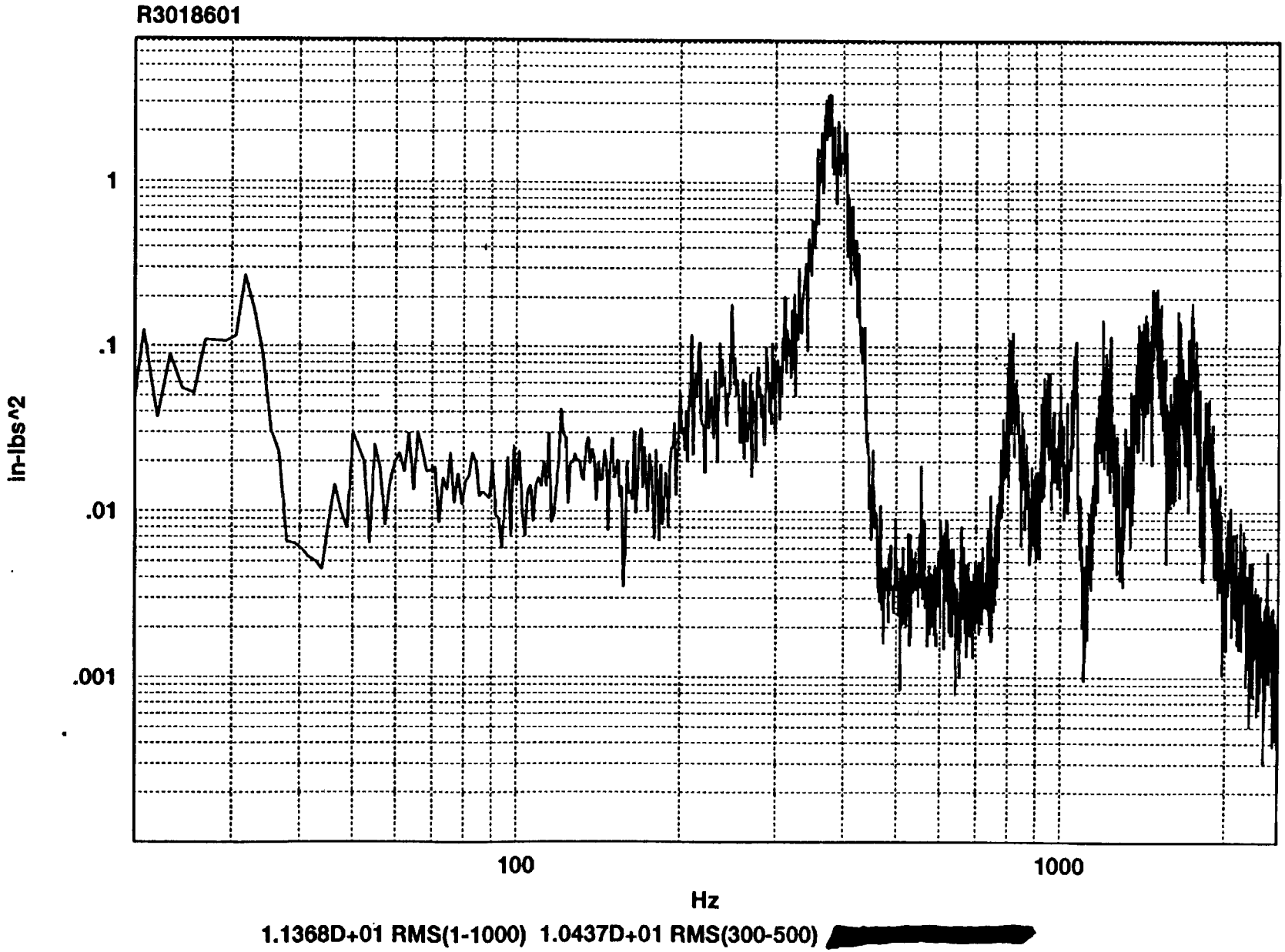
R3018601
1
.1
.01
.001
in-lbs^2
100
1000
Hz
1.1368D+01 RMS(1-1000) 1.0437D+01 RMS(300-500)

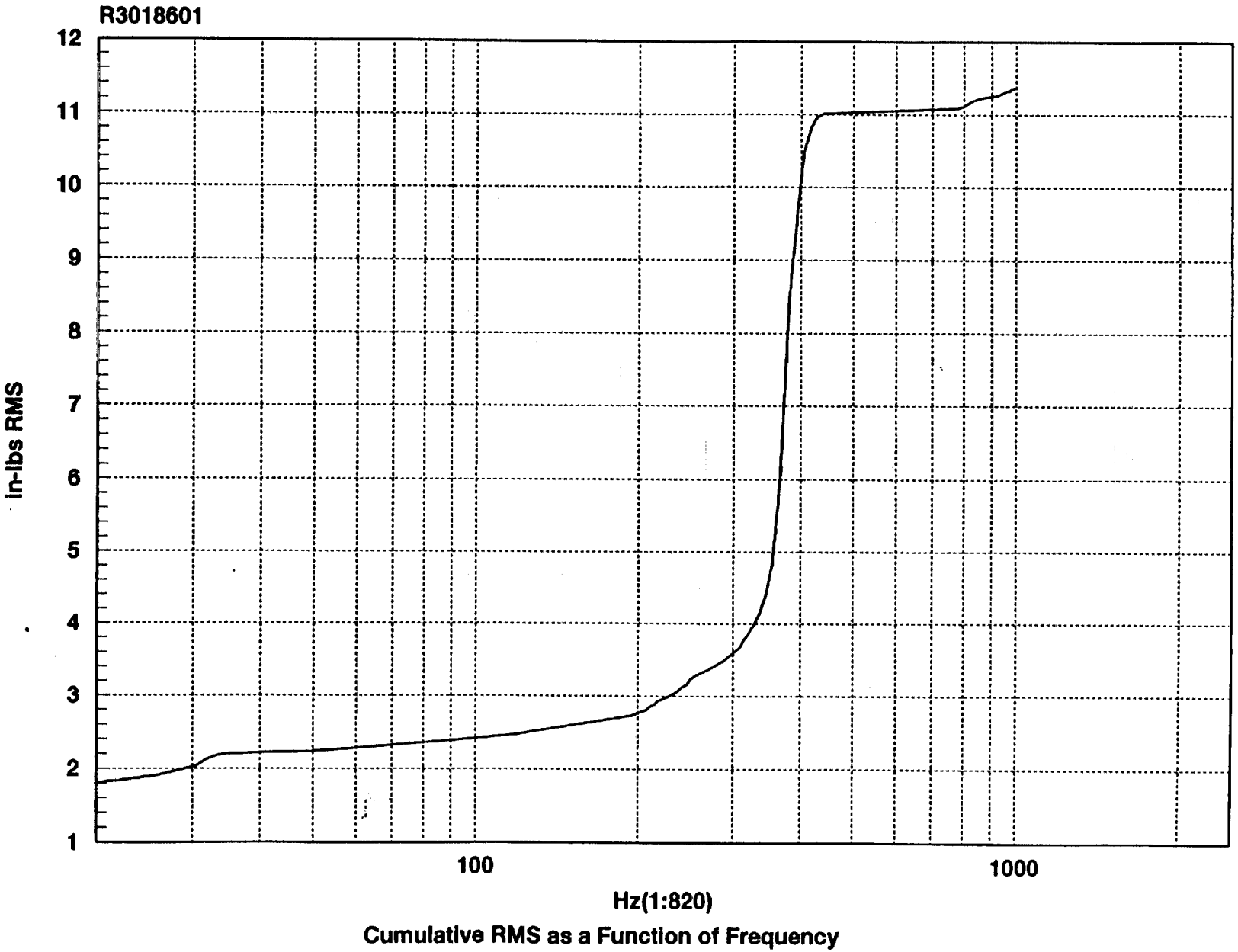

Cumulative RMS as a Function of Frequency

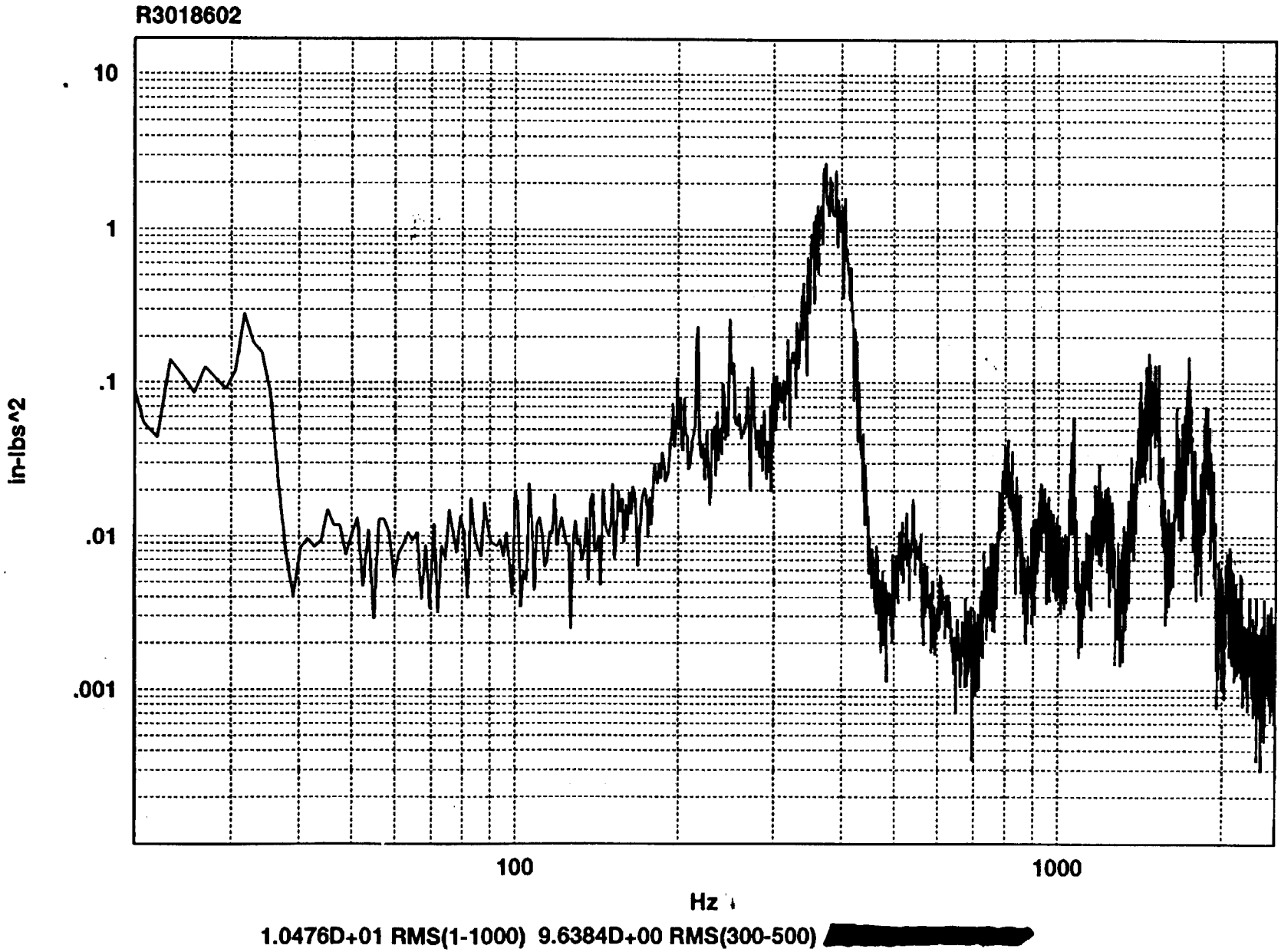
R3018602
10
1
.1
.01
.001
in-lbs^2
100
1000
Hz
1.0476D+01 RMS(1-1000) 9.6384D+00 RMS(300-500)

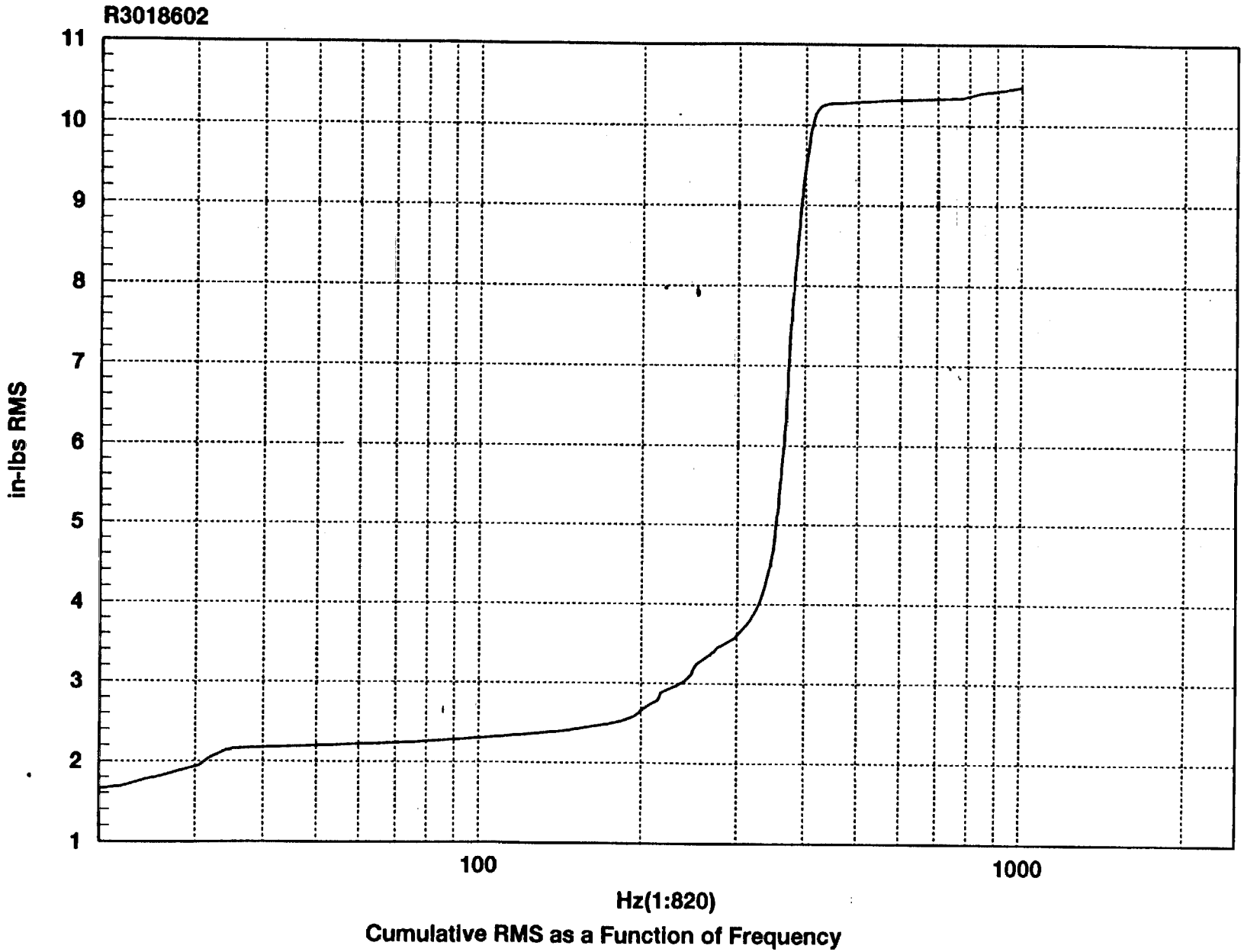
R3018602
11
10
9
8
7
6
5
4
3
2
1
in-lbs RMS
100
1000
Hz(1:820)
Cumulative RMS as a Function of Frequency

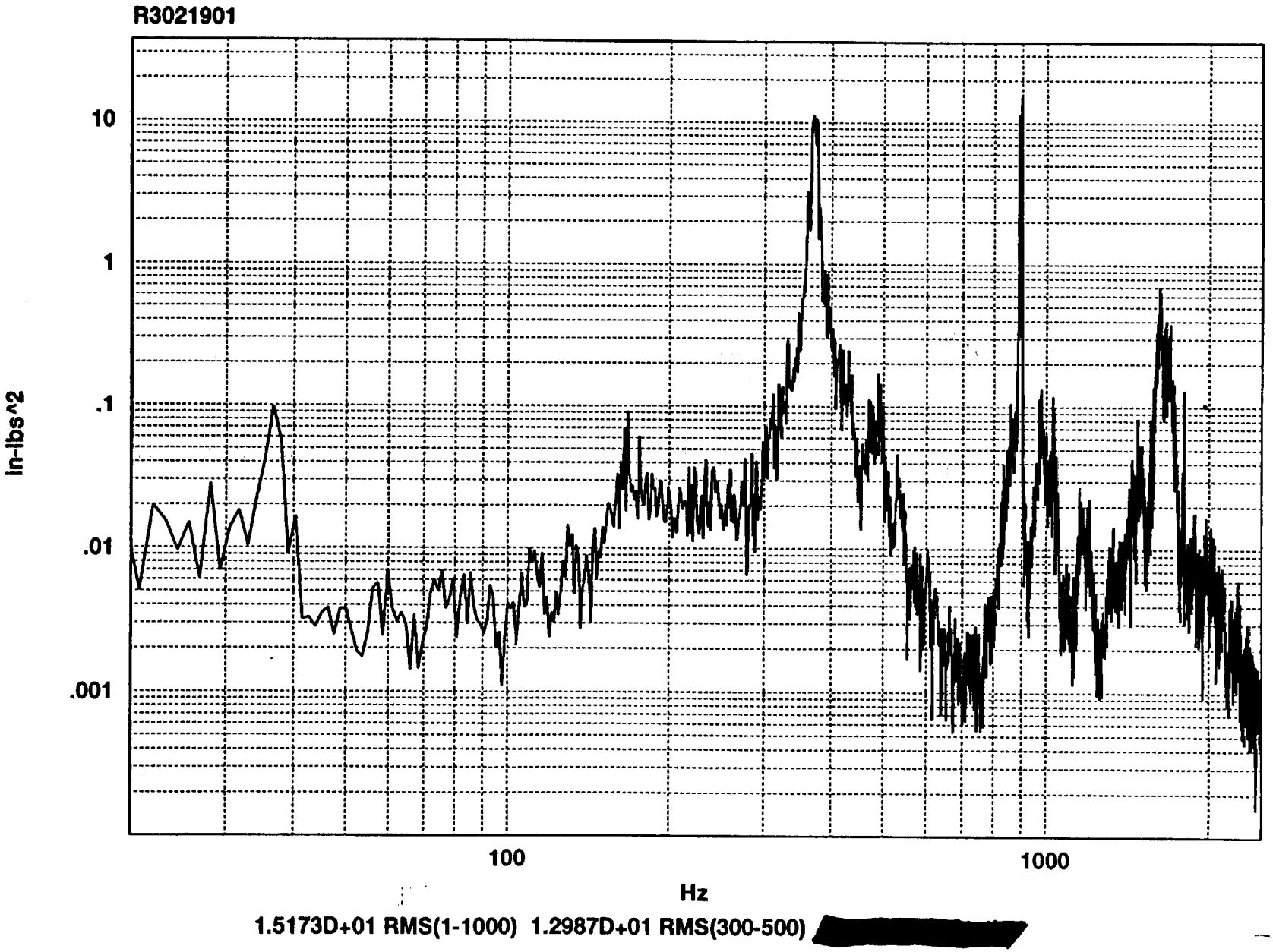
R3021901
10
1
.1
.01
.001
In-lbs^2
100
1000
Hz
1.5173D+01 RMS(1-1000) 1.2987D+01 RMS(300-500)

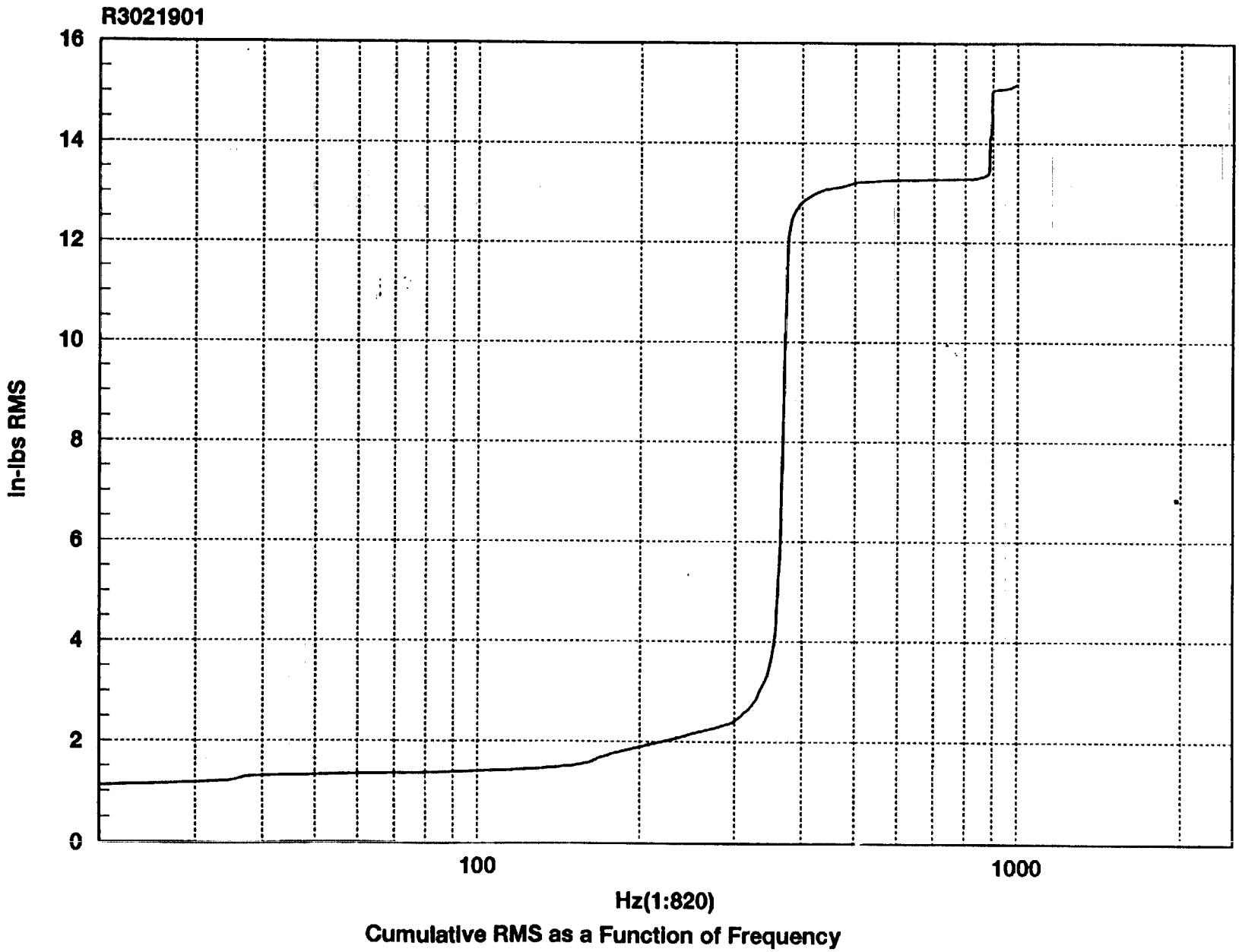
R3021901
16
14
12
10
8
6
4
2
0
In-lbs RMS
100
1000
Hz(1:820)
Cumulative RMS as a Function of Frequency

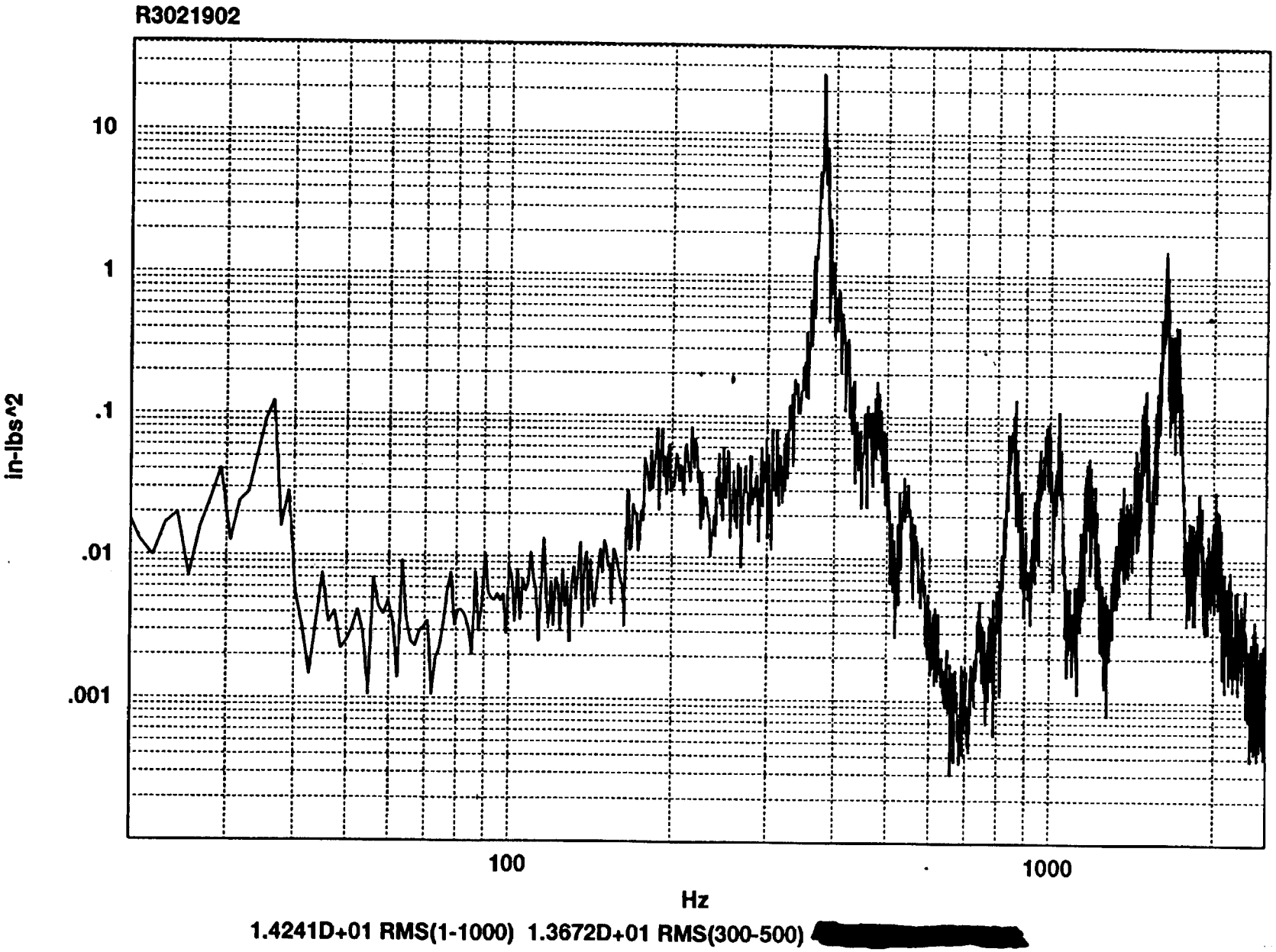
R3021902
10
1
.1
.01
.001
in-lbs^2
100
1000
Hz
1.4241D+01 RMS(1-1000) 1.3672D+01 RMS(300-500)

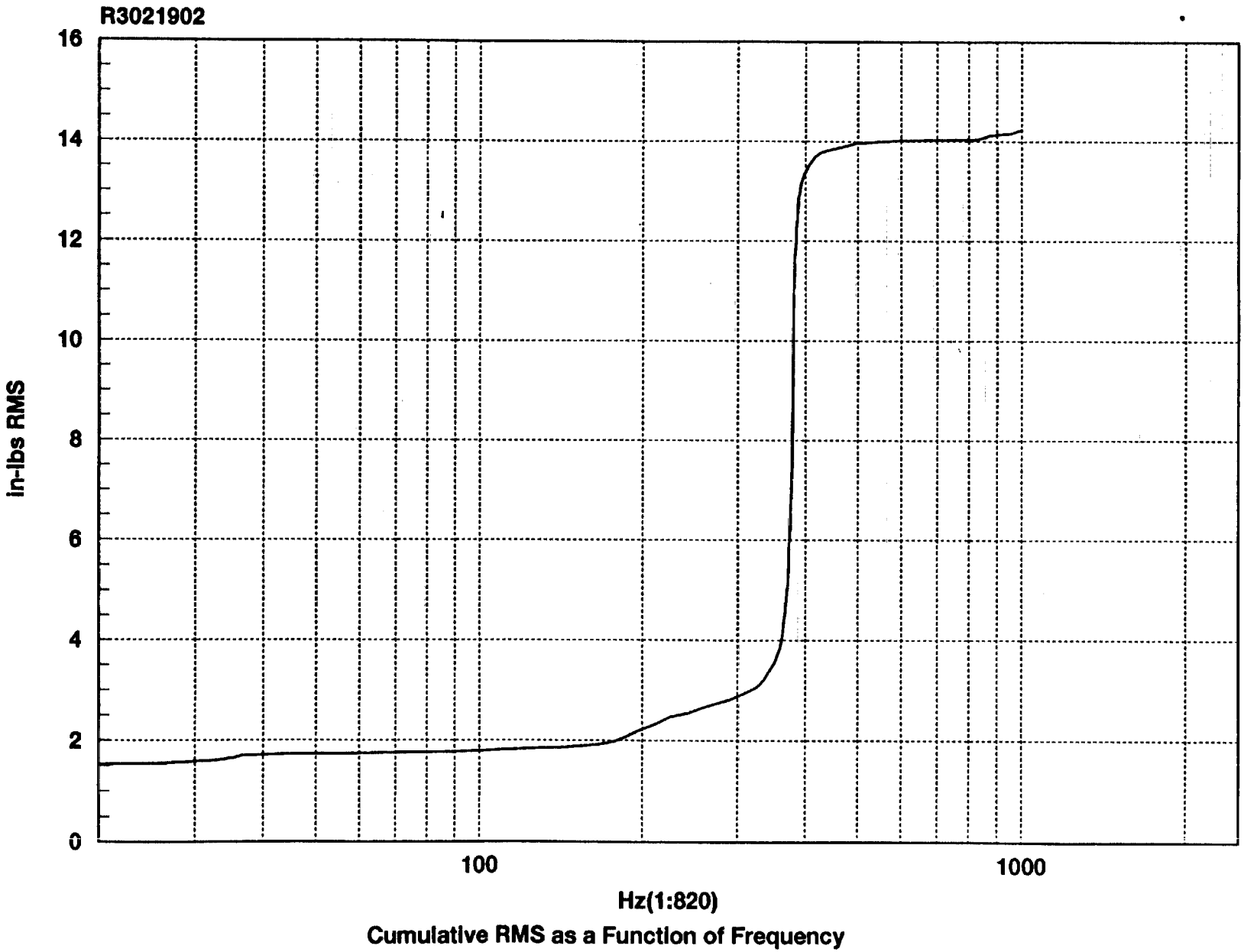

Cumulative RMS as a Function of Frequency

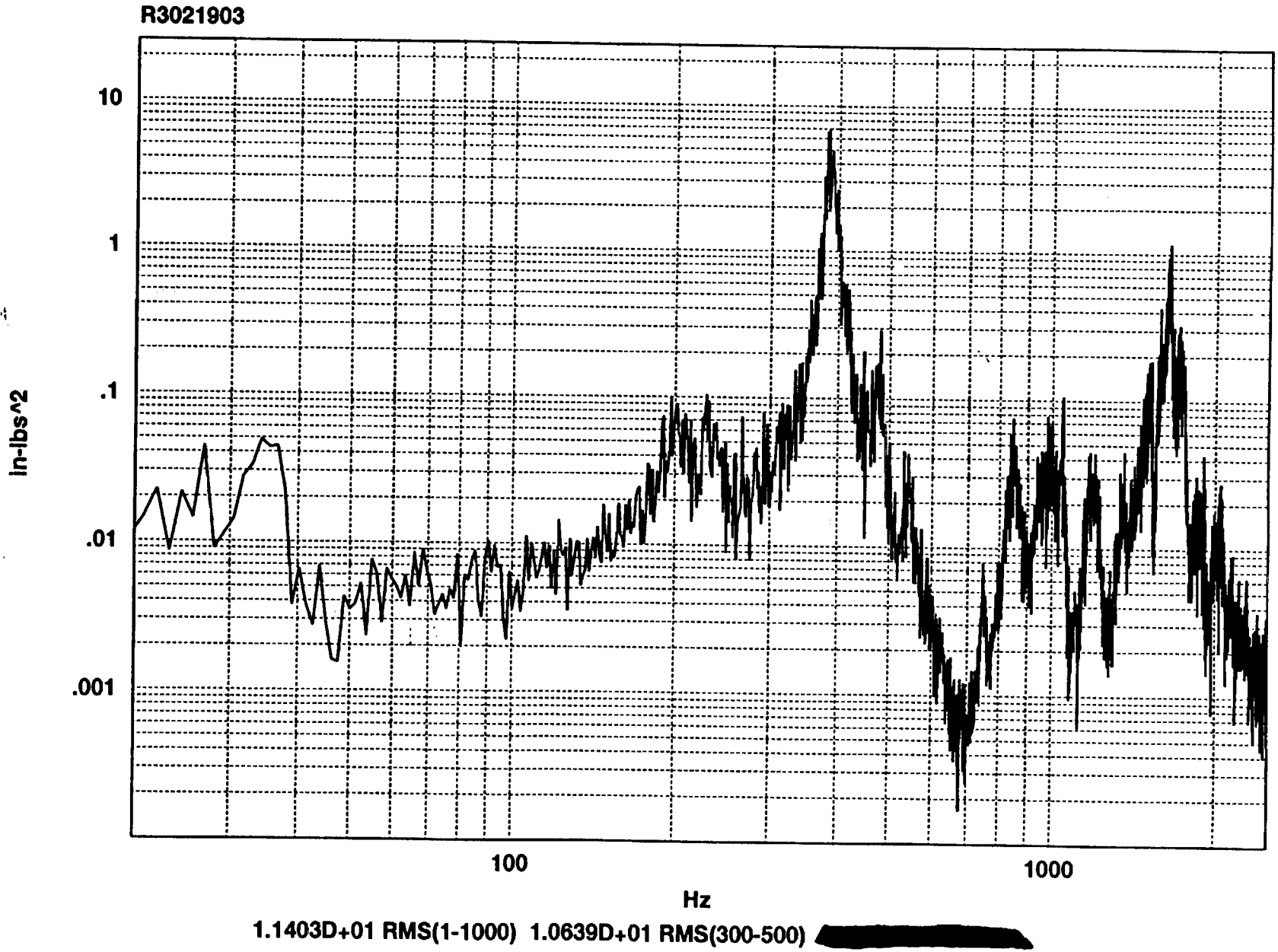
R3021903
10
1
.1
.01
.001
ln-lbs^2
100
1000
Hz
1.1403D+01 RMS(1-1000) 1.0639D+01 RMS(300-500)

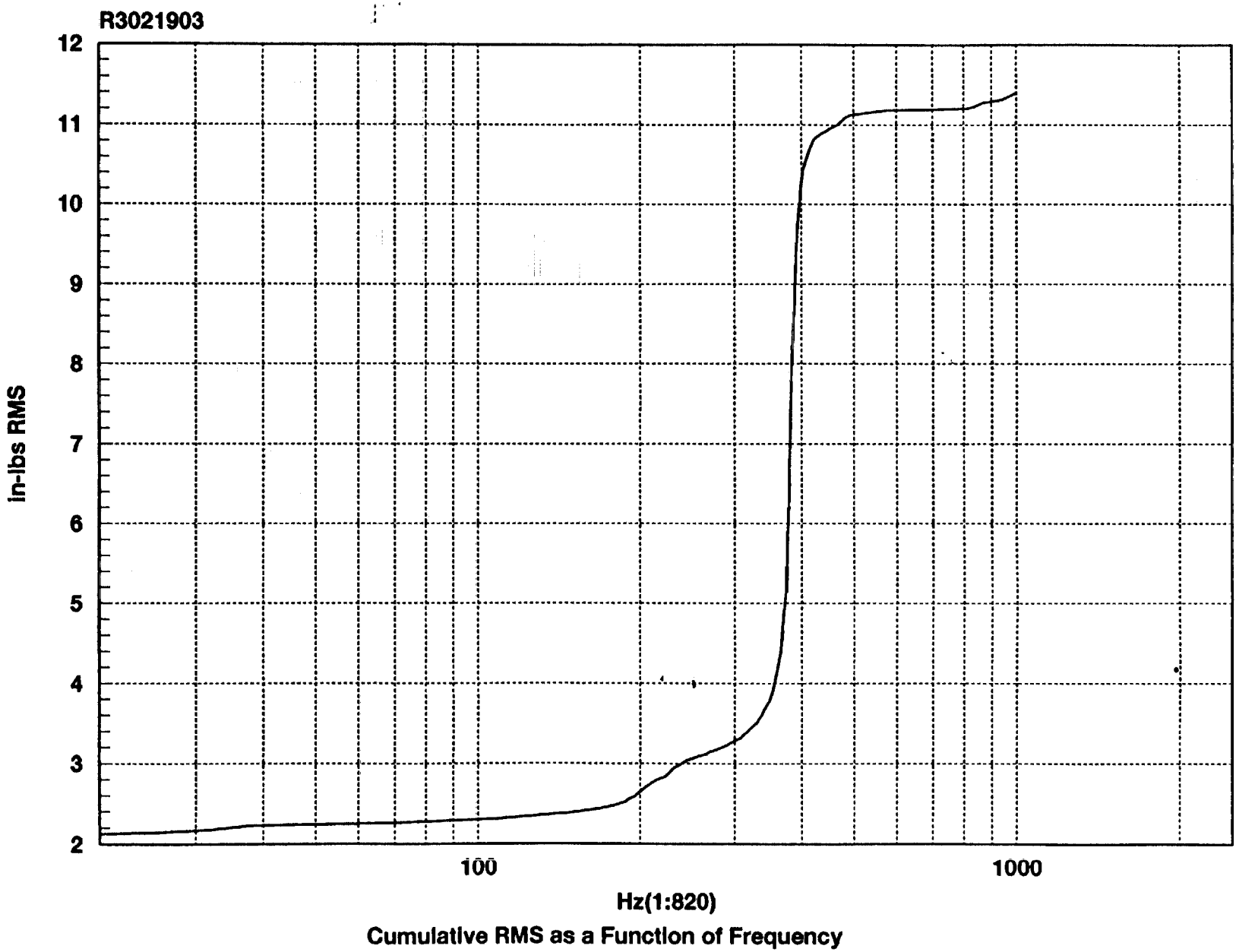
R3021903
12
11
10
9
8
7
6
5
4
3
2
In-lbs RMS
100
1000
Hz(1:820)
Cumulative RMS as a Function of Frequency

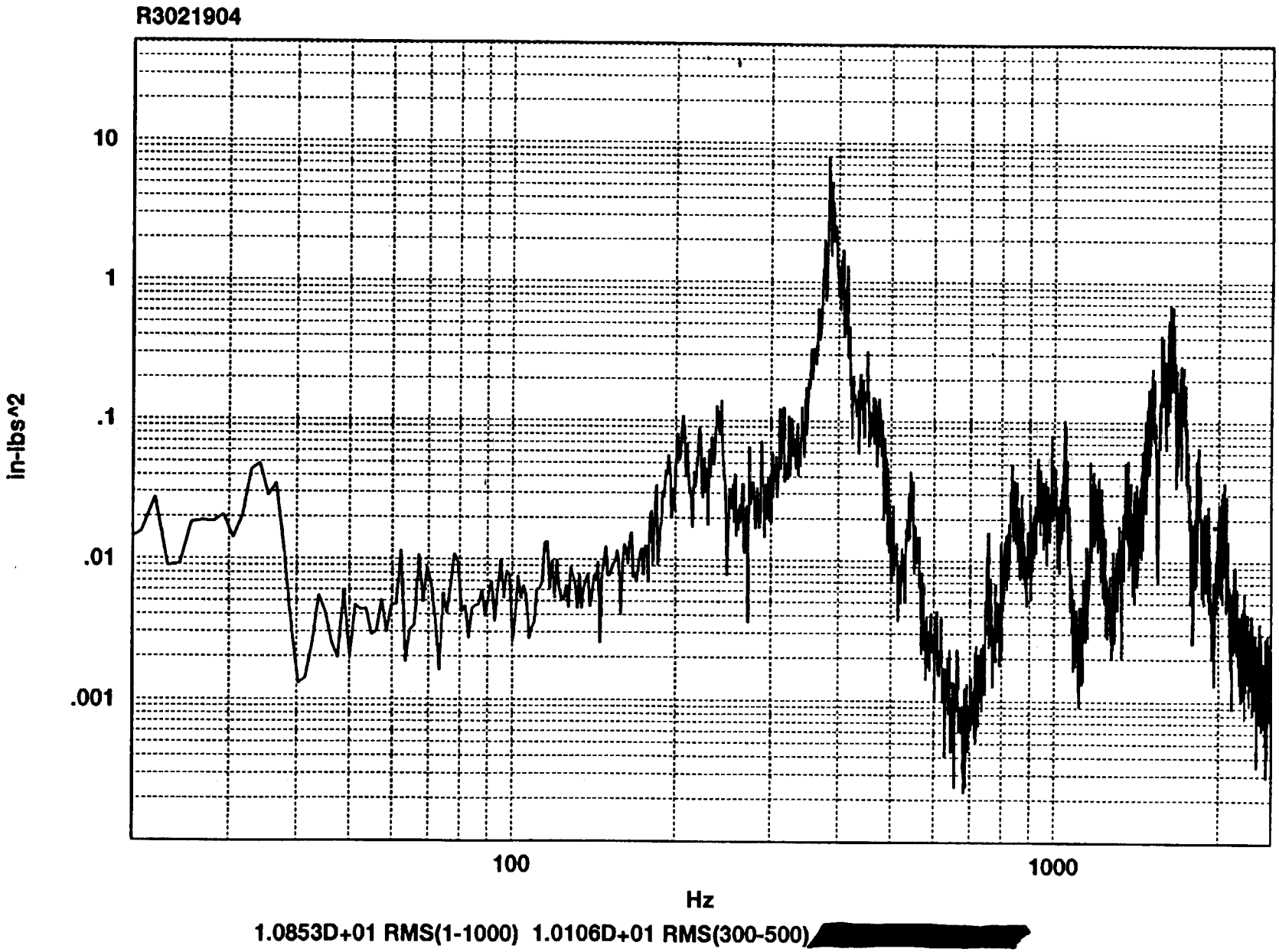
R3021904
10
1
.1
.01
.001
in-lbs^2
100
1000
Hz
1.0853D+01 RMS(1-1000) 1.0106D+01 RMS(300-500)

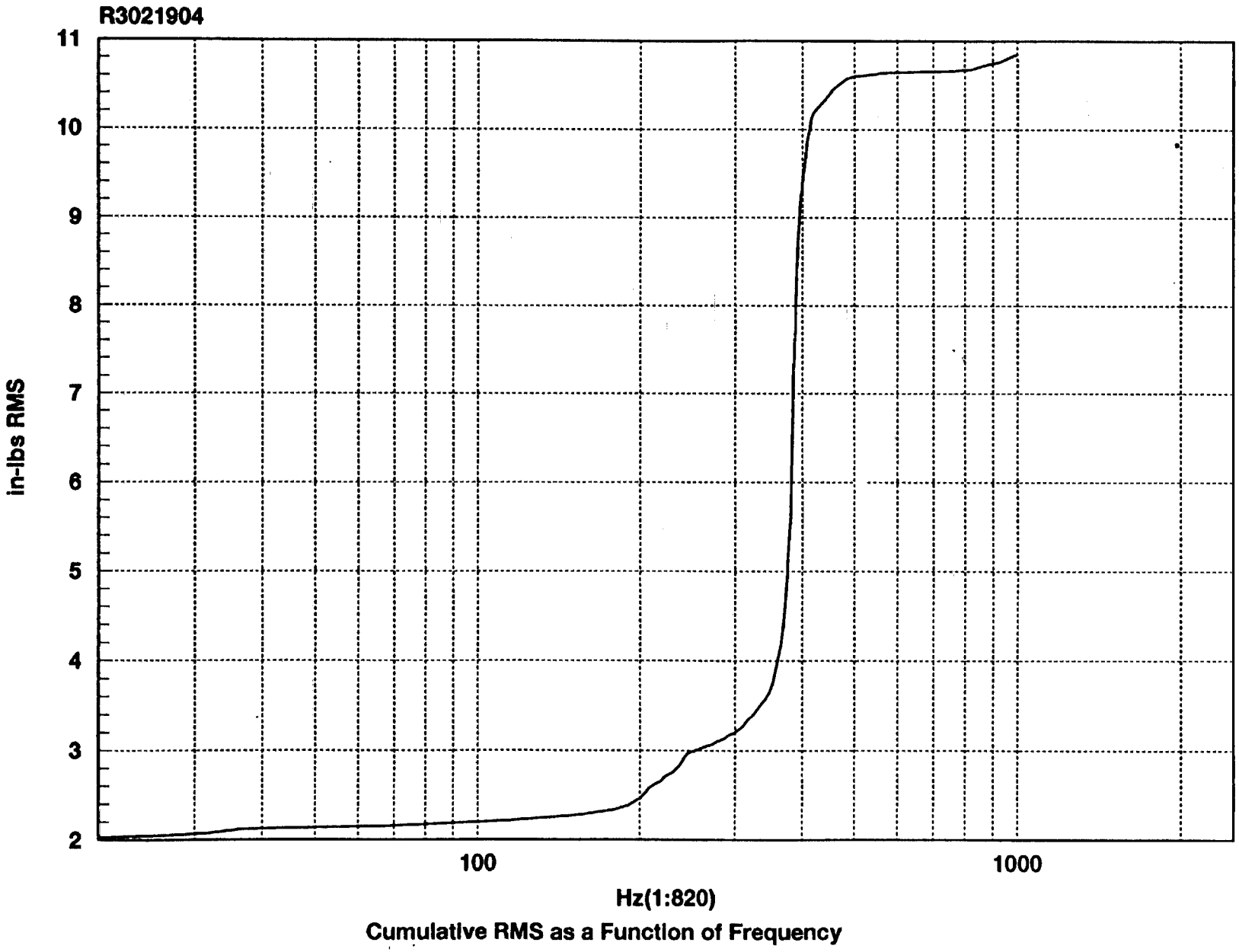
R3021904
11
10
9
8
7
6
5
4
3
2
in-lbs RMS
100
1000
Hz(1:820)
Cumulative RMS as a Function of Frequency

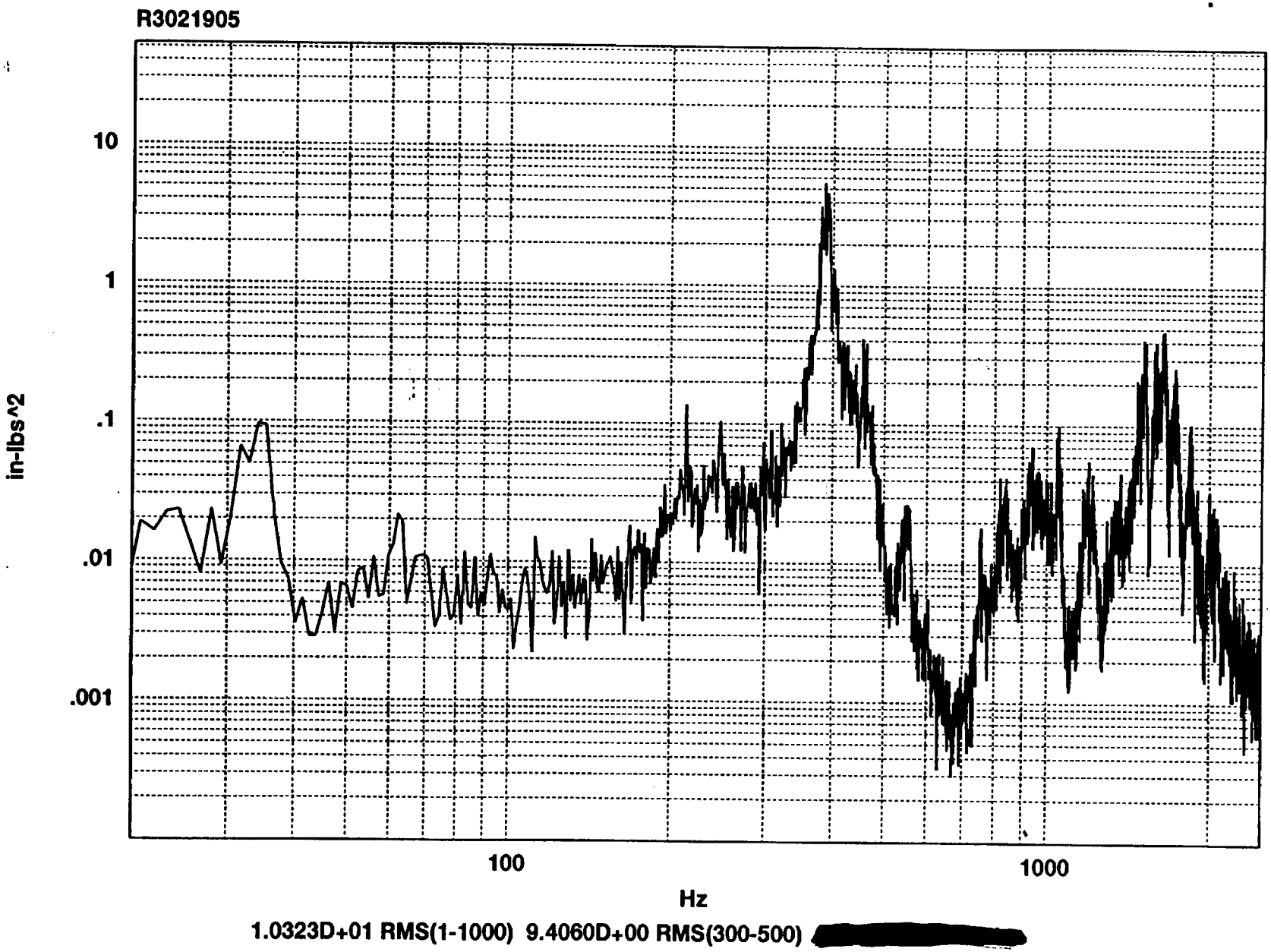
R3021905
10
1
.1
.01
.001
in-lbs^2
100
1000
Hz
1.0323D+01 RMS(1-1000) 9.4060D+00 RMS(300-500)

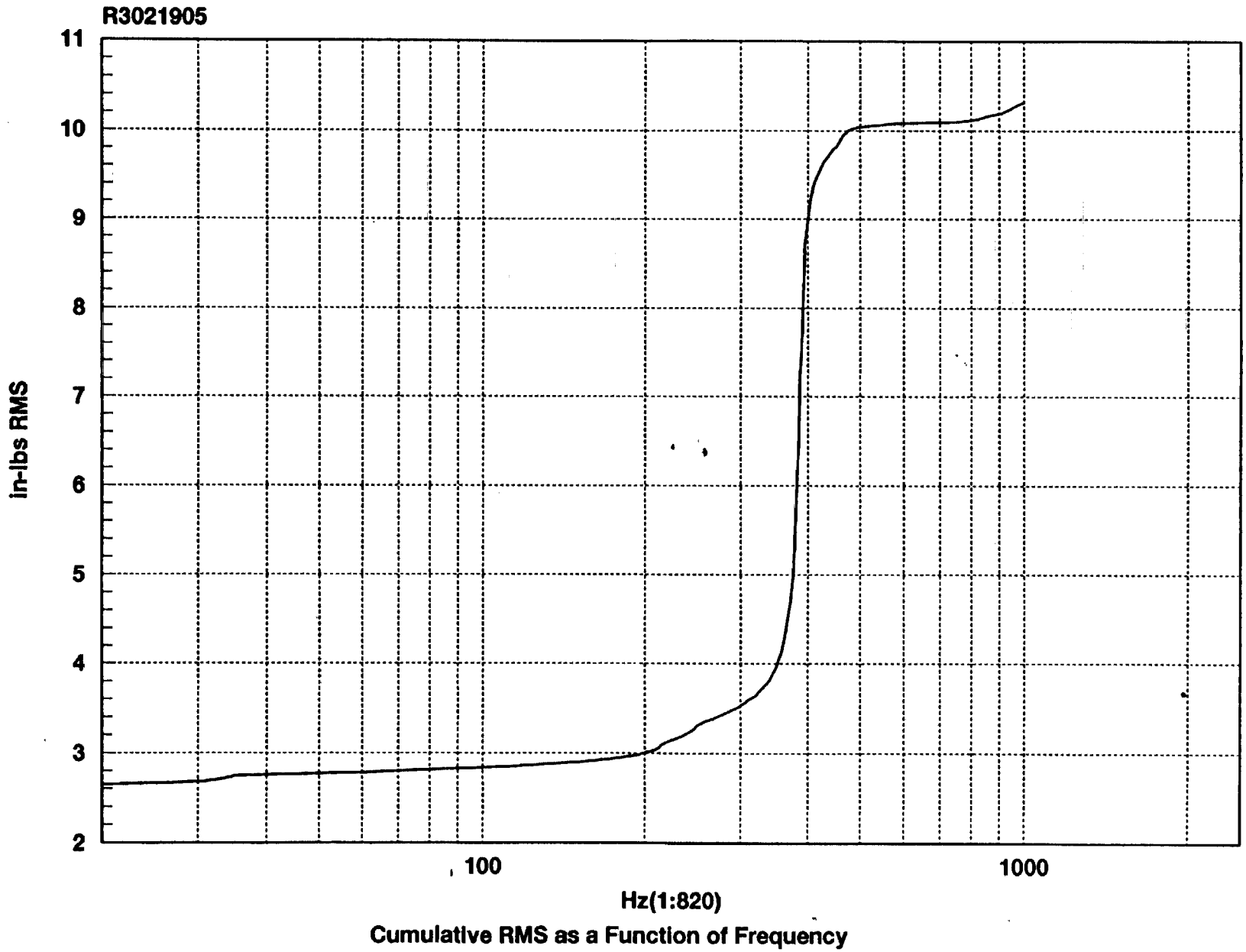
R3021905
11
10
9
8
7
6
5
4
3
2
in-lbs RMS
100
1000
Hz(1:820)
Cumulative RMS as a Function of Frequency

R3021906

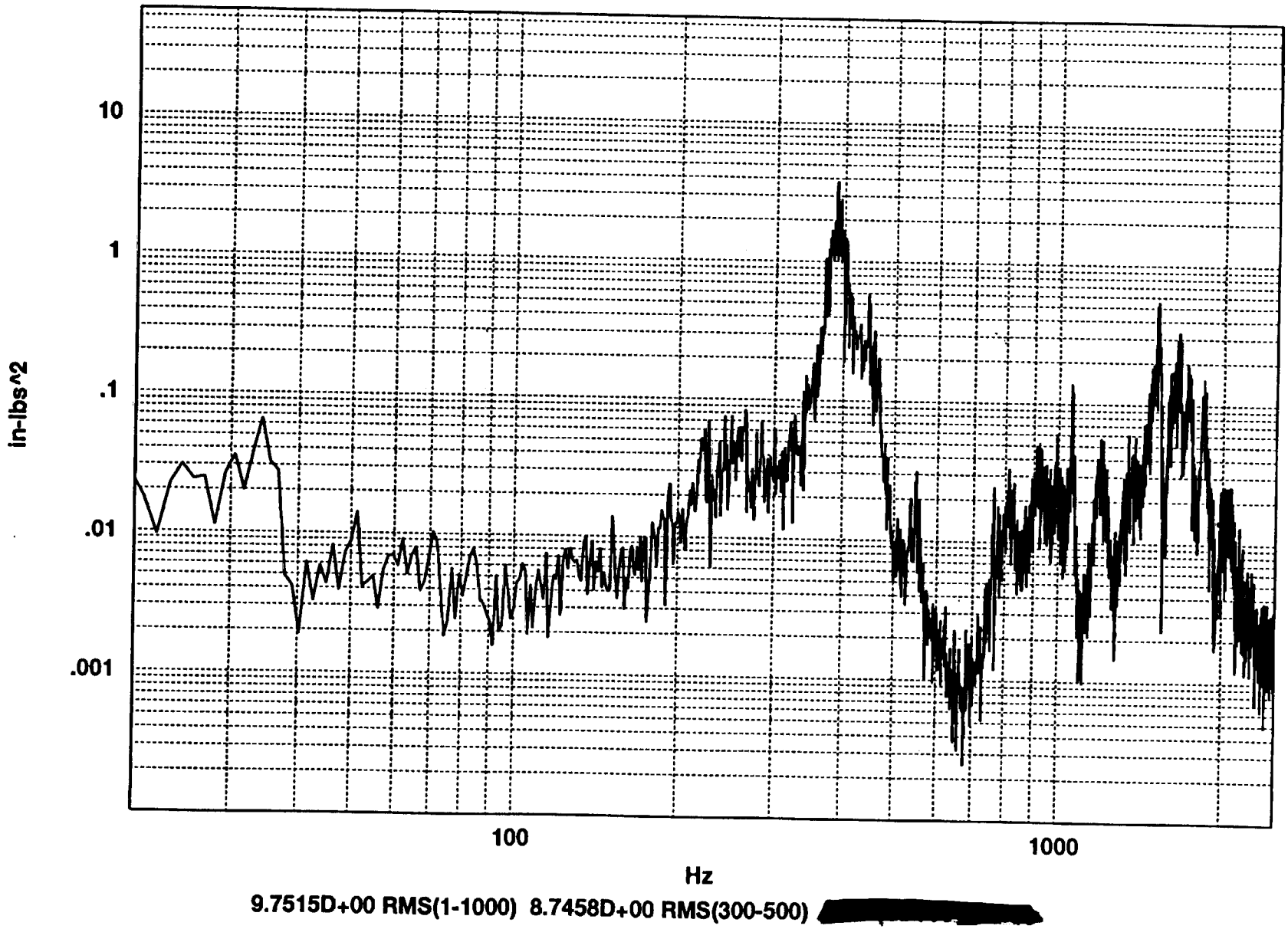

9.7515D+00 RMS(1-1000) 8.7458D+00 RMS(300-500) [redacted]

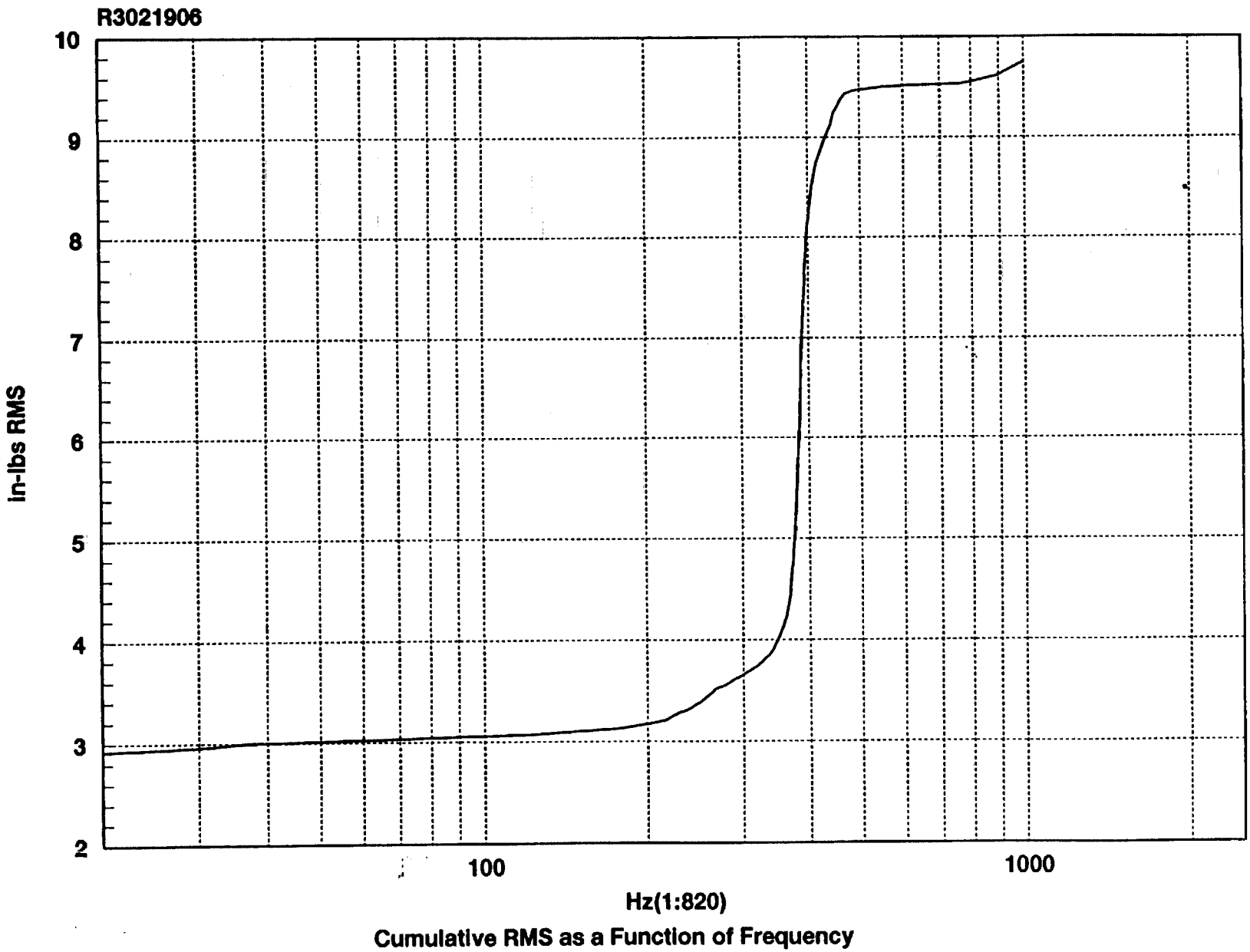

Cumulative RMS as a Function of Frequency

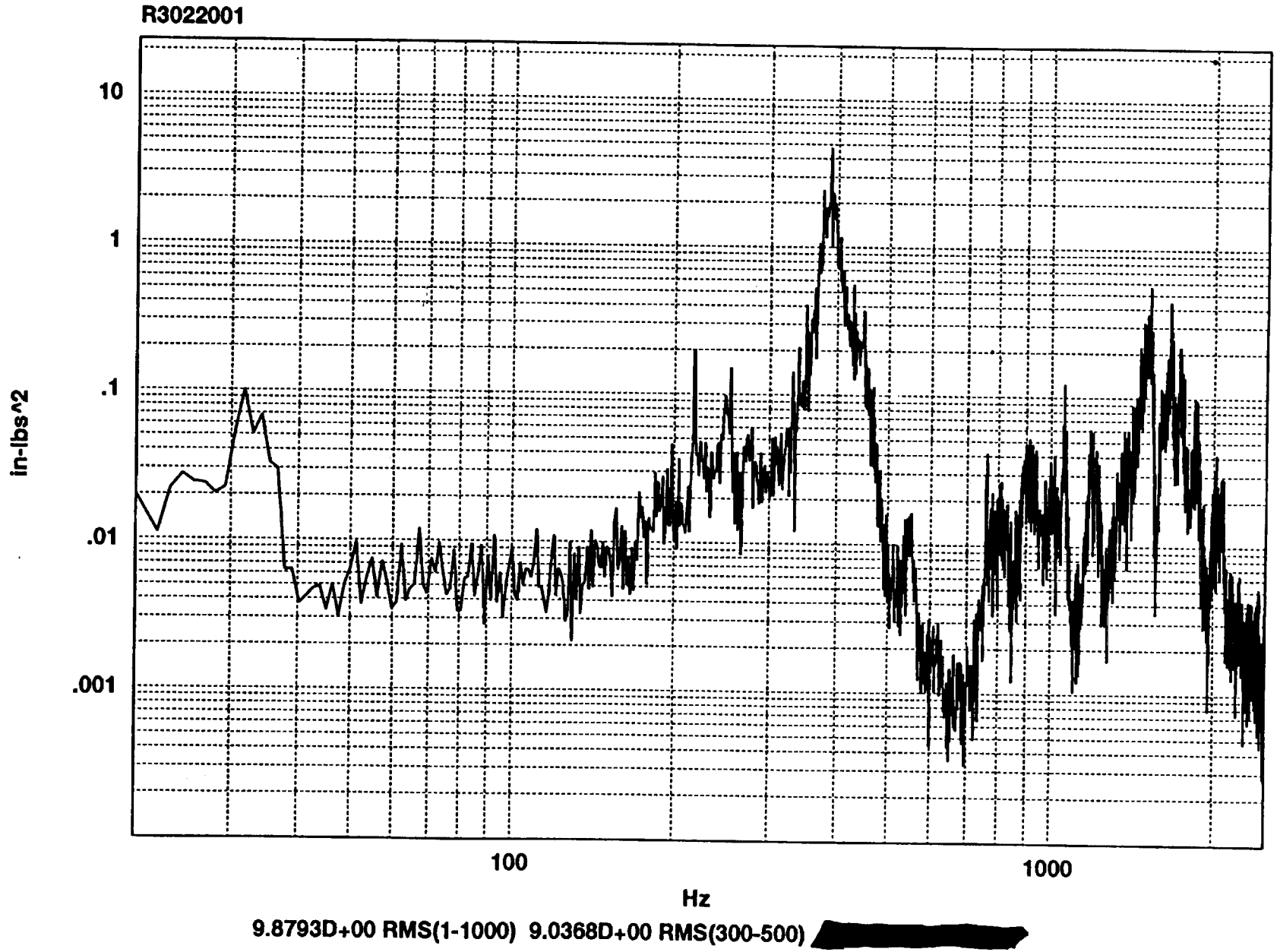
R3022001
10
1
.1
.01
.001
in-lbs^2
100
1000
Hz
9.8793D+00 RMS(1-1000) 9.0368D+00 RMS(300-500)

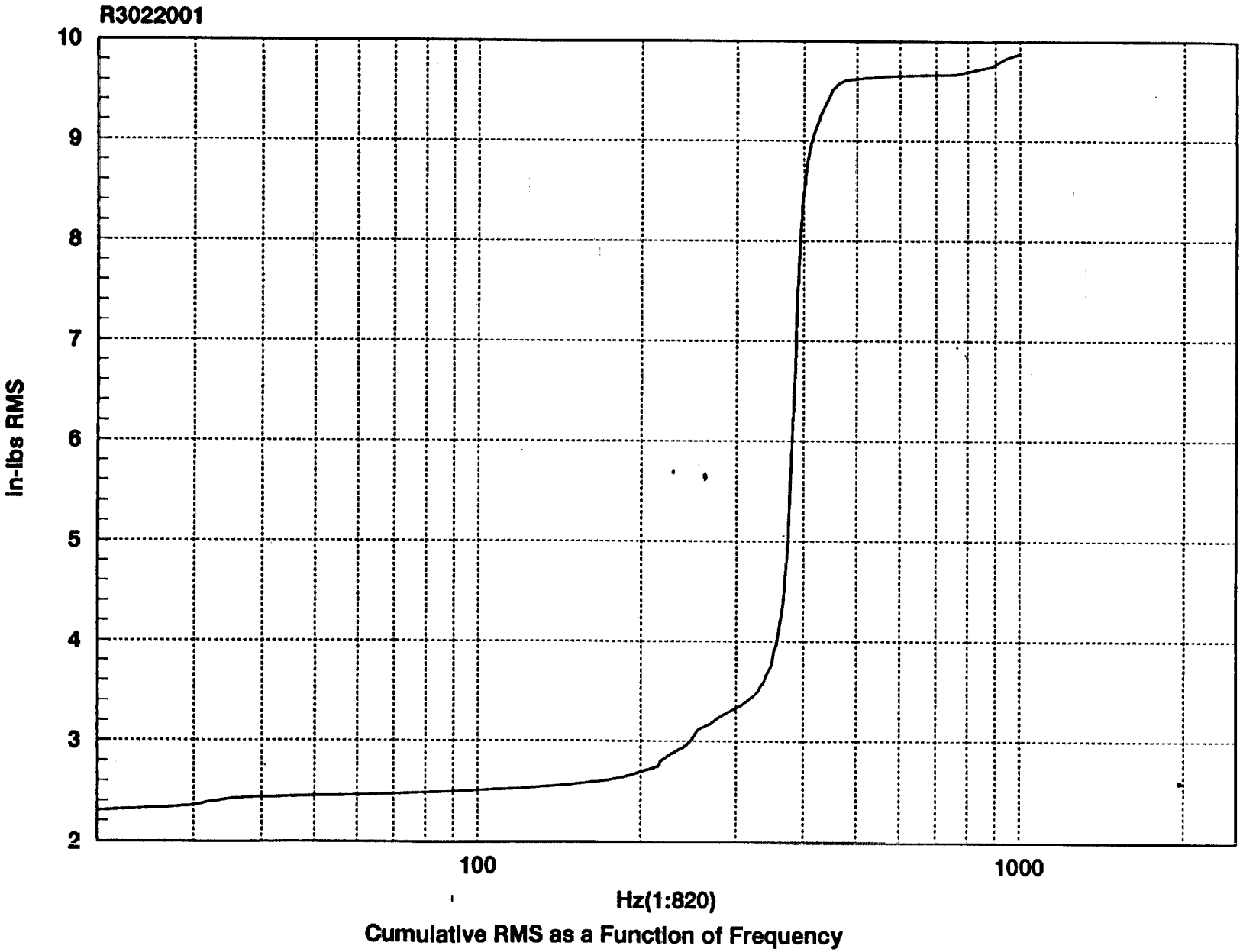

Cumulative RMS as a Function of Frequency

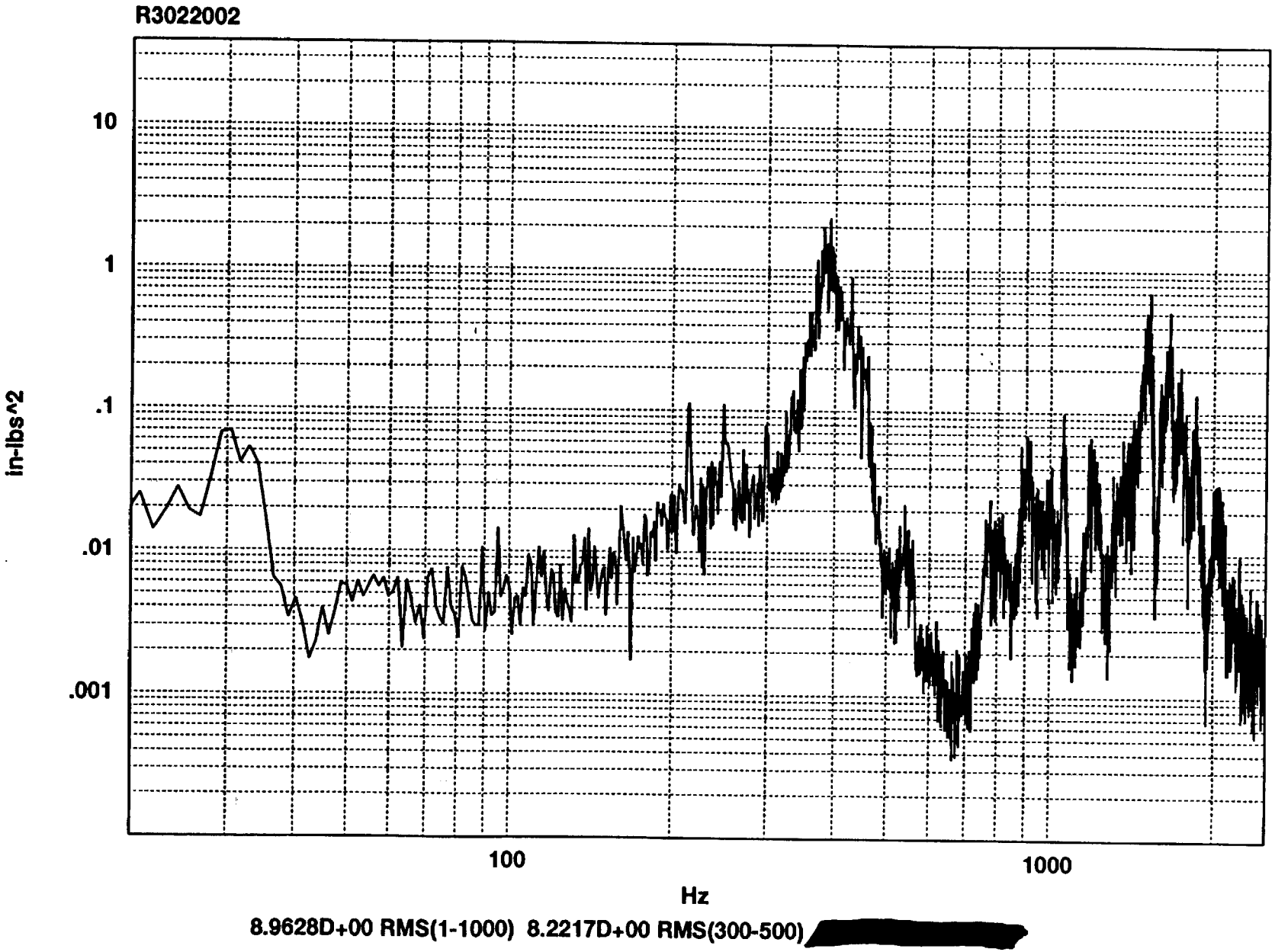
R3022002
10
1
.1
.01
.001
in-lbs^2
100
1000
Hz
8.9628D+00 RMS(1-1000) 8.2217D+00 RMS(300-500)

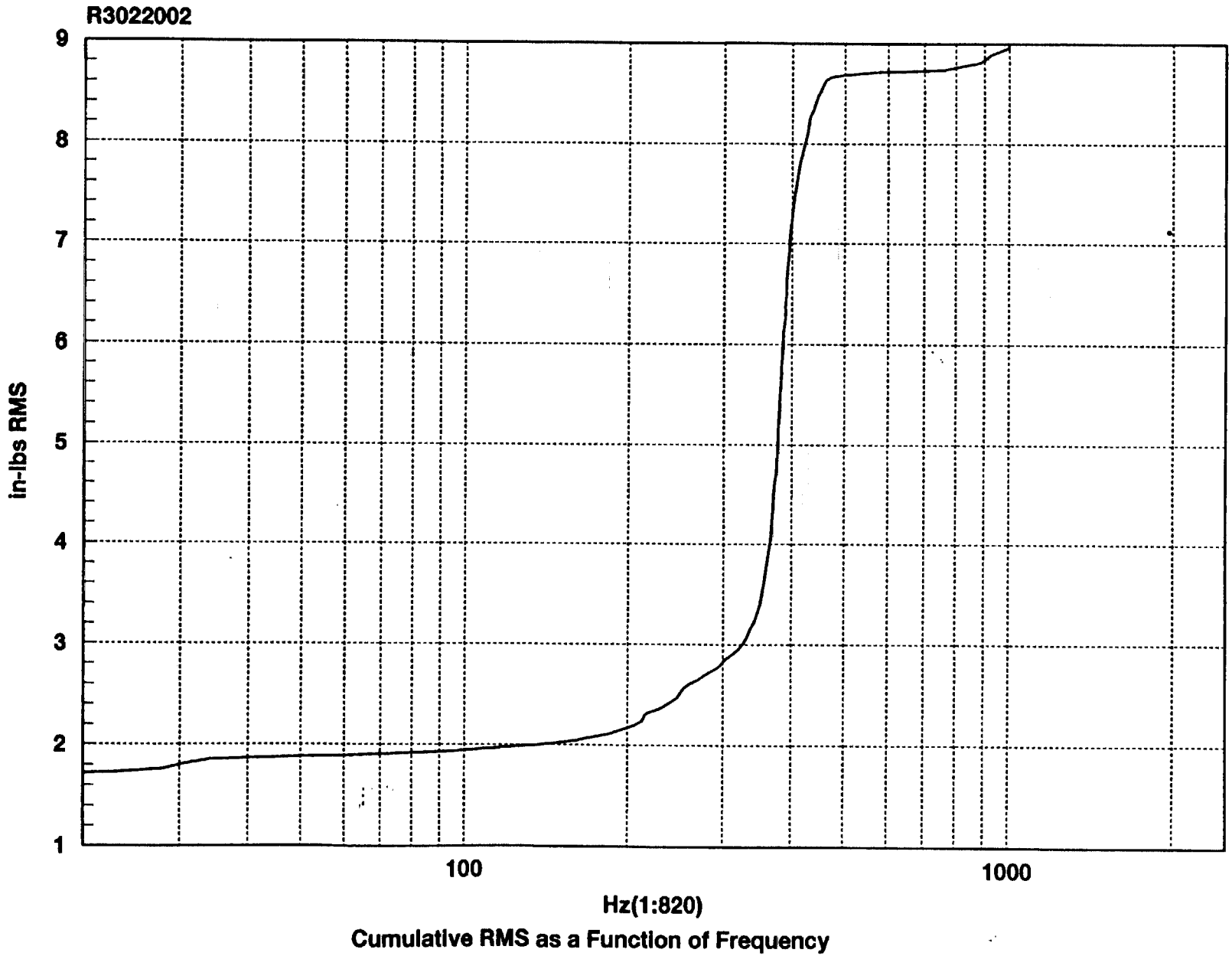

Cumulative RMS as a Function of Frequency

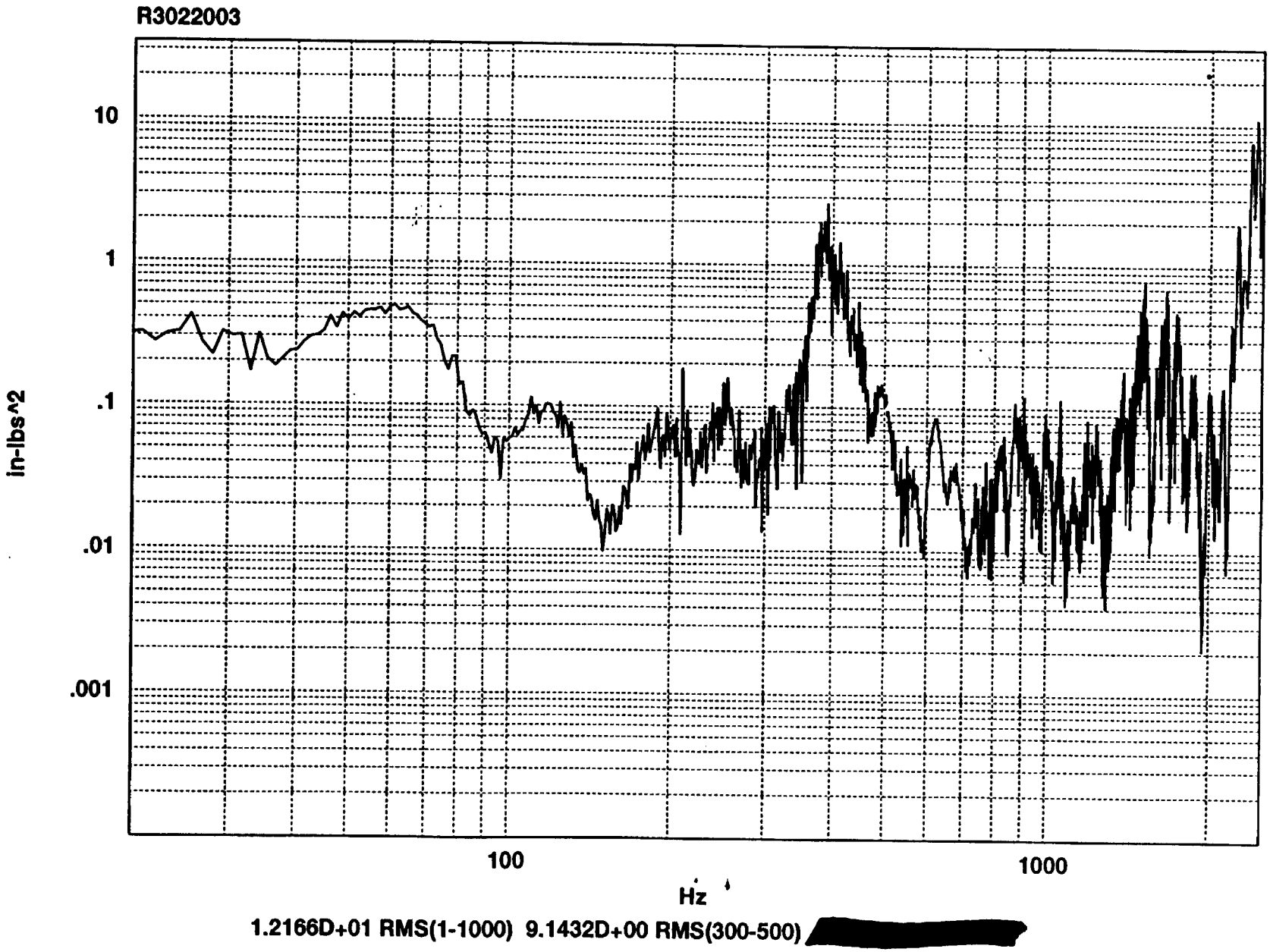
R3022003
10
1
.1
.01
.001
in-lbs^2
100
1000
Hz
1.2166D+01 RMS(1-1000) 9.1432D+00 RMS(300-500)

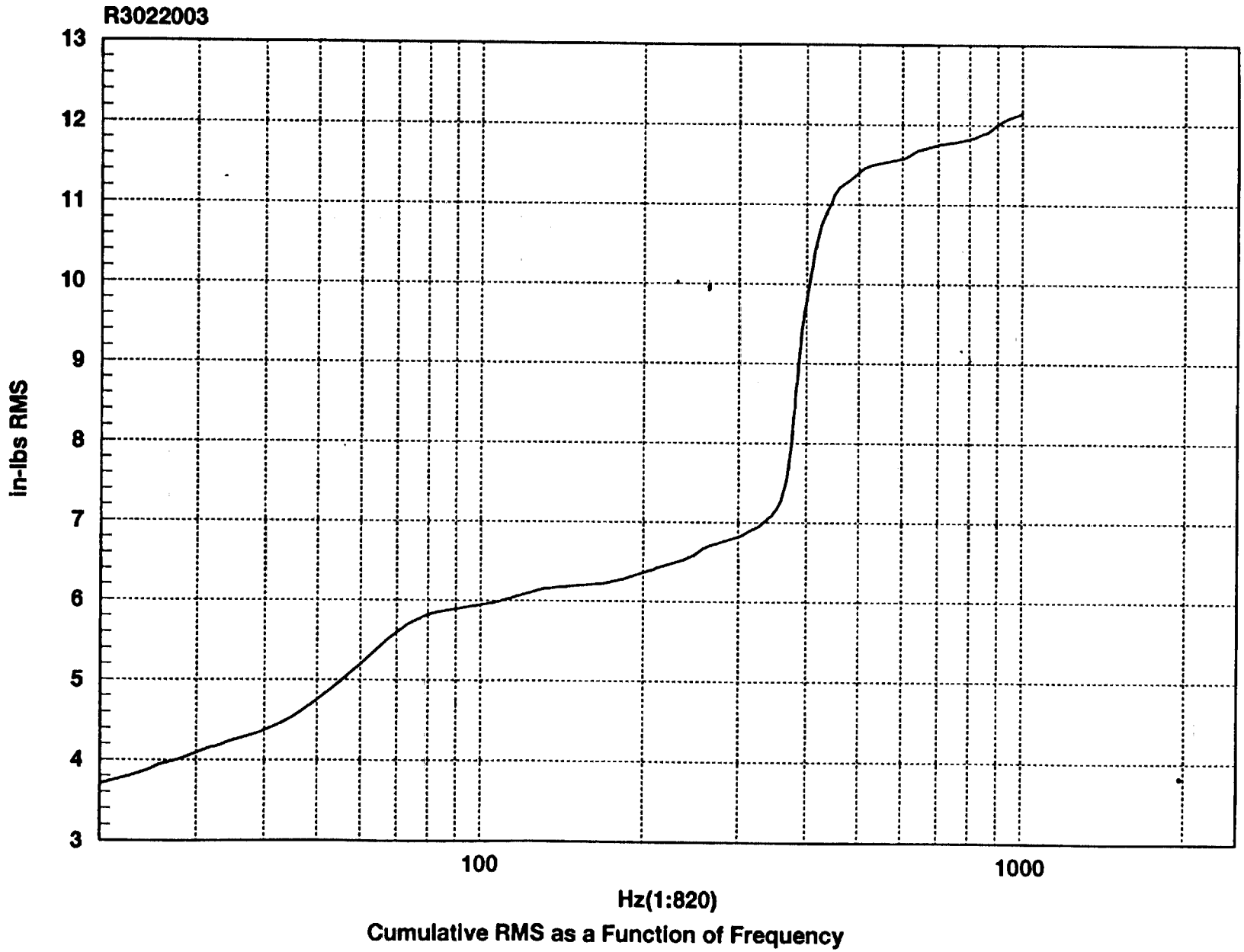

Cumulative RMS as a Function of Frequency

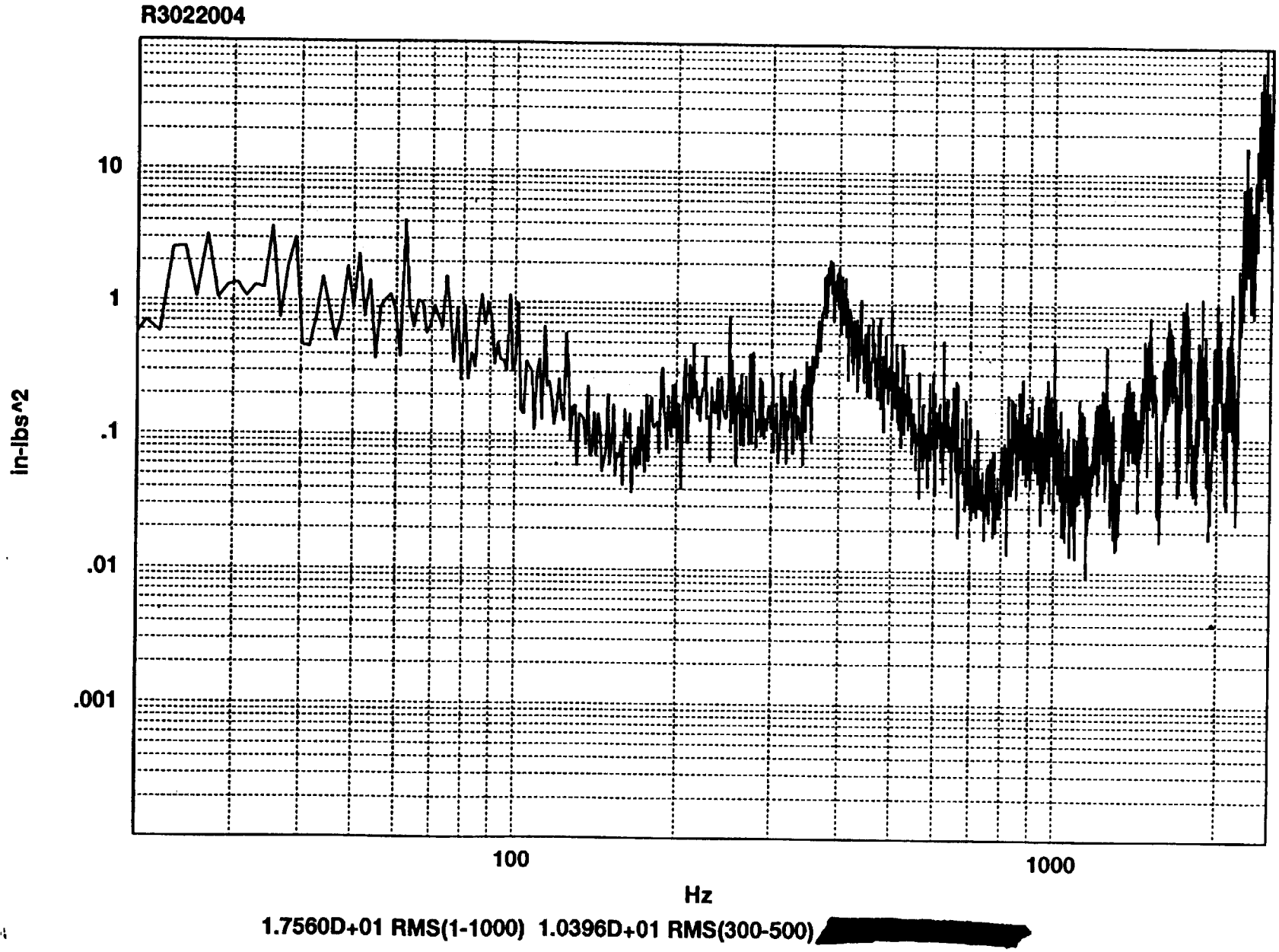
R3022004
10
1
.1
.01
.001
in-lbs^2
100
1000
Hz
1.7560D+01 RMS(1-1000) 1.0396D+01 RMS(300-500)

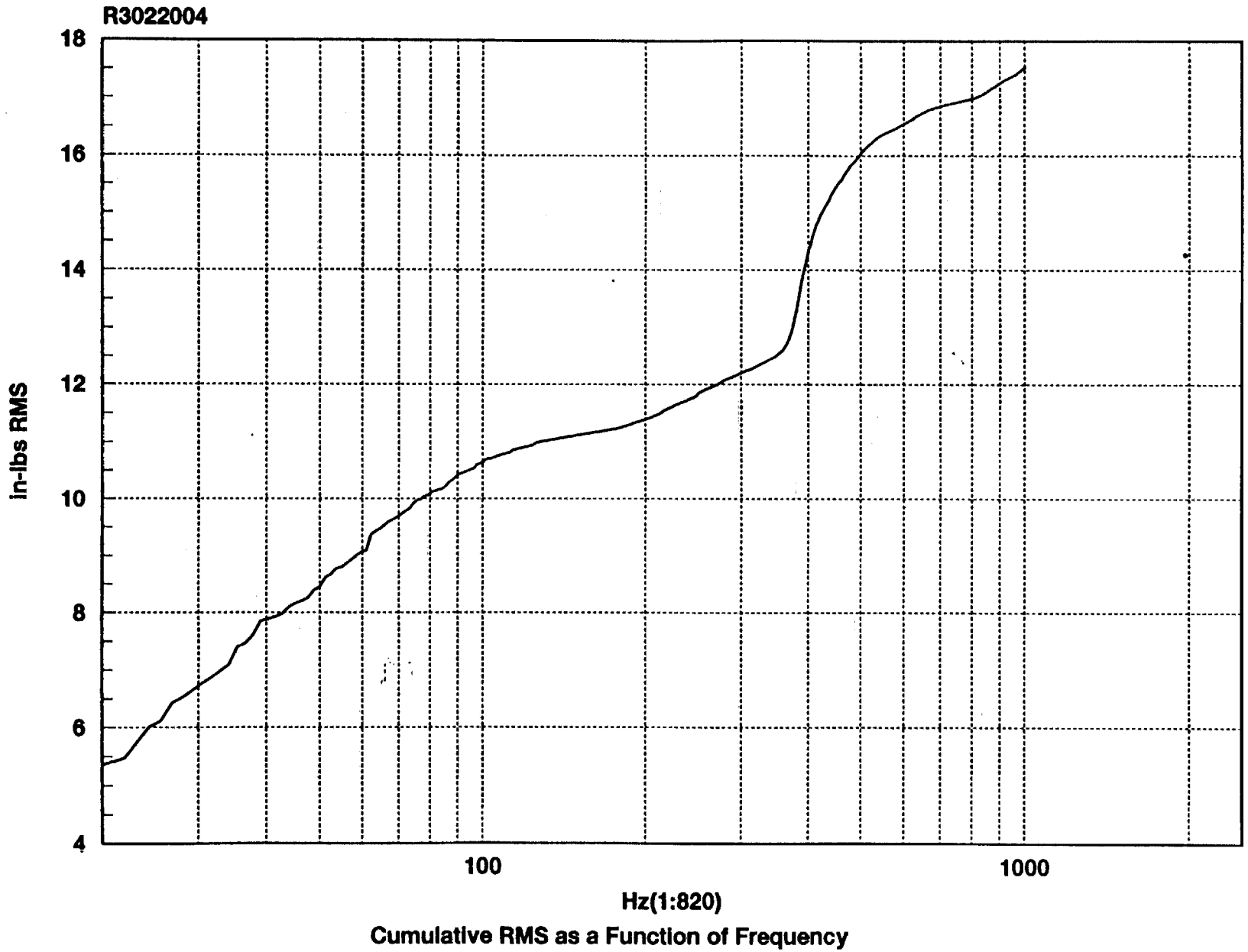

Cumulative RMS as a Function of Frequency

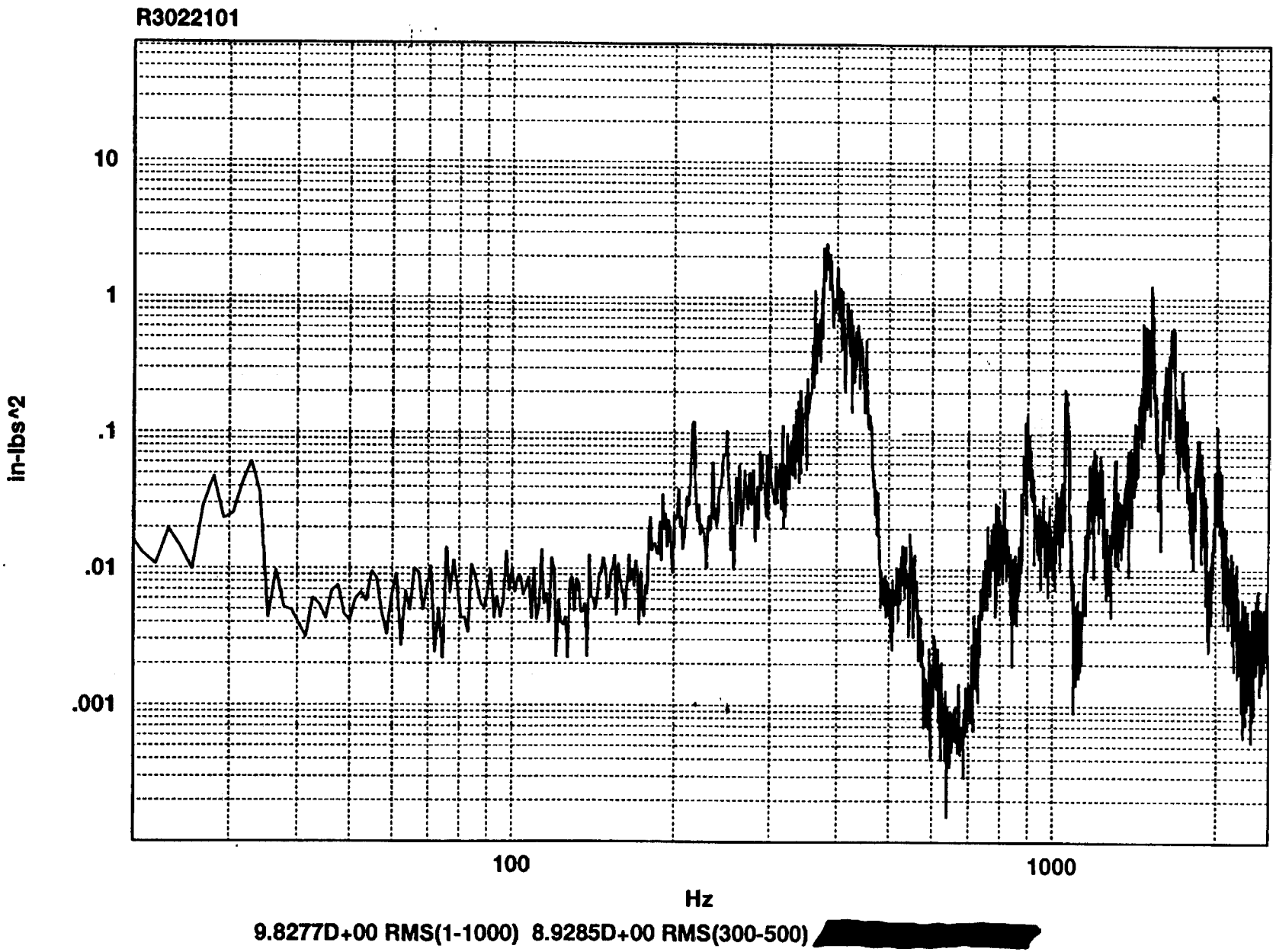
R3022101
10
1
.1
.01
.001
in-lbs^2
100
1000
Hz
9.8277D+00 RMS(1-1000) 8.9285D+00 RMS(300-500)

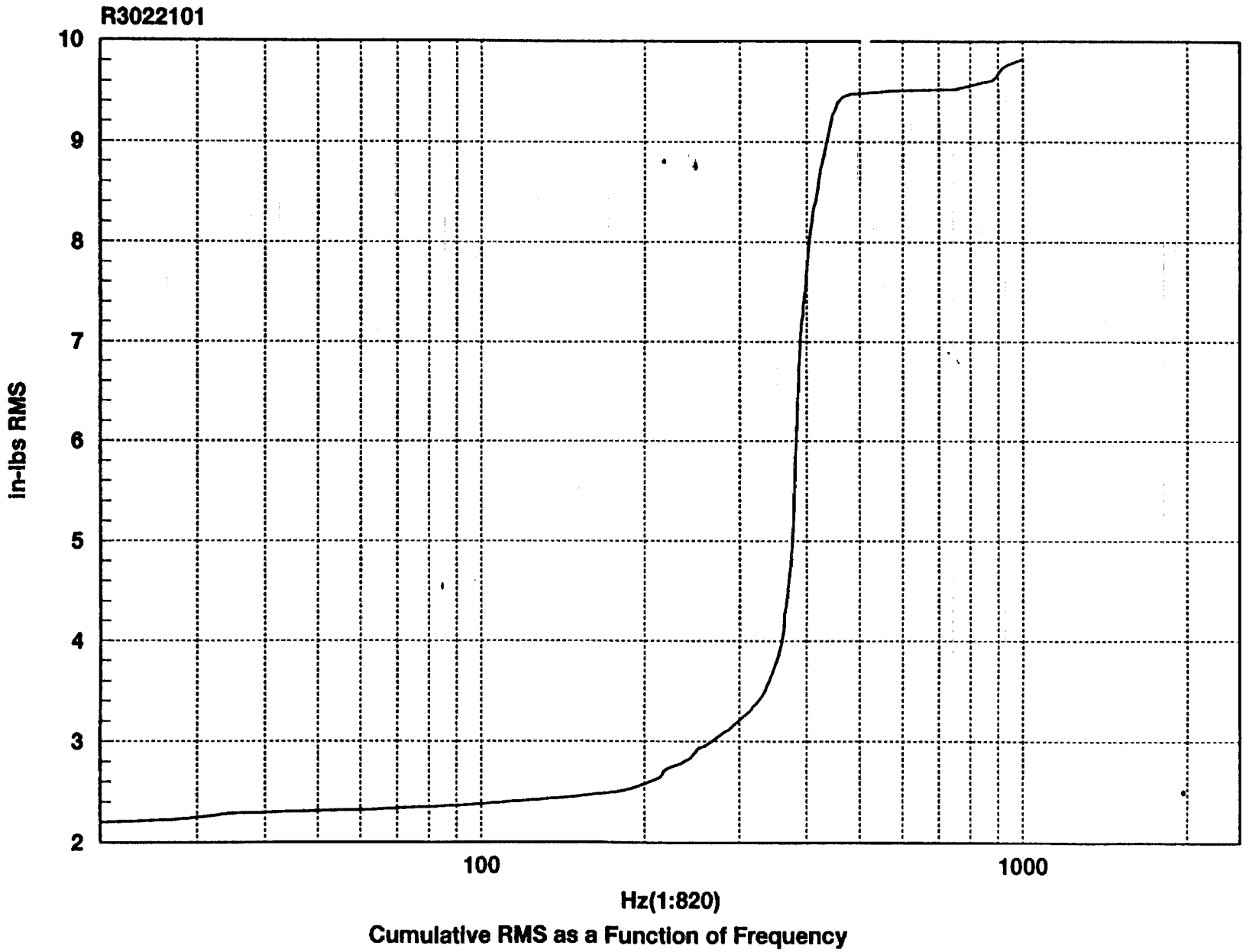

Cumulative RMS as a Function of Frequency

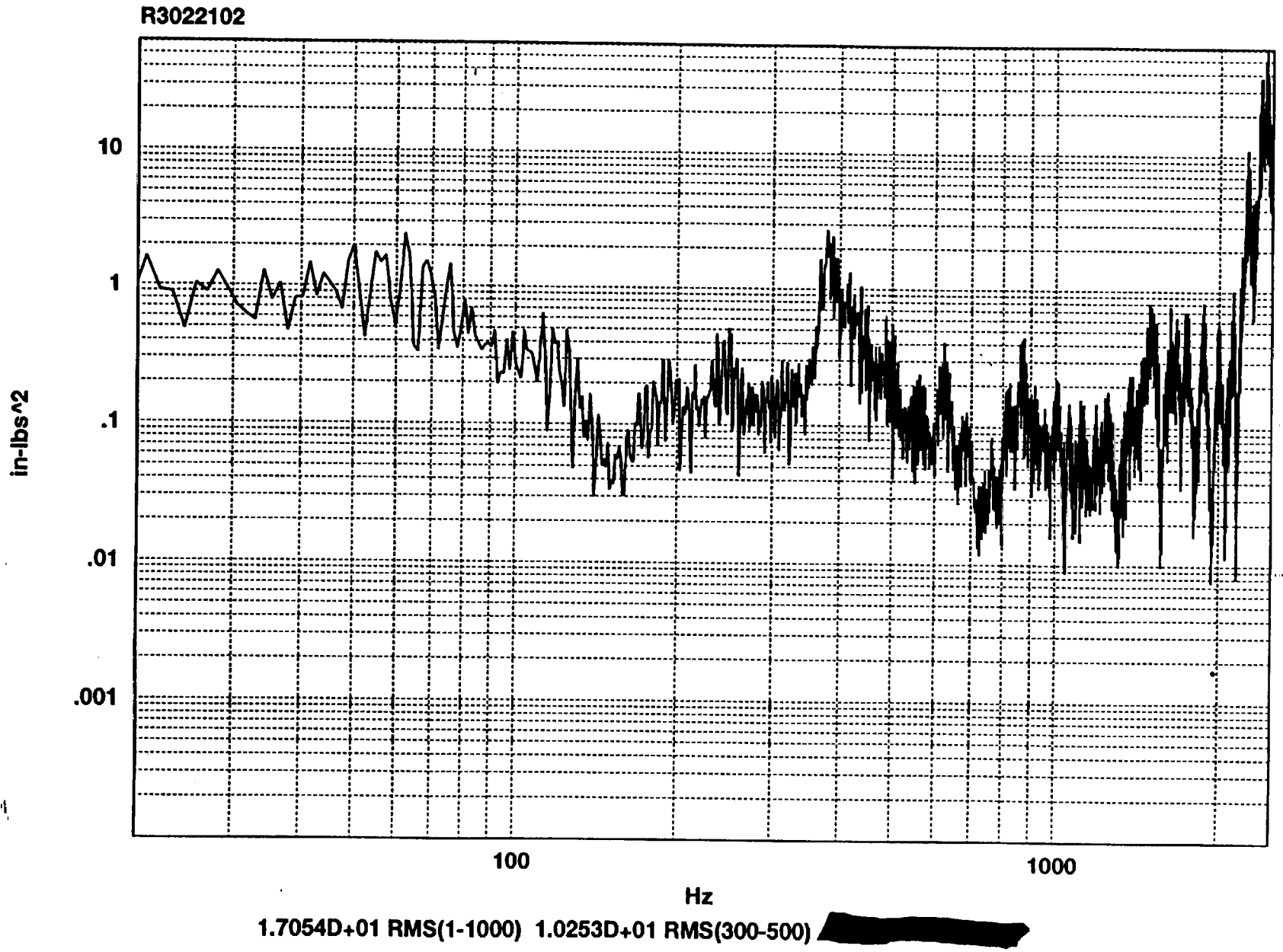
R3022102
10
1
.1
.01
.001
in-lbs^2
100
1000
Hz
1.7054D+01 RMS(1-1000) 1.0253D+01 RMS(300-500)

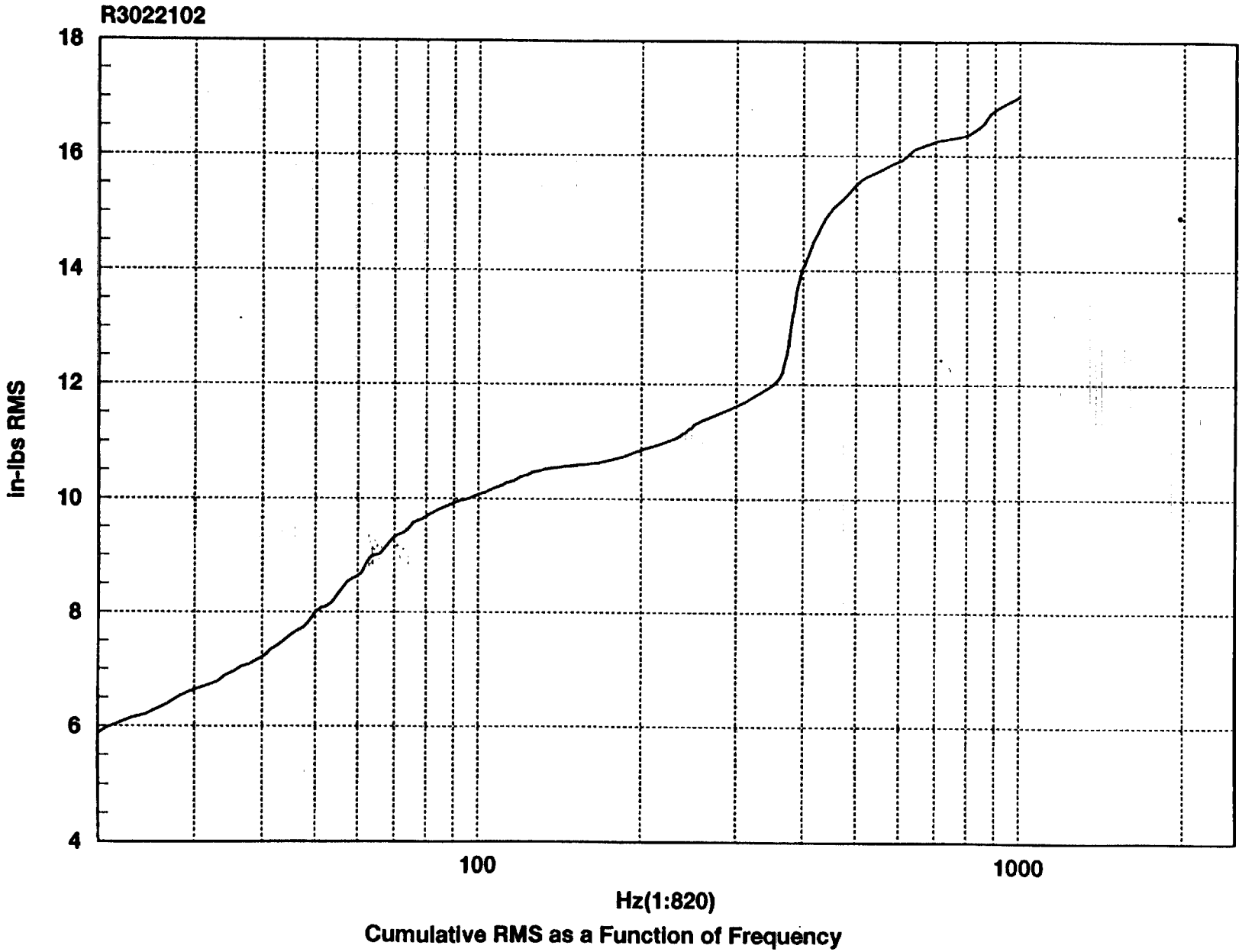

Cumulative RMS as a Function of Frequency

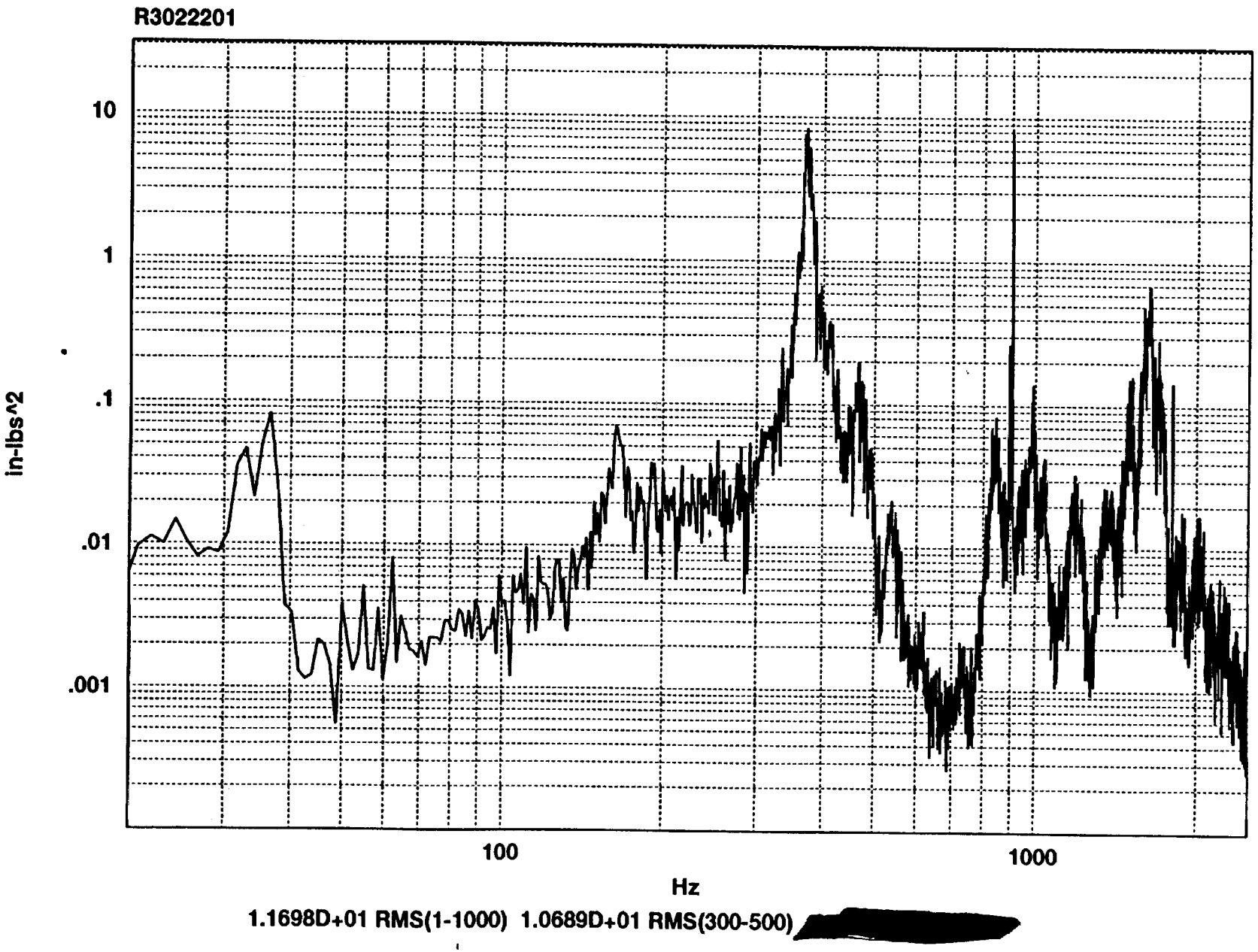
R3022201
10
1
.1
.01
.001
In-lbs^2
100
1000
Hz
1.1698D+01 RMS(1-1000) 1.0689D+01 RMS(300-500)

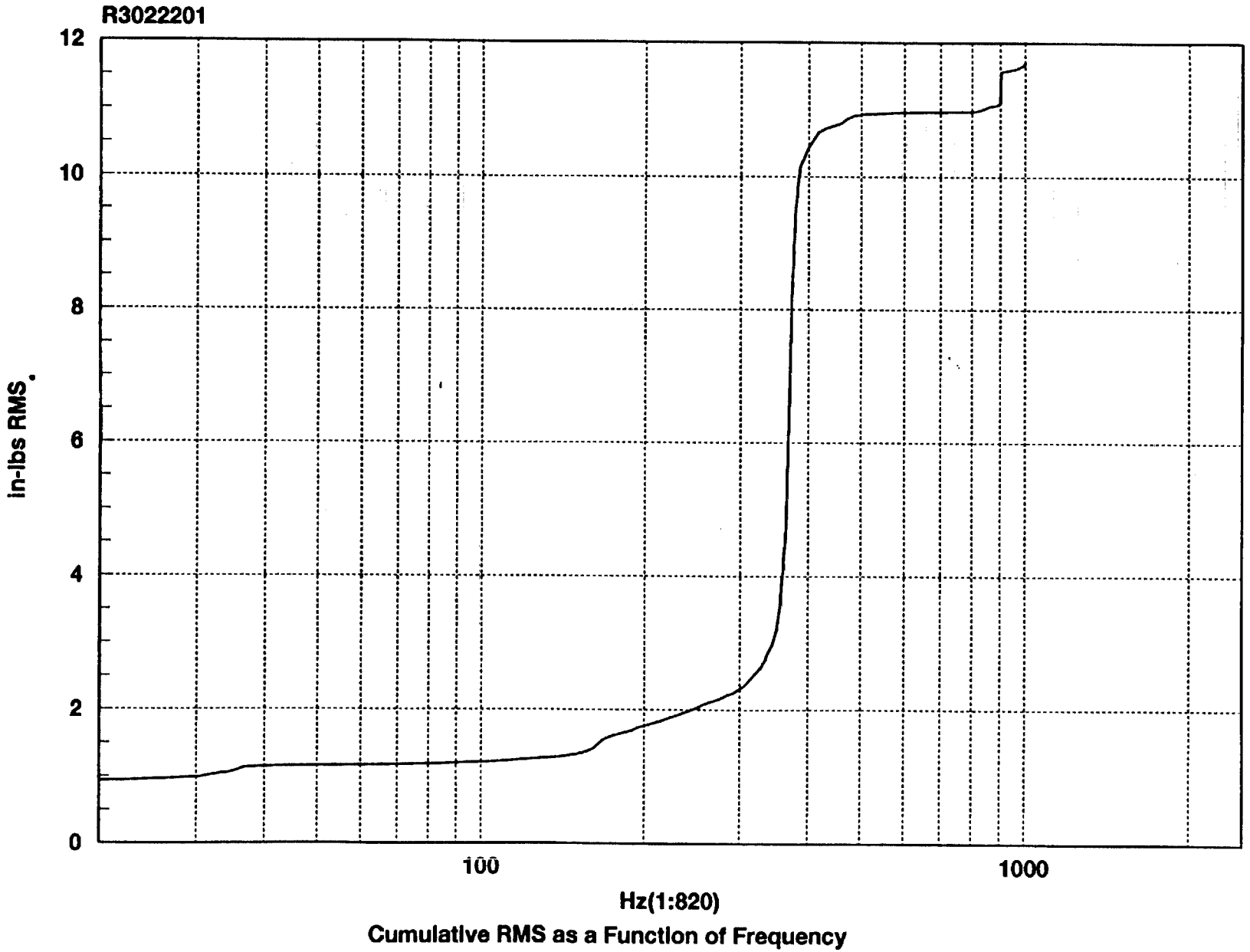

Cumulative RMS as a Function of Frequency

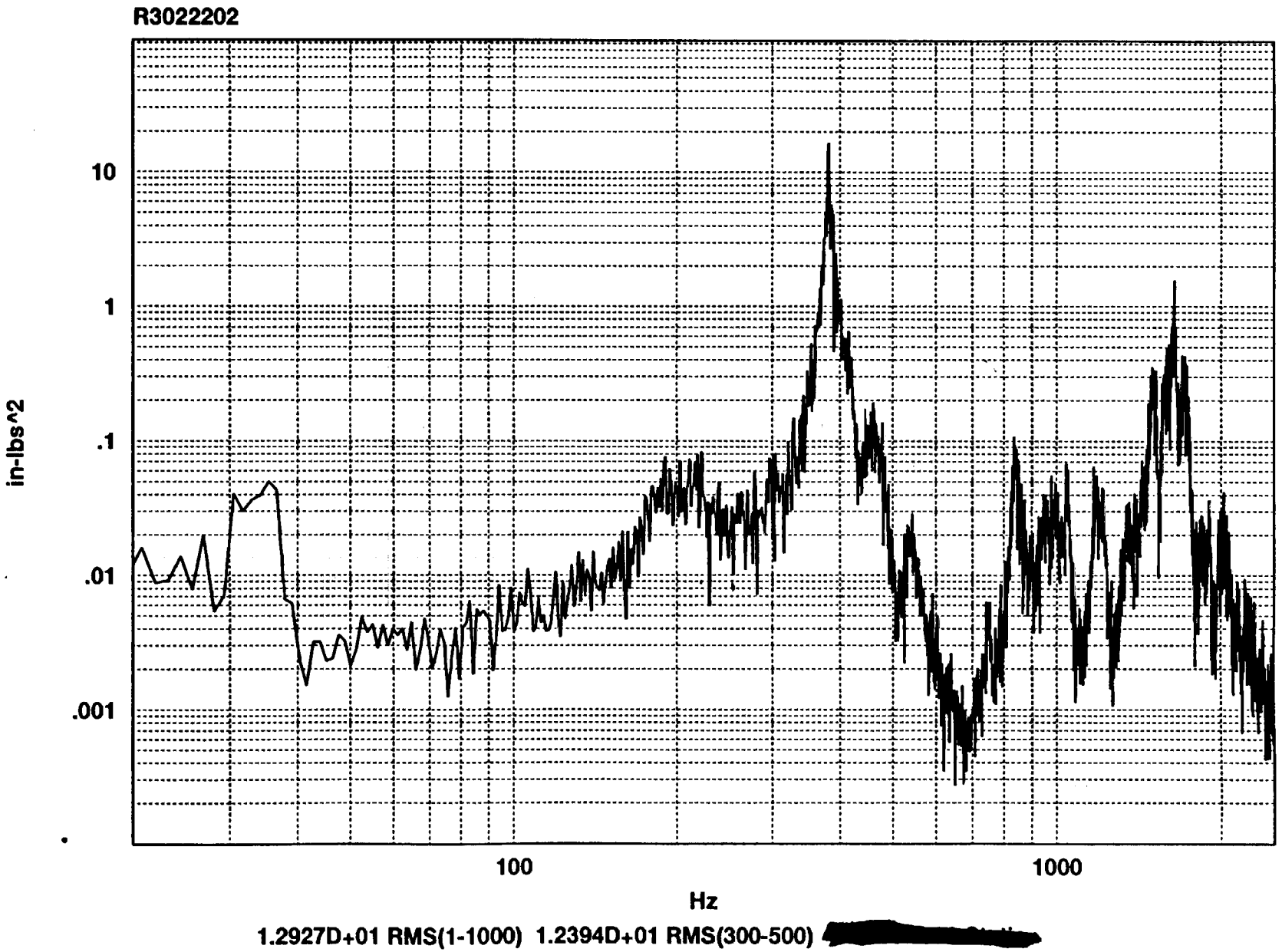
R3022202
10
1
.1
.01
.001
in-lbs^2
100
1000
Hz
1.2927D+01 RMS(1-1000) 1.2394D+01 RMS(300-500)

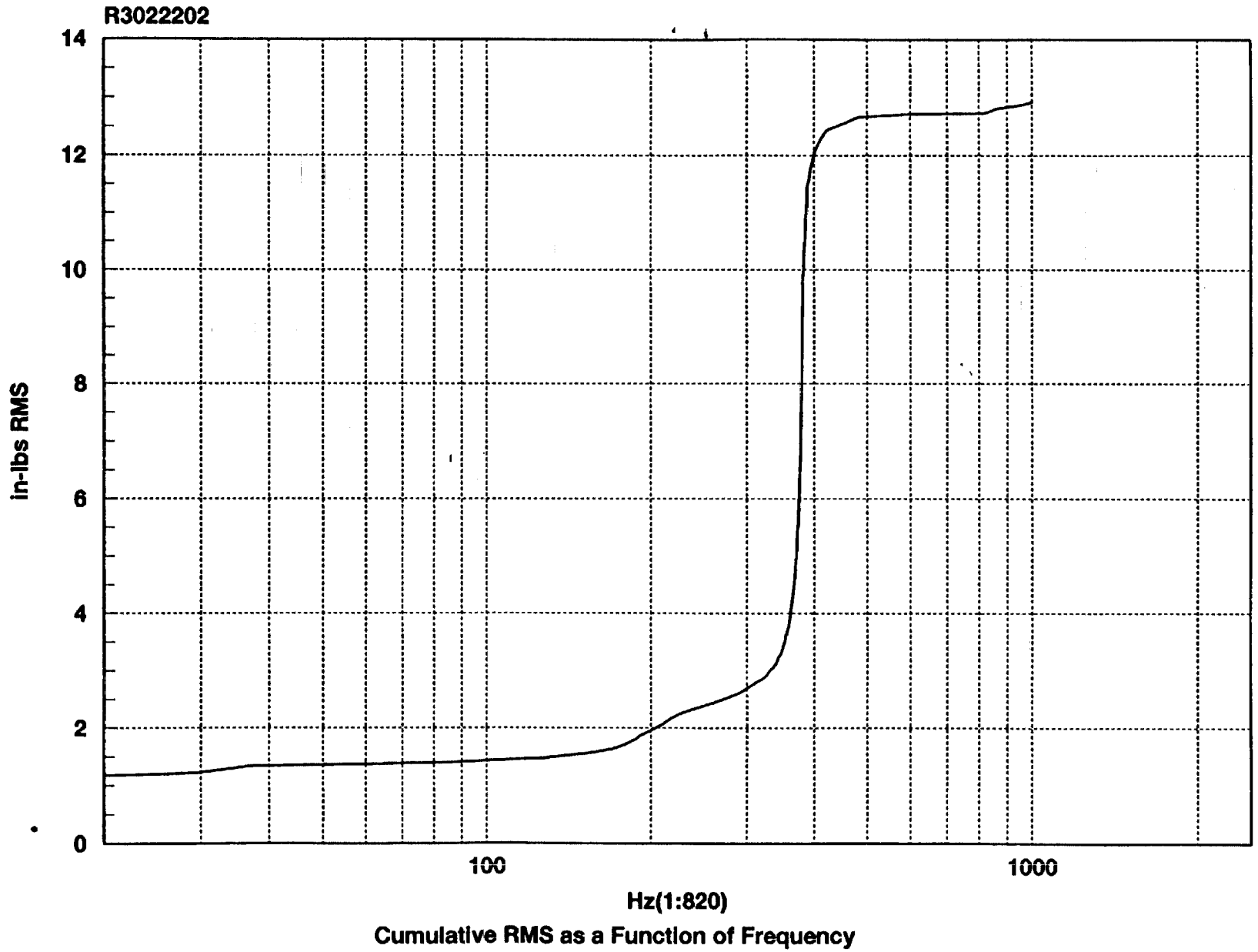

Cumulative RMS as a Function of Frequency

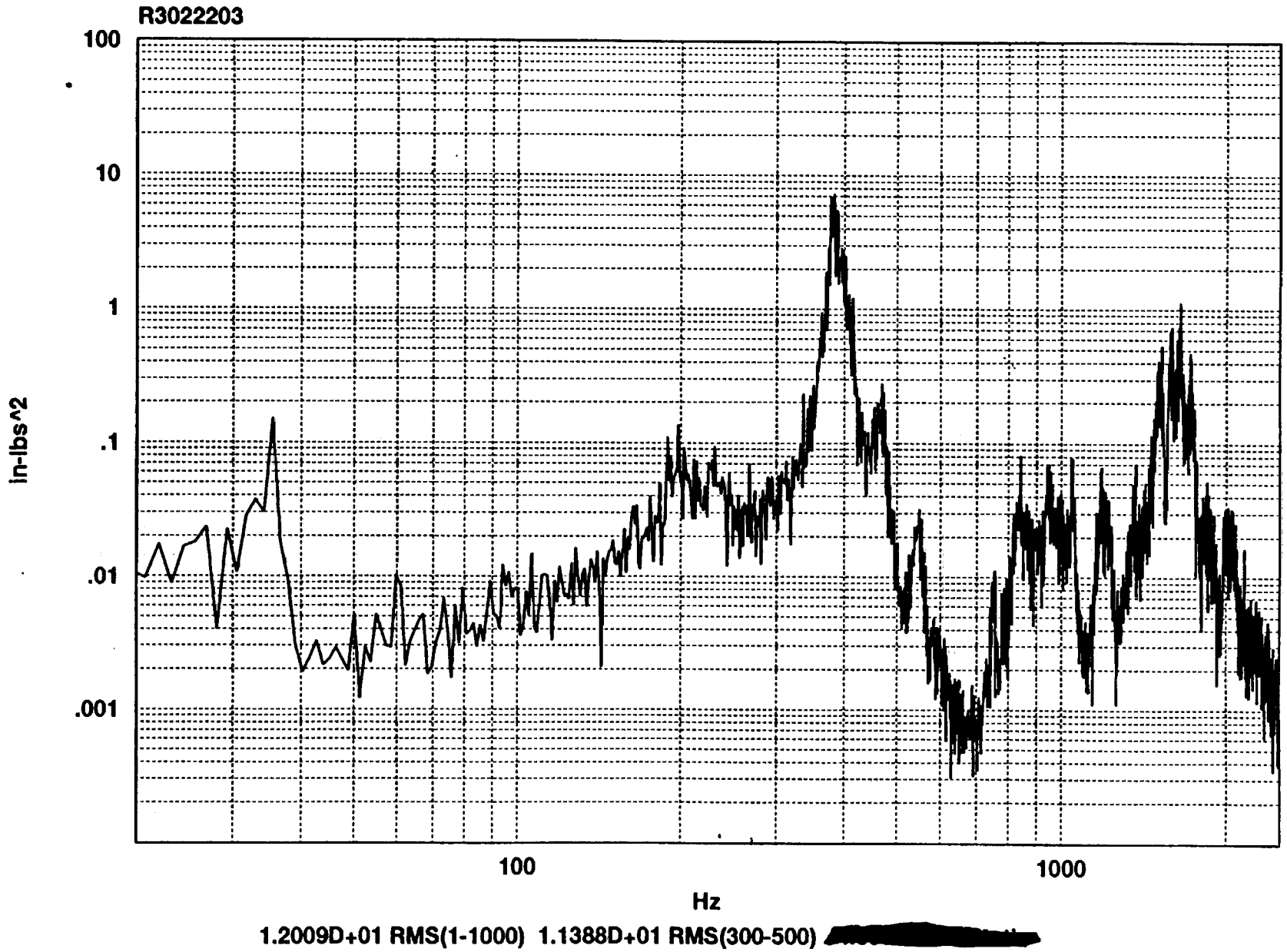
R3022203
100
10
1
.1
.01
.001
in-lbs^2
100
1000
Hz
1.2009D+01 RMS(1-1000) 1.1388D+01 RMS(300-500)

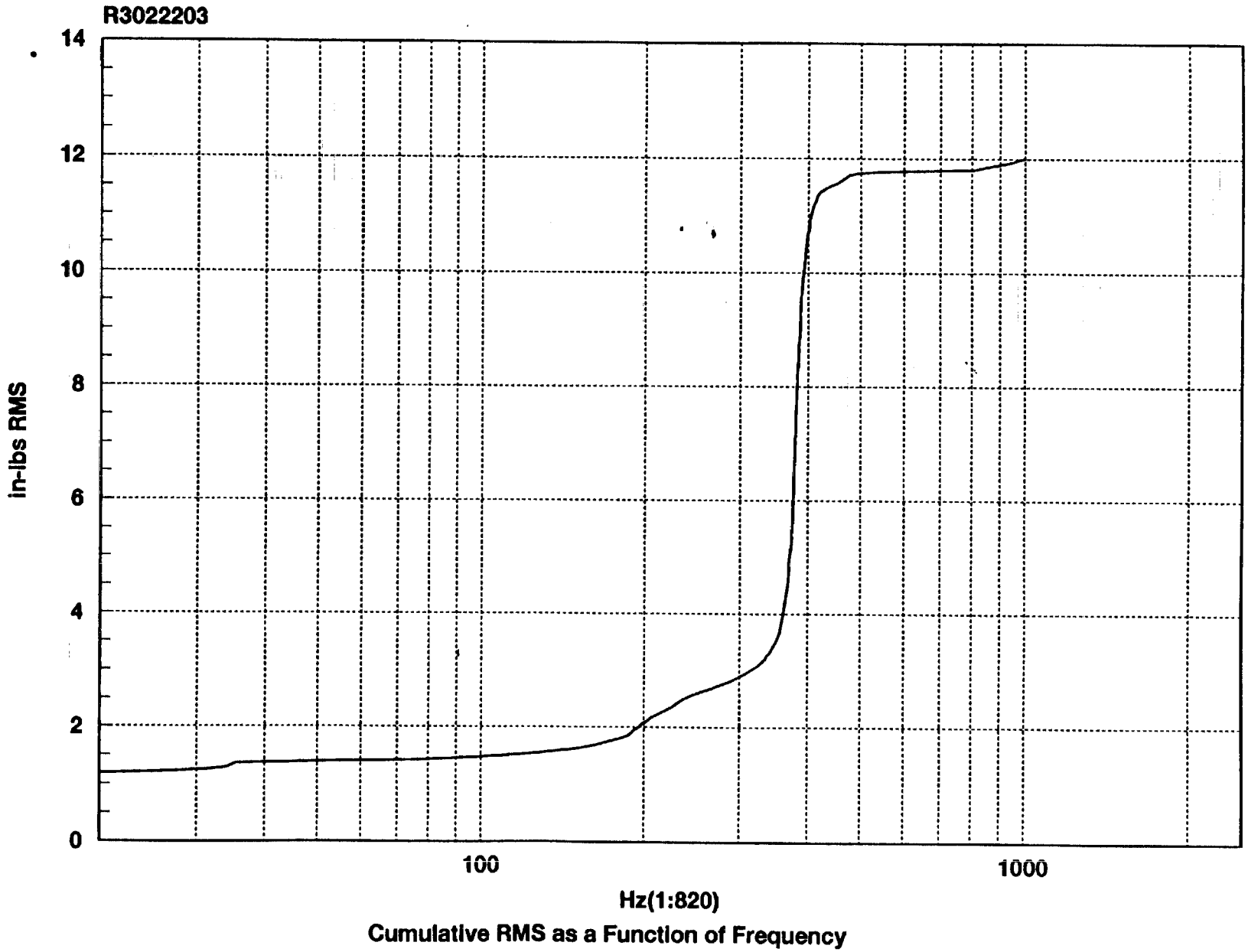

Cumulative RMS as a Function of Frequency

R3022205

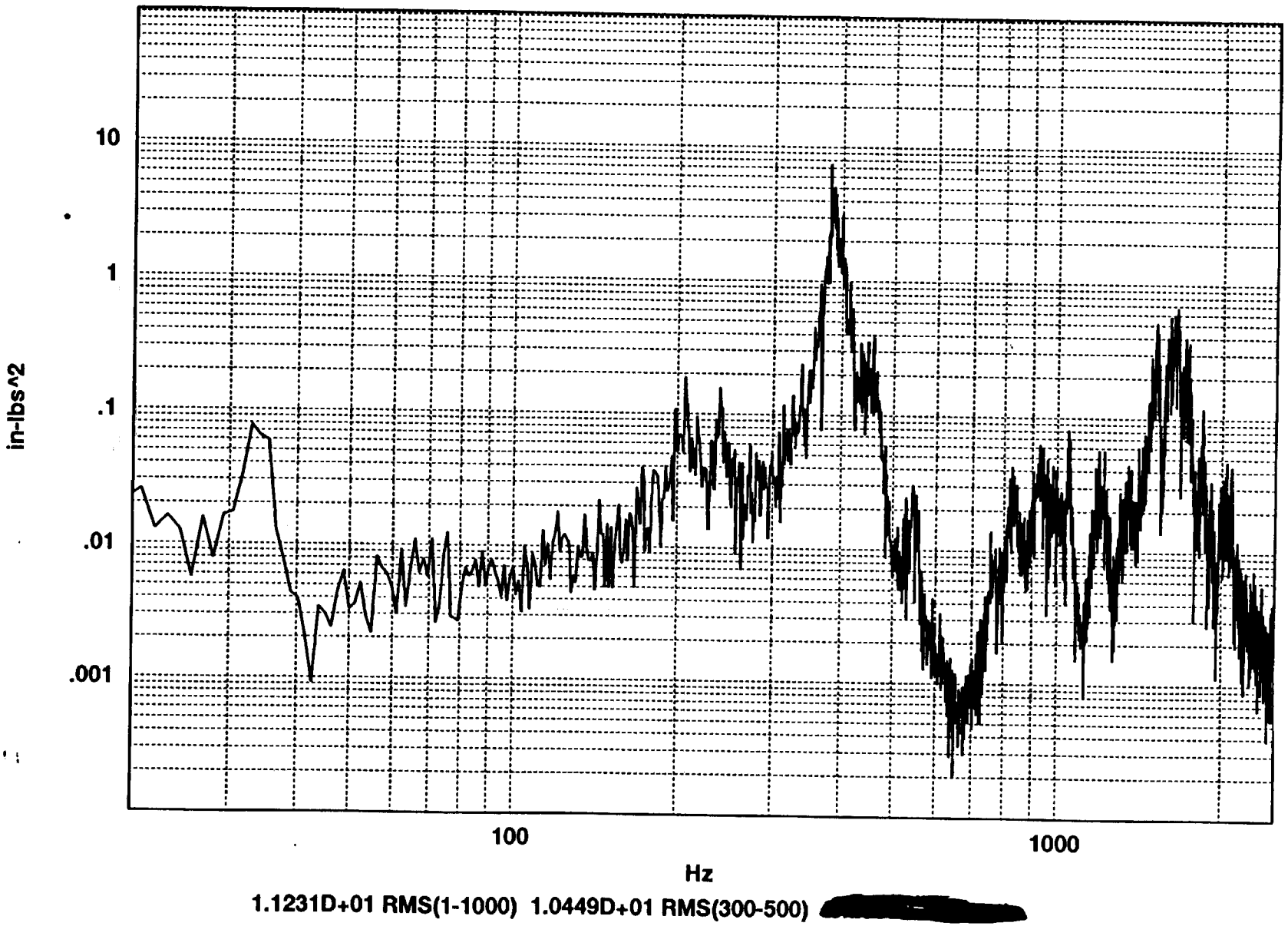

1.1231D+01 RMS(1-1000) 1.0449D+01 RMS(300-500) [redacted]

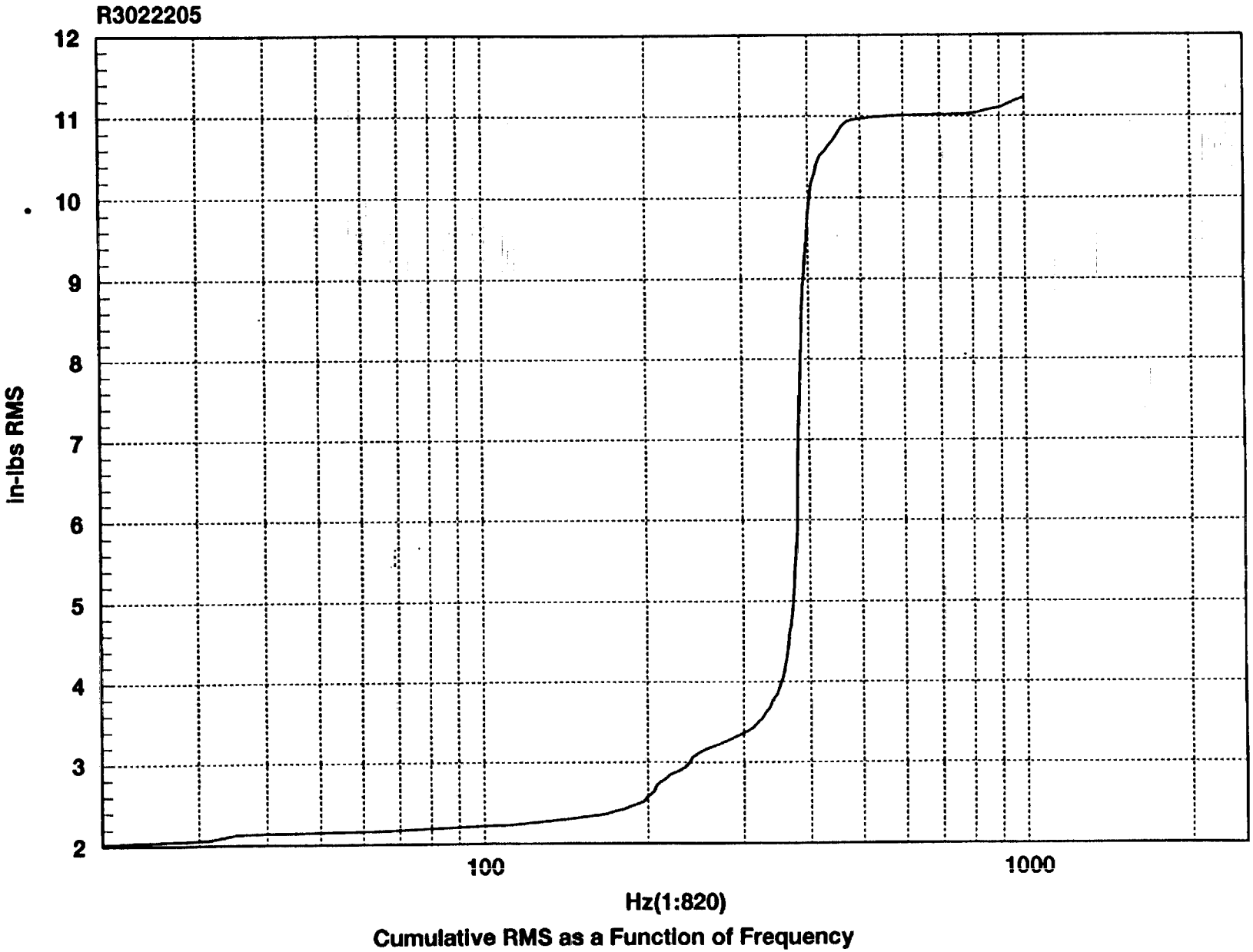

Cumulative RMS as a Function of Frequency

R3022206

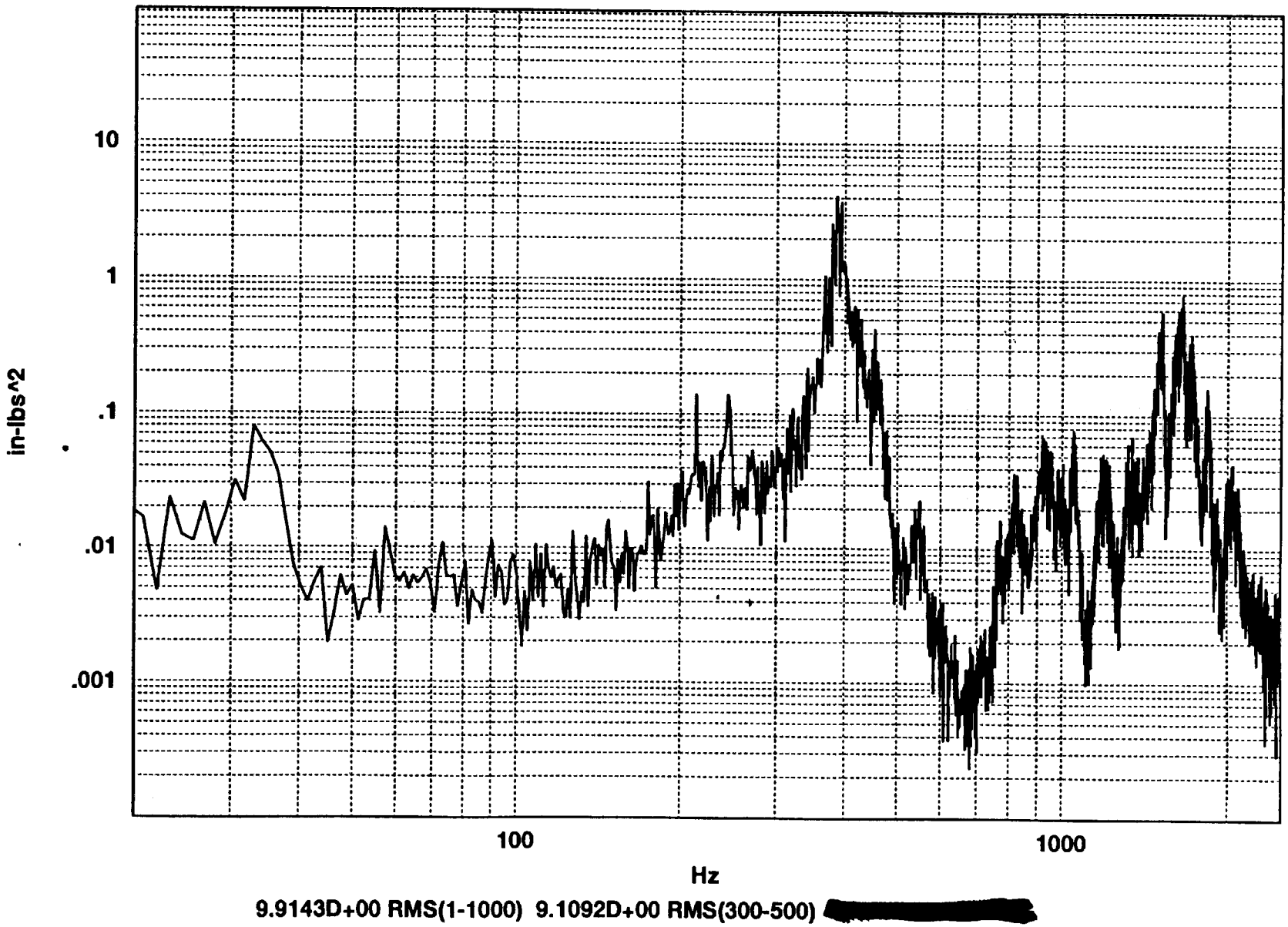

9.9143D+00 RMS(1-1000) 9.1092D+00 RMS(300-500) [redacted]

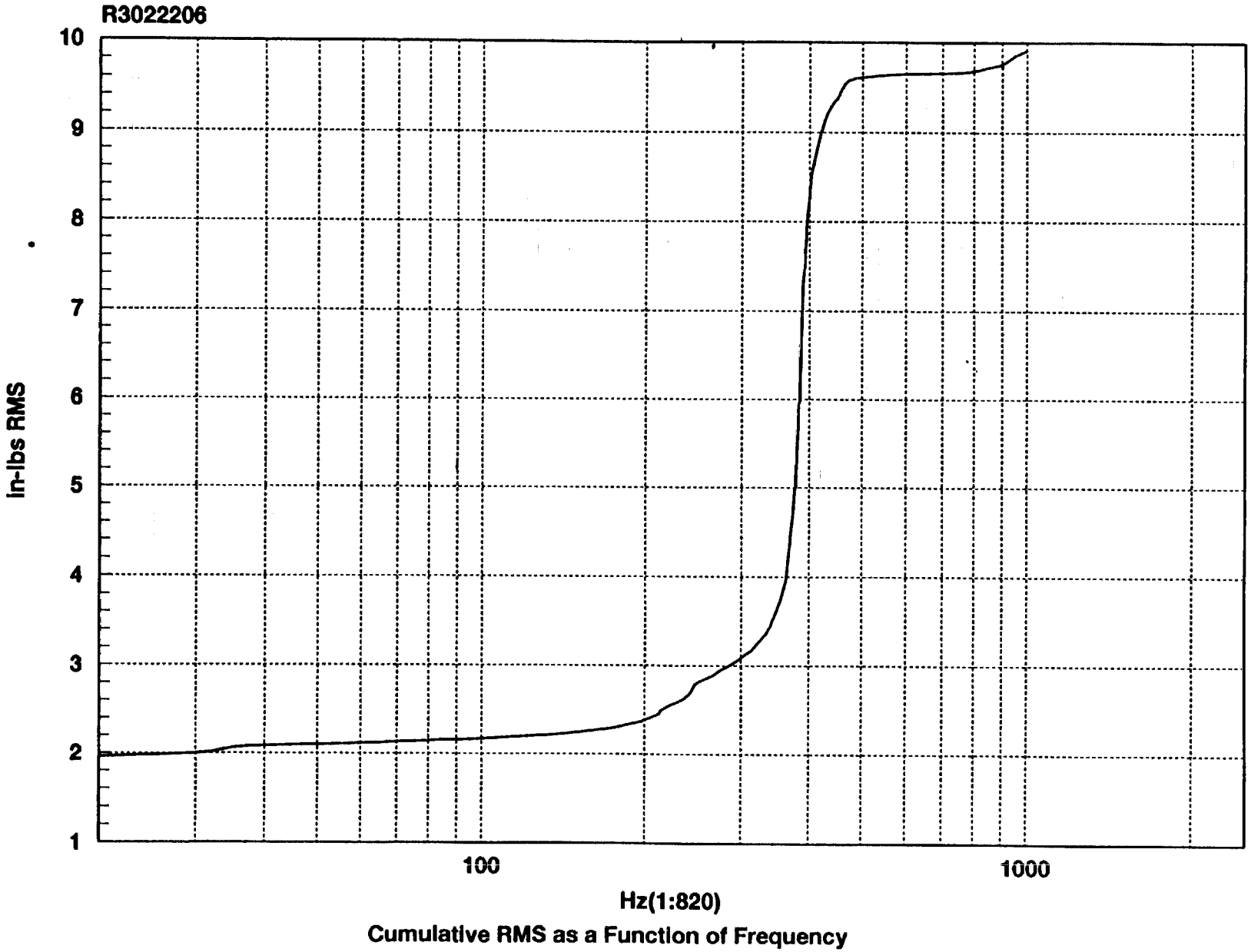

Cumulative RMS as a Function of Frequency

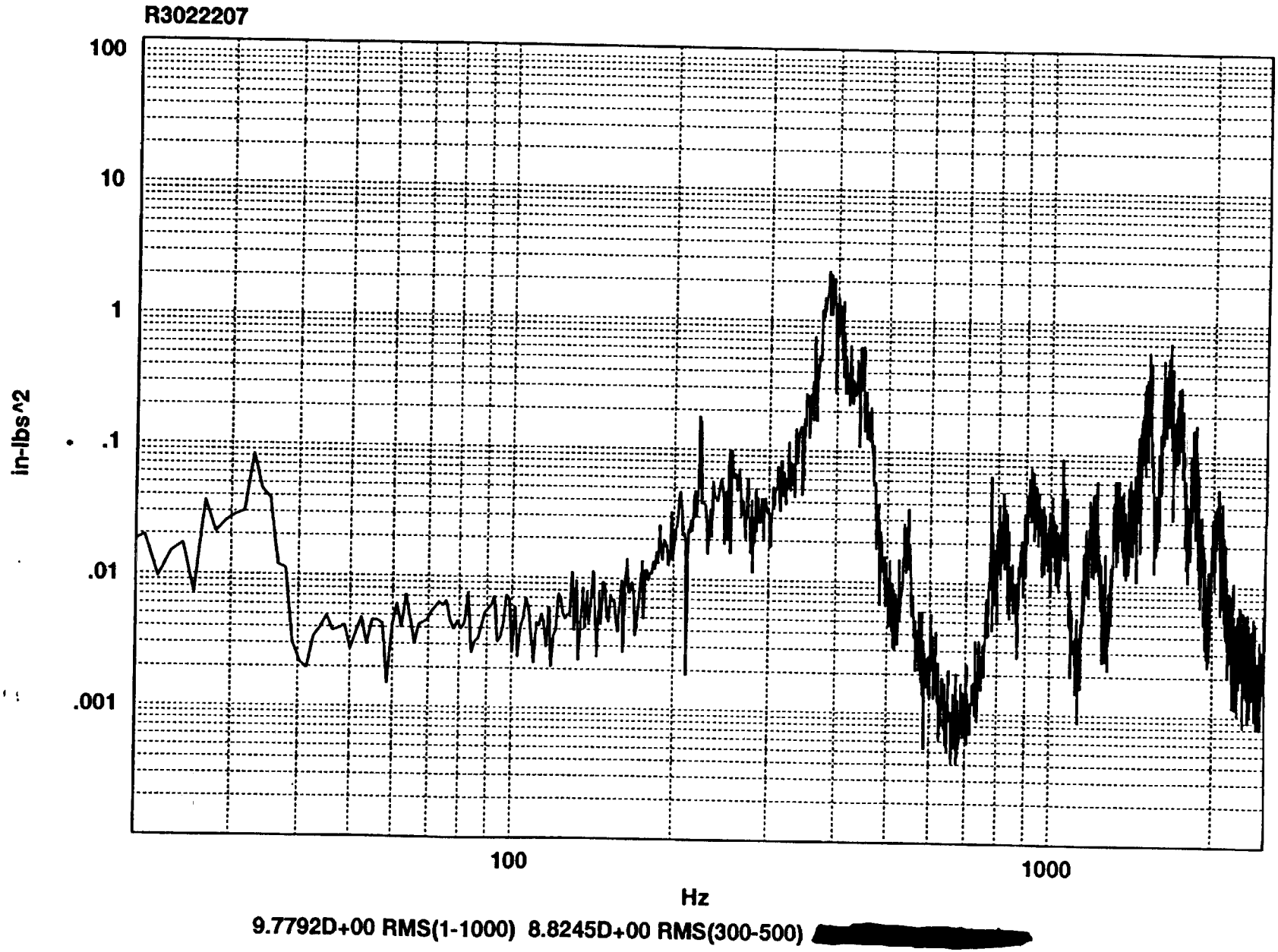
R3022207
100
10
1
.1
.01
.001
in-lbs^2
100
1000
Hz
9.7792D+00 RMS(1-1000) 8.8245D+00 RMS(300-500)

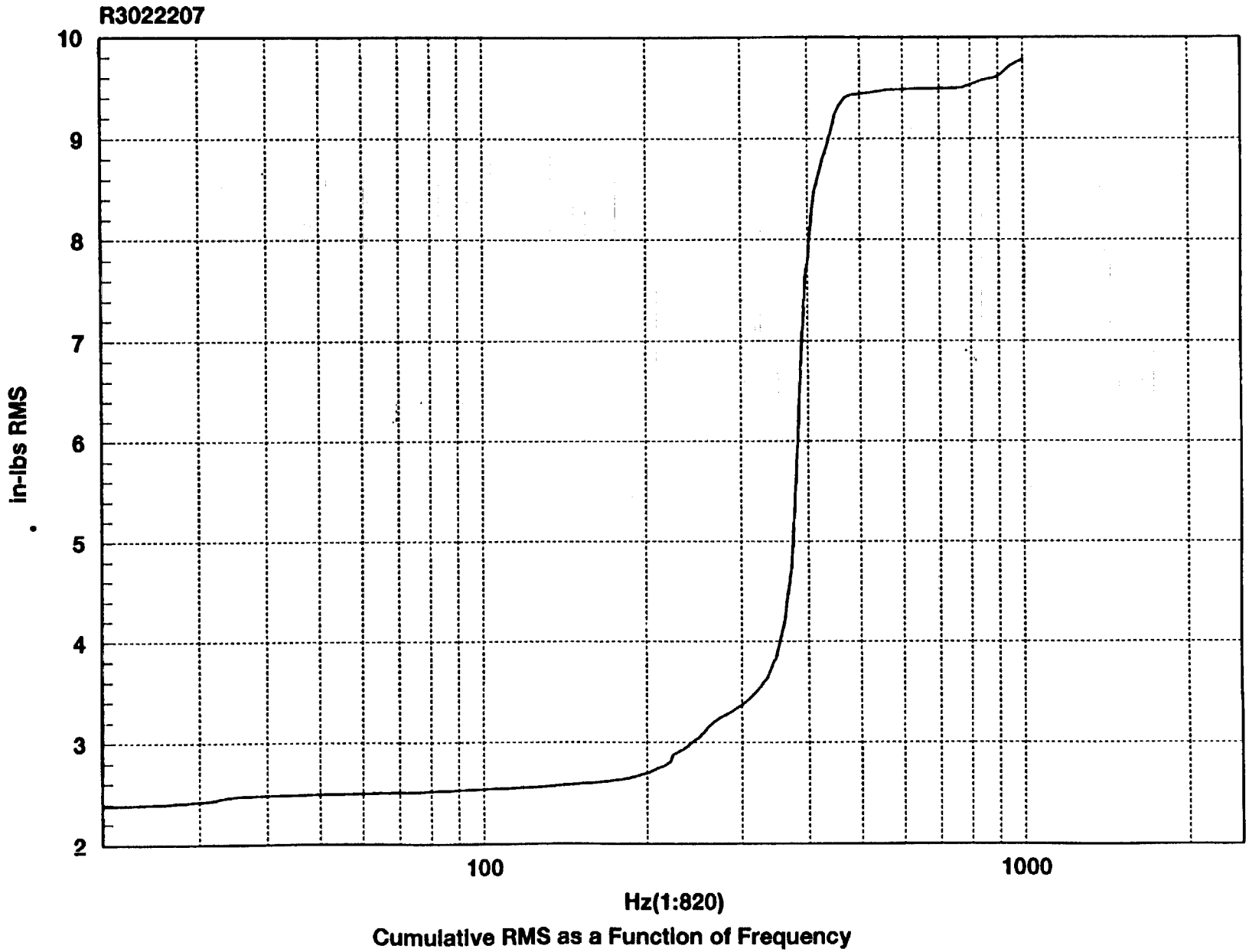

Cumulative RMS as a Function of Frequency

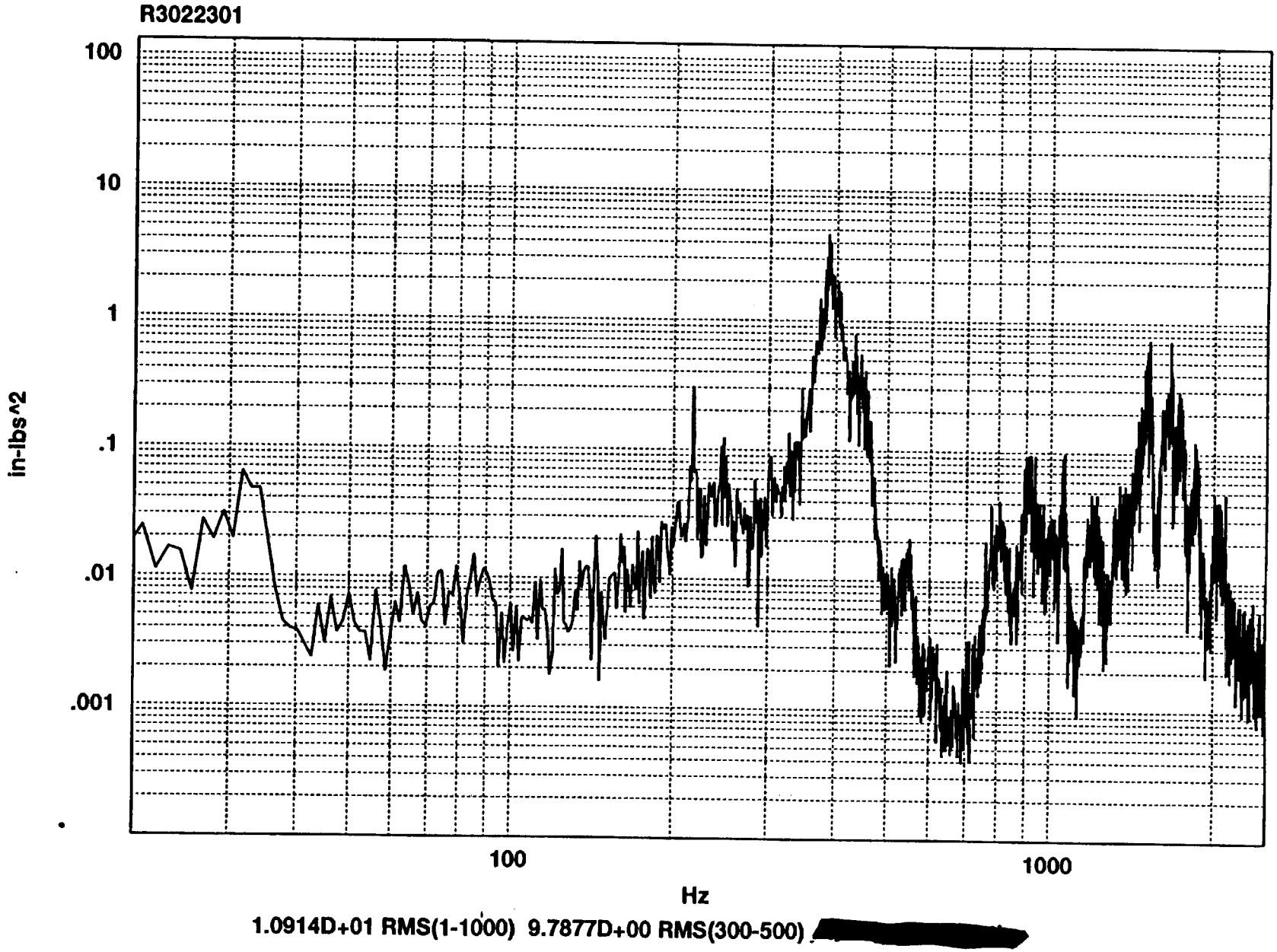
R3022301
100
10
1
.1
.01
.001
in-lbs^2
100
1000
Hz
1.0914D+01 RMS(1-1000) 9.7877D+00 RMS(300-500)

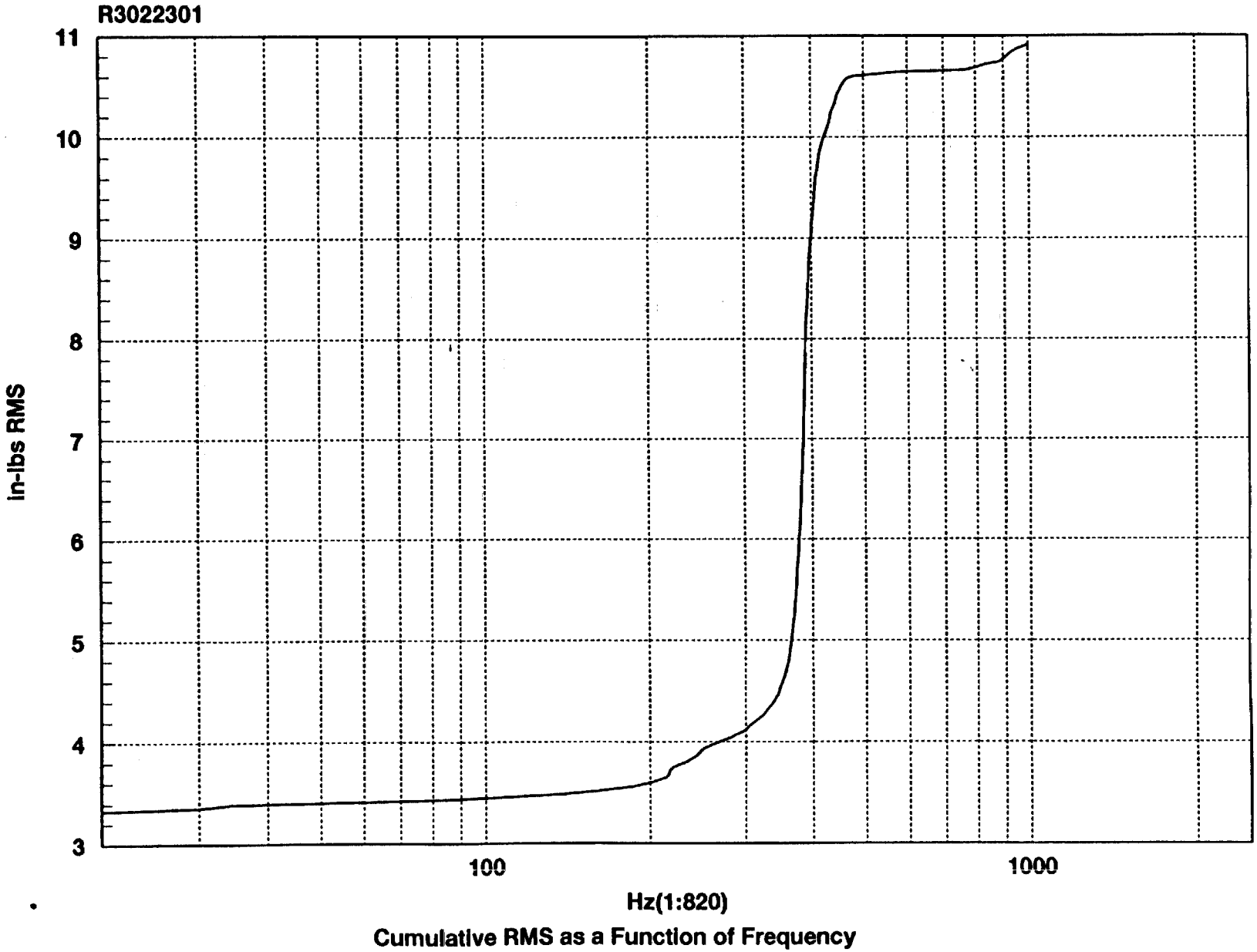

Cumulative RMS as a Function of Frequency

R3022302

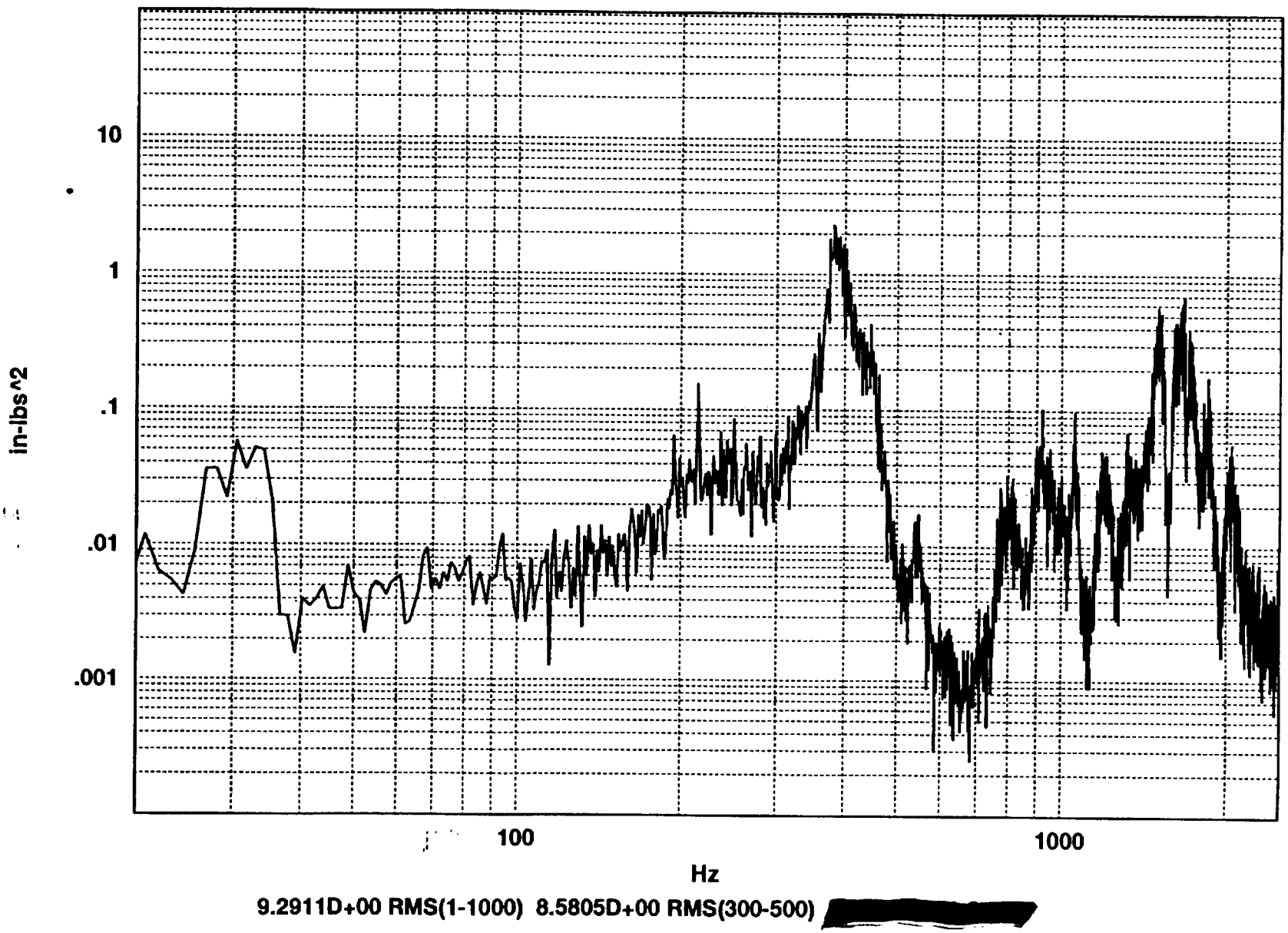

9.2911D+00 RMS(1-1000) 8.5805D+00 RMS(300-500) [redacted]

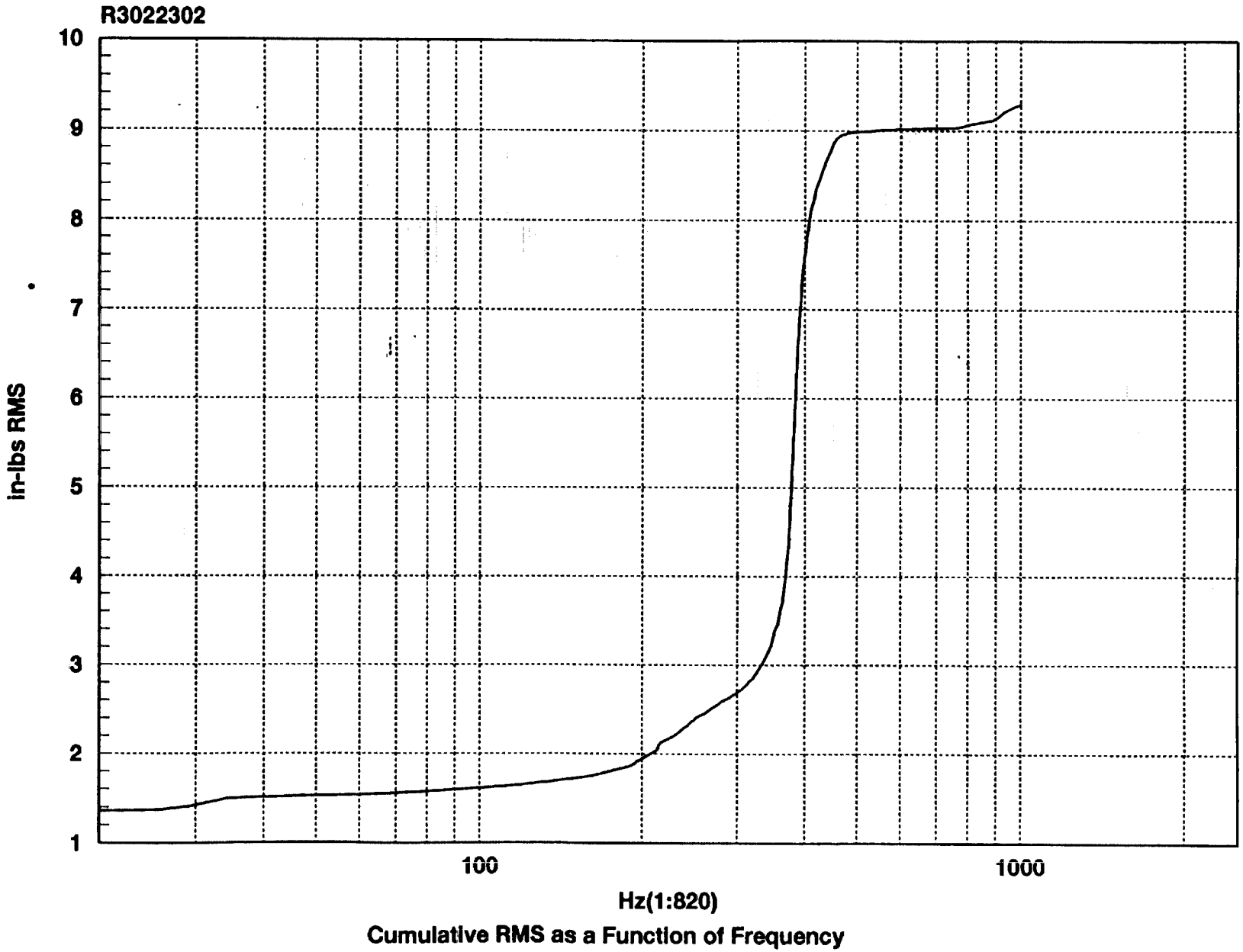

Cumulative RMS as a Function of Frequency

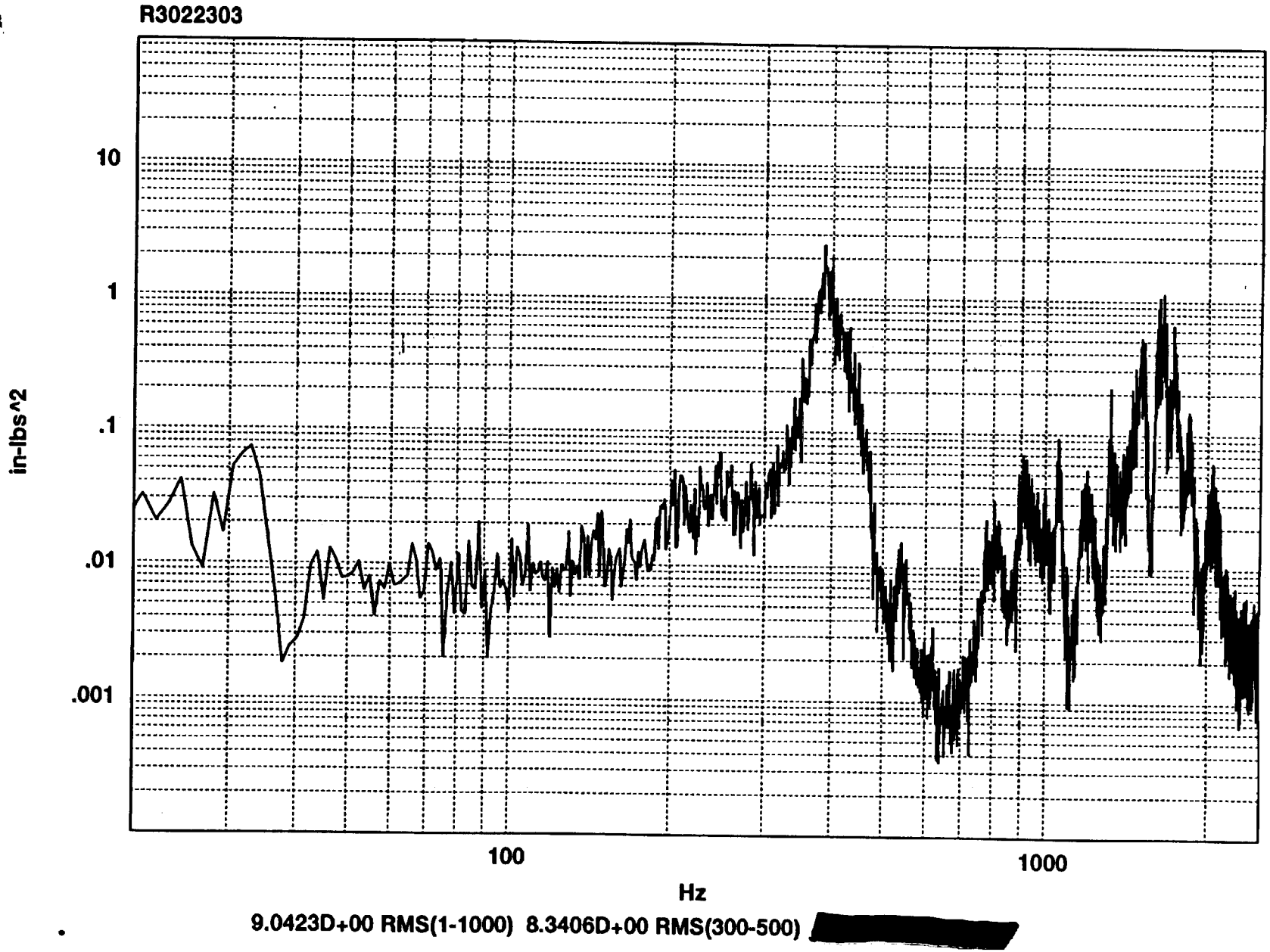
R3022303
10
1
.1
.01
.001
in-lbs^2
100
1000
Hz
9.0423D+00 RMS(1-1000) 8.3406D+00 RMS(300-500)

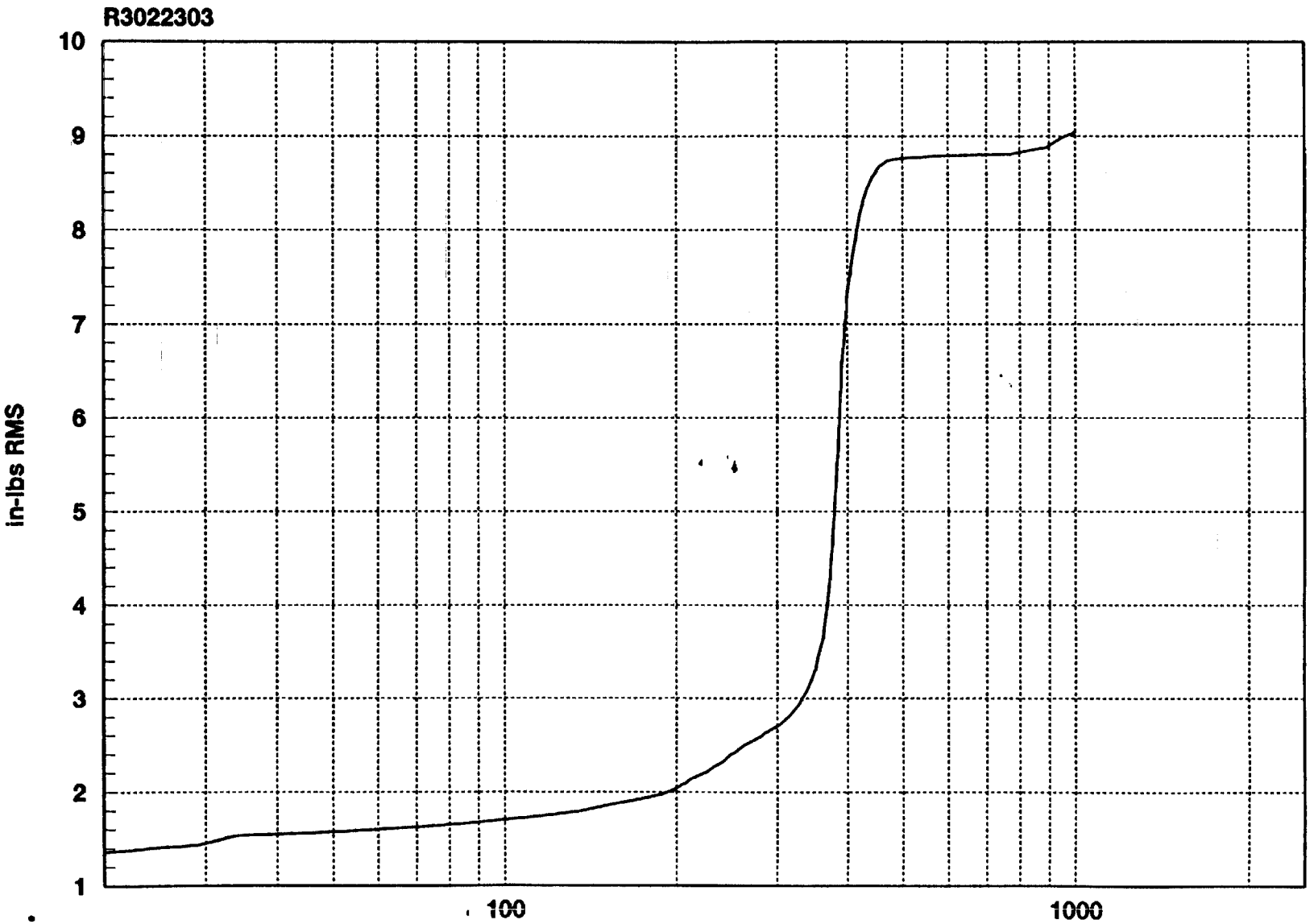

Cumulative RMS as a Function of Frequency

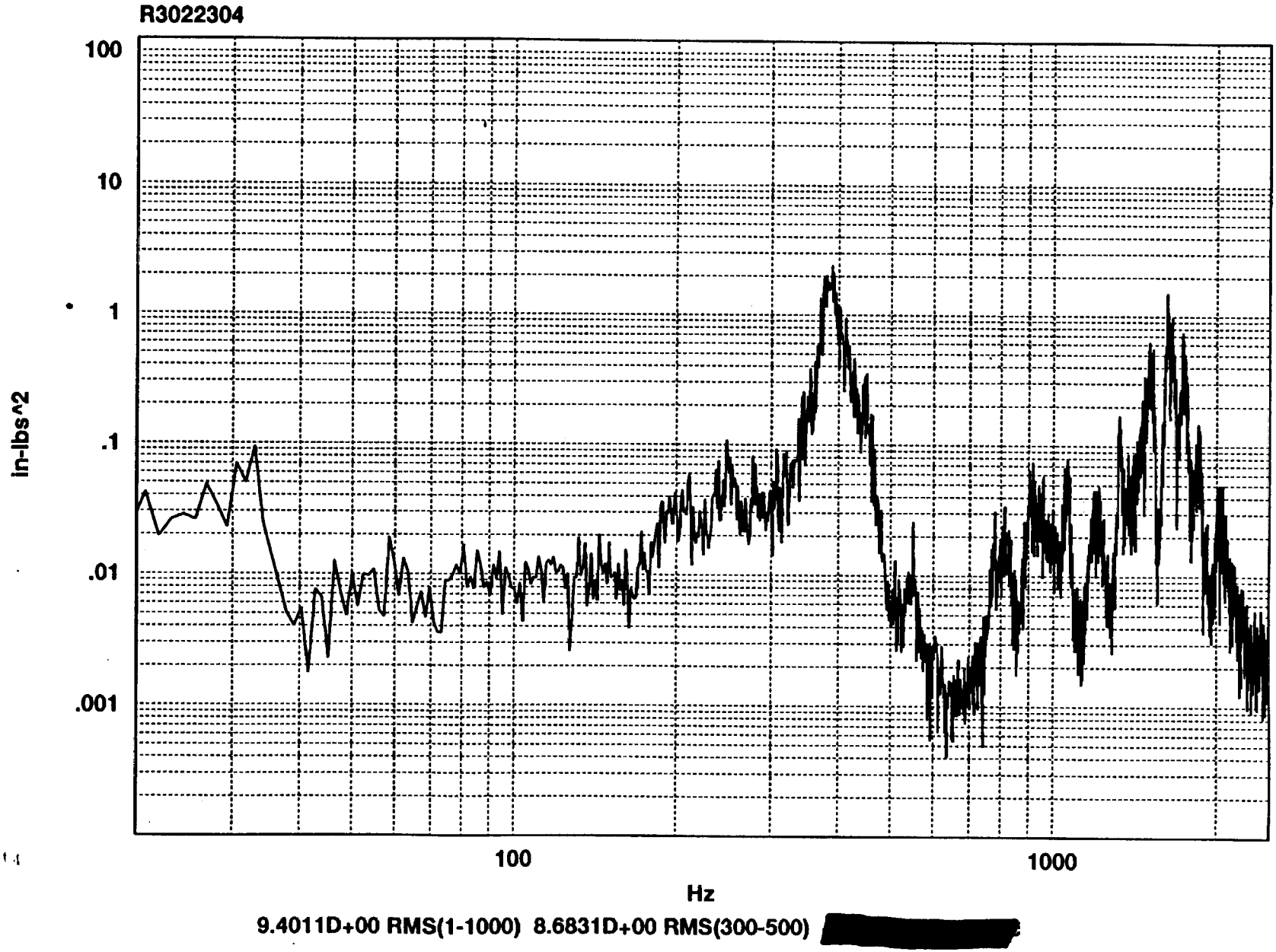
R3022304
100
10
1
.1
.01
.001
in-lbs^2
100
1000
Hz
9.4011D+00 RMS(1-1000) 8.6831D+00 RMS(300-500)

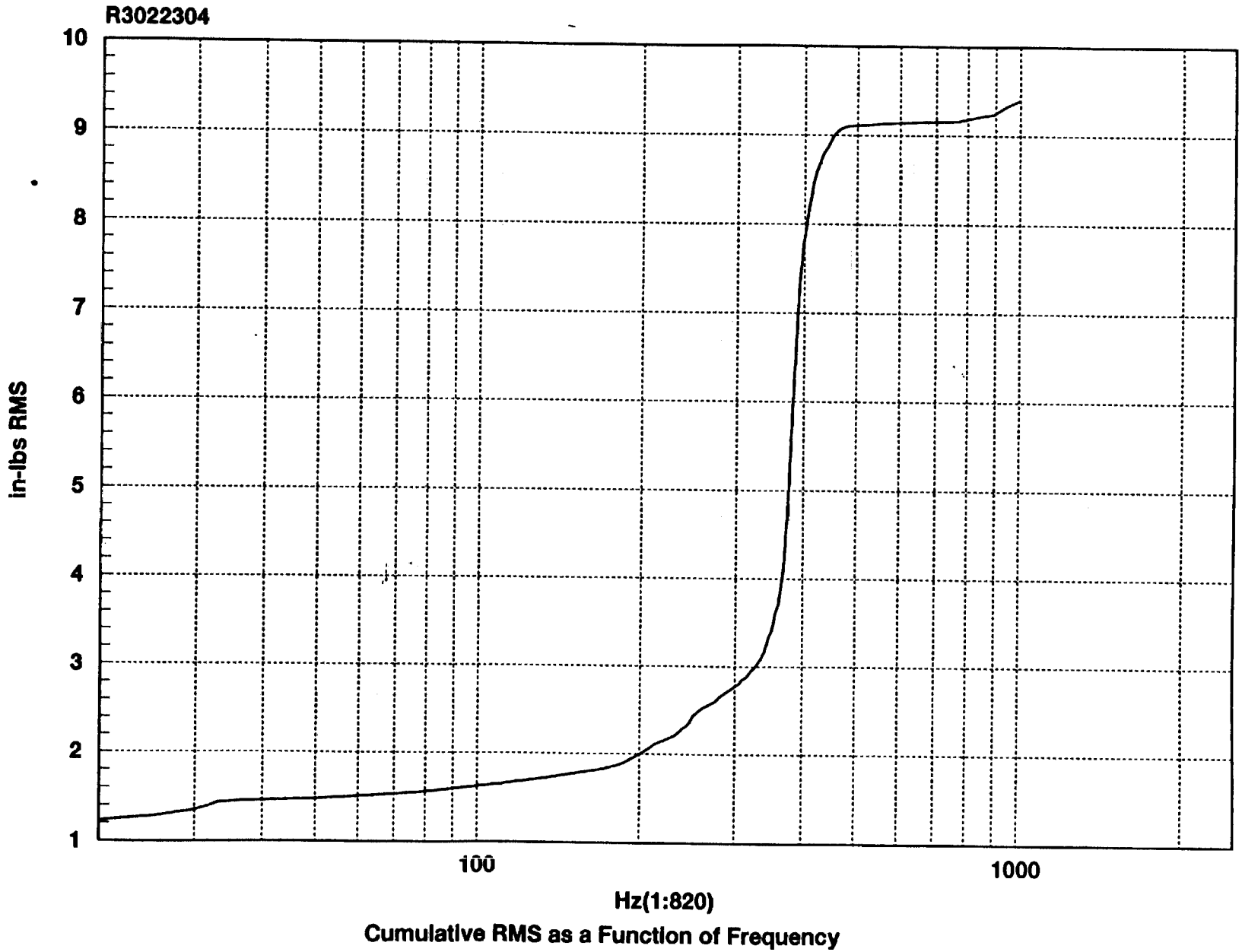

Cumulative RMS as a Function of Frequency

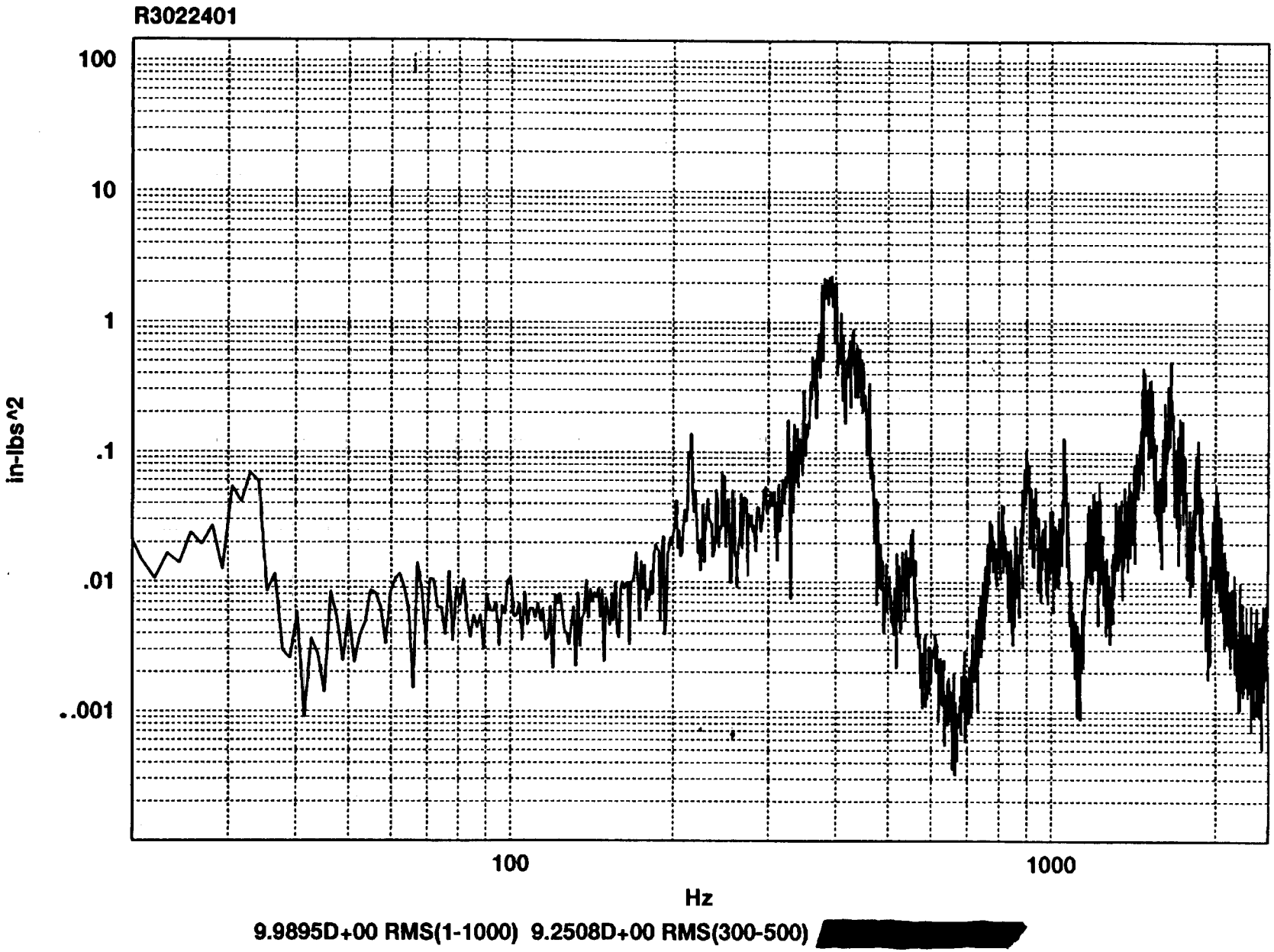
R3022401
100
10
1
.1
.01
..001
in-lbs^2
100
1000
Hz
9.9895D+00 RMS(1-1000) 9.2508D+00 RMS(300-500)

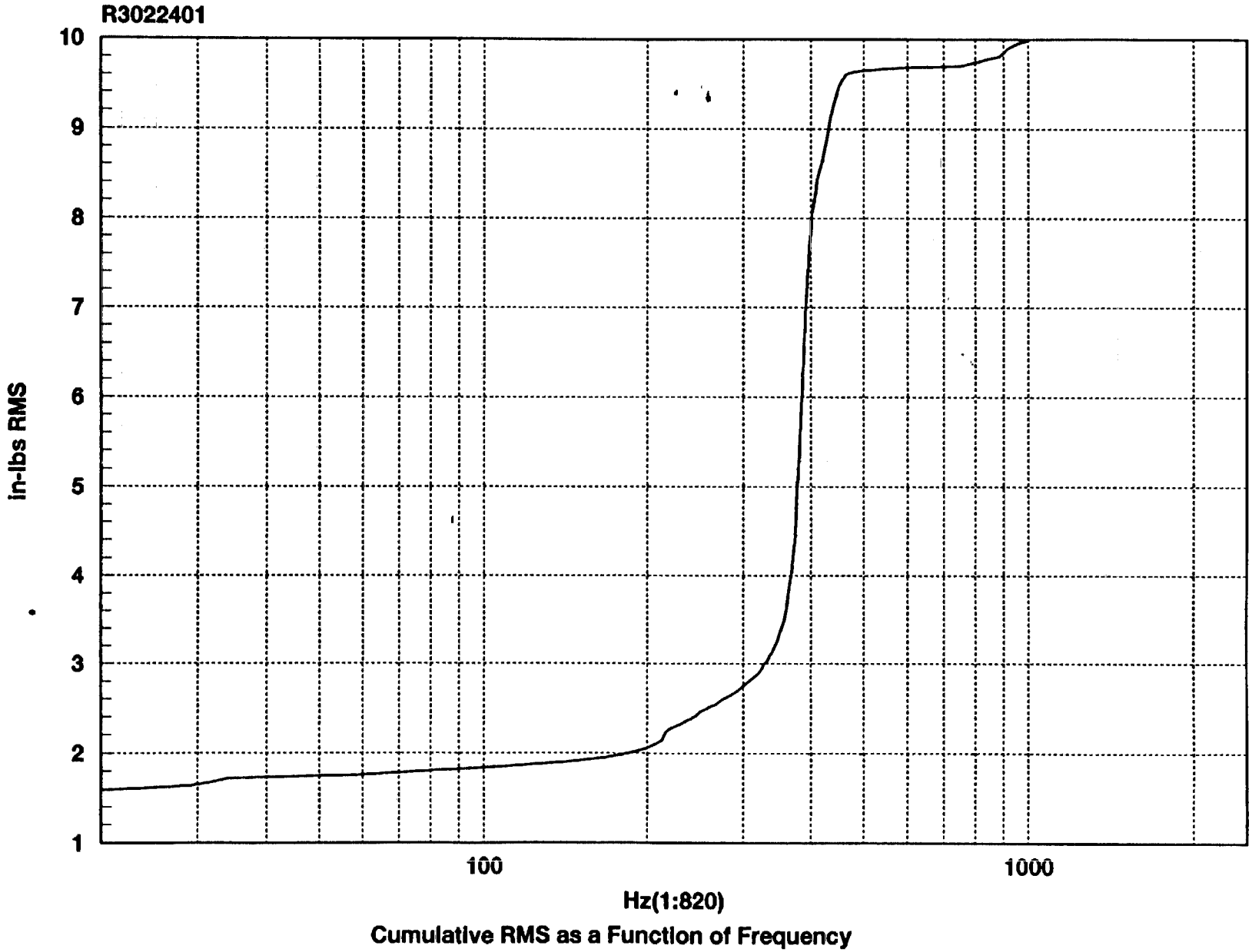
R3022401
10
9
8
7
6
5
4
3
2
1
in-lbs RMS
100
1000
Hz(1:820)
Cumulative RMS as a Function of Frequency

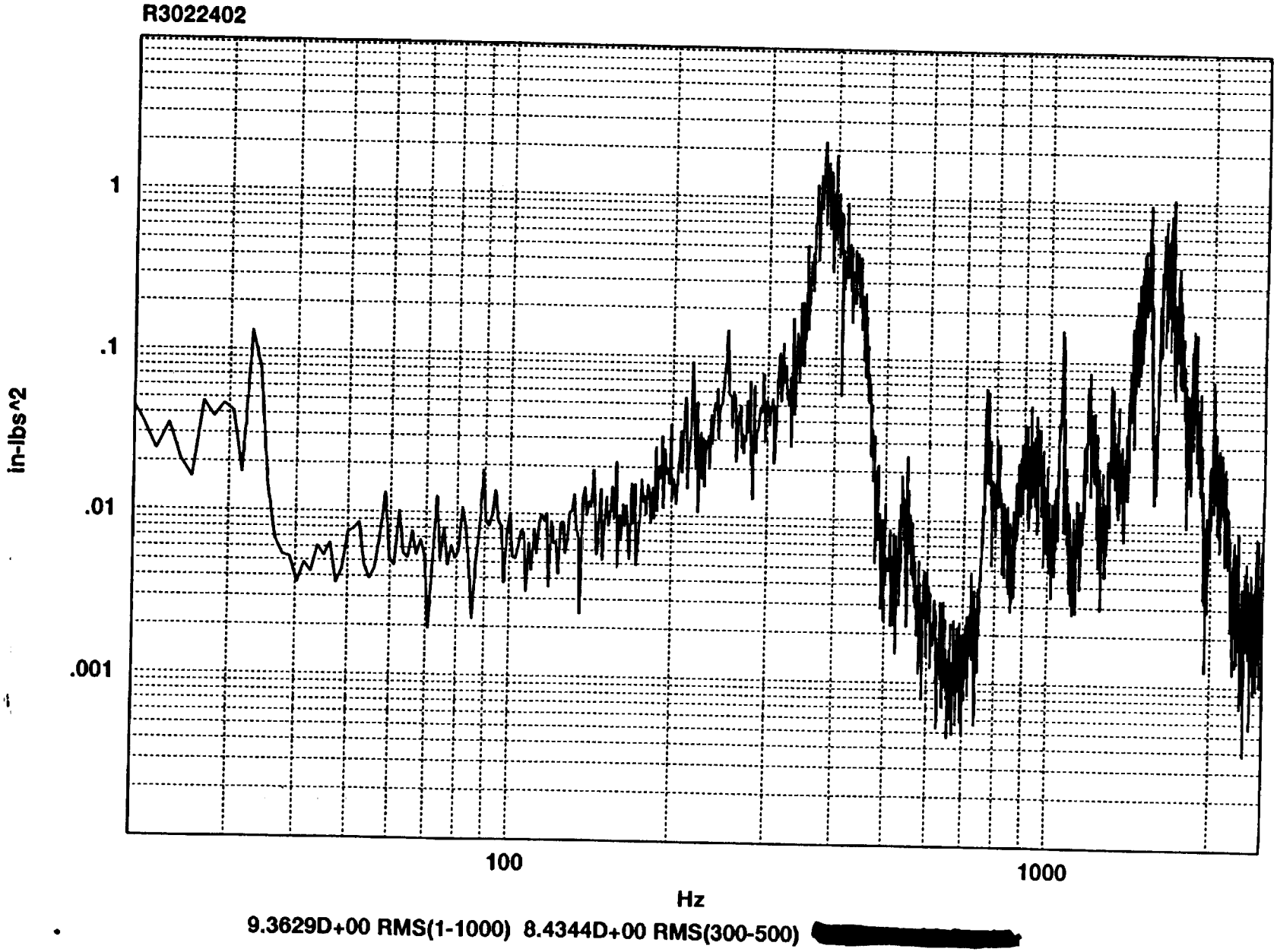
R3022402
1
.1
.01
.001
in-lbs^2
100
1000
Hz
9.3629D+00 RMS(1-1000) 8.4344D+00 RMS(300-500)

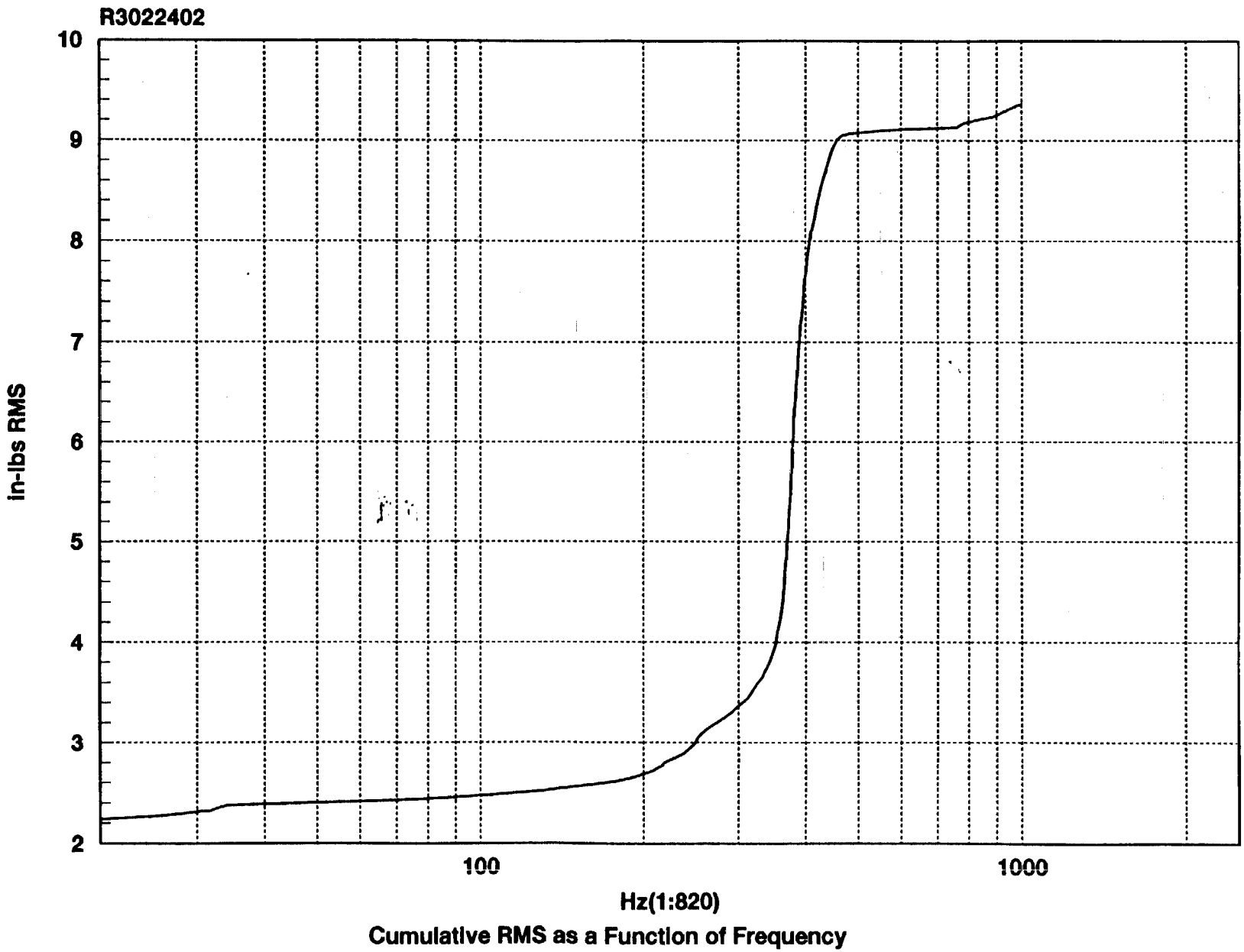

Cumulative RMS as a Function of Frequency

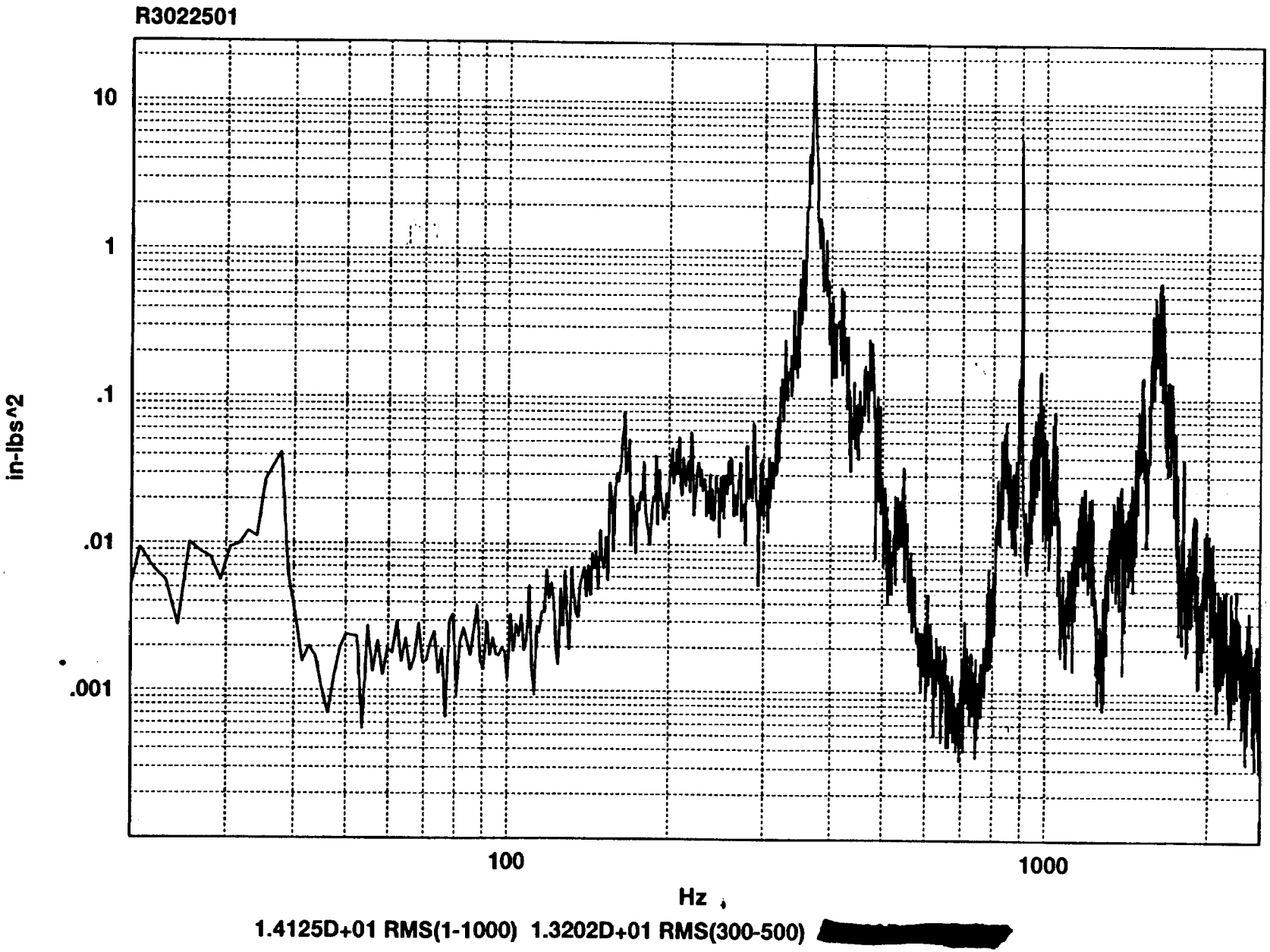
R3022501
10
1
.1
.01
.001
in-lbs^2
100
1000
Hz
1.4125D+01 RMS(1-1000) 1.3202D+01 RMS(300-500)

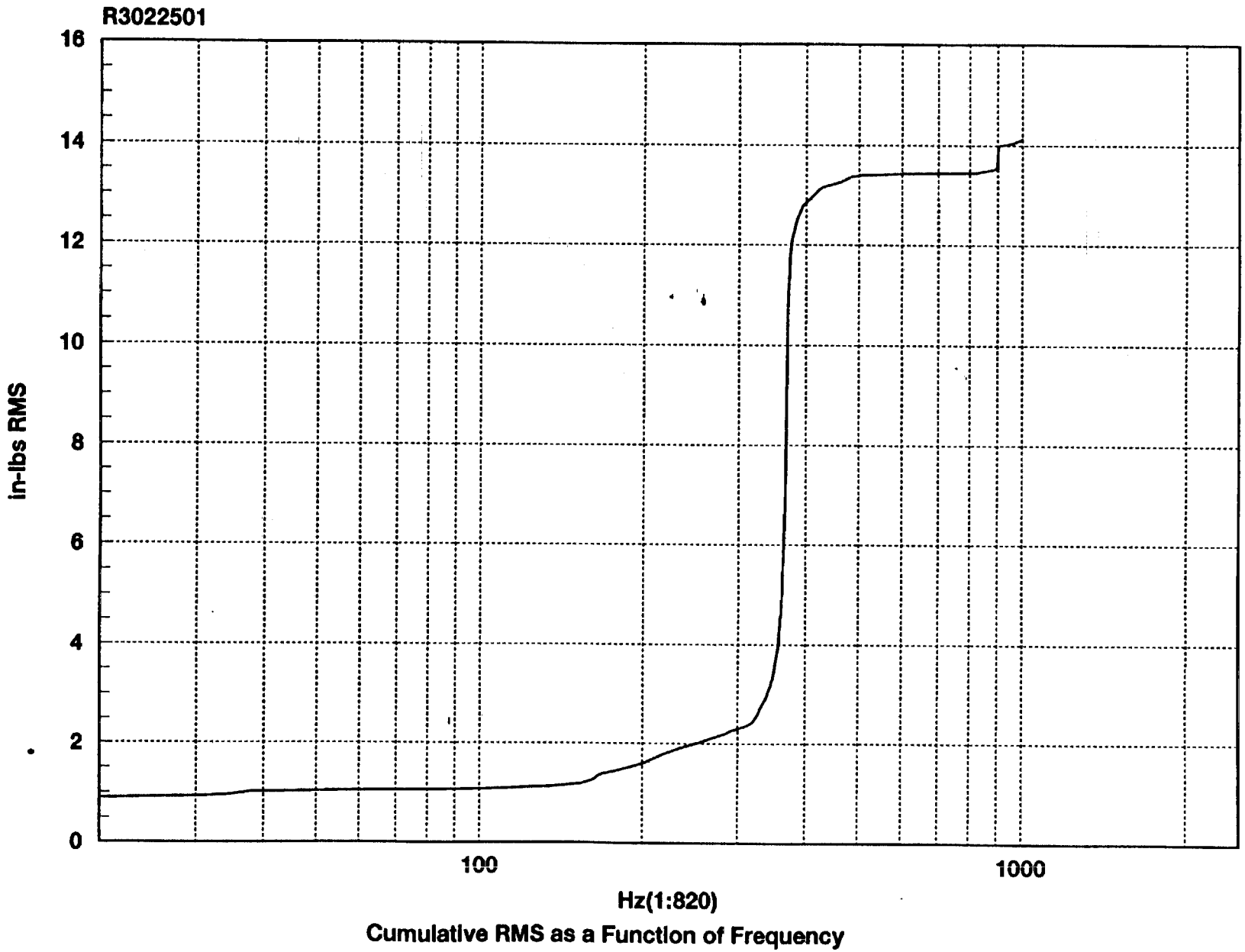

Cumulative RMS as a Function of Frequency

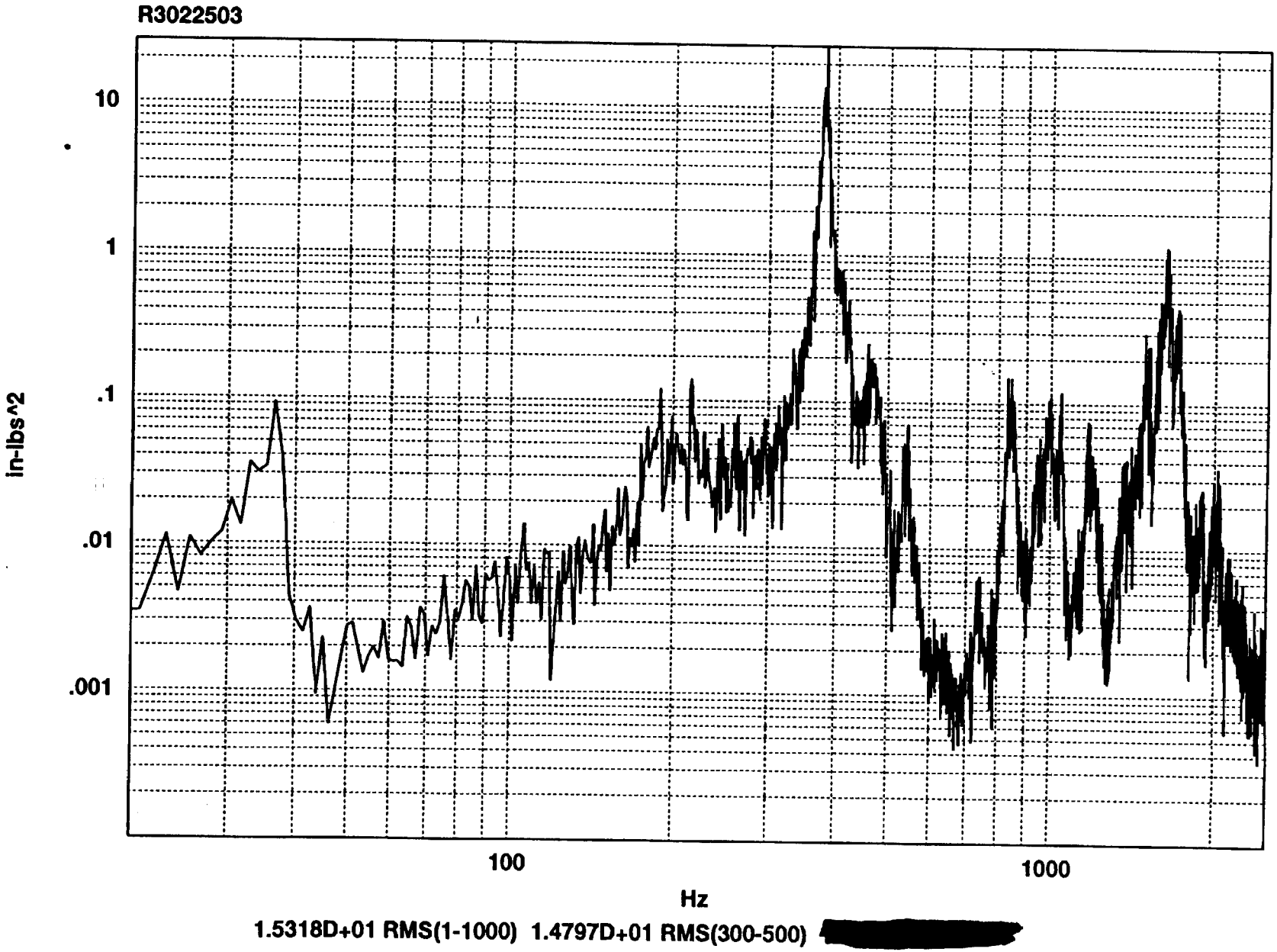
R3022503
10
1
.1
.01
.001
In-lbs^2
100
1000
Hz
1.5318D+01 RMS(1-1000) 1.4797D+01 RMS(300-500)

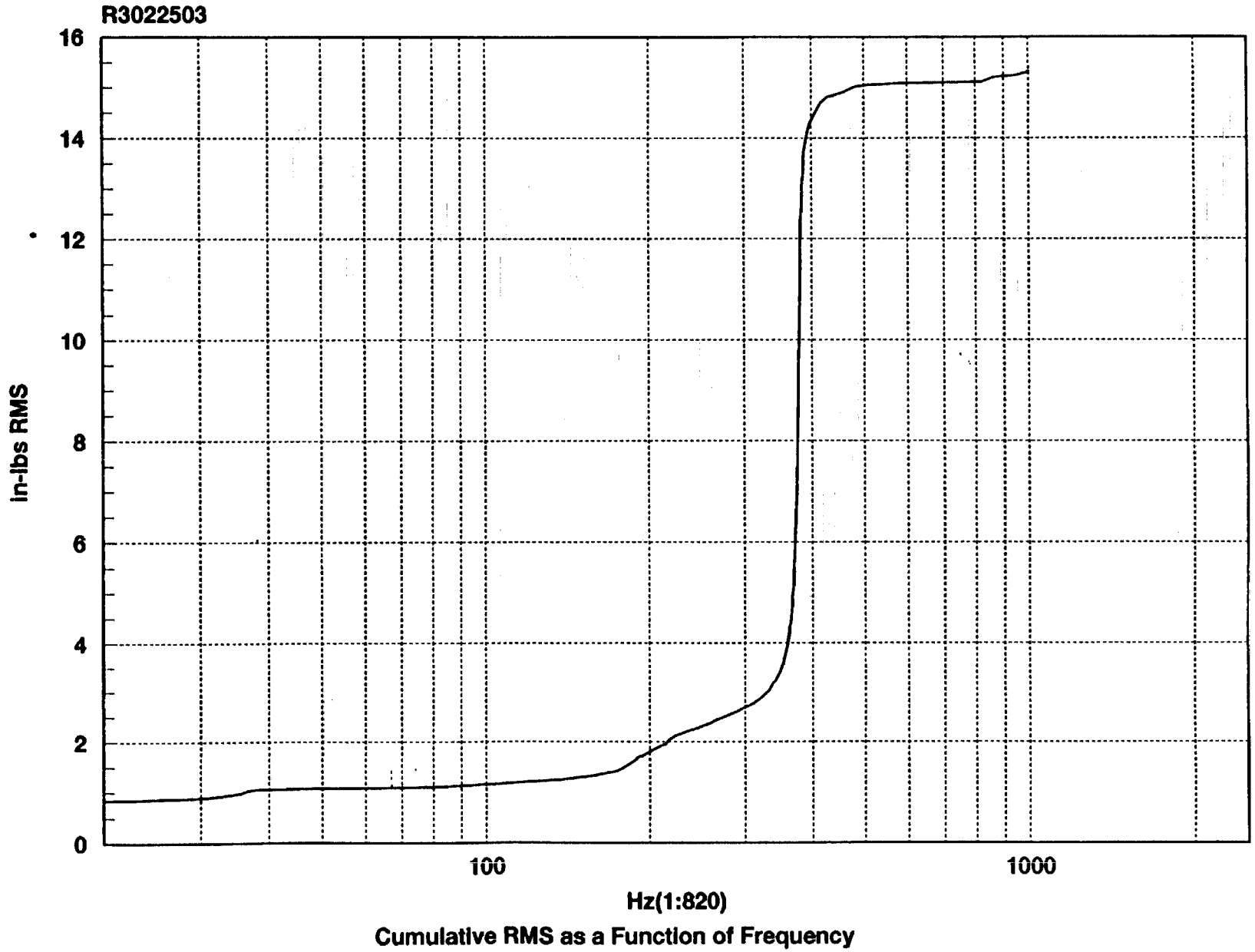

Cumulative RMS as a Function of Frequency

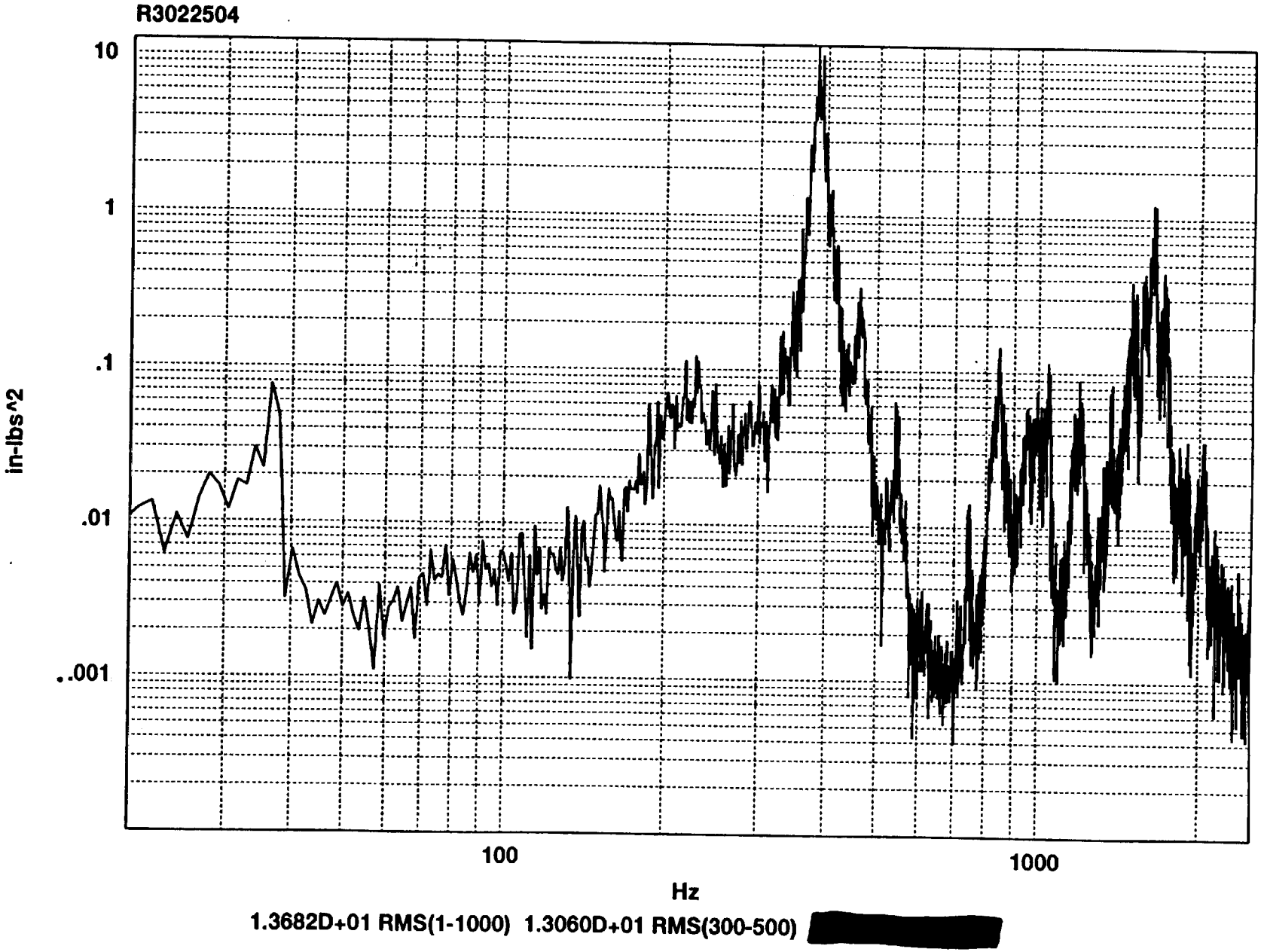
R3022504
10
1
.1
.01
..001
in-lbs^2
100
1000
Hz
1.3682D+01 RMS(1-1000) 1.3060D+01 RMS(300-500)

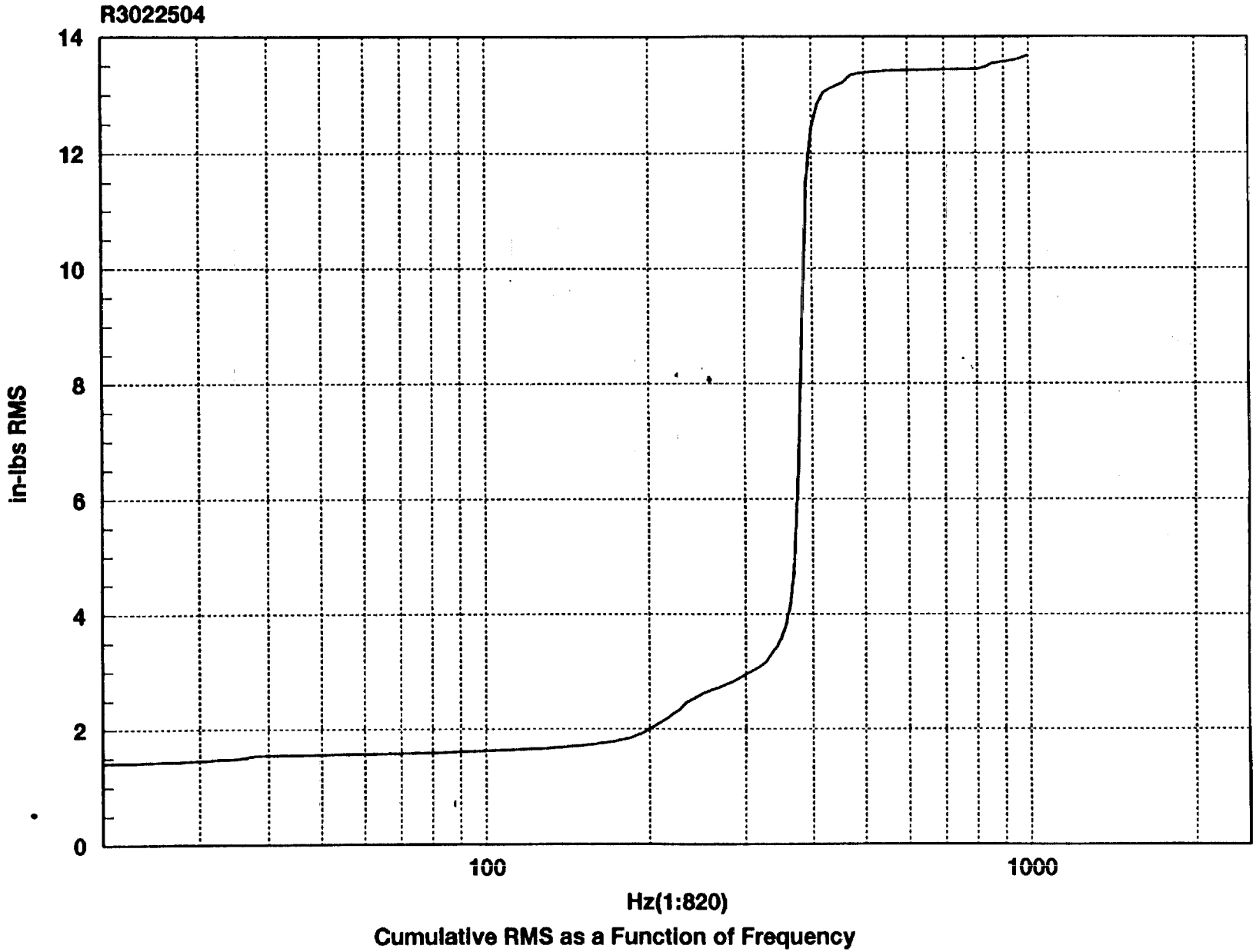

Cumulative RMS as a Function of Frequency

R3022505

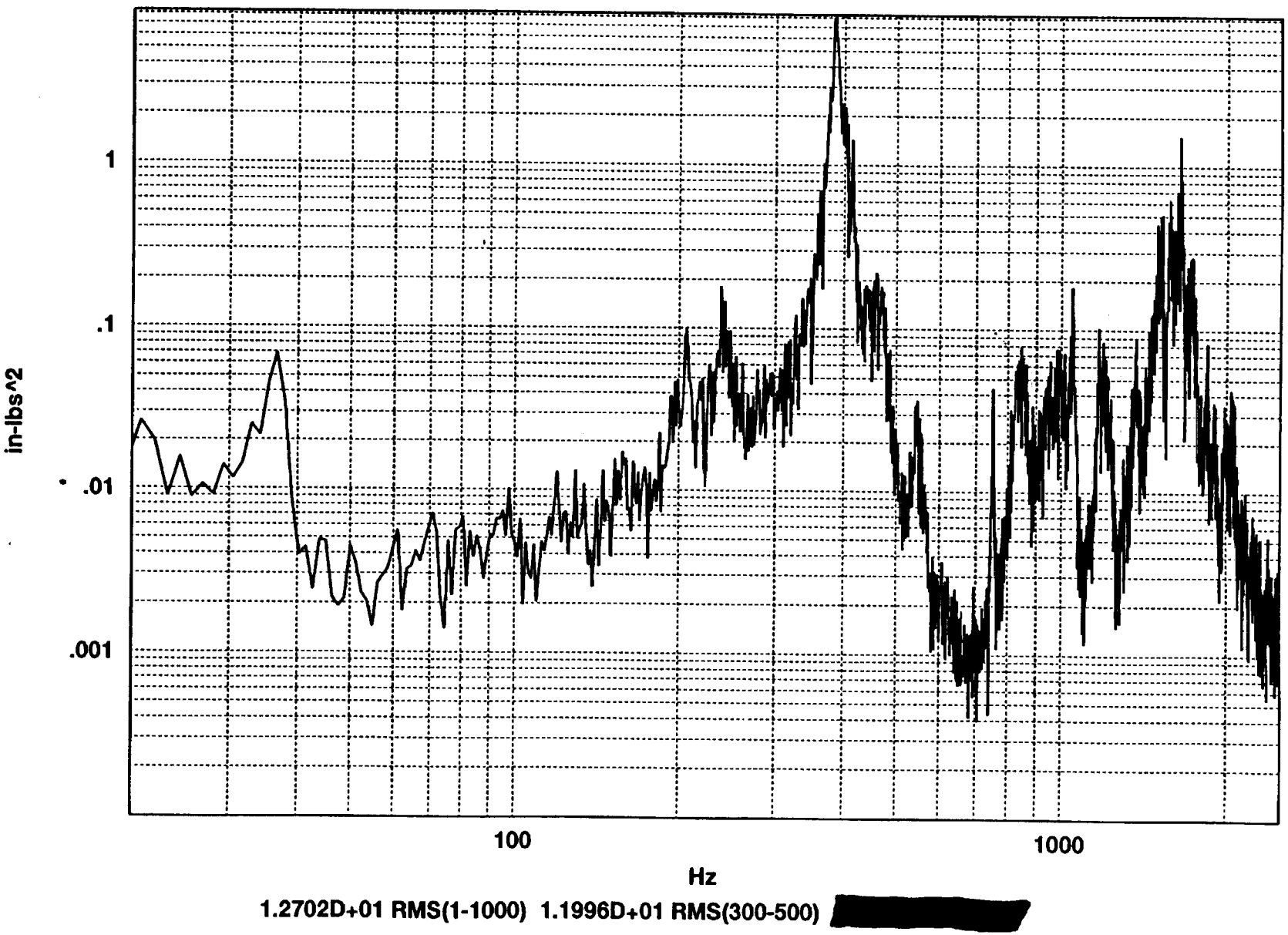

1.2702D+01 RMS(1-1000) 1.1996D+01 RMS(300-500) [redacted]

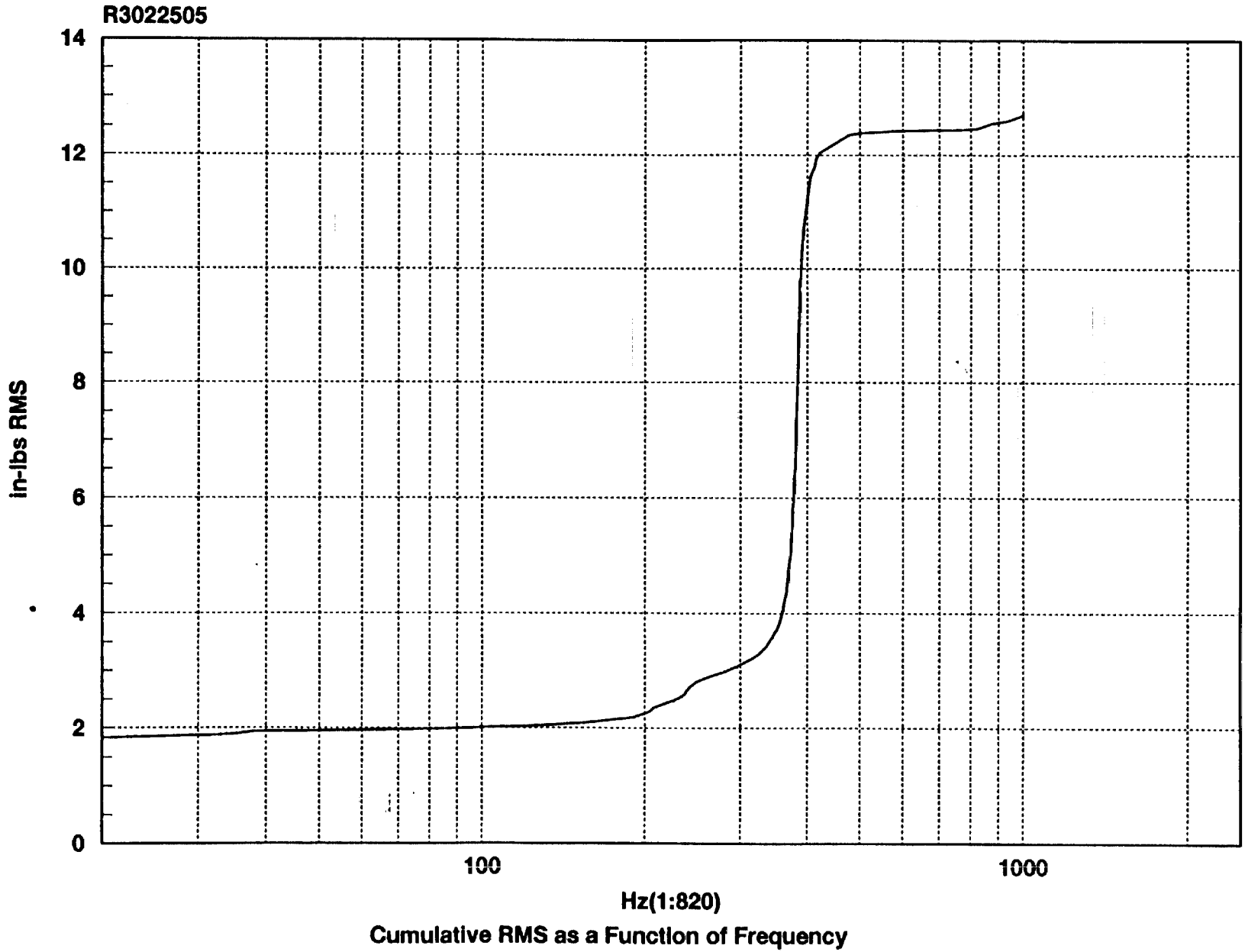

Cumulative RMS as a Function of Frequency

R3022506

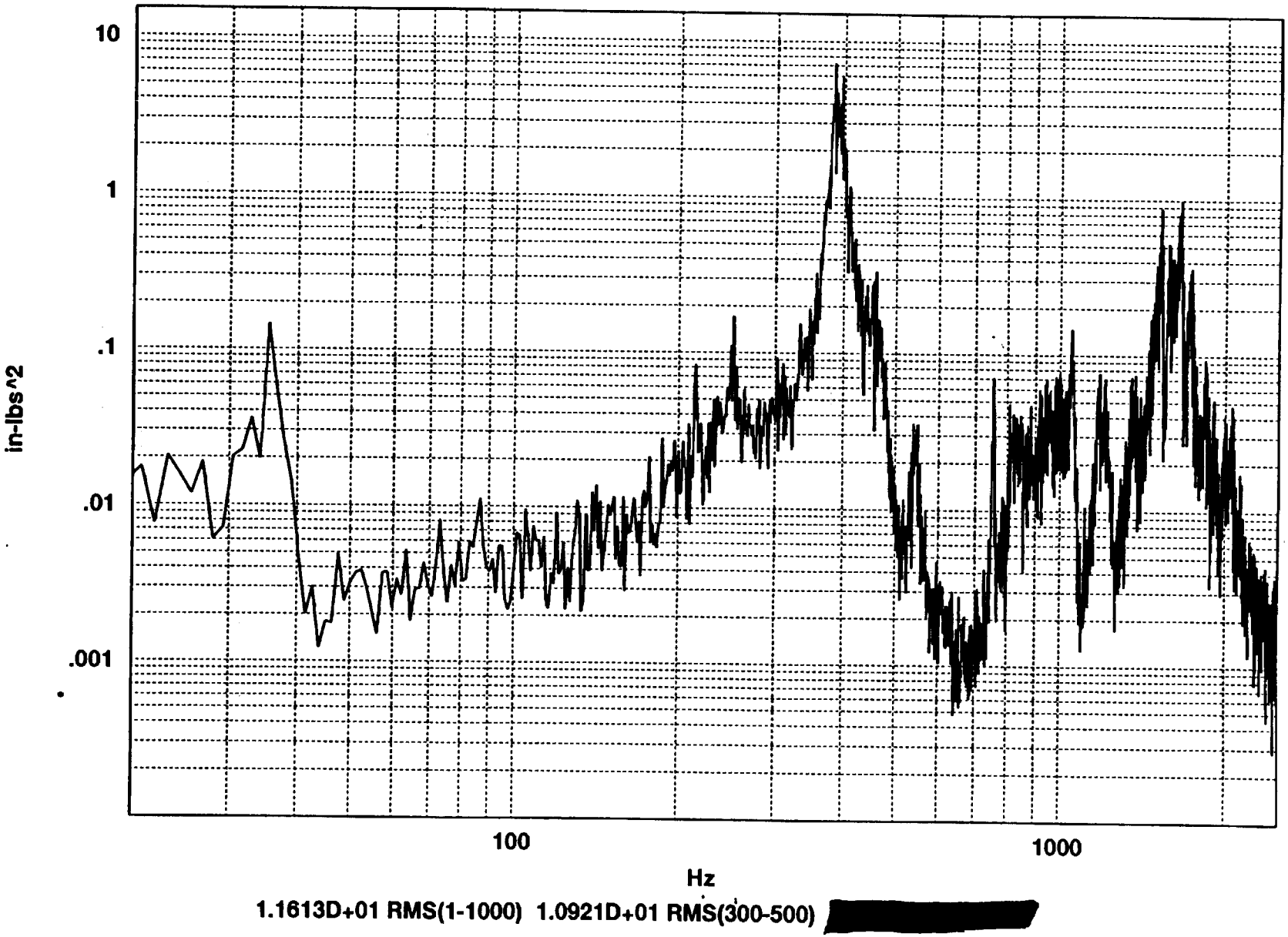

1.1613D+01 RMS(1-1000) 1.0921D+01 RMS(300-500) [redacted]

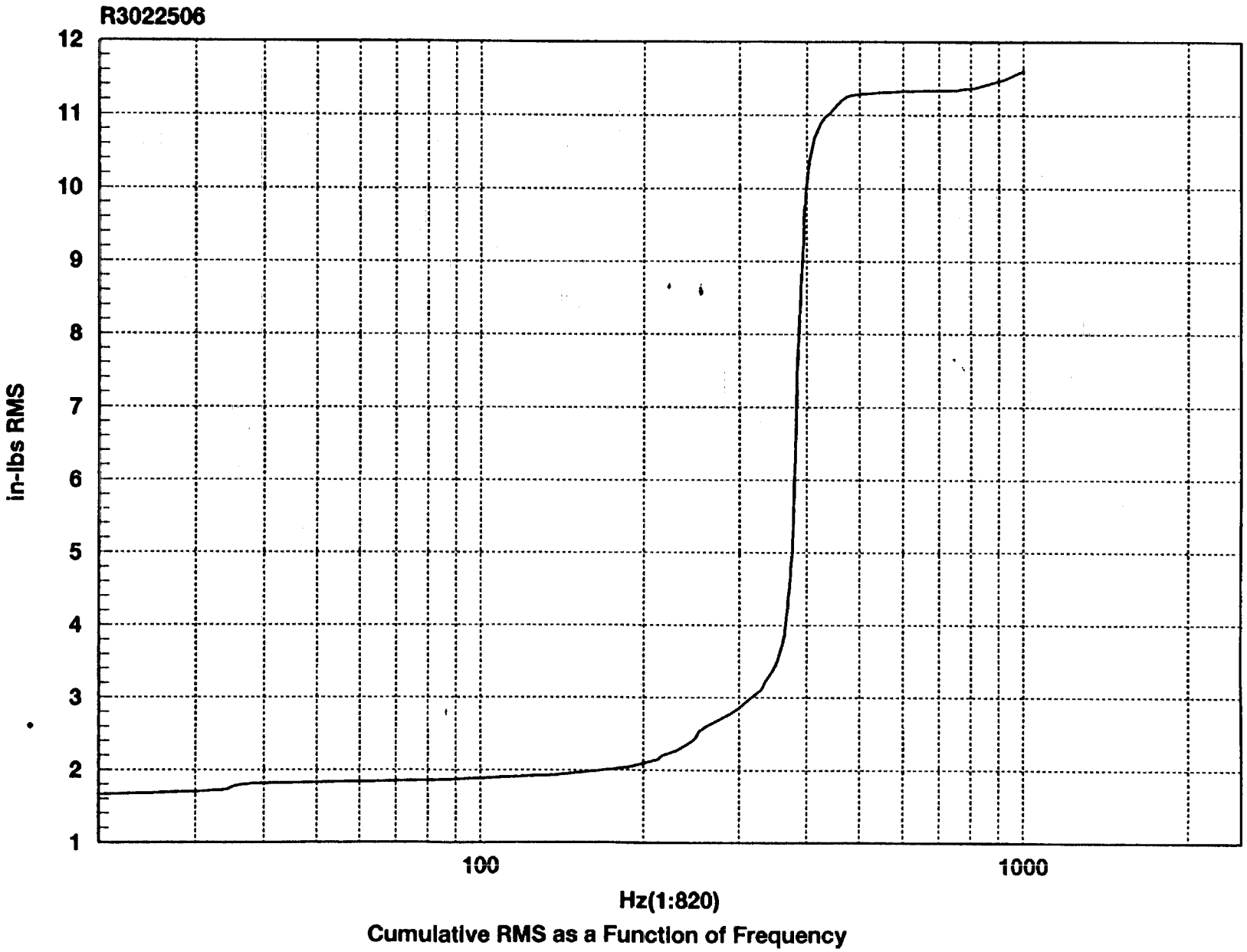

Cumulative RMS as a Function of Frequency

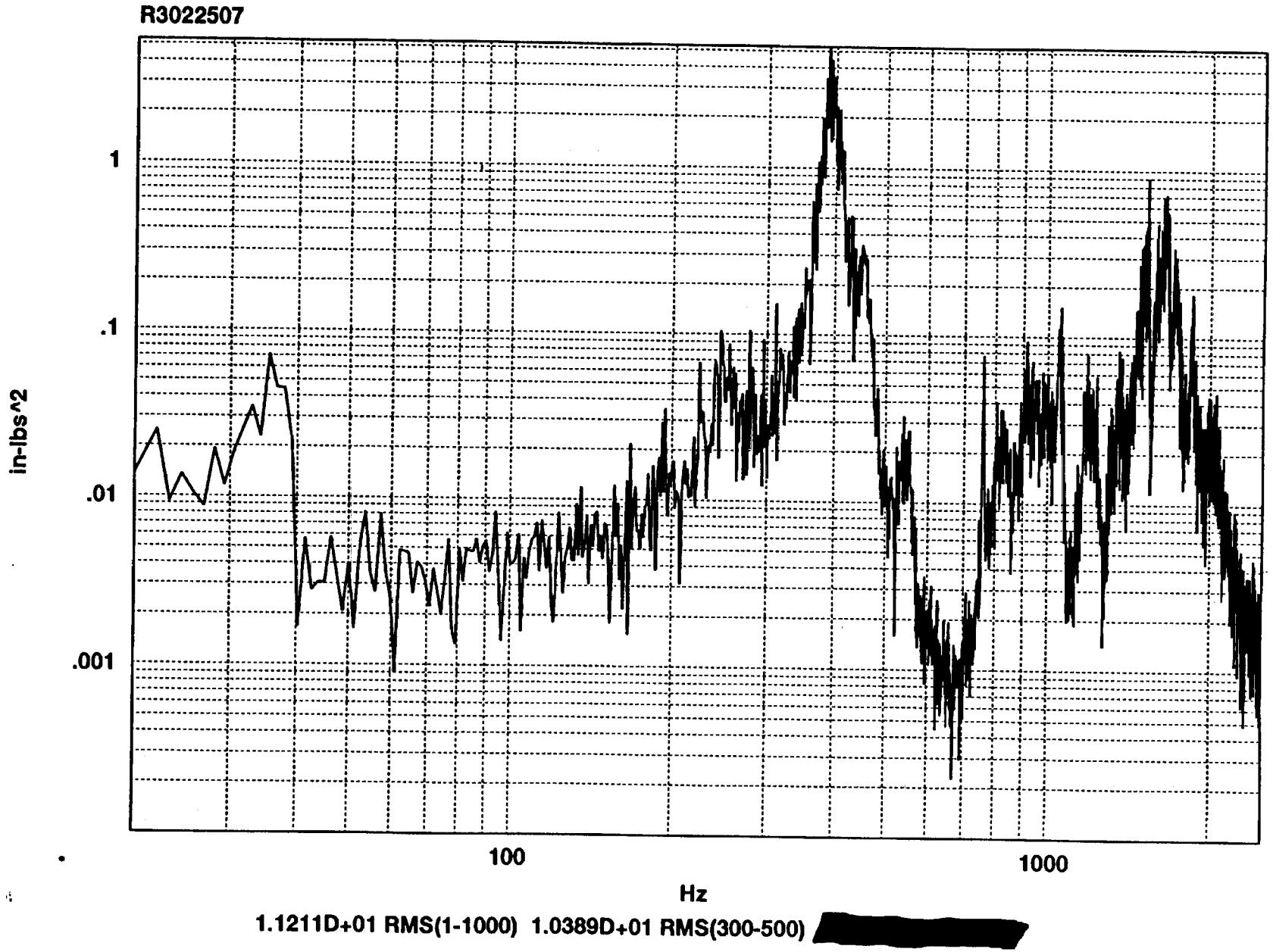
R3022507
1
.1
.01
.001
in-lbs^2
100
1000
Hz
1.1211D+01 RMS(1-1000) 1.0389D+01 RMS(300-500)

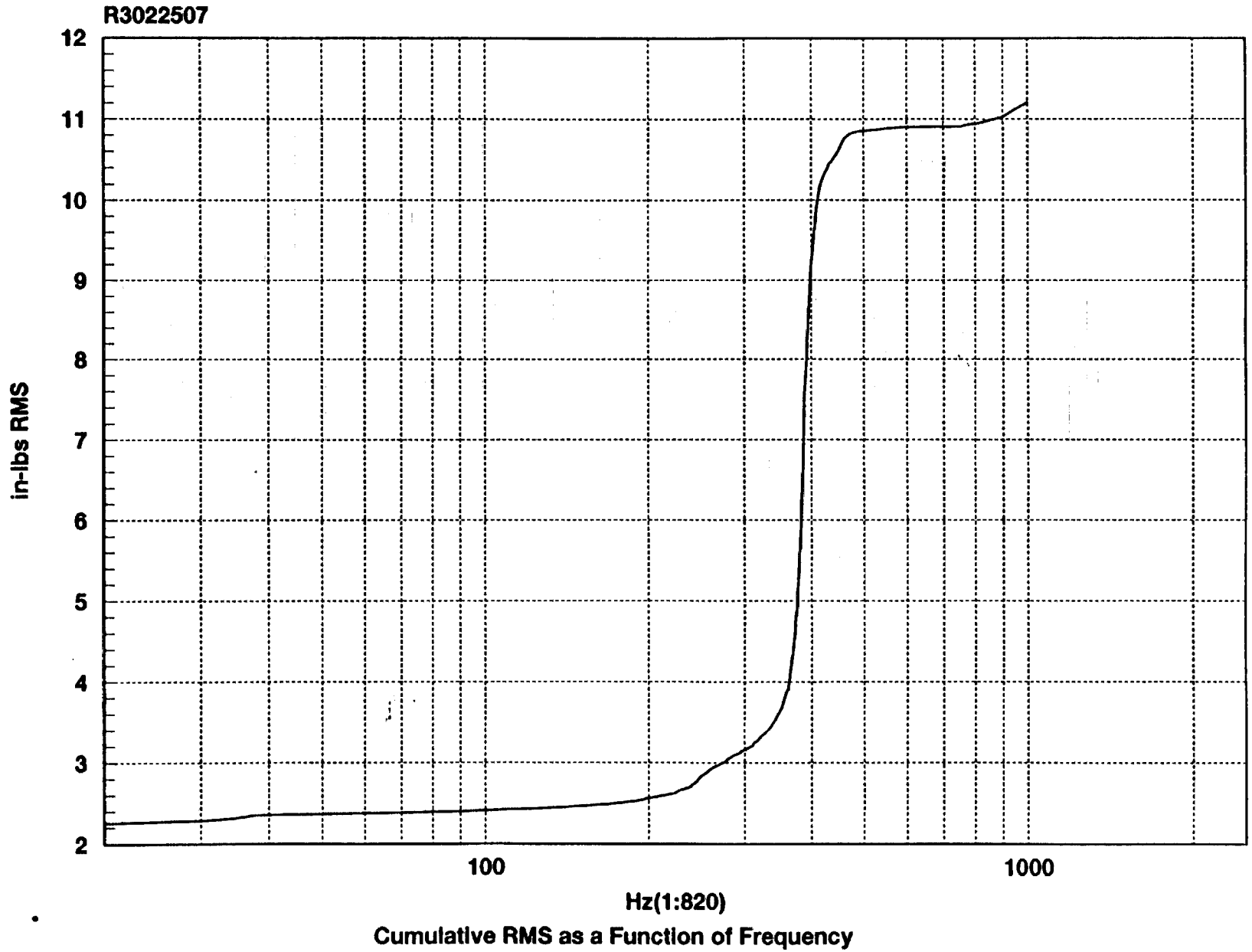
R3022507
12
11
10
9
8
7
6
5
4
3
2
in-lbs RMS
100
1000
Hz(1:820)
Cumulative RMS as a Function of Frequency

R3022601

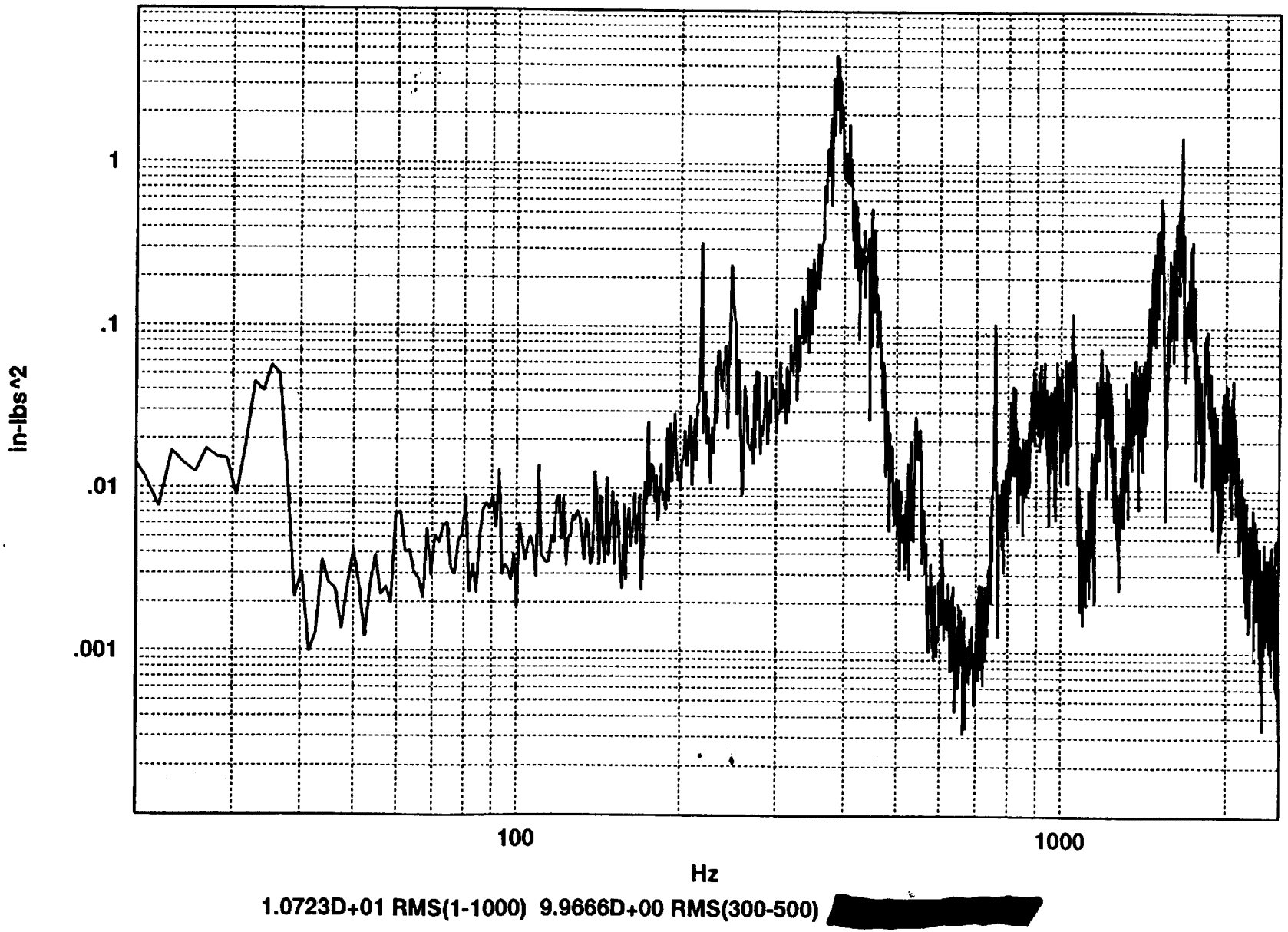

1.0723D+01 RMS(1-1000) 9.9666D+00 RMS(300-500) [redacted]

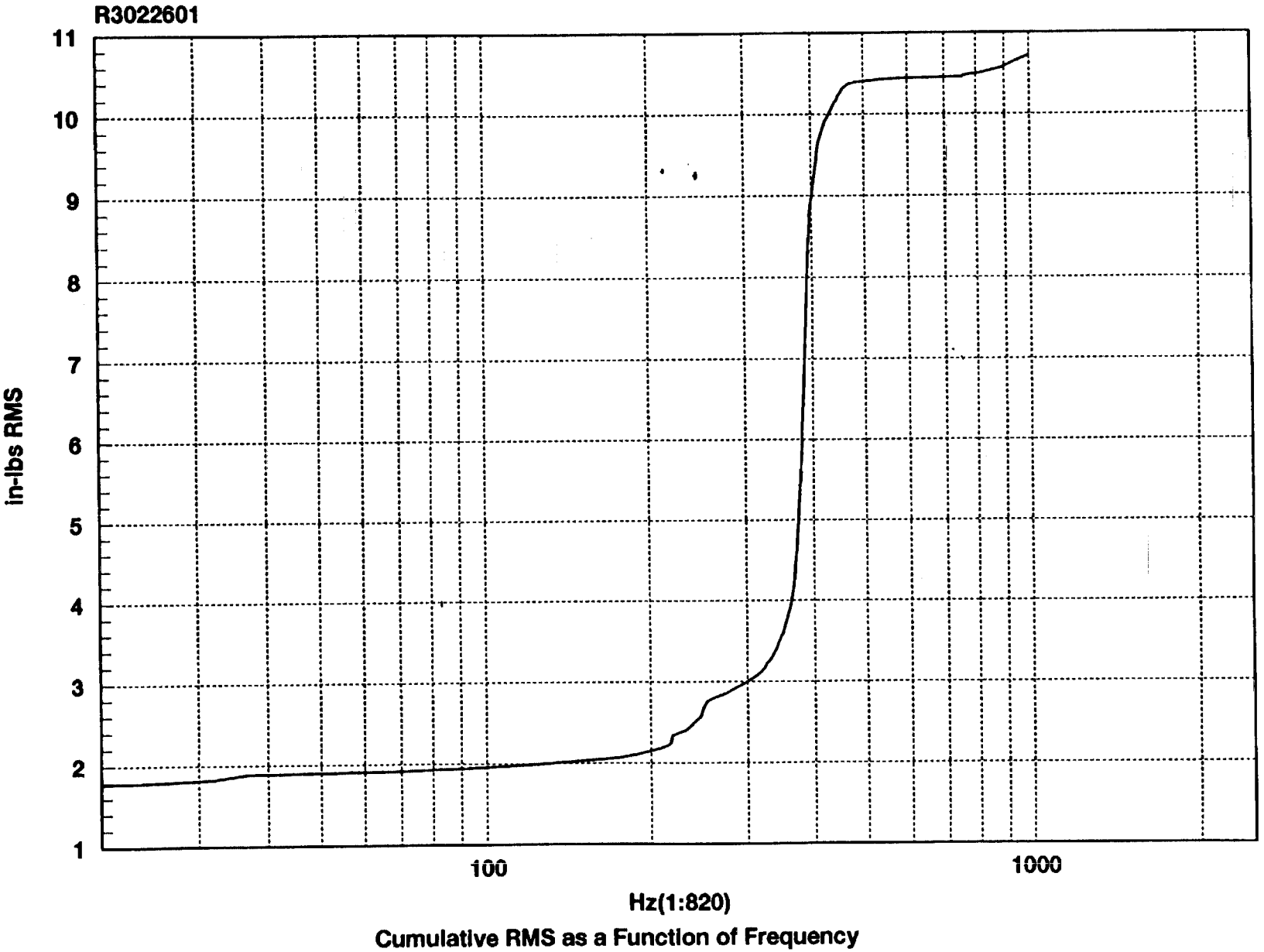
R3022601
11
10
9
8
7
6
5
4
3
2
1
in-lbs RMS
100
1000
Hz(1:820)
Cumulative RMS as a Function of Frequency

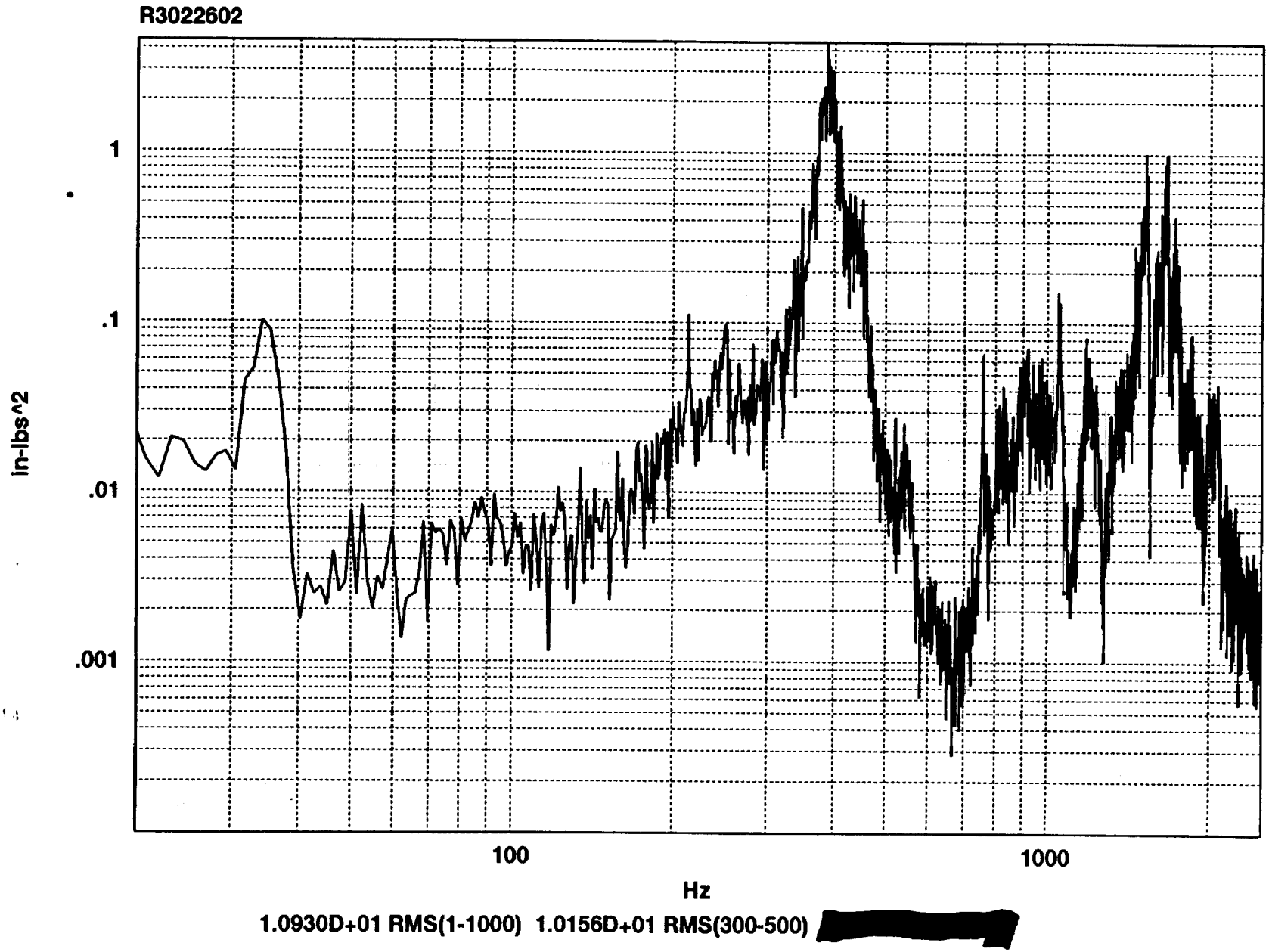
R3022602
1
.1
.01
.001
in-lbs^2
100
1000
Hz
1.0930D+01 RMS(1-1000) 1.0156D+01 RMS(300-500)

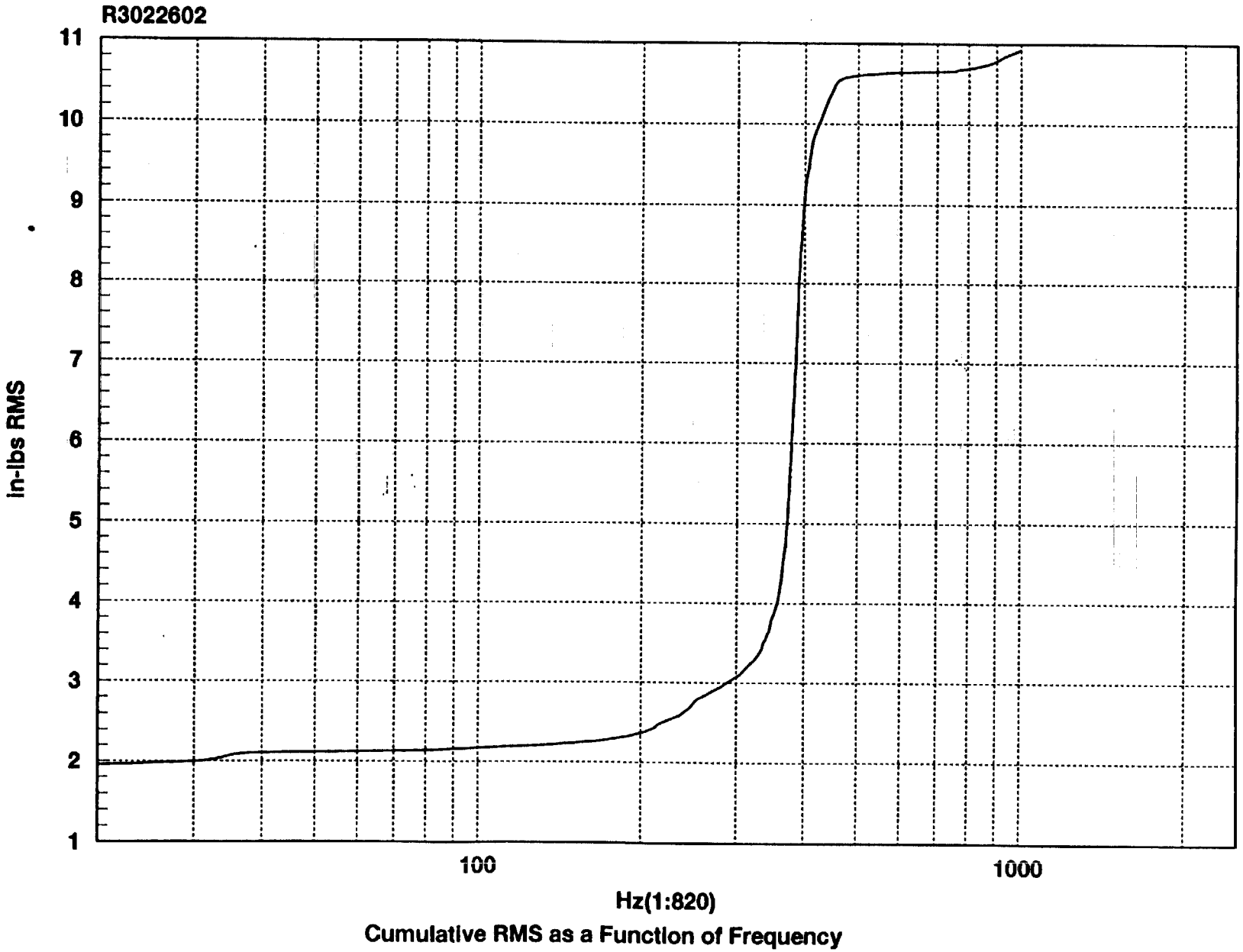

Cumulative RMS as a Function of Frequency

R3022603

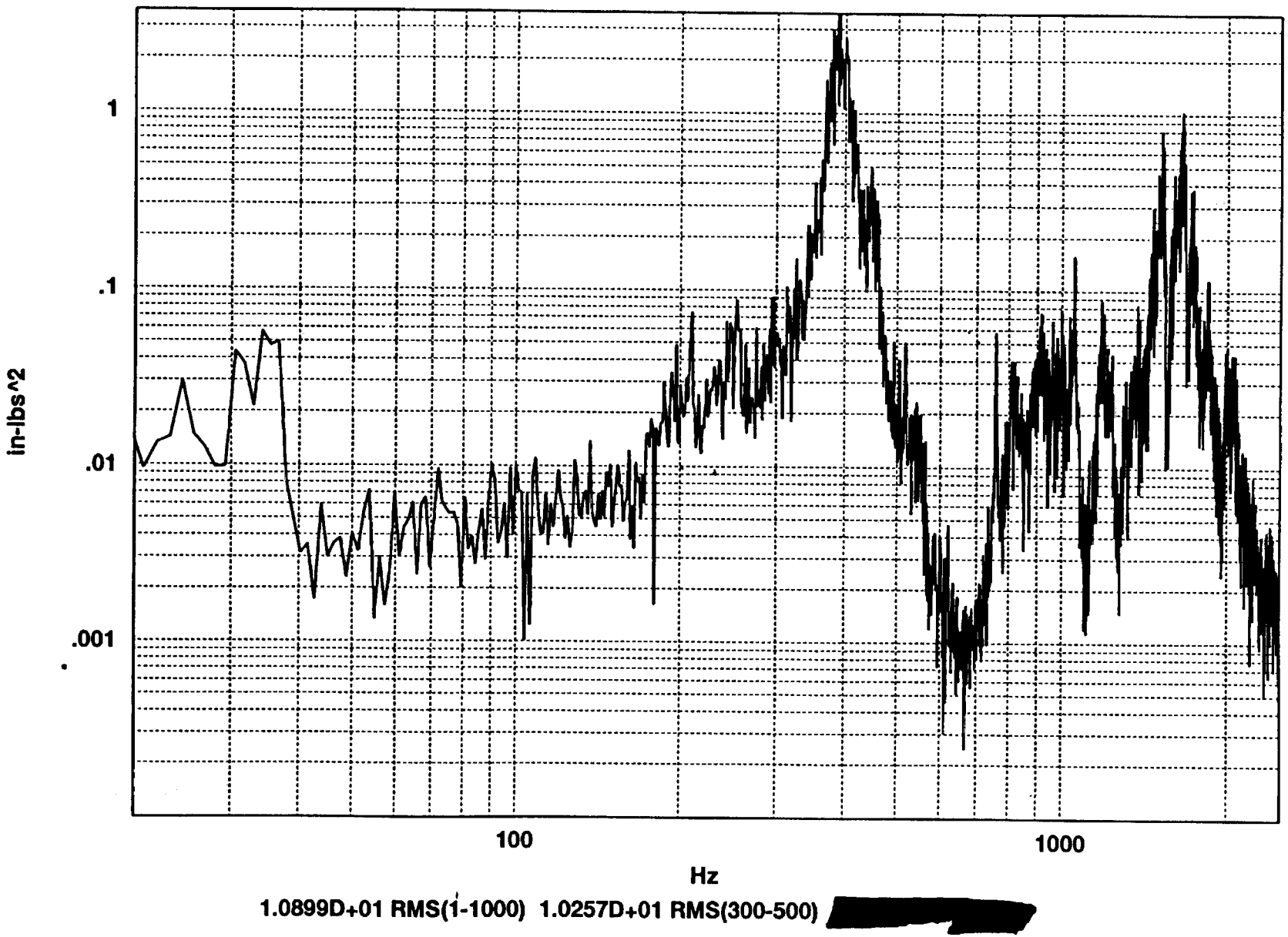

1.0899D+01 RMS(1-1000) 1.0257D+01 RMS(300-500) [redacted]

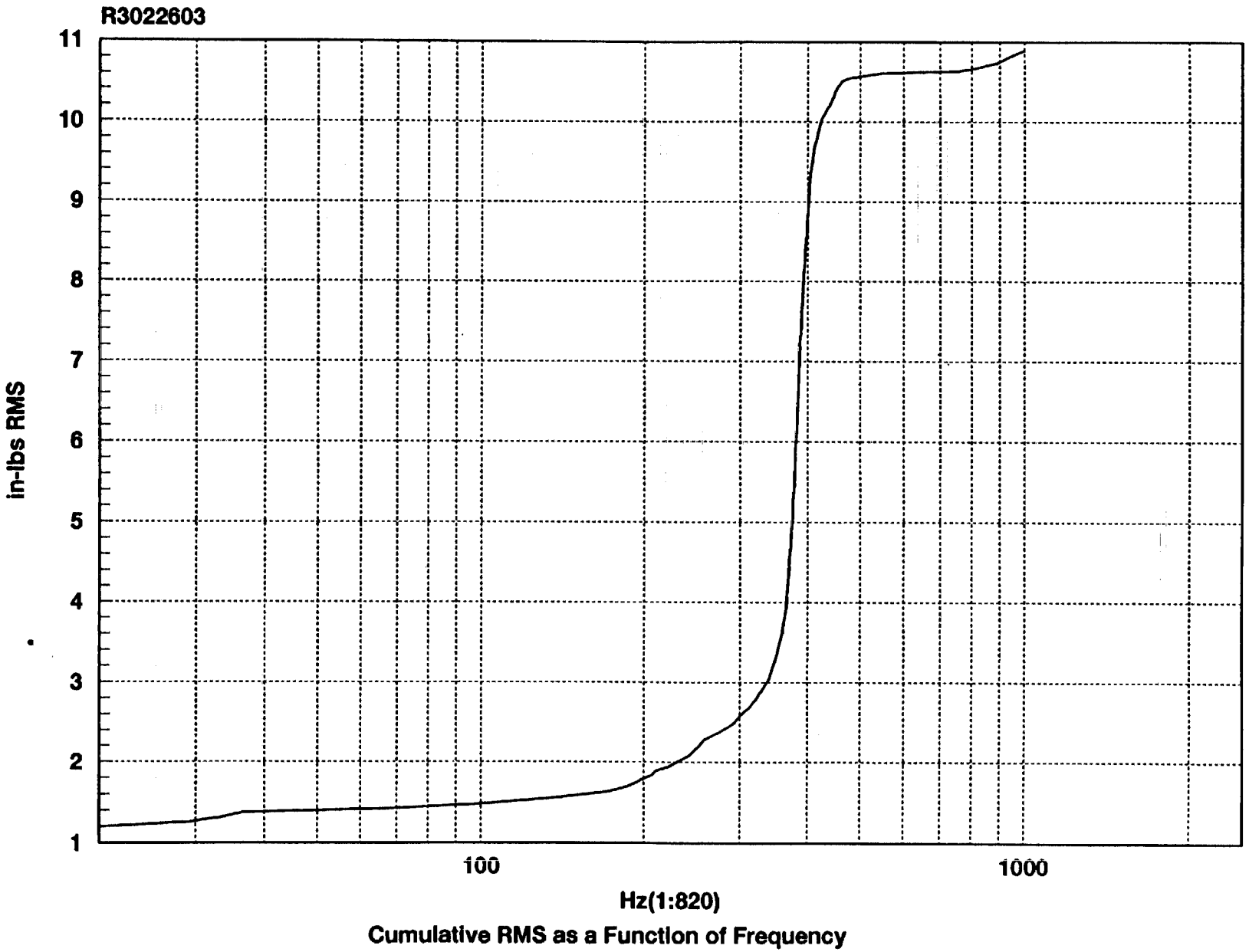
R3022603
11
10
9
8
7
6
5
4
3
2
1
in-lbs RMS
100
1000
Hz(1:820)
Cumulative RMS as a Function of Frequency

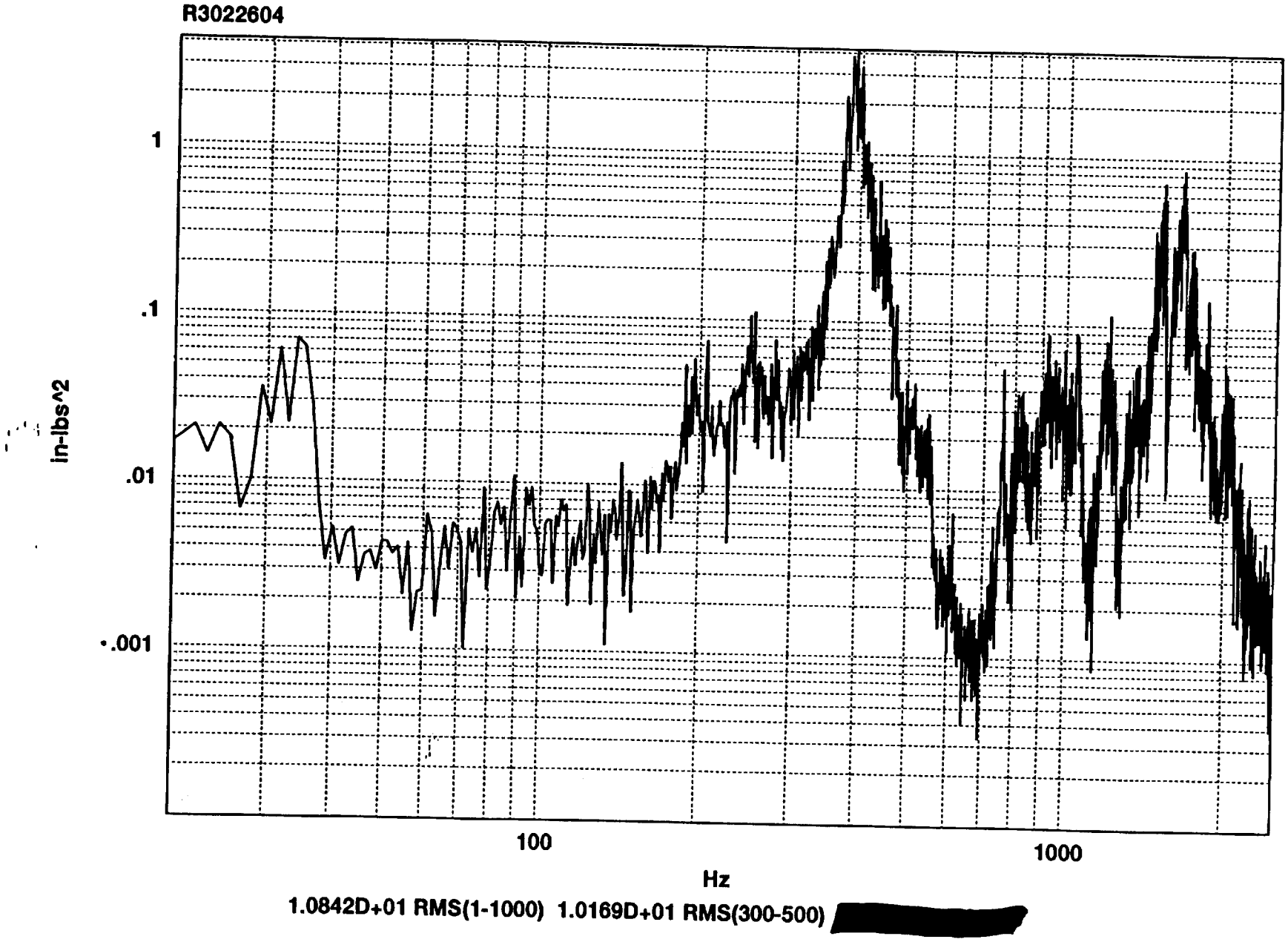
R3022604
1
.1
.01
.001
in-lbs^2
100
1000
Hz
1.0842D+01 RMS(1-1000) 1.0169D+01 RMS(300-500)

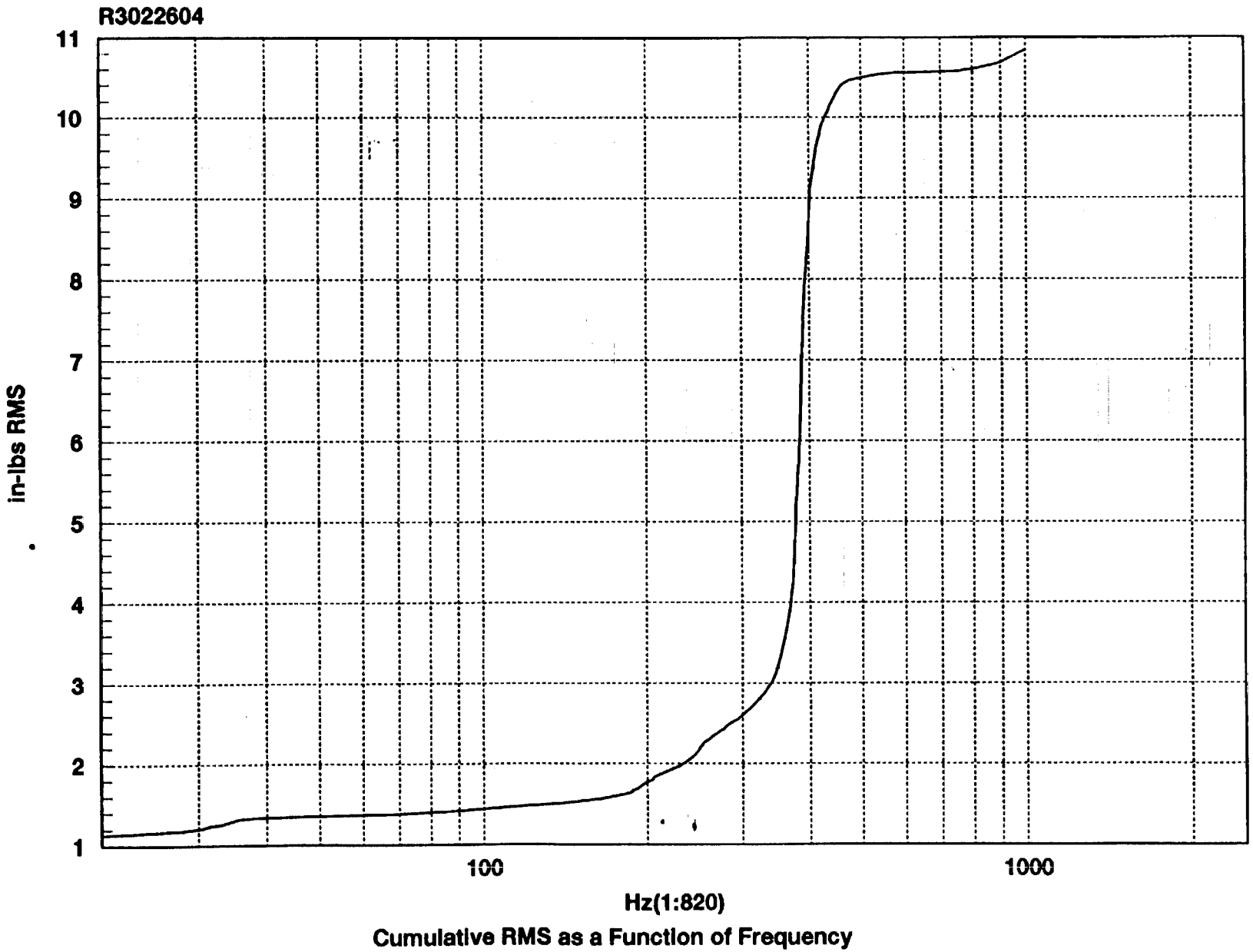

Cumulative RMS as a Function of Frequency

R3022701

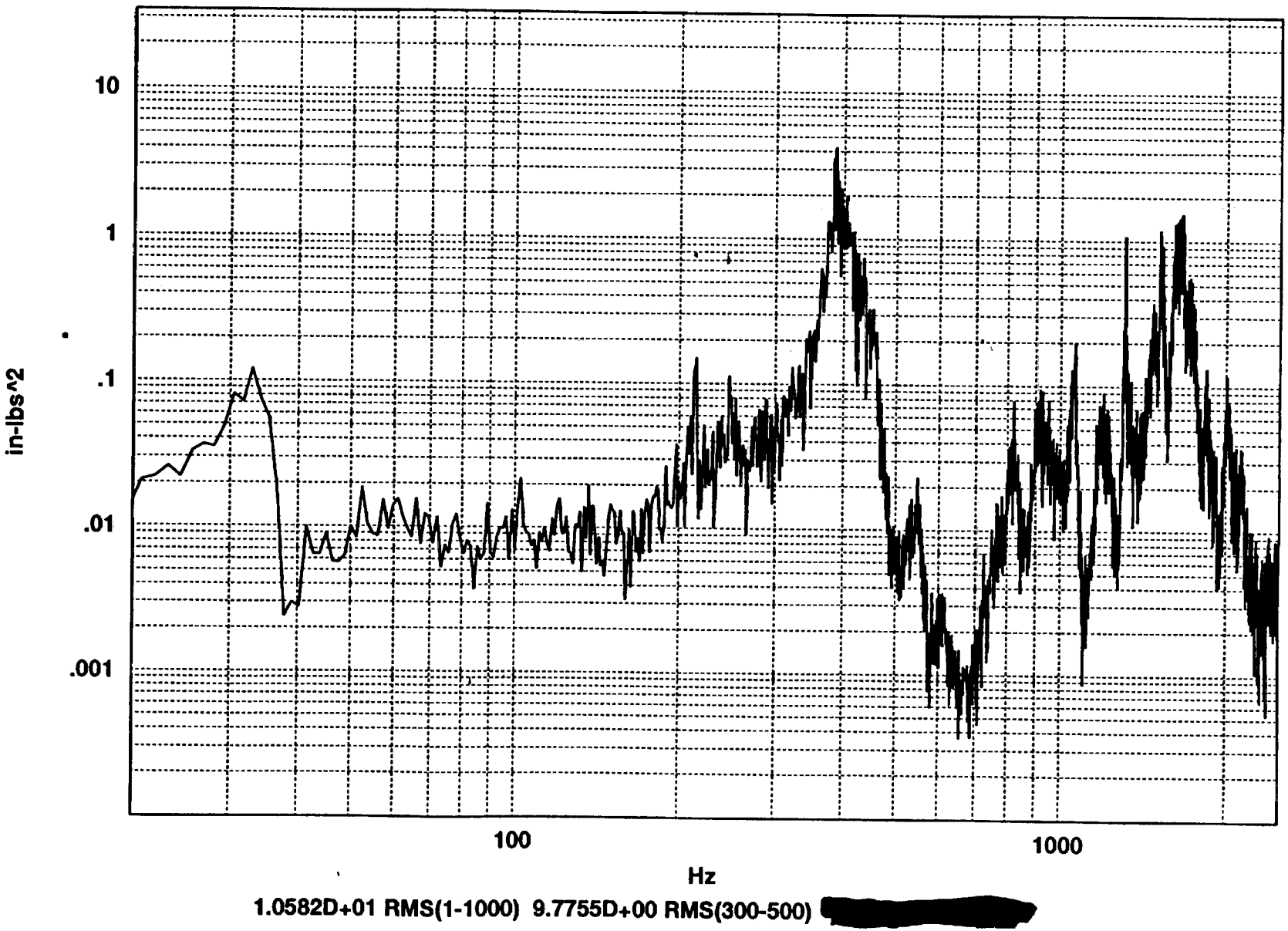

1.0582D+01 RMS(1-1000) 9.7755D+00 RMS(300-500) [redacted]

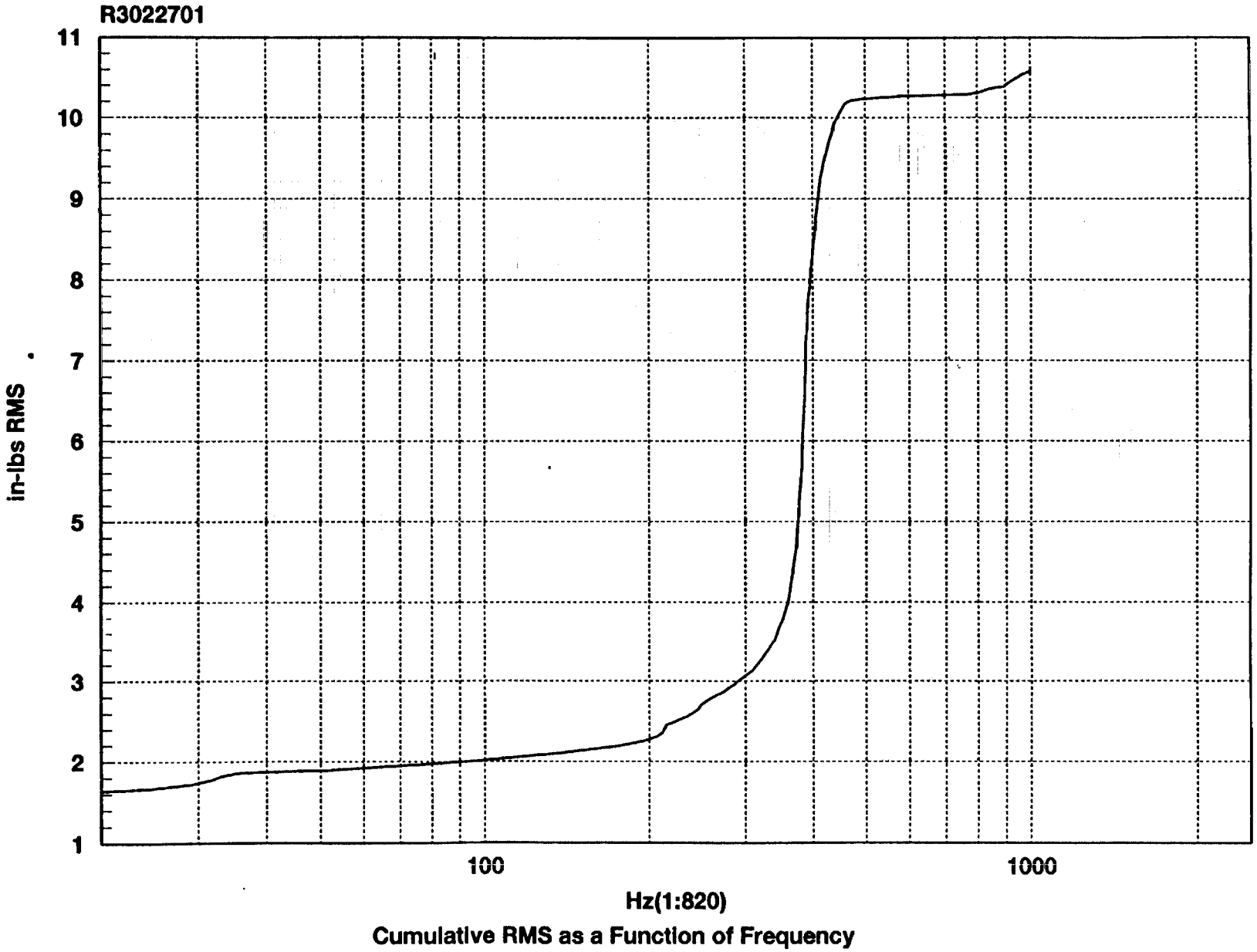

Cumulative RMS as a Function of Frequency

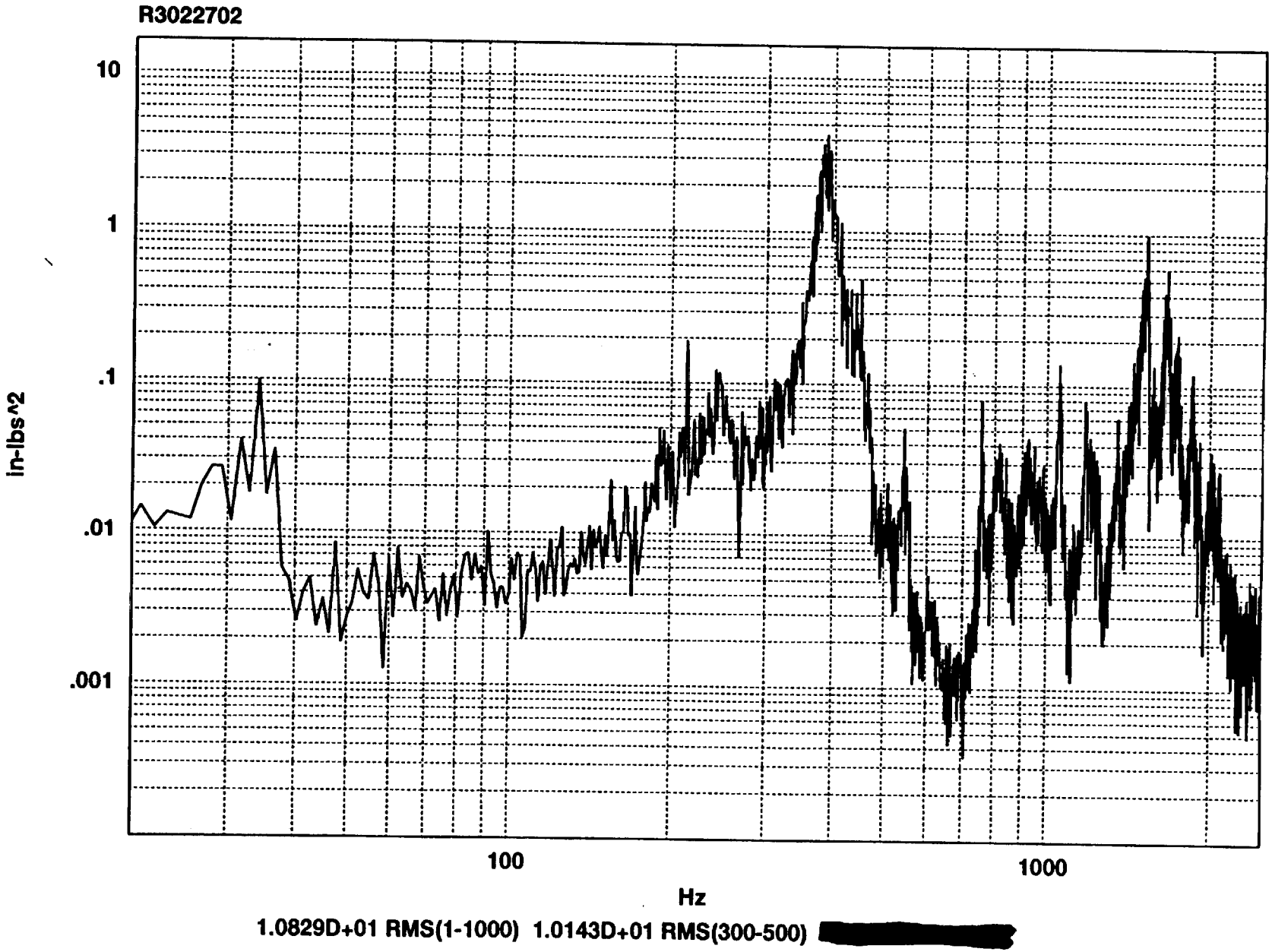
R3022702
10
1
.1
.01
.001
In-lbs^2
100
1000
Hz
1.0829D+01 RMS(1-1000) 1.0143D+01 RMS(300-500)

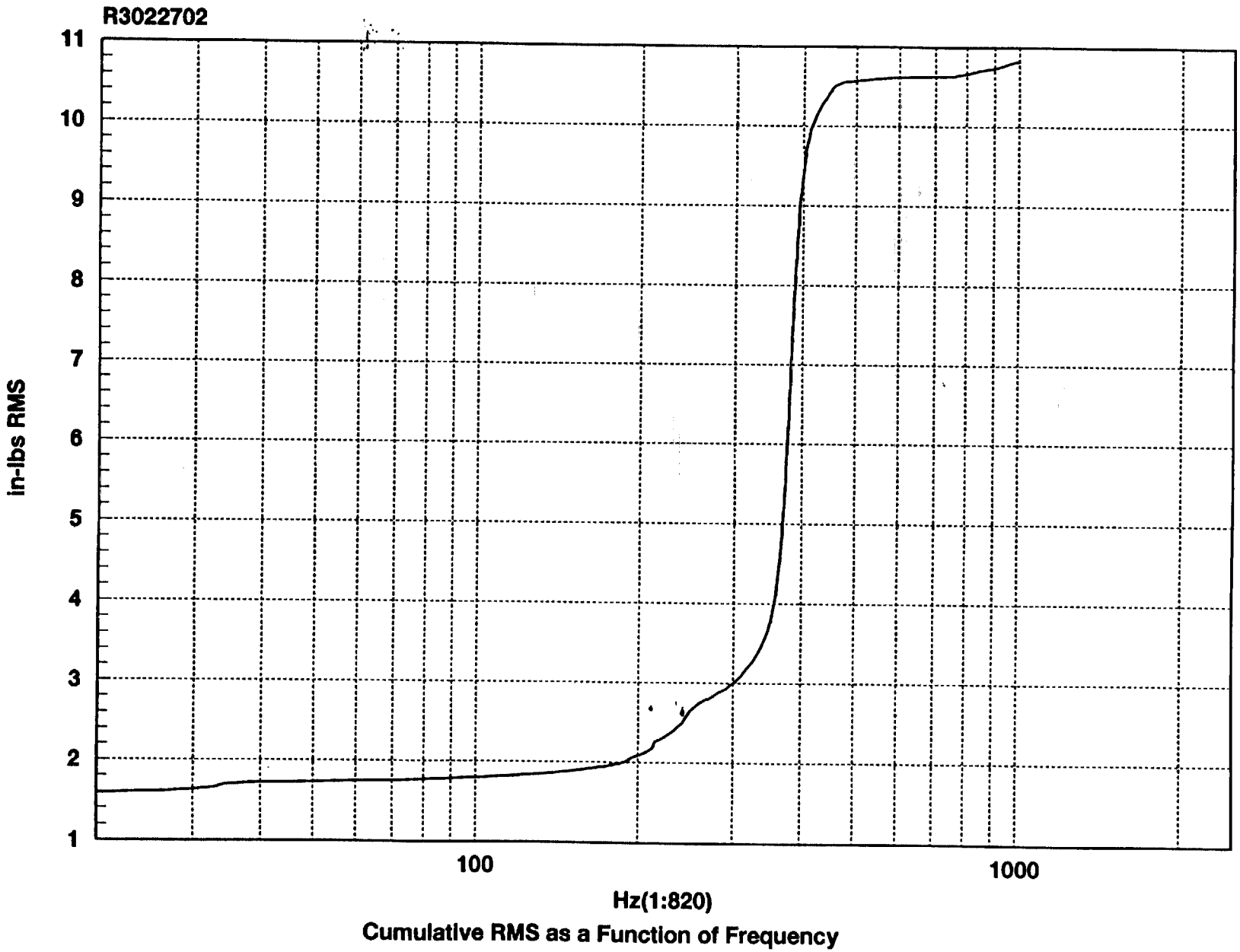

Cumulative RMS as a Function of Frequency

Dynamic Signal Scaling Factors:

The following scale factors were used to convert the raw data recorded on the Metrum to physical units. Each vector was simply multiplied by the scale factor shown, once it was loaded into $MATRIX_x$.

Accelerometer: (Serial#)	Sensitivity (mV/g) (after amplifier)	Metrum A/D (counts/volt)	scale factor (g/count)
a_{z1} (AF9A3)	100	4096/20	25/512
a_{z2} (AF8W2)	100	4096/20	25/512
$accel_x$ (AF9A3)	100	4096/20	25/512

Balance gauge:	Sensitivity (mV/lb)	Metrum A/D (counts/volt)	scale factor (lb/count)
N1	257.286	4096/20	.01898
N2	296.468	4096/20	.01647
AX	119.347	4096/20	.04092

Note: N1, N2, a_{z1}, and a_{z2} were inverted to yield the sign conventions shown on the following page.

PSD Scaling

$MATRIX_x$ was used to do the vector arithmetic, and to calculate PSD's of the calculated disturbance. The calculated disturbance contained 25000 data points representing 5 seconds of data. This was used to calculate six 4096 point PSD's. These PSD's were then averaged. The 4096 point PSD yielded a 1.221 Hz (model scale) frequency resolution. The RMS values for 1-1000 Hz and 300 - 500 Hz were calculated by summing the appropriate PSD points and taking the square root of the sum. As mentioned in the body of the report, the dynamic RMS values did not include the static forces.

The PSD magnitudes (as calculated) are scaled to $in\text{-}lb^2/1.221$ Hz, due to the frequency resolution used. For the PSD plots in appendix B, they were normalized to plot in $in\text{-}lb^2/Hz$.

Dynamic Disturbance Calculations:

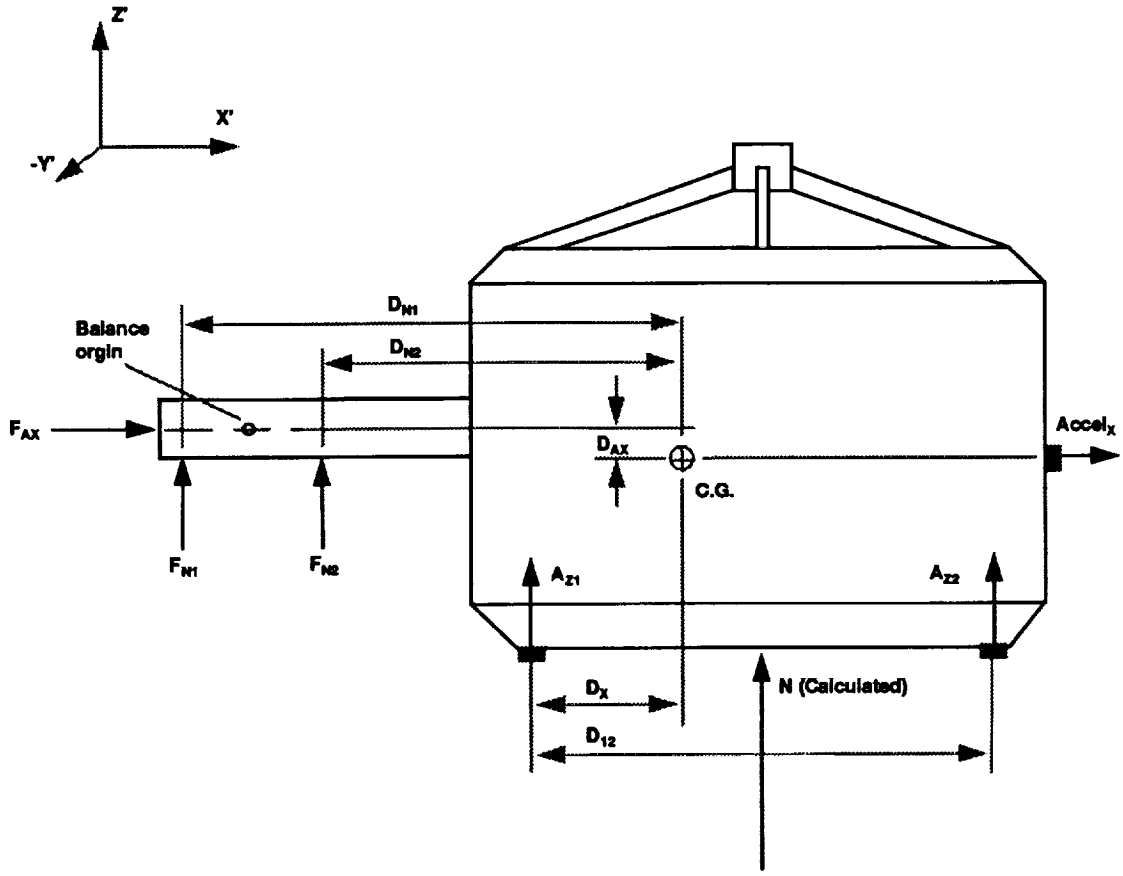

m_t = 1 lb. D_{N1} = 6.844 in. D_{N2} = 4.794 in.
D_{AX} = 0.454 in. D_X = 3.447 in. D_{12} = 8.035 in.
$Accel_X$, A_{Z1}, A_Z (Accelerometer signals, orientation and sign conventions shown above).
F_{AX}, F_{N1}, F_{N2} (Balance force signals, orientation and sign conventions shown above).
N (Unknown external disturbance, orientation and sign convention shown above).

DYNAMIC EXTERNAL DISTURBANCE EQUATIONS:

The model scale resultant Normal force on the primary mirror (in Z' direction) was calculated from the acceleration of the system's mass center and the force balance reaction. The following equation assumes that the telescope model behaves as a rigid body for frequencies under 1000 Hz.

(i) $N = m_t*[a_{Z1}-D_X*(a_{Z1}-a_{Z2})/D_{12}] - F_{N1} - F_{N2}$
$= m_t*[a_{Z1}*(1-D_X/D_{12}) - a_{Z2}*(D_X/D_{12})] - F_{N1} - F_{N2}$ (lb)

Where a_{Z1}, a_{Z2}, F_{N1}, and F_{N2} are phase-locked time function vectors that contain 5 seconds worth of data (25000 samples). The result of the calculation is a time vector N of the same dimension, that represents a 5 second calculated externally applied normal force time function.

Assuming the resultant N is at the center of the primary mirror sail area, the resulting cross elevation moment about the air bearing location can be calculated by multiplying N by the appropriate moment arm:

(ii) N*(model scale moment arm) = N*(7.6 in) (in-lb)

The 7.6 inch moment arm represents the distance from the center of the primary mirror to the point where the model scale air bearing would be located (about 1 inch further away than the balance origin shown on the preceding page, axis out of page).

All six balance static forces and moments were recorded at another location where the static balance signal was periodically re-calibrated to zero between runs. The static forces and moments were the result of longer time averages, and were recorded on the SWTS.